



universität
wien

DISSERTATION

Titel der Dissertation

“Functionalization of metal-based anticancer drugs
in the quest for new chemotherapeutics and
studies on their mode of action”

verfasst von

Mag. Maria Babak

angestrebter akademischer Grad

Doktorin der Naturwissenschaften (Dr. rer. nat.)

Wien, 2014

Studienkennzahl lt. Studienblatt:	A 791 419
Dissertationsgebiet lt. Studienblatt:	Dr.-Studium der Naturwissenschaften (Dissertationsgebiet: Chemie)
Betreuerin / Betreuer:	O. Univ.-Prof. Dr. Dr. Bernhard Keppler A/Prof. Dr. Christian G. Hartinger



universität
wien

Ph.D. Thesis

Title of the thesis

“Functionalization of metal-based anticancer drugs
in the quest for new chemotherapeutics and
studies on their mode of action”

Author

Mag. Maria Babak

Aspired academic degree

Doctor of Sciences (Dr. rer. nat.)

Vienna, 2014

Study code: A 791 419

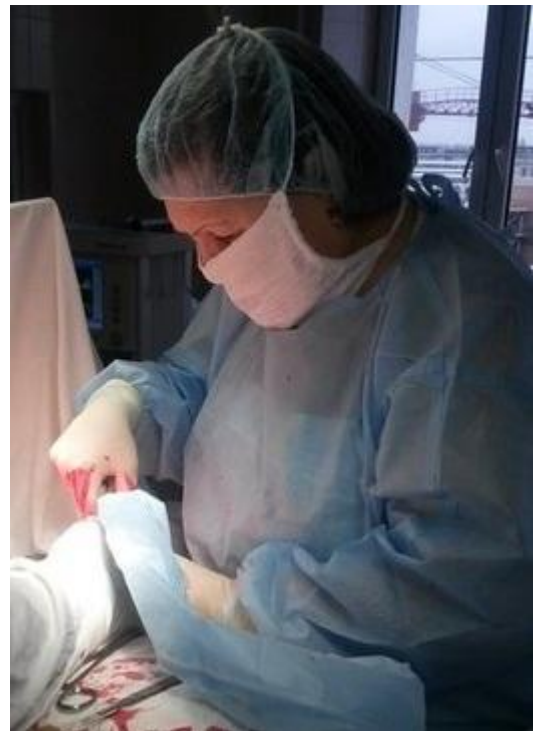
Branch of study: Chemistry

Supervisors: O. Univ.-Prof. Dr. Dr. Bernhard Keppler

A/Prof. Dr. Christian G. Hartinger

This work is solely dedicated to my mother Natalia Babak, who has always been my main support and my dearest friend. Within 45 years of her clinical practice in cancer surgery, she saved and prolonged thousands of lives. I wish I were able to do at least a small part of what she has done for people.

I love you mom!



Acknowledgements

I am heartily grateful to all people who supported and helped me during my PhD thesis. I especially thank:

o. Univ.-Prof. Dr. **Dr. Bernhard Keppler** for the possibility to work in his group

A/Prof. **Christian G. Hartinger** for his inspiring contributions to my work, outstanding supervision at the University of Vienna and the University of Auckland. I am especially thankful to Christian for this chance to work in New Zealand, which was definitely the most fascinating experience of my life

Prof. **Paul J. Dyson** for discovery of my favorite RAPTAs complexes

Dr. Samuel Meier for performing MS experiments, his deep knowledge, fruitful discussions, beautiful graphs and schemes in our papers and amazing contributions to my work

Colleagues from **CeMM** who shared with us sad and happy moments during the development of a drug pull-down method

Mag. Johannes Theiner for his love to elemental analysis measurements

NMR team, especially **Paul-Steffen Kuhn** for NMR measurements

Alexander Roller and **Prof. Arion** for X-ray data collection and structure refinement

Anatoly and **Aliona** for ESI-MS measurements

Jóhannes Reynisson and **John Arabshahi** for performing docking experiments

Dr. Damian Plazuk for a fruitful collaboration

Maria, Mahsa, Dr. Michael Jakupec and especially **Anton** for performing biological tests

Elfriede Limberger and **Harald Fuchs** for their incredible patience in solving bureaucratic and technical issues and problems

Ali and **Marina** for proof-reading my PhD thesis and publications

all my students at the University of Vienna and the University of Auckland, especially **Martin, Matthias, Sebastian, Bjorn, Besnik, Cheyenne, David, Sally and Luke** for their interest in science, devotion to research, love and support

all my kiwi-colleagues, especially **Ali, Muhammad and Farhana** for amazing working atmosphere and wonderful moments

all former colleagues of Lab6@CH, especially **Andrea, Martina and Evelyn** for making Lab6 my second home

Raquel, Sarah, Gabriel, Hristo, Miljan, Aliona, Matthias, Sergey, Anton, Masha, Yulia, Zuhra, Bjorn, Raph, Irena, Joan, Alexey, Ali and Muhammad for being not only the best colleagues I've ever had, but also amazing friends

Evelyn Balsano for being my best student, best colleague and friend, for scientific and non-scientific discussions, infinite moments of laughter, dancing in Lab6 and endless support in the Falling Walls Competition

all my friends who supported me from all places in the world (from America to New Zealand) throughout my life and especially PhD thesis

all zouk dancers who shared my passion to zouk and inspired me when the world was too dark

Wolfgang Kandioller, Melanie Schmiedlehner, Nadine Sommerfeld, Britta Fischer and Verena Pichler for the best motivation and inspiration to learn more, work harder and be better.

The following scientific manuscripts resulted from this Ph.D. thesis:

1. *Maria V. Babak*, Samuel M. Meier, Alexander Roller, Anton A. Legin, Michael A. Jacupec, Bernhard K. Keppler, Christian G. Hartinger. Am(m)ines Make the Difference: Organoruthenium Am(m)ine Complexes and Their Chemistry in Anticancer Drug Development. *Chemistry – A European Journal*, 19(13), 4308-18, **2013**
2. Samuel M. Meier, *Maria V. Babak*, Bernhard K. Keppler, Christian G. Hartinger. Efficiently Detecting Metallodrug-Protein Adducts: Ion Trap versus Time-of-Flight Mass Analyzers. *ChemMedChem*, in press, **2014**
3. *Maria V. Babak*, Samuel M. Meier, Kilian Huber, Jóhannes Reynisson, Anton A. Legin, Michael A. Jacupec, Alexander Roller, Alexey Stukalov, Manuela Gridling, Keiryn L. Bennett, Jacques Colinge, Walter Berger, Paul J. Dyson, Giulio Superti-Furga, Bernhard K. Keppler, Christian G. Hartinger. Target Profiling of RAPTA-drugs by Chemical Proteomics, *JACS*, submitted, **2014**
4. *Maria V. Babak*, Damian Plazuk, Samuel M. Meier, John Arabshahi, Jóhannes Reynisson, Błażej Rychlik, Andrzej Blauż, Muhammad Hanif, Sebastian Ströbl, Bernhard K. Keppler, Christian G. Hartinger. Half-sandwich Ruthenium(II) Biotin-Conjugates as Biological Vectors to Cancer Cells, *Chemistry – A European Journal*, to be submitted, **2014**

The following manuscripts were prepared during the Ph.D. thesis; however, they are not related to the main topic of Ph.D. work:

5. Muhammad Hanif, *Maria V. Babak*, Christian G. Hartinger. Development of Anticancer Agents: Wizardry with Osmium. *Drug Discovery Today*, submitted, **2014**
6. *Maria V. Babak*, Samuel M. Meier, Martin Pfaffeneder-Kmen, Anton A. Legin, Michael A. Jacupec, Muhammad Hanif, Bernhard K. Keppler, Christian G. Hartinger. Rollover Platinum(II) Complexes with a Biological Activity, in preparation.

The following conference contributions resulted from this Ph.D. thesis:

Poster presentations

1. *Maria V. Babak*, Samuel M. Meier, Bernhard K. Keppler, Christian G. Hartinger. Am(m)ines Make the Difference: Organometallic Ruthenium Am(m)ine Complexes and Their Chemistry in Anticancer Drug Development. XXV International Conference on Organometallic Chemistry, Lisbon, Portugal, **2012**, PA. 203
2. *Maria V. Babak*, Samuel M. Meier, Bernhard K. Keppler, Christian G. Hartinger. Inhibition of Cancer Cell Growth by Ruthenium(II)-Arene Complexes with Various Am(m)ine Ligands. 5th EuCheMS Nitrogen ligands conference, Granada, Spain, **2011**, P 159
3. *Maria V. Babak*, Samuel M. Meier, Bernhard K. Keppler, Christian G. Hartinger. Synthesis and investigation of substituted RAPTA-compounds – new potential anticancer drugs. 13th JCF-Frühjahrssymposium, Erlangen, Germany, **2011**, P28

Oral presentations

1. *Maria V. Babak*, Samuel M. Meier, Kilian Huber, Giulio Superti-Furga, Paul J. Dyson, Bernhard K. Keppler, Christian G. Hartinger. How to Find the Needle in a Haystack: Target Profiling of RAPTA Drugs by Chemical Proteomics. Second Whole Action Meeting of the COST Action CM1105, Barcelona, Spain, **2013**.
2. *Maria V. Babak*, Samuel M. Meier, Michael A. Jacupec, Giulio Superti-Furga, Paul J. Dyson, Bernhard K. Keppler, Christian G. Hartinger. Target Profiling of RAPTA Drugs by Chemical Proteomics. Modern Trends in Organometallic Chemistry and Catalysis, Moscow, Russian Federation, **2013**, O16
3. *Maria V. Babak*, Samuel M. Meier, Bernhard K. Keppler, Christian G. Hartinger. Organometallic Ru(ammine) Complexes and Their Chemistry in Anticancer Drug Development. 7. Workshop Anorganische Chemie in Österreich, Innsbruck, Austria, **2012**, O18

The presentation “Breaking the Walls of Classical Anticancer Therapy” was awarded the 1st prize on the international Falling Walls Competition in Vienna 2012. The work was consequently presented on the Falling Walls Lab in Berlin 2012.

Abstract

The discovery of the anticancer activity of cisplatin by Rosenberg has broadened the range of routinely applied chemotherapeutics from organic drugs to metal-based compounds. Nowadays platinum compounds are a treatment of choice for a large number of cancer patients; however, the use of these drugs is limited by severe side-effects, tumor resistance and a narrow window of activity. In order to overcome the limitations of platinum chemotherapeutics, researchers turned to the investigation of other metals of the periodic table. Novel modes of action of anticancer ruthenium complexes, which are substantially different from commonly used platinum-based chemotherapeutics, assured the interest in this compound class. The most well-studied ruthenium drug candidates are the ruthenium(III) coordination compounds NAMI-A and KP1019 and organometallic ruthenium(II)-arene complexes with ethylenediamine or PTA ligands (e.g. RM175 and RAPTA-C). Despite promising results in advanced preclinical studies and clinical trials, the mechanism of action of these compounds remains largely unknown. As a result, the design of next-generation derivatives is hampered by incomprehension of their mode of action.

In order to establish the molecular target profiling of ruthenium-based complexes, we developed a so-called drug pull-down approach. This approach is based on a combination of the design of a drug derivative with similar biological properties as the parent compound, drug affinity purification of cancer cell lysates with subsequent high-end mass spectrometry and bioinformatics. The novel approach was successfully applied for establishing a molecular target profile of RAPTA complexes; consequently, a wide variety of intracellular proteins was identified, including key cancer-related proteins. Our novel drug pulldown approach can be employed for the target profiling of a wide range of metal-based complexes and shed light on their mode of action.

According to the results of the drug pulldown performed on a RAPTA derivative, they interact with a wide range of proteins in a non-specific way; therefore, the next goal of this thesis was an establishment of structure-activity relationships in novel non-specifically targeting ruthenium compounds, namely $\text{Ru}^{\text{II}}(\text{arene})$ complexes with am(m)ine ligands. In the last part of the thesis, we developed a more targeted chemotherapeutic approach for RAPTA-like complexes, where they were derivatized with biotin ligands, specifically targeting cancer cells with an overexpressed level of

sodium multivitamin transporter. We characterized novel ruthenium complexes by standard analytical methods including X-ray diffraction analysis and mass spectrometry. Consequently, we investigated their cytotoxicity as well as interactions with a range of biomolecules and established structure-activity relationships. Additionally, the impact of the mass analyzer on the adduct formation of metal complexes with proteins was explored.

Zusammenfassung

Die Entdeckung der zytostatischen Aktivität von Cisplatin durch Rosenberg hat die Bandbreite der klinisch routinemässig angewandten Chemotherapeutika über organische Verbindungen hinaus auf metallbasierte Substanzen erweitert. Heutzutage sind Platinverbindungen die bevorzugte Behandlungsmethode für eine große Anzahl an Krebspatienten. Jedoch unterliegt die Verwendung dieser Medikamente aufgrund von schweren Nebenwirkungen, der Bildung von Tumorresistenzen und einem schmalen Anwendungsfenster Einschränkungen. Um den therapeutischen Beschränkungen von Platinverbindungen zu begegnen, wurde die Forschung auf andere Metalle des Periodensystems erweitert. Insbesondere die neuartigen Wirkmechanismen von antitumoraktiven Rutheniumverbindungen unterscheiden sich deutlich von denen der etablierten Platinverbindungen und erhöhten das Interesse an dieser Verbindungsklasse. Die bestuntersuchten Rutheniumverbindungen in Entwicklung sind die Ruthenium(III)-Koordinationsverbindungen NAMI-A und KP1019 sowie Ruthenium(II)-Organometallverbindungen mit Ethylendiamin- oder PTA-Liganden (z.B. RM175 und RAPTA-C). Trotz vielversprechender Resultate von präklinischen und klinischen Studien sind die Wirkmechanismen dieser Verbindungsklassen immer noch grossteils unaufgeklärt. Die Unkenntnis dieser Wirkmechanismen hemmt die Entwicklung neuer Medikamentengenerationen.

Um ein molekulares Zielprofiling für Rutheniumkomplexe zu erstellen, haben wir einen sogenannten „drug pulldown“ Ansatz entwickelt. Dieser Ansatz bedient sich einer aus Designs eines Wirkstoffderivates mit ähnlichen biologischen Eigenschaften wie die Mutterverbindung, Wirkstoffaffinitätsreinigung von Krebszelllysaten mit anschließender Hochleistungsmassenspektrometrie und Bioinformatik. Dieser neuartige Ansatz wurde erfolgreich erfolgreich für ein molekulares Zielprofiling für RAPTA-Komplexe angewandt. Daraus folgte die Identifikation einer ganzen Reihe von intrazellulären Proteinen, darunter krebssrelevanten Schlüsselproteine. Unser neuartiger „drug pulldown“ Ansatz kann für das Zielprofiling einer großen Bandbreite an Metallkomplexen verwendet werden und erlaubt einen Einblick in deren Wirkmechanismen.

Die Resultate des „drug pulldowns“ zeigten, dass RAPTA-Komplexe mit einer ganzen Reihe an Proteinen unspezifisch reagieren. Daraus folgte als nächstes Ziel dieser

Dissertation, die Identifikation von Struktur-Aktivitätszusammenhängen in neuartigen unspezifisch wirkenden Rutheniumverbindungen, in diesem Fall $\text{Ru}^{\text{II}}(\text{Aren})$ -Komplexe mit Am(m)in-Liganden. Im letzten Teil der Dissertation wurde ein noch gezielterer chemotherapeutischer Ansatz für RAPTA-ähnliche Verbindungen entwickelt. Dazu wurden die Verbindungen mit Biotinliganden, welche spezifisch auf Krebszellen mit einer Überexpression an Natriummultivitamintransportern abzielen, derivatisiert. Die dabei entstandenen neuartigen Rutheniumkomplexe wurden mittels analytischen Standardmethoden, darunter Röntgendiffraktometrie sowie Massenspektrometrie, charakterisiert. Schließlich wurde deren Zytotoxizität sowie die Wechselwirkungen mit einer Reihe von Biomolekülen untersucht um Struktur-Aktivitätsbeziehungen zu erhalten. Zusätzlich wurde die Protein-Metallkomplex Adduktbildung in Abhängigkeit von der Wahl des Massenanalysators untersucht.

Important abbreviations and symbols

bax – pro-apoptotic protein of Bcl-2 family
bcl-2 family – family of apoptosis regulating proteins
bcl-2 protein – **B**-cell lymphoma **2**, anti-apoptotic protein of bcl-2 family
bcl-x_L – **B**-cell lymphoma-extra large, anti-apoptotic protein of bcl-2 family
BCRP protein (ABCG2) – **B**reast **C**ancer **R**esistance **P**rotein, drug-efflux pump
bFGF – basic Fibroblast Growth Factor
BRCA1 – human **B**reast **C**ancer suppressor gene **1**
carbo-RAPTA – [(η⁶-p-cymene)Ru(PTA)(C₆H₆O₄)]
cat B – cathepsin **B**
CID – Collision-Induced Dissociation
CDKs – Cyclin-Dependent Kinases
CDKIs – Cyclin-Dependent Kinases Inhibitors
Ctr1 – Copper transport protein
Cyt C – Cytochrome **C**
CZE – Capillary Zone Electrophoresis
DAPTA – (3,7-diacetyl-1,3,7-triaza-5-phosphabicyclo[3.3.1]nonane
2D-DIGE – two-Dimensional Difference In Gel Electrophoresis
DFT – Density Functional Theory
DUT– DeoxyUridine 5'-Triphosphate nucleotidohydrolase, mitochondrial
dGMP – deoxyGuanosine MonoPhosphate
DNA – 2'-DeoxyriboNucleic Acid
EPR (effect) – Enhanced Permeability and Retention effect
ER – Estrogen Receptor
ER+ (cancer) – Estrogen Receptor positive cancer (cancer cells with estrogen receptors)
ER- (cancer) – Estrogen-Receptor negative cancer
ERCC1 protein – DNA Excision Repair protein
ESI-IT-MS – ElectroSpray Ionization Ion Trap Mass Spectrometry
ESI-QToF-MS – ElectroSpray Ionization Quadrupol Time-of-Flight Mass Spectrometry
FAD – Flavin Adenine Dinucleotide
FT-ICR – Fourier Transform Ion Cyclotron Resonance
G₀ (phase) – inactive phase of the cell cycle
G₁ (phase) – growth phase of the cell cycle
G₂ (phase) – second growth phase of the cell cycle
GSH – glutathione, intracellular thiol
GST – Glutathione-**S**-Transferase
HOMO – Highest Occupied Molecular Orbital
HSA – Human Serum Albumin
ICP-MS – Inductively Coupled Plasma Mass Spectrometry
ICP-AES – Inductively Coupled Plasma Atomic Emission Spectroscopy
JNKs – c-Jun-NH₂-terminal Kinases, apoptosis regulators
KP46 – tris(8-quinolinolato)gallium(III)
KP1019 – (indazolium *trans*-[tetrachloridobis(1*H*-indazole)ruthenate(III)])
KP1339 – (sodium *trans*-[tetrachloridobis(1*H*-indazole)ruthenate(III)])
LC-ICP-MS – Liquid Chromatography Inductively Coupled Plasma Mass Spectrometry
LUMO – Lowest Unoccupied Molecular Orbital
M (phase) – mitosis
MLCT – Metal-to-Ligand Charge Transfer
MMR (system) – MisMatch Repair pathway
MMPs – Matrix MetalloProteinases, matrix-degrading enzymes
MRE – Metal-Response Element-binding transcription factor -1(MTF-1)
MRP (**MRP1**, **MRP2**, **ABCC** family) – Multidrug Resistance Proteins, drug-efflux pumps
MT – MetalloThioneins
MTT (assay) – (3-[4,5-dimethylthiazol-2-yl]-2,5 diphenyl tetrazolium bromide) assay, a colorimetric assay for determination of cell viability
MTF-1 – Metal-responsive Transcription Factor, signaling pathway
MudPIT – MultiDimensional Protein Identification Technology
NAD⁺ – Nicotinamide Adenine Dinucleotide
NADH – a reduced form of NAD⁺
NADP⁺ – Nicotinamide Adenine Dinucleotide Phosphate
NADPH – a reduced form of NADP⁺

NAMI-A – New Antitumor Metastasis Inhibitor, (imidazolium *trans*-[tetrachlorido(dimethylsulfoxide)(1*H*-imidazole)ruthenate(III)])
NCP – Nucleosome Core Particle
NER (system) – Nucleotide Excision Repair system
NMR – Nuclear Magnetic Resonance
OsPTA – [(η^6 -p-cymene)Os(PTA)Cl₂]
oxali-RAPTA – [(η^6 -p-cymene)Ru(PTA)(C₂O₄)]
p53 – tumor suppressor protein, pro-apoptotic protein
p21 – pro-apoptotic protein, CDKI
2D-PAGE – two-Dimensional PolyAcrylamide Gel Electrophoresis
PARPs – Poly(Adenosine diphosphate (ADP)-Ribose) Polymerases, DNA repair proteins
PCR – Polymerase Chain Reaction
PDT – PhotoDynamic Therapy
Pgp (ABCB1) – P-glycoprotein, drug-efflux pump
POLE3 – DNA Polymerase Epsilon subunit 3
QM/MM – Quantum Mechanics/Molecular Mechanics
RNA – RiboNucleic Acid
PTA – 1,3,5-triaza-7-phosphatricyclo-[3.3.1.1]decane
ptn – 3,7-dimethyl-7-phospha-1,3,5-triazabicyclo[3.3.1]nonane
RAPTA-C – [(η^6 -p-cymene)Ru(PTA)Cl₂]
RAPTA-T – [(η^6 -toluene)RuCl₂(PTA)]
RAPTA-CF3 – [(η^6 -C₆H₅CF₃)RuCl₂(PTA)]
RM175 – [(η^6 -biphenyl)Ru(ethylenediamine)Cl](PF₆)
ROS – Reactive Oxygen Species
S (phase) – DNA synthesis phase of the cell cycle
SEC-ICP-MS – Size-Exclusion Chromatography Inductively Coupled Plasma Mass Spectrometry
SOD – SuperOxide Dismutase
Tf – human serum Transferrin
Trx – Thioredoxin
TrxR – Thioredoxin Reductase
Ub – Ubiquitin
VEGF – Vascular Endothelial Growth Factor
ZnT-1 – Zn transporter 1
ZF (protein) – Zinc Finger protein

Table of contents

Abstract.....	XII
Zusammenfassung.....	XIV
Important abbreviations and symbols.....	XVI
Table of contents.....	XVIII
I. Introduction	1
1. Introduction into the molecular biology of cancer	2
1.1 Understanding cell division	2
1.2 Carcinogenesis. Tumor formation.....	2
1.3 Unique properties of cancer cells.....	4
1.4 Drug resistance.....	5
2. Cancer treatments	7
2.1 Conventional cancer treatments	7
2.2 Chemotherapy	7
2.3 Clinical trials.....	8
2.4 Targeted chemotherapy.....	9
2.5 Antimetastatic drugs	9
3. Metal-based anticancer drugs	11
2.1 General information	11
2.2 Resistance of metal-based drugs	12
2.3 Categorization of metal-based drugs	15
4. Development of RAPTA-complexes	20
4.1 <i>Primitive era</i> . Who are you, RAPTA?.....	21
4.1.1 General information	21
4.1.2 Hydrolysis.....	22
4.1.3 Structure-activity relationships.....	24
4.1.4 Anticancer properties.....	29
4.2 <i>DNA era</i> . Is DNA the main target?	31
4.3 <i>Proteins era</i> . If not DNA, then what?	34
4.3.1 Thioredoxin reductase (TrxR).....	34
4.3.2 Cathepsin B (Cat B).....	35
4.3.3 Ubiquitin (Ub) and cytochrome C (cyt C)	36
4.3.4 Lysozyme and superoxide dismutase (SOD)	38
4.3.5 Glutathione (GSH)	40
4.3.6 Metallothioneins (MTs)	41
4.3.7 Poly(adenosine diphosphate (ADP)-ribose) polymerases (PARPs)	42
4.3.8 Human serum albumin (HSA) and human serum transferrin (Tf)	43
4.3.9 Subcellular localization	45
4.3.10 Nucleosome core particle (NCP)	47

4.4 <i>Advanced proteins era</i> . The role of proteomics in metallodrug research	48
4.4.1 Protein targets determined by 2D-DIGE	49
4.4.2 Protein targets determined by MudPIT	51
4.5 <i>Modern times</i> . Towards targeted therapy with RAPTA complexes	53
4.5.1 Targeting DNA.....	53
4.5.2 Targeting glutathione-S-transferase (GST)	55
4.5.3 Targeting human serum albumin (HSA). Exploiting the EPR effect.....	56
4.5.4 Metallodendrimers. Further exploiting the EPR effect	58
4.5.5 RAPTA complexes with thermomorphic properties	59
4.5.6 Fluorescent postlabeling.....	60
4.5.7 Metallacages. Multifunctional drugs.....	61
4.6 <i>New era</i> . Conclusions. What comes next?	63
5. References	66
II. Results	70
1. Target profiling of RAPTA-drugs by chemical proteomics	71
1.1 Supporting information.....	81
2. Half-sandwich ruthenium(II) biotin-conjugates as biological vectors to cancer cells	95
2.1 Supporting information.....	121
3. Am(m)ines make the difference: organoruthenium am(m)ine complexes and their chemistry in anticancer drug development	129
3.1 Supporting information.....	141
4. Efficiently detecting metallodrug-protein adducts: ion trap versus time-of-flight mass analyzers	150
4.1 Supporting information.....	157
III. Conclusions and prospects	164
IV. Curriculum Vitae	166

I. Introduction

“All truths are easy to understand once they are discovered; the point is to discover them”

Galileo Galilei

1. Introduction into the molecular biology of cancer

1.1 Understanding cell division¹

The main characteristic of cancer is an abnormal cell proliferation. Cell proliferation is a process involving the reproduction of a cell to form two daughter cells, where each of them subsequently forms two other daughter cells, and so on. The sequence of events repeated every time a cell passes between one cell division and the next is called the **cell cycle**. It is made up of four stages and is usually illustrated in a clockwise manner. Each cell cycle starts with interphase, followed by mitosis. In the interphase, the cell passes through a **growth phase (G₁)**, followed by a **DNA synthesis phase (S)** and a **second growth phase (G₂)**. At the end of G₂, the cell enters into **mitosis (M phase)**, where the division itself occurs. Whereas G₁ and G₂ phases are the preparation steps where the cells wait for the next phase, the S phase is characterized by the replication of the genetic material and the M phase implicates the division of the parent cell into two daughter cells. The average cell cycle lasts 16 hours, where 15 hours are given for the interphase and 1 hour for mitosis; however, the length of the cycle depends on the cell type. Notably, most cells in an adult are not dividing; they are quiescent and rest in the **inactive phase G₀** outside the cycle. Nevertheless, they can be activated by several factors to re-enter the cycle. Cells travelling through the cycle are strictly controlled and coordinated at every transition to the new phase by a set of proteins called **cyclins** and **cyclin-dependent kinases**. These **checkpoints** are important in maintaining the genome integrity, since they sense and induce a cellular response to DNA damage. The **G₁ checkpoint** is responsible for the cell cycle arrest as a consequence of DNA damage; as a result, this damage is not replicated in the S phase. The **G₂ checkpoint** arrests the cell cycle so that the replication in the S phase is properly completed. The **M checkpoint** leads to the arrest of chromosomal segregation. Cyclins and corresponding kinases regulate each checkpoint at each transition of the cell cycle. The regulation of cyclin production is regulated by growth signals, which can be positive and negative; therefore, the cell cycle can be either stimulated or arrested every moment. Disruption of any checkpoint function (e.g. overexpression of cyclins) results in mutations which can induce carcinogenesis.

1.2 Carcinogenesis. Tumor formation

All cancer cells are characterized by unregulated cell growth. Dorothy Lobo in the book "Biology of cancer" gave an excellent explanation "*cancer is cell division gone bad*".² It is

hard to imagine that cancer arises from *one* faulty cell that underwent a sequence of mutations. In 1970s, a two-step cancer development model was proposed, based on the knowledge that every person has two copies (alleles) of every gene (from mother and father). Thus, in order to initiate cancer progression, both copies of an **oncogene** or **tumor suppressor** (two major types of mutated genes) must be mutated.

The process of tumor formation is called **carcinogenesis**; it involves initiation, promotion, progression and invasion (see Figure 1). The **initiation** is the genetic mutation itself that predisposes a cell to cancer. During the **promotion** step, the mutation of the second copy of the same gene occurs, which results in a total failure of its function. Notably, there are a number of mutations happening daily in a human body; however, the good news is that in order to cause **progression** of a cell into a cancerous one, a number of mutations should occur *in the same cell*, which is quite unlikely. When a cell accumulates mutations leading to a significant increase in the cell division, the patch of tissue forms a **benign** tumor. This is an area characterized by an enhanced growth but the tumor is not cancerous. It is not capable of invading other tissues or exhibiting other properties specific for cancer. That means that such tumors do not metastasize but they can still be life-threatening due to their location (*e.g.* in the brain). An important prerequisite for the formation of a **malignant** tumor is the occurrence of additional mutations. Malignant tumors do not remain encapsulated and spread to other tissues, showing the features of **invasion**.

The mutation sequence is as follows:

- 1) one cell undergoes a mutation
- 2) growth-stimulating signals increase, whereas growth-inhibiting signals decrease
- 3) daughter cells divide much faster than normal cells, resulting in a formation of a small benign tumor
- 4) within a tumor an additional set of mutations occurs
- 5) apoptosis is blocked
- 6) cells divide fast and do not die
- 7) within these immortal cells, an additional set of mutations occurs
- 8) Vascular Endothelial Growth Factor (VEGF, see Table 1) is released
- 9) blood vessels that supply tumors with nutrients are formed
- 10) an additional set of mutations occurs
- 11) the cell motility is activated, as a result mutated cells move from their original locations

- 12) at the new sites an additional set of mutations occurs
- 13) telomerase is activated
- 14) cells become immortal

It can take a long time for numerous mutations to change the cell from its healthy state to dangerous cancer conditions, although carcinogenesis is a self-accelerating process, with every mutation accelerating the appearance of new ones. Therefore, carcinogenesis takes more than 20 years from the moment of the first mutation; as a result, the cancer incidence markedly increases with the age.

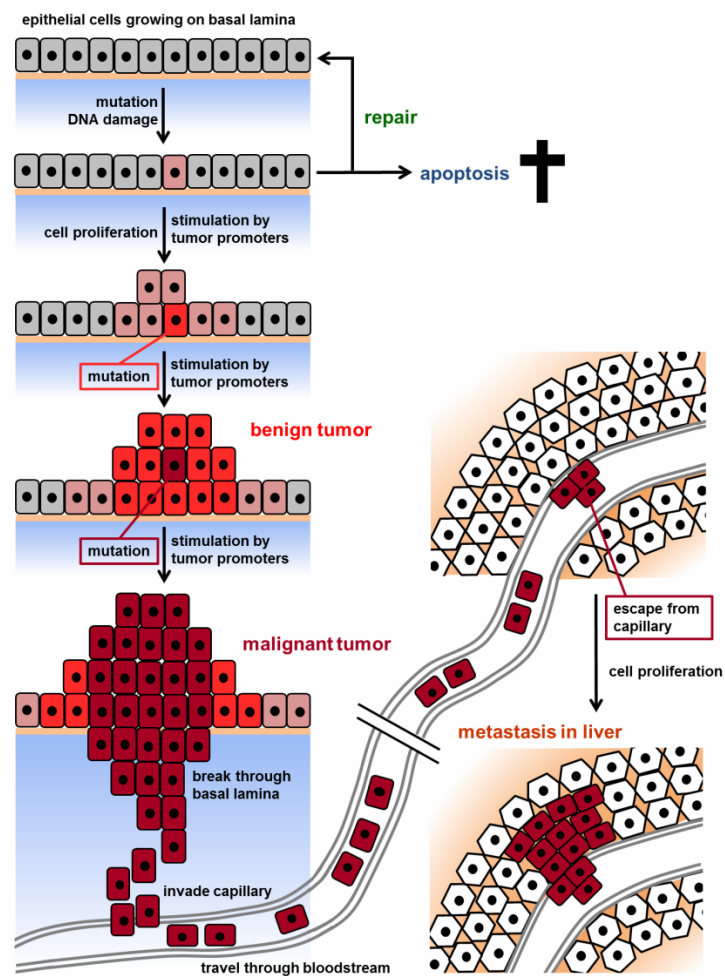


Figure 1. The process of carcinogenesis. The picture was taken from the PhD thesis of Dr. Andrea Kurzwernhart (2013) with her kind permission.

1.3 Unique properties of cancer cells³

A number of people mistakenly think that cancer is a disease which originates and develops similarly in all patients. However, it is a group of diseases, with more than 100 types of cancer identified and classified; therefore, there is no universal treatment for all

cancer types. Cancer cells have at least several features in common, which distinguish them from healthy cells and which might be exploited for the development of cancer treatments. These features are called “hallmarks” of cancer and were described by Douglas Hanahan and Robert Weinberg in 2000 as follows:

- 1) Growth signal autonomy (growth without “go” signals)
- 2) Evasion of growth inhibitory signals (failure to respond to “stop” signals)
- 3) Evasion of a programmed cell death (**apoptosis**)
- 4) Uncontrolled cell division (unlimited replicative potential)
- 5) **Angiogenesis** (the formation of new blood vessels)
- 6) Tissue invasion and metastasis

The detailed examination of hallmarks of cancer along with representative characteristics of cancer and healthy cells is presented in Table 1.

1.4 Drug resistance

One of the main limitations for the curative treatment of cancer is chemotherapy resistance characterized by rapid adaptation of cancer cells to the aggressive chemotherapeutic treatment or intrinsic resistance of the tumor. **Acquired resistance** reflects the instability of tumor cells, whose genome might be easily modified in course of the disease. **Intrinsic resistance** is mainly associated with normal cells (especially, epithelial) constantly protected against toxins exposure; however, tumor cells can also be intrinsically resistant. There is no universal resistance mechanism for all drugs; therefore, the resistance mechanism has to be determined experimentally for every novel drug. There are several reasons for the development of drug resistance:

- 1) the drug may not reach the cell target in a concentration needed for a proper therapeutic effect due to the blocked uptake (e.g. **Ctrl1**) or increased efflux (e.g. **Pgp, MRP**)
- 2) the drug reaches the cell; however, it is inactivated by protein binding, e.g. to metallothioneins (**MT**), glutathione (**GSH**), or thioredoxin reductase (**TrxR**), before it damages the cellular target the drug reaches the cell and damages the target; however, the damage is repaired (**NER system**) or cells become tolerant to this damage (**MMR system**)
- 3) the drug reaches the cell and damages the target; however, this damage does not cause cell death (e.g. **bcl-2, p53**)

Several possible explanations for metal-based drug resistance will be discussed later in a respective chapter.

Table 1. The hallmarks of cancer

	Healthy cells	Cancer cells
Growth without “go” signals	- Need “permissive” signals from growth factors ^{a)} to divide.	- Independent of normal growth factor signaling - Mutations of proteins encoded by oncogenes (can be compared to gas pedal stuck in the accelerated position)
Failure to respond to “stop” signals	- Respond to inhibitory signals - Do not divide if there is no space (contact inhibition) - Never form several layers of cells	- Do not respond to growth inhibitory signals - Mutation of proteins encoded by tumor suppressors (can be compared to the failure of the car breaks) - Do not follow the rules of contact inhibition; that is, cells continue to divide, when there is no space - Form several layers of cells, resulting in tumors
Evasion of apoptosis	- Are removed by apoptosis, if DNA is damaged	- Evade apoptotic signals
Unlimited cell division	- Can divide maximum 60 times as a result of a senescence, caused by shortening of telomeres ^{b)}	- Maintain the length of their telomeres due to the activation of telomerase ^{c)} - Exhibit unlimited replicative potential
Angiogenesis	- Depend on blood vessels to supply of nutrients and oxygen - Do not significantly alter the vascular architecture	- Induce the release of proteins that trigger the growth of new blood vessels important for tumor survival and expansion (two most critical proteins are Vascular Endothelial Growth Factor (VEGF) and Basic Fibroblast Growth Factor (bFGF)) - Induce angiogenic switch by altering the balance between angiogenic inducers and inhibitors
Tissue invasion and metastasis	- Do not migrate	- Move to other parts of the body, which is a major cause of cancer deaths - Affect the activity and/or levels of enzymes responsible for cell-cell or cellular-extracellular adhesion

^{a)} **Growth factors** are proteins on the surface of cells permitting them to carry out cell division

^{b)} **Telomeres** are repetitive DNA sequences and special proteins at the ends of double-stranded DNA, which control the replication of the cells. Telomere sequences do not code for any proteins; therefore, during the lifetime of cell some of the sequences are lost. As a result, DNA becomes so short that the cell cannot divide anymore.

^{c)} **Telomerase** is a protein which constantly adds nucleotides to the telomeres, thus making them longer. Consequently, the DNA replication is not limited.

2. Cancer treatments

2.1 Conventional cancer treatments

After a patient has been diagnosed with cancer, doctors decide how the disease should be treated. The course of treatment they suggest depends on multiple factors and is highly personalized. Different people tolerate the same treatment differently. Therefore, it is important to pay attention to the general health of the patient, the location of the tumor and the extent of metastasis formation. Clearly, the main purpose of the initial treatment is to remove as much of the cancer as possible. Subsequently, remaining tumor cells must be killed or their growth should be significantly inhibited. The best way to remove cancer is surgery, which is the easiest and the earliest therapeutic strategy. Obviously, surgery is impossible in case of leukemia and sometimes it is not possible to access the tumor due to its specific location in a body. In other cases, surgery might not be the first course of treatment because of the size of the tumor, which cannot be removed from the body without risk to the patient. Then, the tumor has to be “shrunked” prior to its removal. If it is not clear if a tumor has been removed completely, additional treatments are suggested. In addition, surgery cannot address the question of metastasized cells. To inhibit the growth of remaining or metastasized tumors, chemotherapy and radiotherapy have been used. Cancer therapies aim to prevent the proliferation of cancer cells (**cytostatic** effect) and to kill them (**cytotoxic** effect). Ideally, this should be achieved with a minimum level of side-effects.

2.2 Chemotherapy

Chemotherapy is a term used to describe the implication of active chemical substances in treatment of a disease. Conventional chemotherapies are aimed to target highly proliferating cells and consequently they display a broad specificity. There are three different ways to affect rapid cell division:

- 1) drugs damage DNA in order to prevent its replication, e.g. cisplatin (Platinol), Doxorubicin (Adriamycin)
- 2) drugs interfere with DNA replication itself, e.g. 5-Fluorouracil (Efudex, Aduvicol), methotrexate (Trexall)
- 3) drugs interfere with the mechanisms of cell division, e.g. paclitaxel (Taxol), Vinblastine (Velban), Vincristine (Oncovin)

The main drawback of this approach is the negative effect on rapidly dividing healthy cells (e.g., epithelial cells or cells that line the digestive track), which are harmed during chemotherapy. This leads to well-known side-effects such as **alopecia** (loss of hair), ulcers, nausea and anemia. Traditional therapies are very successful in extending patients' lives. Nevertheless, there is an urge in a development of new therapies with better efficiencies and less severe side-effects.

2.3 Clinical trials

All new cancer treatments, as well as diagnostic and prevention methods must be studied for their safety and effectiveness. Therefore, testing in humans progresses through staged clinical trials (see Table 2). Depending on their purposes and end goals, the phases of clinical trials are assigned as Phase I, Phase II or Phase III. Testing in **Phase I** is performed in a small number of healthy volunteers (20-100) or terminally ill patients and mainly concentrated on the determination of the optimal given doses in order to estimate the safety of the new treatment. At this stage, the first information about pharmacokinetics (e.g. how fast is the drug released from the body?) is obtained. It is worth noting that about 70% of the tested drugs succeed in this phase of clinical trials and enter Phase II. **Phase II** is dedicated to the understanding of the efficacy of the drug in a larger group of people (100-300). Usually, a drug is tested against a specific type of cancer. **Phase III** is the most expensive phase of clinical trials, since it implicates large-scale studies (up to 3000 people) with the main goal of comparison of the drug with the existing treatments. During Phase III the effectiveness of a new drug is confirmed and side-effects are closely monitored. As a consequence, only 30% of the drugs tested successfully complete this phase of clinical trials. It is worth noting that experimental drugs are not used as a sole treatment during the trials; they are often given in a combination with existing treatments. All new drugs are tested against control groups, which either receive no treatment or a placebo substance.

Table 2. Clinical trials*

	Purpose	Number of patients
Phase I	Safety	20-100
Phase II	Efficacy	Up to several hundred
Phase III	Efficacy often tested against conventional treatments	Several hundred to several thousand

* Table was taken from reference ².

2.4 Targeted chemotherapy¹

Classical anticancer drugs affect cells depending on the speed of their division. However, they cannot distinguish between cancer cells and rapidly dividing cells of the epithelium, which leads to severe side-effects, such as nausea, loss of hair, damage of nails and development of ulcers. As a result, a number of patients refuse or stop post-operational therapy.⁴ Therefore, a key feature in developing a new chemotherapeutic agent should be selectivity for cancerous cells over healthy cells. To achieve this selectivity, more intrinsic differences between normal and tumor cells should be exploited, rather than the speed of their division. A revolution in cancer treatment has come with the development of targeted drugs, capable of “understanding” the individual mutations that occur in specific cancers. This strategy takes advantage of the fact that cancerous cells over-express various proteins in tumor cells which are not over-expressed in healthy cells. Thus, the therapeutic effect of targeted drugs correlates with an over-expression or multiplication of specific oncogenes. These drugs are aimed to be activated only in defective cancer cells. The good news is that this treatment does not severely affect normal cells and leads to fewer side-effects. However, blocking one type of specific mutations is not enough to kill all cancer cells taking into account a large number of mutations occurring in cancer cells during carcinogenesis. That is why targeted therapy is usually performed in combination with traditional drugs.

One of the pioneering targeted drugs was **imatinib (Gleevec®)** specifically inhibiting BCR-ABL tyrosine kinase activity (the main cause of abnormal proliferation of leukocytes). The implication of this drug into leukemia treatment led to the remission of tumors of >95% of patients at early stages of disease. One of the most powerful targeted drugs applied for the treatment of breast cancer is **tamoxifen (Nolvadex®)**. This drug blocks estrogen receptors overexpressed in a number of breast cancers. Another strategy is based on targeting of inducers of angiogenesis, both non-specific growth factors (**Erlotinib, Tarceva®**) and VEGF (**bevacizumab, Avastin®**). The knowledge of molecular biology of cancer is essential for coping with the major flaw of most conventional therapies, namely, the lack of selectivity towards tumor cells versus healthy ones. The identification of cancer-specific molecular targets will lead to the successful design and development of effective low-toxicity therapeutics.

2.5 Antimetastatic drugs

Despite the extensive research on the phenomenon of metastasis, it still remains the main cause of cancer patients' deaths. After a sequence of mutations, cancer cells

acquire the ability to detach from the neighboring cells, travel in the surrounding tissues and finally re-attach in a new organ. As a result, the tumor derived from metastatic cells reveals characteristics similar to those of a primary tumor (e.g. doctors may identify cancer cells found in lungs as breast cancer cells). The invaders disturb the normal functioning of the host organ, which consequently leads to additional difficulties in cancer treatment. The journey of a metastatic cell includes multiple hurdles (see Figure 2) and the probability of its “success” is low; therefore, the surviving cells display low sensitivity to conventional chemotherapies. Moreover, metastatic cells might be detected in distant organs years after the original cancer was eradicated, which means that these cells are capable of sustaining chemotherapy in an inactive state (“dormant cells”) with subsequent reactivation.

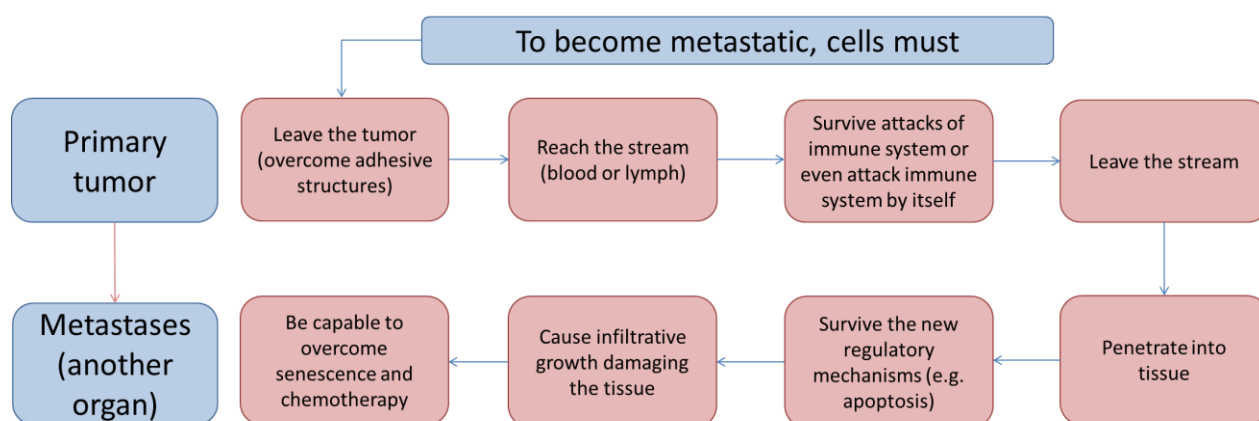


Figure 2. Requirements for metastatic cells

Despite the high incidence of deaths (more than 90%) due to metastasis formation, yet there is no effective antimetastatic drug on the market and most of the existing anticancer drugs rely on the inhibition of the active division of cancer cells. However, chemotherapeutic agents for primary tumors do not effectively affect metastatic cancer cells due to their specific properties (see Figure 2). All drugs and drug candidates with antimetastatic properties can be divided into two categories, namely drugs which hamper the dissemination of cancer and drugs which damage already existing metastases.⁵ In hospitals conventional antimetastatic drugs are represented by a number of **matrix metalloproteinase (MMP)** inhibitors and compounds with antiangiogenic properties. However, no significant benefits in such treatments were achieved, since MMP inhibitors and antivascular agents work properly only on the early stage of metastatic cancer detection. Therefore, there should be a better correlation between the stage of metastasis and antimetastatic treatment.

3. Metal-based anticancer drugs

3.1 General information

The investigation of metal-based compounds with biological activity is nowadays an extremely fashionable area of research. Several decades ago, the terms “bioinorganic” or “bioorganometallic” chemistry did not exist but in the last 40 years the situation has markedly changed and the number of research groups interested in the application of metal complexes in medicine significantly increased. In the field of cancer research, the main trigger for extensive investigations of cytotoxic metal-based compounds was Barnett Rosenberg’s serendipitous discovery of cisplatin. This platinum-based complex quickly went through clinical trials and successfully penetrated to clinical practice worldwide. Its way to the hospitals was followed by two Pt compounds of the second and third generations, namely carboplatin and oxaliplatin (see Figure 3).

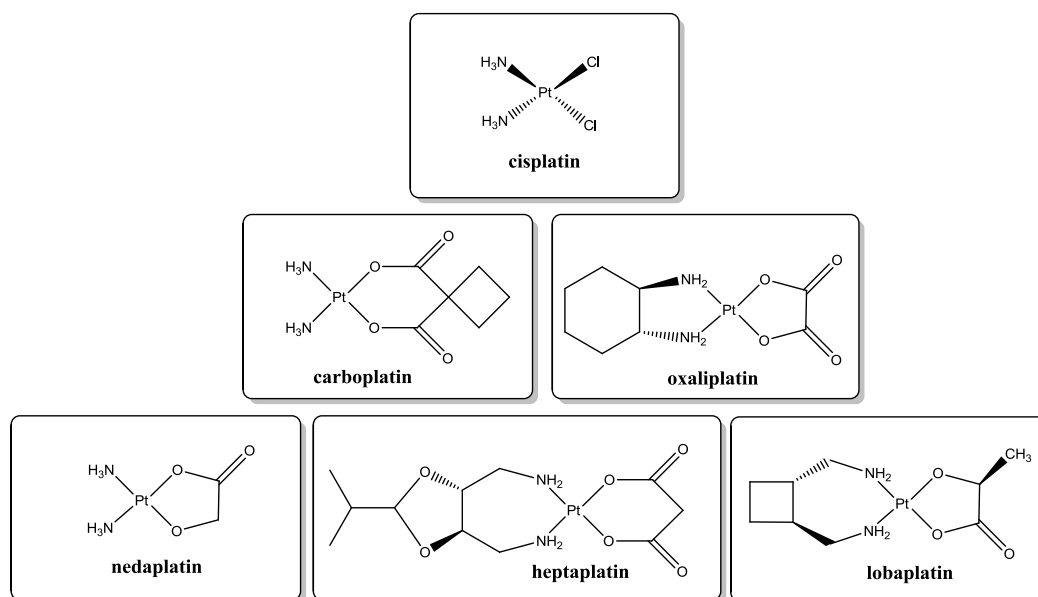


Figure 3. Structures of clinically approved (the third row – not worldwide) platinum drugs.

The advantages of the new chemotherapeutic agents over existing organic drugs were undeniable. Therefore, it was expected that in the nearest future metal-based anticancer drugs would be as widely represented as organic chemotherapeutics. However, besides compounds like nedaplatin, lobaplatin, and heptaplatin (see Figure 3) which are used in clinical practice in several countries and not worldwide like cisplatin, carboplatin and oxaliplatin, no other transition metal-based complexes from a huge library of screened compounds succeeded to be approved for treatment of patients. The most promising candidates, namely, the Ru^{III} coordination compounds NAMI-A and KP1019/KP1339,

Ga^{III} compounds KP46 and gallium maltolate and Gd-texaphyrin complex motexafin gadolinium, reached at best phase II of clinical trials (Figure 4).

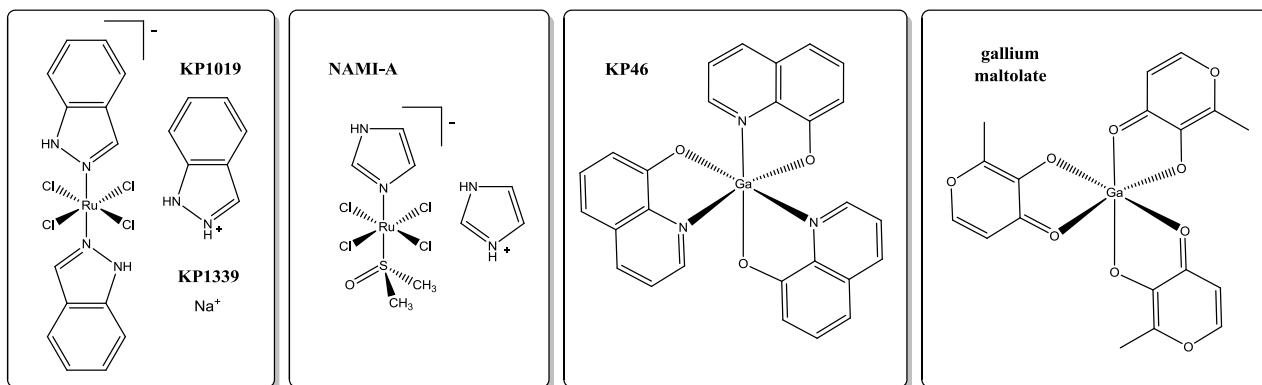


Figure 4. Several non-platinum complexes currently undergoing clinical trials.

What is the reason for the discrepancy between great expectations of bioinorganic chemists and the disappointing outcome? The common strategy for development of novel bioactive complexes is the synthesis of a large library of different compounds (usually structurally similar ligands and corresponding complexes) and their subsequent screening by available *in vitro* methods, e.g. the MTT assay. If complexation results in improvement of biological properties, the most promising compounds are chosen for additional and more complicated biological tests. The image of therapeutic potential of novel complexes is usually based on the *in vitro* results, which do not provide reliable assumptions about the corresponding *in vivo* activity of the compounds. In addition, very often researchers do not have resources and access to *in vivo* tests. Moreover, screening methods of metal compounds are not universal and significantly vary between research laboratories. As a result, their direct comparison is impossible. Consequently, the design of reliable screening tests and the unification of results worldwide, the old-fashioned “serendipitous” way of drug discovery as well as skeptical view of medicinal chemists towards “toxic” metals as medicines should be reconsidered.

3.2 Resistance of metal-based drugs⁶

As it was discussed in “Drug resistance” section (see Chapter 1.4), one possible explanation for insufficient intracellular drug concentration is a *reduced drug uptake*. The uptake of cisplatin is associated with copper influx transporters **Ctr1**. Therefore, knock-out of these genes resulted in a reduced uptake of cisplatin, carboplatin and oxaliplatin.

On the other hand, a sufficient amount of drug ends up in a cell but then quickly removed by *efflux pumps*. These are ATP-driven transmembrane proteins that eject

anticancer drugs before they display any therapeutic effect. Among the most prominent efflux pumps are the members of ABC-transporter family, namely, **P-glycoprotein (Pgp, ABCB1)**, BCRP protein (ABCG2) and multidrug resistance proteins (**MRP1, MRP2, ABCC** family). Whereas P-glycoprotein mainly transports unmodified molecules, MRP is capable of transporting metabolized compounds (e.g. GSH or glucuronide). With the increasing expression of Pgp or MRP protein, the cells improve their capacity to pump drugs out, which leads to a reduced effectiveness of the chemotherapeutic. There is no evidence of transport of platinum complexes by Pgp, MRP1, or BCRP proteins. Nevertheless, it was reported that MRP2 might be involved in efflux of cisplatin. Notably, the Ru compound KP1019 is not affected by MRPs or BCRP proteins; in turn, its chemotherapeutic effect is highly dependent on P-glycoprotein.

Drugs may successfully cross the cellular membrane. However, as soon as they reach the intracellular space, they may be *inactivated by endogenous thiols*, such as **glutathione (GSH)** catalyzed by **GSH S-transferase (GST)** or **metallothioneins (MT)**. The interaction with intracellular thiols is believed to be one of the main reasons for resistance of metal-based drugs, since platinum metals reveal high affinity to sulfur atoms. It was reported that the action of several platinum drugs in cancer cells was not interrupted by MT, but glutathione was involved in drugs detoxification.

The role of glutathione (GSH) in the acquired resistance of ruthenium compounds was extensively studied by various analytical and molecular biology methods; however, the contribution of GSH to resistance is still ambiguous. On the one hand, it was shown that in cell-free conditions high levels of GSH interfered with their DNA binding properties of Ru^{III} compounds; similar observations were reported for Ru^{II} complexes.⁶ On the other hand, it is believed that GSH is able to activate Ru^{III} compounds, such as KP1019 or NAMI-A, by reduction (“activation-by-reduction pathway”) to Ru^{II} species. Notably, when Ru compounds were tested in cisplatin-resistant cell lines with enhanced level of GSH, no cross-resistance with cisplatin was observed for any Ru compound tested. Moreover, the activity of KP1019 and NAMI-A *in vivo* was not affected by GSH. This is an important finding, since it is believed that the interaction with GSH is one of the main reasons for cisplatin resistance. However, Ru compounds are less susceptible to enhanced GSH levels. Additionally, it is known that drug resistance is also caused by overexpression of **thioredoxin reductases (TrxR)** which control the cellular redox metabolism. Therefore, these enzymes might be potential targets redox active metallodrugs (see “Thioredoxine reductase” section, Chapter 4.3.1).

There is evidence that under specific conditions the **MTF-1** signalling pathway may be another reason for acquired drug resistance. The expression of metallothioneins **MT**, as well as zinc (**ZnT-1**) and copper (**Ctr1**) transporters is controlled by a zinc finger protein, the Metal-responsive Transcription Factor (**MTF-1**) and its corresponding DNA-binding site, Metal-Response Element (**MRE**). In order to protect the cell from zinc toxicity, the MTF-1 pathway induces the production of MT and ZnT1; therefore, it might induce similar overexpression to protect cells from metal-based complexes. However, this hypothesis was not closely investigated and requires a justification.

Since the main cellular target of a number of chemotherapeutic agents (especially, Pt complexes) is believed to be DNA, another factor contributing to the resistance of Pt drugs is associated with DNA targeting. Tumor cells which undergo specific mutations are characterized by an *enhanced DNA repair*, established by the **Nucleotide Excision Repair (NER)** system, particularly, the protein **ERCC1**. NER is associated with a resistance to clinically used Pt drugs. The question of Ru drug resistance was not investigated so far, although some Ru complexes may target DNA in a way comparable to Pt drugs.

Another factor, which represents drug resistance, reflects the ability of cancer cells to detect DNA damage and consequently activate apoptosis. In normal cells, the DNA damage is preceded by the activation of the DNA detection system, which is called **mismatch repair pathway (MMR)**. Subsequently, apoptosis is triggered. In tumor cells, the function of MMR is lost, leading to an *increased tolerance to DNA damage*; as a result, DNA targeting chemotherapeutic agents do not induce apoptosis. It was reported that cisplatin and carboplatin adducts were recognized by MMR, whereas, oxaliplatin and satraplatin, as well as ruthenium(II)-arene complexes, were recognized to a much lesser extent, leading to diminished drug resistance.

Going back to the hallmarks of cancer, the evasion of programmed cell death is one of the main characteristics of tumor cells. Notably, the *dysfunction of apoptosis* is a serious barrier for effective chemotherapy treatment. Normally, the question if a cell should “live or die” is solved by pro- and anti-apoptotic members of the **bcl-2** gene family. In cancer cells, the evasion of apoptosis is established by over-expression of anti-apoptotic proteins, such as **bcl-2** and **bcl-x_L**, or decreased expression of pro-apoptotic proteins **bax** and **p21**, mediated by the **tumor suppressor protein p53**. High levels of **bcl-2** and

bcl-x_L hamper the efficacy of chemotherapeutic agents. It was demonstrated that all clinically-used Pt drugs are sensitive to bcl-2; however, the efficacy of novel Pt drugs, such as picoplatin, was bcl-2 independent. The dysfunction of **p53** causes the cellular protection against a number of drugs, e.g. clinically used Pt complexes. It is known that cells are chemoresistant to cisplatin, when bax translocation in mitochondria is blocked as well as the release of mitochondrial proteins into cytosol.⁷ The mutations of p53 did not affect the activity of KP1019; nevertheless, the efficacy of several arene ruthenium complexes was dependent on the p53 status.

It was clearly shown that not all metal-based drugs have identical intracellular targets and their modes of action depend on diverse signaling and survival pathways. The differences were observed not only between Pt and Ru compounds, but also between compounds with identical metal center (cisplatin and picoplatin, KP1019 and arene Ru complexes). The main advantage of existence of numerous drug-resistance pathways is a low probability that cells would develop cross-resistance to all drugs. Therefore, to reach the optimal therapeutic effect, drugs are applied in a combination regimen.

3.3 Categorization of metal-based drugs

There is an urge for a rational design of metal-based drugs. Therefore, it is important to predict potential benefit of metal complexes over structurally similar organic ligands *prior* to their synthesis. Clearly, in a metal complex the metal center serves multiple functions. The introduction of a metal fragment significantly alters physical and chemical characteristics of organic ligands, such as solubility, reactivity, lipophilicity, biodistribution, *etc.* Moreover, these parameters might be affected by other ligands coordinated to the same metal center and based on the chemical structure of the complexes.

Metal-based drugs may be classified by looking at the chemical structure of the metal complex.⁸ If the ligand *per se* is a biologically active compound (e.g. hydroxytamoxifen, staurosporine or a DNA intercalator) (see Figure 5), the ligand may be released from the complex. This depends on the nature of the chemical bonds between the ligand and the metal fragment, e.g. a strong covalent bond between the ligand and arene moiety of the half-sandwich complex or a labile dative bond between the ligand and the metal.

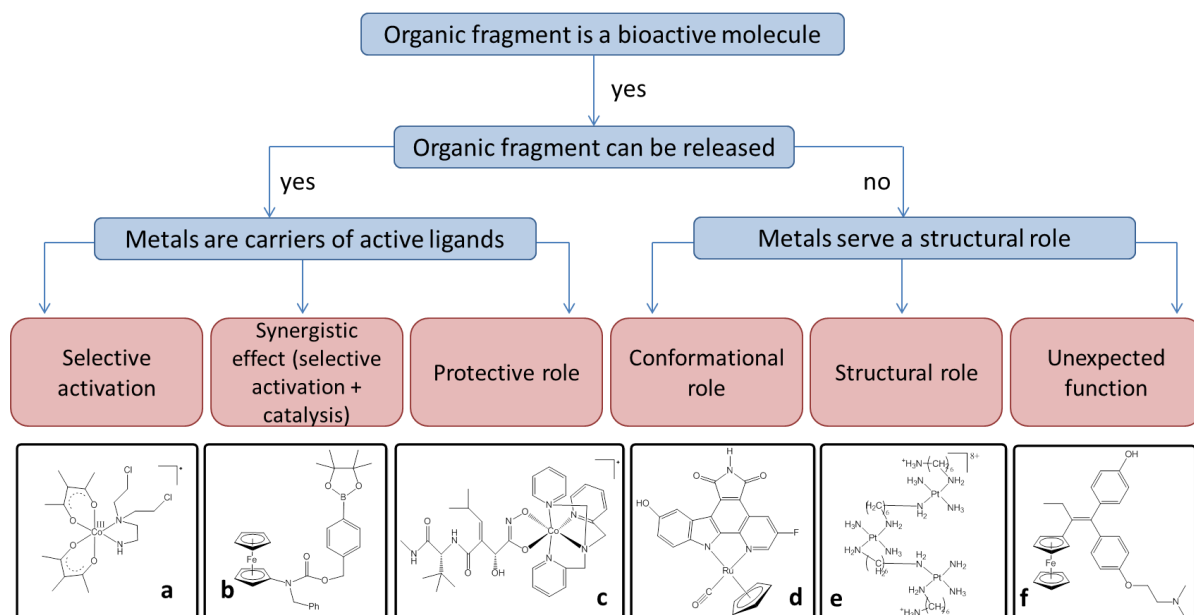


Figure 5. Categorization of the metal-based drugs based on the role of the metal (references: a,^{9,10} b,¹¹⁻¹³ c,¹⁴ d,¹⁵ e,¹⁶ f¹⁷).

If an organic ligand is bioactive and might be released once inside the cell, metals serve as their **carriers**. The metal complex to serve a **protective function** may be stable and inert outside the cell to avoid quick release of the ligand upon administration and unstable once inside the cell, otherwise the coordination of the ligand to the metal would not be beneficial. One of the examples of metal complexes with protective function is the Co^{III} complex of matrimastate (see Figure 5, box c), where coordination of the organic active moiety to the metal center results in the decrease of unwanted reactivity *in vivo*. A metal fragment might also play a **conformational role** by stabilizing a particular conformation or a tautomer of the ligand. The metal might enable **triggered activation** of a drug at the diseased site, e.g. substitutionally inert Co^{III} complex reduces cytotoxic nitrogen mustards only in hypoxic conditions of cancer cells (see Figure 5, box a).^{9,10} If a metal fragment itself possesses biological activity, its combination with an active organic ligand would result ideally in a **synergistic effect** of the components (e.g. platinum complexes conjugated to DNA intercalators).^{18,19} Mokhir *et al.* developed an elegant series of aminoferrocenyl-based prodrugs, which generate selective anticancer agents upon elevation of reactive oxygen species (ROS).¹¹⁻¹³ Cancer cells generally produce a markedly higher amount of ROS than normal cells and aminoferrocenyl complexes can be selectively activated only in tumor tissue. Such activation results in the formation of quinone methides and iron/ferrocenium ions. These species exhibit a synergistic effect, since iron species act as catalysts and quinone methides are capable of inhibiting antioxidative cell systems by alkylation of glutathione (see “Glutathione” section, Chapter

4.3.5). Interestingly, iron and ferrocenium ions catalyze the generation of ROS species; therefore, the reaction proceeds autocatalytically.

If the active ligand cannot be released from the metal fragment, it means that the metal coordination sphere is stable and inert. Since no activation is required, the metal complex remains unchanged *in vivo*. In such cases, metal fragments play a **structural role**. It is worth noting that metal complexes with non-active ligands rarely serve structural roles. However, such complexes exist and Triplatin NC would be an example (Figure 5, box e).¹⁶ In this complex three platinum(II) centers are linked by amine ligands and the coordination sphere of the Pt centers features no leaving groups. Consequently, unlike cisplatin the Pt centers are not capable to bind DNA in a coordinative manner. The cytotoxic activity of this compound is attributed to the distortions in DNA resulting from multiple hydrogen bonds of the am(m)ine ligands to the phosphate backbone of DNA. Inert metal complexes might also serve a **conformational** role by stabilizing the ligand in a structure complementary to the active site of a bio-target. Thus, the metal itself is not involved in any *direct* interaction with the biological target (e.g. the complexes of Meggers *et al.*, Figure 5, box d).¹⁵ However, it has been demonstrated that the introduction of the metal fragment, which is expected to act only as a modifier of the structure of the ligand, may serve some **unexpected functions**. The best example is ferrocifen, where the introduction of a ferrocene moiety into the hydroxytamoxifen backbone resulted in an unexpected mechanism of action (Figure 5, box f).¹⁷ More precisely, the combination of ferrocene and a para-hydroxy substituted phenyl ring allowed production of reactive oxygen species resulting from a cascade of redox processes including semiquinonoids. Ferrocifen was able to modulate positive and negative estrogen receptor (ER+/ER-) breast tumors, whereas commonly used in hospitals tamoxifen affects only ER+ tumors.

If an organic ligand is not an active biomolecule, the metal is expected to interact directly with a biological target, serving a **functional role** (see Figure 6). However, the activity of the metal complex might also derive from some specific properties of compounds. Metal complexes may behave as **catalysts**, e.g. by activating the oxidation of glutathione with a subsequently increased production of reactive oxygen species (ROS)²⁰ or by participating in transfer hydrogenation from NAD⁺ to NADH which causes depleted NAD⁺ pools and subsequent apoptosis (Figure 6, box d).²¹ Some metal complexes, such as Ru^{II} or Os^{II} complexes with polypyridine²² or polyaaromatic ligands,²³ as well as Pt^{II}-

porphyrine derivatives,^{24,25} might be used in photodynamic therapy due to their **photosensitizing properties** (Figure 6, box e).

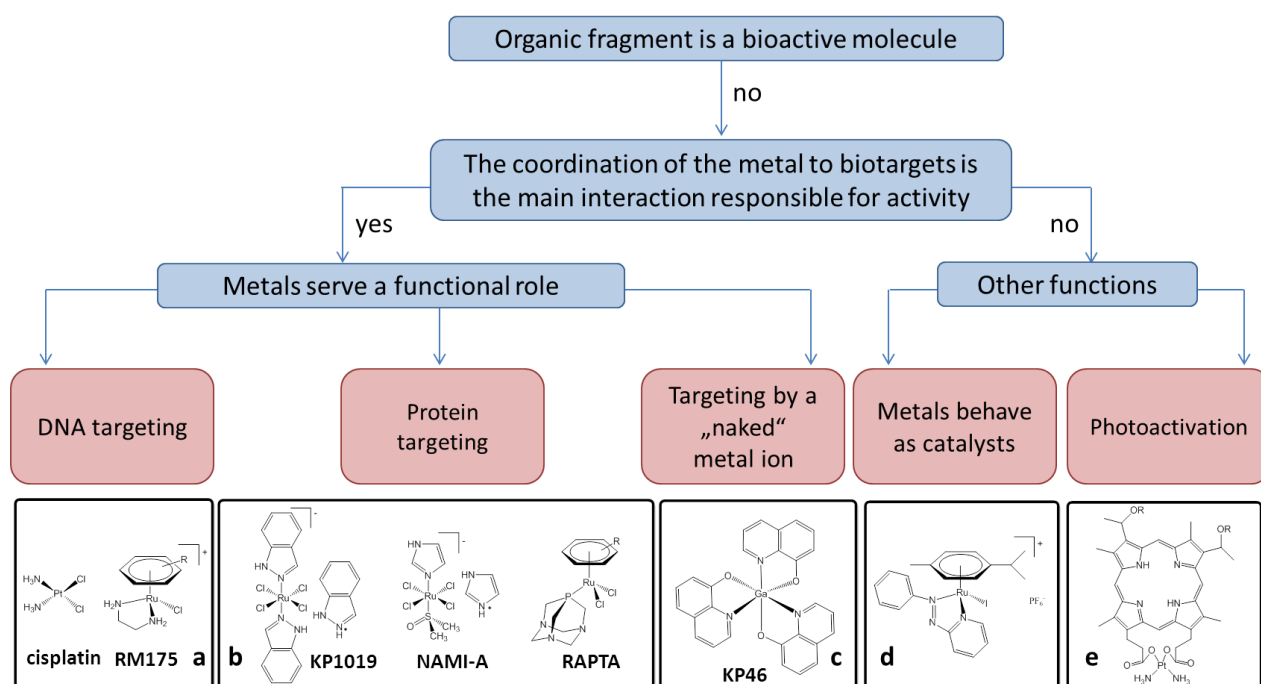


Figure 6. Categorization of the metal-based drugs based on the role of the metal (references: a cisplatin,²⁶ RM175,²⁷ b KP1019,^{28,29} NAMI-A,³⁰ RAPTA,^{31,32} c,³³⁻³⁵ d,²⁰ e^{24,25}).

The majority of metal-based compounds belong to the group of **functional** complexes. Therefore, this class of compounds is more precisely discussed. All functional compounds contain non-leaving ligands and at least one leaving group, where the latter provides a free site for coordination of biomolecules. It is known that the structure of these drugs is altered after administration and they usually serve as prodrugs. The most advanced metal-based compounds, *i.e.* platinum drugs in hospitals and ruthenium compounds in clinical trials belong to the group of functional complexes.

Functional complexes can be further classified dependent on the biomolecules which they bind to. In order to facilitate this classification and improve the understanding of the mode of action of metal complexes, Barry and Sadler defined biological targets for a number of metal-based complexes and explicitly described their targeting behavior.³⁶ It is known that the mode of action of traditional platinum drugs is based on **DNA** damage but the targets of ruthenium complexes are still not clear. It is believed that KP1019, NAMI-A and complexes of RAPTA family preferentially target **proteins**, whereas the main target of the family of “Sadler complexes” (such as RM175) is DNA (Figure 6,

boxes a, b). Upon administration all above mentioned compounds are activated by chloride/water ligand exchange and, in case of ruthenium(III) compounds, reduction to more active ruthenium(II) species in the tumor cell. However, it was shown that for the family of RAPTA complexes hydrolysis is not an important prerequisite for their modes of action (see Chapter 4.1.2).

Another type of functional metal complexes is represented by gallium(III) compounds, namely KP46 and gallium maltolate (Figure 6, box c). In contrast to metal carriers of bioactive ligands serving a protective role for the organic ligands, the ligands serve a protective function for the metal preventing rapid hydrolysis and unwanted reactivity of the complex as well as providing hydrophobicity to make the compounds suitable for oral administration. It was reported that upon aquation gallium(III) complexes release Ga^{III} ions which consequently may replace essential metals in the binding sites of enzymes, e.g. iron in ribonucleotide reductase. This results in a disruption of important cell metabolism pathways and leads to apoptosis. Such mode of action is called “multistage-rocket model”, since only the “**naked**” ion reaches the biotargets.³⁷

In conclusion, design of a new drug is closely associated with the understanding of its mode of action and pre-determination of its biological target (DNA, protein, enzyme, etc.). Nevertheless, the real targets of the majority of metal complexes remain elusive. The development of a universal strategy for determination of the targets of metal-based compounds may significantly improve the understanding of their behavior in the body and accelerate the long way of metal complexes from bench to clinic.

4. Development of RAPTA complexes

*Before I moved to the field of medicinal chemistry, I was working with organometallic compounds for a very long time. I had a prejudice that all organometallic complexes are difficult to work with and require a lot of patience and attention (like kids). They need inert atmosphere, they do not like water and oxygen, and they quickly decompose unless treated properly. That is why I have always been fascinated by RAPTA compounds. This is a class of organometallic ruthenium(II) complexes which possess anticancer activity in vivo, especially in lung metastases, at the same time being only marginally active in vitro. Why is it so? How can these fragile organometallic complexes reach their bio-targets without being destroyed along the way? And **what are these mysterious targets?** When I started my PhD, I realized that this was a mystery not only for me, but for the whole scientific world. Despite extensive research of RAPTA complexes, their biomolecular targets still remained elusive. Therefore, I fell in love with my project from the first sight. Who knows, maybe we would be able to identify these secret targets and shed light on how RAPTA complexes really work...*

4.1 Primitive era. Who are you, RAPTA?

4.1.1 General information

The class of RAPTA compounds was developed by the group of Paul Dyson at the École Polytechnique Fédérale de Lausanne (EPFL) in Switzerland. The abbreviation RAPTA stands for Ruthenium Arene PTA complexes, where PTA is the monodentate phosphorous-containing ligand 1,3,5-triaza-7-phosphatricyclo-[3.3.1.1]decane. The RAPTA scaffold reveals the typical piano-stool structure for half-sandwich Ru^{II} complexes, where a η^6 -arene ligand bound to the metal center represents the stool and the three remaining ligands represent the legs of the stool (see Figure 7). One of the legs is PTA or a PTA analogue and two other legs are labile ligands, such as chlorides. If an arene fragment of the complex is cymene or toluene, abbreviations of the complexes are RAPTA-C or RAPTA-T, correspondingly.

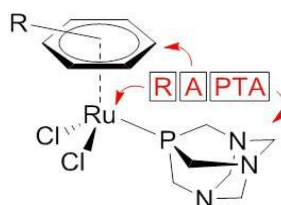


Figure 7. Schematic representation of the RAPTA framework components

The electronic configuration of ruthenium is $[\text{Kr}]4d^75s^1$ and the main contribution in the complex formation was demonstrated to be made by the 4d orbitals rather than the 5s orbital, which confirms that 4d orbitals locate at lower energy than 5s orbitals. The arene moiety (π -ligand) predominantly contributes to the LUMO, while the HOMO is dominated by the d orbitals of the ruthenium center and the PTA ligand. Notably, if chloride ligands are replaced with carboxylate ligands (carbo-RAPTA and oxali-RAPTA, see below), the HOMO is dominated by orbitals of the ruthenium ion and the bidentate ligands, rather than of PTA. RAPTA complexes are characterized by metal-to-ligand charge transfer (MLCT) mainly from the ruthenium lone pair to carbon atoms of π -ligand arene. In turn, the arene ligand takes part in the back-bonding of electrons to the bonding orbitals of a metal-ligand bond, especially that of Ru-P (or Ru-O), which is a common feature of metal complexes with a π -ligand. Metal-ligand bonds are characterized as non-covalent bonds which were suggested to be dative-covalent except for the Ru-Cl suggested to be an ionic bond. The bond order of the dative ligands is the following: Ru-P > Ru-O > Ru-C.³⁸

The interest in this family of compounds was awoken by the versatile solubility properties of PTA, which is soluble not only in a range of organic solvents (chloroform, dichloromethane, acetone, methanol), but also in water and aqueous buffers. High hydrosolubility of the PTA ligand derives from its ability to form hydrogen bonds *via* three N-donor atoms of the lower rim of the adamantane skeleton which serve as hydrogen bonding acceptors, as well as hydrogen bonding donors (when protonated).³⁹ Upon the protonation of the ligand, the solubility of PTA in organic solvents decreases. Therefore, the corresponding half-sandwich Ru^{II} complex with the PTA ligand was developed in order to exhibit similar pH-dependent solubility. It was expected that the novel RAPTA complex would easily cross cellular membranes at physiological pH. In diseased tissues, this complex would be protonated and subsequently trapped in the cell, leading to enhanced selectivity and therapeutic effect. Moreover, it was anticipated that the protonation of a neutral ruthenium complex in cancer cells would enhance its interaction with negatively charged DNA.

The first communication about the cymene complex RAPTA-C was published in 2001, which described the synthesis of the complex and briefly its effect on the DNA binding in correlation with the pH of the medium.⁴⁰ Indeed, in accordance with the hypothesis, the pH range at which the investigated complex retarded DNA migration was found to match the pK_a of the PTA ligand (from 5.63 to 6.07). Later on, it was shown that depending on the labile ligand coordinated to the ruthenium center, RAPTA complexes with various leaving groups exhibit quite different antimicrobial properties, being generally non-toxic, air-stable and thermodynamically stable, revealing that the RAPTA family is a promising class for development of biologically active compounds.⁴¹ Herein, the focus is on the anticancer activity of RAPTA compounds.

4.1.2 Hydrolysis

In order to understand the mechanism of action of RAPTA complexes and the role of their structural components, it is essential to delineate what happens with these compounds in body fluids and in the cell itself. It is generally believed that the key activation step of drugs in the cells is hydrolysis. Whereas this process was thoroughly investigated for cisplatin⁴², KP1019⁴³ and [Ru(arene)(en)Cl]⁺,⁴⁴ hydrolysis of RAPTA complexes for a long time was not fully understood. The behavior of RAPTA compounds in aqueous solution was studied by means of UV-vis^{45,46} and ³¹P NMR spectroscopy,⁴⁶

ion-exchange chromatography,⁴⁵ capillary electrophoresis⁴³ and theoretical calculations.⁴⁷

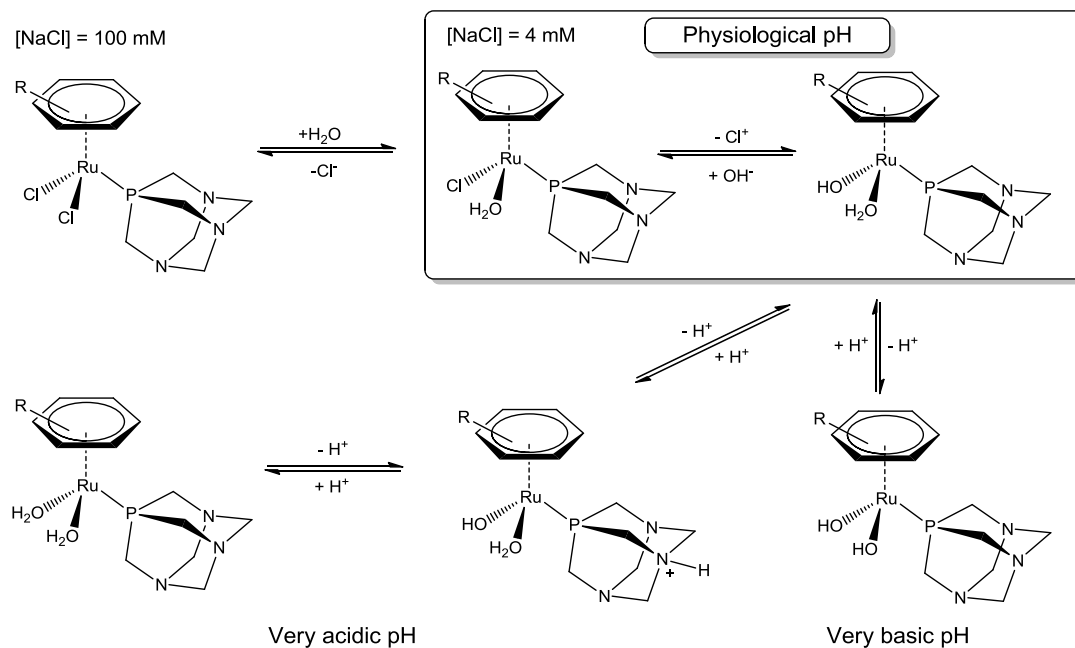


Figure 8. Hydrolysis of RAPTA complexes

In aqueous solutions RAPTA complexes undergo rapid hydrolysis and emerge into aqua species with a retained PTA ligand. Subsequently, these intermediates quickly react with nucleophilic components of various biomolecules. In 4 mM NaCl solutions, corresponding to the intracellular concentration of Cl^- in blood plasma, the same rapid process takes place; however, in 100 mM NaCl solution, corresponding to the extracellular medium, hydrolysis is suppressed. The work of Scolaro *et al.* suggested that hydrolysis of RAPTA compounds occurs *via* the simultaneous loss of both chloride ligands. This is in contrast to the behavior of cisplatin, which rapidly substitutes one chloride with water once inside the cell, with the second hydrolysis step being considerably slower.⁴⁵ Ion exchange chromatography with a basic eluent was used to determine the concentration of chloride ions. Therefore, the experimental setting was far from physiological conditions and did not mimic the processes occurring in cells. It was theoretically predicted that under very basic conditions the complex with hydroxide ligands rather than aqua ligands formed, whereas the formation of dihydroxo species at physiologically relevant pH is unlikely.⁴⁷ The dominant species in intracellular medium were shown to be the monohydrolyzed (*ca.* 70%) and the hydroxo-aqua complex (*ca.* 12%) (see Figure 8).⁴⁶ Under physiological conditions complete hydrolysis of the second chloride could be achieved only by adding $AgNO_3$. Hydrolysis studies by capillary zone electrophoresis (CZE) revealed that under physiological conditions the equilibrium

between the RAPTA complex and its hydrolysis products was established rather quickly.⁴³ Interestingly, one of the most intense peaks was assigned to doubly positively-charged species, possibly the bis-aqua complex. It should be noted that complexes containing arenes with highly electron-withdrawing substituents reveal a profoundly different hydrolytic behavior, since these complexes undergo arene loss upon aquation.⁴⁸

4.1.3 Structure-activity relationships

In order to reveal the importance of every structural unit of the RAPTA scaffold, *i.e.* the ruthenium core and arene, PTA and chlorido ligands, and their effect on the biological activity, a series of structurally similar compounds was synthesized and extensive structure-activity relationships were obtained. Some examples are illustrated in Figure 9.

Arene (π -ligands). It was demonstrated that the variation of the arene moiety induces significant alterations of the biological properties of RAPTA complexes. Arene ligands exhibit pronounced effects on the solubility, reactivity, biodistribution and lipophilicity of RAPTA compounds. Lipophilic arenes significantly facilitate transmembrane transport, which results in a higher accumulation of the drug and a more pronounced therapeutic effect. Moreover, arene ligands affect properties of the PTA ligand. By varying the arene moiety, the pKa of the PTA ligand can be adjusted. In addition, the arene ligand induces different orientations of PTA. Consequently, this affects the reactivity of RAPTA complexes with biomolecules, such as DNA, since several orientations of PTA prevent formation of a DNA twist (see “DNA era” section, Chapter 4.2).⁴⁹

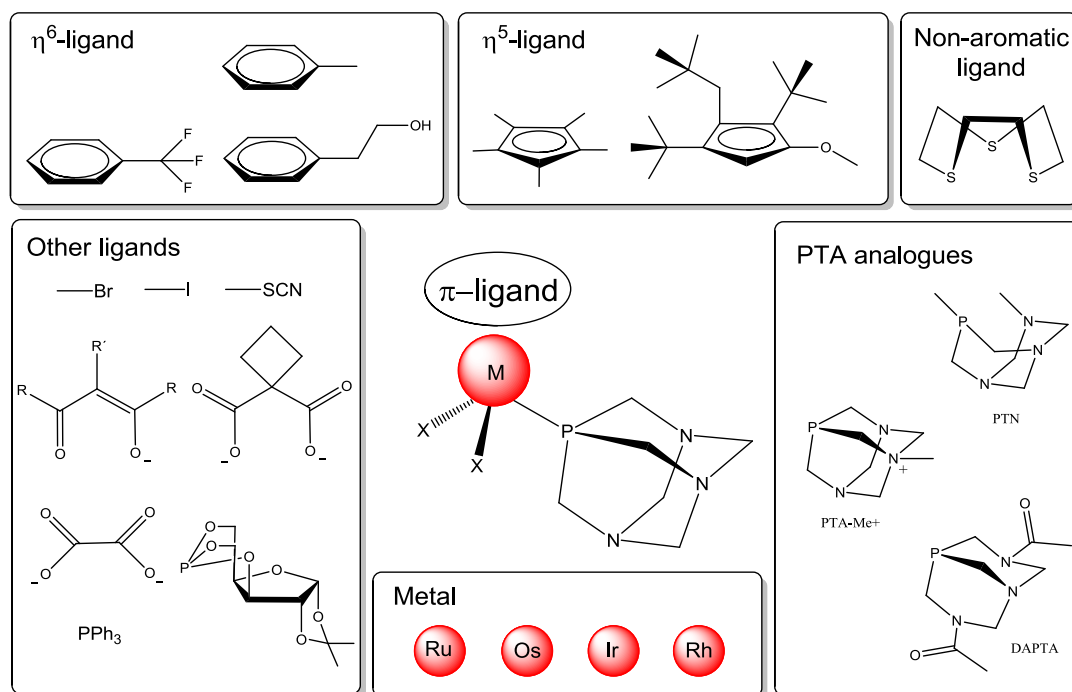


Figure 9. Selected structural units modified in the RAPTA scaffold.

Some of the most interesting findings were the unusual cytotoxicity and hydrolytic behavior of RAPTA derivatives with weakly coordinating arenes containing highly withdrawing substituents, such as $-\text{CF}_3$ or $-\text{F}$.⁵⁰ The increase in the number of electron-withdrawing substituents resulted in a profound decrease of the pK_a of the complexes, which signifies the higher stability of the complexes at low pH. Notably, RAPTA- CF_3 is one of the most cytotoxic compounds of the RAPTA series known by now ($\text{IC}_{50} \approx 38 \mu\text{M}$ in A 2780 cells), which can be possibly explained by its different hydrolytic behavior. RAPTA- CF_3 demonstrated pH-dependent hydrolysis. More precisely, the rate of hydrolysis markedly increased upon addition of an acid. According to theoretical calculations, at the cellular pH this RAPTA complex exists in its mono-hydroxy form (see Figure 8); however, in tumor tissue more reactive aqua species form. The major difference of RAPTA- CF_3 to other members of the RAPTA family is a weakly coordinated arene. Therefore, RAPTA- CF_3 loses its arene upon hydrolysis. Consequently, the incubation with various biomolecules revealed a number of adducts different from those formed by “classic” RAPTA complexes (see “Ub and Cyt C” section, Chapter 4.3.3).⁴⁸ This may be another feature responsible for the unusual cytotoxicity of this complex.

Arene ligands can also be replaced by cyclopentadienyl derivatives.^{51,52} Whereas the Cp complex with two PTA ligands did not show any proliferative activity, the cytotoxicity of the analogous Cp* complex was moderate. However, similar complexes with water-soluble lipophilic Cp derivatives exhibited excellent cytotoxicity in the micromolar range.⁵¹

Surprisingly, an aromatic fragment is not an essential attribute for anticancer activity of RAPTA complexes. Alessio *et al.* developed an elegant series of ruthenium complexes where the arene moiety was replaced by the sulfur macrocycle 1,4,7-trithiacyclononane ([9]aneS₃).⁸ In RAPTA-C and $\text{CpRu}(\text{PTA})_2\text{Cl}$, π -coordinated ligands were substituted by the macrocycle, whereas the rest of the coordination sphere remained unchanged. Contrary to the complexes with aromatic ligands, the $[[9]\text{aneS}_3]\text{Ru}(\text{PTA})_2\text{Cl}]^+$ complex was significantly more cytotoxic and selective than its mono PTA analogue and the parent compound RAPTA-C. This is an interesting result, since this complex is remarkably inert both in water and at physiological pH, revealing that hydrolysis is not essential for biological activity of PTA compounds.

Overall, a pronounced effect on the biological activity can be achieved by varying the π -ligand and therefore, variations of the arene might represent a step to rational compound design.

Metal. Since the electronic configurations of ruthenium and osmium are similar due to their position in the periodic table, it is not surprising that osmium analogues of RAPTA complexes (OsPTA) were prepared and their biological activity was evaluated.⁵³⁻⁵⁶ Osmium complexes were significantly less cytotoxic than ruthenium complexes and displayed lower reactivity toward DNA and other biomolecules, perhaps due to slower ligand exchange kinetics. It is worth noting that adducts between OsPTA and biomolecules assigned by ESI-MS did not contain the PTA moiety, which is not common for their ruthenium congeners.

η^6 -Arene PTA complexes based on other metals, such as Ir and Rh, would be charged. In order to keep complexes neutral, the arene ligand was substituted by η^5 -cyclopentadienyl ligand and its derivatives which resulted in a series of different Ir and Rh complexes with one or two PTA ligands.^{53,57,58} While neutral mono-PTA complexes revealed the same order of cytotoxicity as the parent RAPTA, bis-PTA complexes were significantly less cytotoxic. This is an expected result, since highly charged compounds might not be able to penetrate the cell membrane. Contrary to RAPTA and OsPTA complexes, hydrolysis of $\text{Cp}^*\text{Rh}(\text{PTA})\text{Cl}_2$ was not suppressed in saturated NaCl solution. Due to their similar order of cytotoxicity it may be suggested that all complexes in the cell are almost completely hydrolyzed. This, in turn, does not mean that complexes are equally reactive toward their biomolecular targets in cells. By means of ESI-MS it was demonstrated that all complexes form adducts with oligonucleotides.⁵⁸ Nevertheless, Ir and Rh analogues were essentially inactive in the inhibition of thioredoxin reductase and cathepsin B (see Chapters 4.3.1 and 4.3.2).⁵⁷ These results are in agreement with DFT calculations which demonstrated that Ir and Rh complexes form the weakest M-S bonds (ΔE for the M-S dissociation = 56.8 and 61.5 kJ/mol and ΔG = -15.5 and -13.2 kJ/mol for Ir and Rh, correspondingly. For RAPTA-C, ΔE for the M-S dissociation = 80.5 kJ/mol, ΔG = 16.4 kJ/mol).

PTA. For a long time the protonated form of the PTA ligand was considered to be responsible for the unique properties of RAPTA compounds. Therefore, their methylated (PTA-Me^+) and diacetyl derivatives (DAPTA) were prepared for comparison purposes. It was shown that PTA-Me^+ complexes were indiscriminate and damaged both cancer and healthy cells. Ruthenium complexes with DAPTA were less cytotoxic but still slightly

more toxic than RAPTA analogues with similar structures. In addition, the rate of nucleotide binding was found to be significantly lower.⁵⁹

In subsequent studies, the effect of P,N coordination was evaluated on the cytotoxicity, by replacing PTA with its chelating PTN analogue.⁵⁵ All PTN complexes were considerably more cytotoxic than RAPTA-C. The rate of their reactivity with biomolecules was markedly reduced, probably as a consequence of the decreased rate of hydrolysis.

The effect of a number of PTA ligands on the antiproliferative effect of the complexes and their reactivity towards biomolecules was also investigated.^{51,60} It was found that ruthenium(II) cyclopentadienyl complexes with two PTA fragments did not show any cytotoxicity or reactivity towards oligonucleotides,⁵⁸ probably due to the bulkiness of two PTA ligands in close proximity to each other. ESI-MS showed that in most cases RAPTA complexes do not tend to release PTA upon binding to biomolecules (see Chapter 4.3). Therefore, two PTA ligands might sterically hinder the access to the ruthenium center. To conclude, the PTA ligand appears to be an essential moiety of RAPTA complexes in terms of their therapeutic effect and *selectivity*.

Other ligands. In order to develop hydrolysis-resistant compounds, the chlorido ligands were replaced by an oxalate or a cyclobutyldicarboxylato ligand, resulting in the formation of half-sandwich ruthenium(II) analogues of oxaliplatin and carboplatin (carbo-RAPTA and oxali-RAPTA, respectively).⁶¹ The presence of chelating ligands demonstrated a significant influence on the pK_a of the coordinated PTA ligand with values being significantly lower than for RAPTA-C. The replacement of chlorido by oxalato ligands resulted in increased stability of the complexes at low pH before their protonation. Despite significant suppression of hydrolysis, the formation of equivalent adducts with DNA was still observed, revealing that the aquation step is not an essential prerequisite of RAPTA compounds' activity. These complexes showed a similar order of the antiproliferative activity as RAPTA-C. However, carbo-RAPTA and oxali-RAPTA were demonstrated to be more effective inhibitors of cathepsin B.⁵⁶ It was determined by computational methods that higher solubility and stability of carbo-RAPTA and oxali-RAPTA compared to RAPTA-C might be associated with their high hydrogen bonding stability and stronger non-covalent ligand bonds.³⁸ A possible explanation for complete hydrolysis resistance of oxali-RAPTA was offered from data obtained by theoretical calculations. While Ru-O bonds in oxali-RAPTA are almost the same, significant differences between the two Ru-O bonds exist in carbo-RAPTA leading to imbalance facilitating hydrolysis. This in turn might explain the lower antiproliferative activity of

oxali-RAPTA in comparison with traditional RAPTA complexes with labile chloride ligands.

Inspired by hydrolysis-resistant RAPTA complexes with carboxylate ligands, Vock *et al.* developed a series of RAPTA derivatives with different acac ligands (R-CO-C(-R')-CO-R, where R = Me, *t*Bu, Ph and R' = H or Cl).⁶² The novel derivatives displayed high cytotoxicities and almost complete resistance to hydrolysis, again indicating that hydrolysis is not an important prerequisite for the mode of action of RAPTA complexes. However, the acac ligand with an electron-withdrawing chloro substituent induced rapid hydrolysis of the corresponding RAPTA complex with the loss of the arene ligand. The activity of the complexes relies on the cytotoxicity of acac ligands. It is however not clear whether the acac ligands are released in the cells or remain coordinated to the metal center.

The replacement of a chlorido ligand by a phosphine resulted in increased hydrophobicity of the complexes and enhanced interactions with DNA possibly due to a better hydrogen bonding network.⁶³ However, in contrast to the traditional RAPTA complexes, no detectable adducts were observed upon incubation of PPh₃ complexes with ubiquitin and cytochrome C (see "Ubiquitin and Cytochrome C" section, Chapter 4.3.3). It is likely that when DNA is markedly favored over proteins as a target of a metal complex, this metal complex reveals higher toxicity and lower selectivity for cancer cells. When replacing the triphenylphosphine ligand by bidentate PPh₂(*o*-C₆H₄OH) ligand,⁶⁴ the corresponding RAPTA complex was almost 3-fold more active than parent RAPTA-C, despite its inertness under biological and acidic conditions. However, the cytotoxicity of this complex was not determined for non-tumorigenic cells. Therefore, it is not possible to directly compare this complex with the toxic triphenylphosphine analogue.

An interesting alternative to PTA as a ligand is the class of 3,5,6-bicyclophosphite- α -D-glucofuranosides. Since cancer cells require substantial energy to sustain their rapid proliferation, they up-regulate glycolysis in order to increase the uptake of glucose. Therefore, it was expected that water-soluble Ru^{II} complexes with carbohydrate-based phosphites would be preferentially accumulated in tumors.⁶⁵ It was demonstrated that aquation of the Ru center induced hydrolysis of the phosphite ligand. The complexes were only moderately cytotoxic *in vitro*. Nevertheless, they were selectively cytotoxic towards tumorigenic cells and markedly more cytotoxic than RAPTA-C. RAPTA complexes were also derivatized with fluorescent anthracene moiety in order to be used as model compounds for intracellular visualization.⁶⁶

4.1.4 Anticancer properties

In general, RAPTA complexes are moderately or non-cytotoxic in classic *in vitro* screens for antiproliferative activity with IC₅₀ values of 40-500 µM in cancer cell lines and >1000 µM towards healthy cells. However, these compounds exhibit very interesting behavior *in vivo* in a MCa mammary carcinoma model. This is a murine transplantable tumor, which spontaneously metastasizes to lungs. Therefore, the model can be used for investigations of the RAPTA complexes' effect on primary tumor growth and metastatic progression. It was demonstrated that the primary tumor growth was only slightly inhibited by RAPTA derivatives and reduction in tumor growth was not maintained after administration of the complexes was terminated. Despite unsatisfying results in primary tumors, RAPTA complexes demonstrated a pronounced activity against metastases. 75% percent of the treated mice showed a decrease in the number of large dimension metastases. One of the most distinct advantages of RAPTA compounds over the other ruthenium-based metastasis inhibitor NAMI-A is high clearance rate of RAPTA complexes from the organs (with the highest rate values for lungs and the lowest for spleen).⁴⁵

Despite significant advances in tumor detection methods and cancer therapeutics, unpredictable formation of metastases remains the key problem in cancer treatment. Whereas there is a plethora of drugs and new potentially active compounds with pronounced activity in primary tumors, metastases progression can be hardly inhibited. Therefore, the unique biological properties of RAPTA compounds inspired researchers to learn more about their mechanism of action. To shed light on the ability of RAPTA-T, the toluene derivative, to interact with metastases, Bergamo *et al.* performed an *in vitro* study, where they emulated detachment, migration, invasion and re-adhesion of cells in three different breast cancer cell lines and followed the interference of the complex with every step of the metastatic process.⁶⁷ RAPTA complexes were shown to interfere more selectively with tumor cells with the highest inclination to invade and metastasize such as the highly invasive MDA-MB-231 in comparison to non-invasive MCF-7 cells.

RAPTA-T showed the greatest effect in cell detachment and re-adhesion assays which mimic de-adhesion of cells from a primary tumor and their subsequent attachment to a new organ. The plasticity of cells, which is a prerequisite for successful metastatic processes in the body, was lost as a result of cell body stiffening upon incubation with RAPTA-T. This suggested that the mechanism of RAPTA complexes activity involves the modulation of the cell cytoskeleton.

Whereas RAPTA-T significantly inhibited the detachment of cells from fibronectin or collagen IV, no inhibition was observed from poly-L-lysine where cells adhere only by electrostatic interactions. Such selectivity can possibly indicate the inhibition of proteases. Consequently, down-regulation of matrix metalloproteinases (MMP) was also observed. **Matrix metalloproteinases (MMP)** are a group of extracellular enzymes with a matrix-degrading function. MMP inhibitors inhibit cell migration and consequently reveal antiangiogenic effects. Therefore, down-regulation of MMP by RAPTA-T is in correlation with its antiangiogenic properties.

In independent studies, the molecular mechanism of RAPTA-C was investigated by means of flow cytometry, western blotting and annexin V binding assays in Ehrlich Ascites Carcinoma (EAC), which is a highly proliferative and fluid tumor.⁶⁸ It was shown that RAPTA-C caused arrest of G2/M phase of the cell cycle by **up-regulation of p53**, triggering the mitochondrial apoptotic pathway. P53 is a tumor suppression gene which plays a crucial role in the induction of cell cycle arrest and apoptosis as a result of DNA damage and cellular stress. A probable downstream mediator of p53 is the cell-cycle-related cofactor p21. The experiments showed that the p21 level increased after treating cells with RAPTA-C. Additionally, cells incubated with RAPTA-C revealed the **reduced cyclin E expression**, which is a key regulator in the G1-S and G2-M transitions. Considering that RAPTA-C is involved in the induction of apoptosis, the balance between proapoptotic (Bax protein) and antiapoptotic (Bcl-2) factors was investigated. Following the treatment of cells with the compound, a significant **increase of Bax** level with a simultaneous **decrease of Bcl-2** level was observed, consequently promoting apoptosis.

Another possible mechanism of apoptosis is a pathway involving caspase activation by cytochrome C as a consequence of procaspase cleavage. RAPTA-C was shown to be involved in this pathway, as RAPTA-C treatment resulted in an increased level of cytosolic cytochrome c and a **decreased amount of procaspase-9**. In addition, proapoptotic factors can also be activated by **over-expression of c-Jun-NH₂-terminal kinase (JNK)**, which was found to be activated by RAPTA-C treatment. These findings indicated that RAPTA compounds are involved in multiple apoptotic pathways, including the mitochondrial pathway, which can possibly result in reduction of acquired drug resistance.

The above-mentioned biological processes and mechanisms of cell proliferation and invasion are not only involved in metastatic processes, but also in the process of

angiogenesis. Therefore, RAPTA compounds were tested for angiostatic effects on epithelial cells *in vitro* and on the chicken embryo chorioallantoic membrane (CAM) *in vivo*. Inhibition of angiogenesis by RAPTA complexes resulted in the formation of large avascular zones in the CAM.⁶⁹

RAPTA compounds also have an effect on cells treated with photodynamic therapy, known to induce angiogenesis. Whereas in the control sample (CAM after treatment with PDT alone), new vessels formed and replaced the originally occluded capillary plexus, CAM after treatment with PDT and subsequent topical administration of ruthenium compounds showed a significant inhibition of vascular regrowth. Overall, these promising results show that RAPTA complexes can also be potentially used in combination with photodynamic therapy. Based on these findings, RAPTA complexes were found to be promising candidates for clinical trials.

4.2 DNA era. Is DNA the main target?

Since it was shown that RAPTA compounds induced inhibition of DNA migration probably due to the protonation of the PTA ligand, DNA was considered to be a potential RAPTA target.⁴⁰ To prove this hypothesis, numerous mechanistic, analytical and theoretical studies were performed. Binding studies with 14-mer DNA oligonucleotides by mass spectrometry showed that RAPTA complexes coordinate to DNA *via* the loss of labile chlorido ligands and an arene ligand with retention of the PTA ligand, as shown in Figure 10. The loss of arene may allow formation of π -bound DNA adducts *via* coordination of aromatic rings of nucleobases to a metal center but DFT computations demonstrated that π -binding is not favored energetically. It is more likely that single-stranded oligomers wraps around the metal center with subsequent formation of multiple σ -bonds.⁵⁴ According to these results, **besides DNA, single nucleotides, oligonucleotides and RNA might be potential targets** of RAPTA complexes.

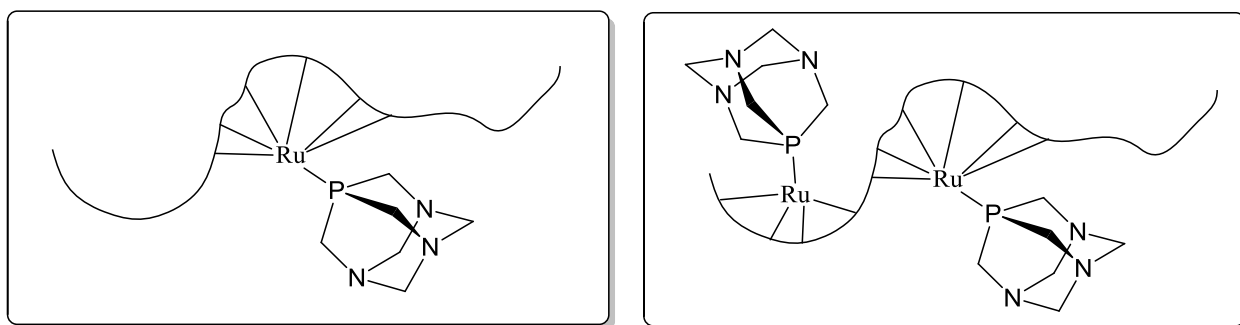


Figure 10. Proposed schematic structure of RAPTA-DNA conjugates

The high reactivity of RAPTA-C to dGMP in acidic conditions was confirmed by CZE-ICP-MS experiments. Based on the migration behavior, it was suggested that the structure of adducts corresponds to mono-dGMP species with either chloride or aqua ligands.⁴³

The computational work of Gossens *et al.* was one of the key milestones of the “DNA era”.⁴⁷ pH-dependent DNA binding of RAPTA complexes was attributed to protonation of a PTA ligand. However, Gossens *et al.* demonstrated that under acidic conditions RAPTA complexes existed mainly in the mono-aqua form. Therefore, they pointed out the role of a labile aqua ligand in the reactivity of complexes. Subsequently, Dorcier *et al.* determined the adducts of Ru, Os and Rh PTA complexes with various DNA model compounds by means of ESI-MS and ¹H NMR spectroscopy.⁵⁸ The most abundant signals were indeed attributed to mono-chlorido complexes with purine bases or nucleosides coordinated via N7 in a η^1 -mode formed possibly *via* the replacement of an aqua ligand. In addition, DNA binding mechanisms of RAPTA-C and Sadler’s [(cymene)Ru(en)Cl]⁺ complex were compared by means of classical and QM/MM molecular dynamics simulations using a 12 base-pair DNA duplex as a model target.⁴⁹ It was shown that both compounds bind the major groove of DNA but both induce different local and global changes in the DNA structure. The calculations demonstrated that RAPTA compounds induce DNA bending towards the major groove without breaking Watson-Crick base pairs or intercalate between them, which is different from [(cymene)Ru(en)Cl] (see Figure 11). Such differences can explain different cell responses to different families of compounds.

Furthermore, the reactivity of RAPTA-T towards different double-stranded nucleotides was analyzed by ESI-MS in comparison with platinum complexes, NAMI-A and KP1019.⁷⁰ Within all the ruthenium complexes tested, RAPTA-T did not reveal the highest reactivity, since NAMI-A modified double strands to a higher extent. Even though Ru^{II} compounds are known to be more reactive than Ru^{III}, hydrolysis kinetics might be the main reason for the observed reactivity trends. Previously, NAMI-A was demonstrated to undergo hydrolysis more rapidly than RAPTA compounds and in a strongly pH dependent manner with regard to the hydrolysis products formed.⁴³ In addition to the characterization of DNA-metallodrug adducts, binding sites of metal complexes were detected. A preferred binding partner for ruthenium complexes is guanine, which is known to be the main binding partner of platinum-based compounds as well. However, it should be noted that formation of adducts of ruthenium complexes with adenine or thymine is also possible, although to a smaller extent.

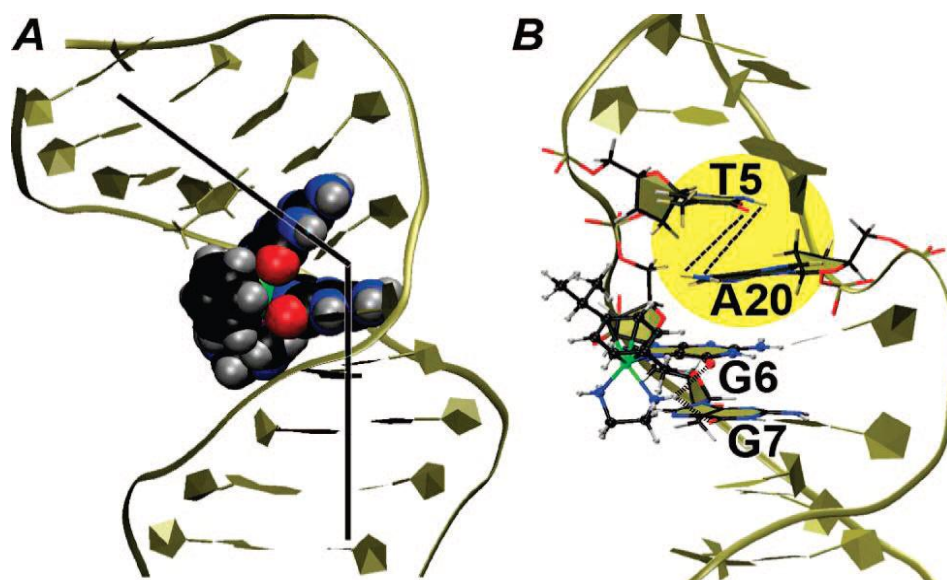


Figure 11. Representative snapshots of 12-mer DNA upon covalent compound binding. (A) The benzene derivative of RAPTA induces a global bend toward the major groove. (B) [(cymene)Ru(en)Cl]⁺ bound to DNA after breaking the Watson-Crick base-pair T5/A20. The figure was reproduced with a kind permission of Prof. Ursula Röthlisberger from reference ⁴⁹.

Subsequently, the nature of interactions of RAPTA-C and carbo-RAPTA-C with the DNA sequence of the human breast cancer suppressor gene 1 (BRCA1) was investigated using conformational analysis of ruthenated DNA, cross-linking assays and semi-quantitative PCR.⁷¹ In accordance with the results described above, it was shown that ruthenation induced unwinding of the supercoiled DNA. These studies revealed that RAPTA complexes preferentially bind to adenine and guanine. The role of thymine and cytosine as binding partners is not yet clear.

In subsequent studies, RAPTA compounds were specifically tuned in order to increase possible interactions with DNA.⁵⁹ One possible way to enhance interactions with DNA is to modify RAPTA complexes to contain functionalities which enable hydrogen-bonding, such as alcohol or amino groups. Surprisingly, complexes bearing these functionalities were either equivalent or less cytotoxic than their non-modified analogues. Moreover, the modification of the complexes with alcohol or amino groups resulted in their inhibited uptake by cancer cells. It should be noted that there was no distinct difference between the uptake of charged and neutral species, suggesting an **active transport** mechanism for delivery of the complexes to the cells. This led to the conclusion that **DNA might not be the primary target** of RAPTA compounds. Even though RAPTA complexes readily

bind to DNA upon incubation in a test tube, in complex biological media the binding to other biomolecules might be dominating.

4.3 Proteins era. If not DNA, then what?

Dyson and Sava pointed out in their review “Metal-based antitumor drugs in the post genomic era” published in 2006 that: “*it seems likely that protein targets are more important than DNA in the activity of RAPTA-T*”.⁷² Consequently, extensive research on the potential protein targets of RAPTA compounds has been performed. It was shown that the complexes of the RAPTA family readily bind proteins such as lysozyme,⁷³ ubiquitin,^{73,74} cytochrome C,^{73,74} superoxide dismutase,⁷⁴ the human serum proteins albumin and transferrin,⁷⁵ poly(adenosine diphosphate (ADP)-ribose) polymerases (PARPs),⁷⁶ and metallothioneins.⁷⁷ Such reactivity is perhaps not unexpected since the structure of RAPTA compounds is simple and the complexes can bind to numerous targets by ligand exchange reactions of labile chloride with nucleophilic atoms of biomolecules.

One of the most popular techniques for the determination of drug-protein adducts is electrospray ionization mass-spectrometry (ESI-MS). Determination of the molecular species formed between metallodrugs and single biomolecules is relatively easy and quick. Therefore, initial studies on the characterization of RAPTA-protein adducts were performed by ESI-MS. However, besides ESI-MS there are numerous bioanalytical techniques which are used for determination of interactions between drugs and biomolecules.⁷⁸

4.3.1 Thioredoxin reductase (TrxR)

Casini *et al.* explored the ability of RAPTA complexes to inhibit cathepsin B (Cat B) and thioredoxin reductase (TrxR).⁵⁶ **Thioredoxin reductase (TrxR)** is the only enzyme known to reduce thioredoxin (Trx). Its structure is similar to the structure of glutathione reductase and consists of several structural components such as FAD, NADPH and the active site with redox-active disulfide bonds. Thioredoxin reductase together with thioredoxin and NADPH maintain the redox state in cells. The role of TrxR in cancer is ambiguous⁷⁹; on the one hand, due to its antioxidative properties it is able to reduce the amount of reactive oxygen species produced in tumors. On the other hand, it is involved

in the process of cell division. Therefore, highly proliferating cells are always marked by overexpressed levels of TrxR protecting them from the immune system. It is important to emphasize that the functions of TrxR are antiapoptotic, which means that up-regulation of TrxR might be one of the reasons for drug resistance. Consequently, drugs capable of TrxR inhibition, acting *via* interaction with one of the redox active residues (e.g. Cys), are promising to overcome drug resistance. It was shown that TrxR is highly sensitive to metallodrugs, such as gold(I), platinum(II) and ruthenium(III) complexes. Therefore, the potency of the RAPTA family was also evaluated. Since RAPTA complexes reveal a high affinity to sulfur atoms, it is possible that TrxR might be a potential biological target of RAPTA complexes after the reduction of a disulfide bond.

Several RAPTA compounds were screened towards cytosolic or mitochondrial thioredoxin reductases.⁵⁶ None of the compounds was an effective inhibitor of mitochondrial TrxR, while inhibition of cytosolic TrxR was more pronounced. It was demonstrated that complexes with sterically demanding arenes exhibited a decreased ability of enzyme inhibition, since proteins cannot easily accommodate bulky substituents. Interestingly, carbo-RAPTA, which does not contain labile chloride ligands in its structure, was found to be a more effective inhibitor than RAPTA-C. This might be due to stabilization of the adduct between TrxR and carbo-RAPTA by interactions of a protein with the 1,1-cyclobutanedicarboxylato ligand which is not cleaved upon protein-metallodrug interactions. Despite the observed inhibition of cytosolic thioredoxin reductase in the 45-200 μ M range, these findings seem to be modest or scarcely relevant *in vivo*.⁵⁶

4.3.2 Cathepsin B (Cat B)

Cathepsin B (Cat B) is an enzymatic protein of the peptidase or protease family (enzymes known to degrade proteins) located in lysosomes. Its biological function is the maintenance of the normal cell metabolism by degradation of the components of extracellular matrix. Cat B acts as an oncomarker, since in tumors its expression is markedly up-regulated. The exact role of cat B in cancer is not fully understood; however, its overexpression correlates with metastatic and invasive processes. Inhibition of cat B results in reduced cell mobility and diminished invasiveness *in vitro*. Similarly to thioredoxin reductase, cat B contains disulfide bridges and its active site contains activated Cys residues, as well as His and Asp.

RAPTA compounds are effective inhibitors of cat B in the low micromolar range.⁵⁶ Notably, carbo-RAPTA was significantly less effective in cat B inhibition than RAPTA-C, indicating that the release of leaving groups is crucial to exhibit inhibitory activity. In order to get further insight on the binding mode of RAPTA-C and active sites of cat B, docking studies were performed. As expected, cysteine (more precisely, Cys-29) was proposed to be the anchoring site for the ruthenium center. This was further stabilized by a number of additional contacts forming hydrogen bonds. In addition to these studies, DFT calculations were performed to estimate how the metal center affects the binding of the complexes to the protein.⁵⁷ While metal-sulfur binding was shown to be thermodynamically favored for RAPTA-C and its osmium analogue, the Ir^{III} and Rh^{III} analogues form very weak metal-sulfur bonds. The free energies for M-S dissociation are 61.5 and 56.8 kJ, while they are 80.5 and 82.9 kJ for RAPTA-C and OsPATA-C, correspondingly. The Ir and Rh derivatives do not inhibit cathepsin B which may be explained by their lower affinity to sulfur as compared to RAPTA complexes.

4.3.3 Ubiquitin (Ub) and cytochrome C (cyt C)

Ubiquitin (Ub) and **cytochrome C (cyt C)** have been widely used as model proteins in ESI-MS experiments to study protein-metallodrug adduct formation due to their solubility, stability and low molecular weight.^{80,81} In addition to their structural properties, these proteins have important biological functions related to cancer.

Ubiquitin (Ub) is an abundant small (9 kD) protein used by cells to covalently modify other proteins in order to activate their functions and target them for degradation.⁸² It was found that numerous oncogenes and gene suppressors were the targets of ubiquitination. The malfunction of proteasomal degradation could either increase the number of oncoproteins or decrease the amount of suppressor proteins. Intuitively, inhibition of the proteasome is expected to result in selective inhibition of malignant growth. **Cytochrome C (cyt C)** is an abundant small heme protein (12 kD) located in mitochondria and playing an essential role in energy production and in apoptotic pathways.⁸³ Apoptosis and cancer are closely related together, since the dysregulation of apoptosis results in the survival of tumor cells. Therefore, the development of compounds capable to interfere with cyt C-mediated pathways which are able to block or trigger apoptosis is important for cancer treatment.

Casini *et al.* demonstrated that the reaction of cyt C with RAPTA-C resulted in extensive protein metallation, whereas only moderate or very low ruthenation was observed with carbo-RAPTA and oxali-RAPTA, correspondingly.⁷³ The results are in good correlation with the ability of the complexes to release their leaving groups upon hydrolysis.⁶¹ The incubation of cyt C with RAPTA-C for 48 hours in water resulted in the formation of four different species, which were assigned to mono-ruthenated species, namely “cyt C + $[(\eta^6\text{-cymene})\text{Ru}]$ ” and “cyt C + $[(\eta^6\text{-cymene})(\text{PTA})\text{Ru}]$ ”, and doubly-ruthenated species with either two $[(\eta^6\text{-cymene})\text{Ru}]$ fragments or one $[(\eta^6\text{-cymene})\text{Ru}]$ and one $[(\eta^6\text{-cymene})(\text{PTA})\text{Ru}]$ fragment. It is worth noting that only 30% of the ruthenated species after 3 hours were detected, whereas after 24 h the signal of free cytochrome C was no longer observed.

On the contrary to RAPTA-C, the adduct with carbo-RAPTA did not retain the arene ligand. As a result, coordinative unsaturation was compensated by coordination of aqua or hydroxido ligands. The signal of the cytochrome C–carbo-RAPTA adduct was assigned to “cyt C + $[(\text{PTA})\text{Ru}(\text{C}_6\text{H}_6\text{O}_4)(\text{OH})]$ ”; however, no doubly ruthenated species were detected. In case of oxali-RAPTA, only one Ru-containing peak with very low intensity was observed which was attributed to a monoruthenated species with a $[(\eta^6\text{-cymene})\text{Ru}]$ fragment.

It is interesting that under equivalent conditions (Pt/cyt C ratio 10:1, one week incubation time, 37 °C) cisplatin forms mono-, bis- and tris-adducts with cyt C,⁸⁰ while $[(\eta^6\text{-cymene})\text{Ru}(\text{en})\text{Cl}]^+$ forms exclusively mono-ruthenated species.

The incubation of RAPTA complexes with ubiquitin for 5 hours in water resulted in the same adducts as with cytochrome C; however, the intensity of signals was significantly higher. Only monoruthenated adducts were detected with the most abundant peak assigned to “Ub + $[(\eta^6\text{-cymene})\text{Ru}]$ ”. Even after 2 days of incubation no doubly ruthenated species were observed. Notably, the complexes containing both PTA and PPh_3 ligands did not form any detectable adducts with any of the proteins tested.

In numerous cases protein-metallodrugs adducts detected by different mass spectrometry techniques were different at least in relative abundance of the peaks. Thus, the signals described above were detected by ESI-IT-MS (Electrospray Ionization Ion Trap Mass Spectrometry). One additional peak with low intensity was detected by ESI-QToF-MS, that is “Ub + $[(\eta^6\text{-cymene})\text{Ru}(\text{PTA})]$ ”.

RAPTA-CF3 behaves significantly different from all other members of the RAPTA family.⁵⁰ This was demonstrated by ESI-MS and NMR studies⁴⁸ in which upon hydrolysis the complete cleavage of the arene and chlorido ligands occurred. This resulted in the formation of unusual adducts with ubiquitin. For example, after 1 day of incubation the most abundant signals were assigned to [Ub-Ru(pta)(H₂O)_x] (x = 0-2). Notably, ubiquitin adducts with solely ruthenium ion were also observed.

4.3.4 Lysozyme and superoxide dismutase (SOD)

For comparative purposes, RAPTA complexes were also incubated with lysozyme, which is relevant in certain defense mechanisms. Again, only monoruthenated species were observed after 48 h incubation in water with either [(η^6 -cymene)Ru] or [(η^6 -cymene)Ru(PTA)] fragments. However, the reactivity of the complexes was markedly lower than in case of cytochrome C.

All these binding studies provided information about the nature of species formed between the metal complex and a protein, but did not give any insight into the selectivity of RAPTA complexes with respect to protein binding. ESI-MS allows identification of various species from the complicated mixtures of compounds and simultaneous screening of drug interactions with different biomolecules. To shed light on the reactivity of RAPTA-C towards a certain protein in presence of other proteins, this metal complex was incubated with a mixture of cytochrome c, ubiquitin and superoxide dismutase (SOD).⁷⁴

Superoxide dismutases (SODs) belong to the group of metalloenzymes found in cytosol and mitochondria that catalyze the dismutation of superoxide into oxygen and hydrogen peroxide. There are several families of SOD which vary in metal cofactor, that is 1) dismutases which bind both Co and Zn, 2) dismutases which bind either Fe or Mn and 3) dismutases which bind Ni. Cancer cells are characterized by a reduced activity of Mn-containing superoxide dismutases and Co/Zn dismutases, which results in a significant increase of the superoxide ion level in cells with the subsequent production of reactive oxygen species.⁸⁴

It was demonstrated that after incubation with a mixture of three proteins RAPTA complexes readily bound to ubiquitin and cytochrome C, which matches well with the data obtained for the binding studies to single proteins.⁷⁴ However, only low intensity signals were observed for RAPTA-SOD adducts. In the competitive binding of cisplatin

and RAPTA towards the same mixture of proteins no signals of cisplatin-Ub were detected, whereas equal intensity signals were assigned to RAPTA-Cyt and cisplatin-Cyt adducts. Notably, in such experiments only platinum adducts with SOD were detected. Therefore, it was concluded that RAPTA-C and cisplatin compete for the same binding sites on proteins which is an important finding.

ESI-MS analysis provided clear evidence that RAPTA complexes readily form identical adducts with different proteins and reactivity decreases in the order **Ub>Cyt C>Lys>SOD**. This is somewhat counter-intuitive in terms of reaction kinetics, since as cytochrome C contains a significantly higher number of metal-binding sites than ubiquitin.

Modern ESI-MS techniques enable reliable determination of metal-binding sites in proteins and other biomolecules. Top-down MS can be used to analyze the sequence of intact proteins, whereas for bottom-up MS smaller peptides obtained from the enzymatic digestion of proteins are characterized. A top-down method displays a number of advantages over the bottom-up method, as the latter requires the digestion of proteins, which can possibly lead to the altering of metal-binding pockets, shift of equilibria and formation of artefacts. On the other hand, top-down MS cannot cover the whole proteome and is technically demanding. Nowadays, both methods are widely used for the determination of metallodrug binding sites and top-down MS slowly increases its popularity.⁸⁵⁻⁸⁹ Casini *et al.* employed a bottom-up method for the identification of RAPTA-C binding sites on cytochrome C.⁷³ In cytochrome C only Met65, His26 and His33 are freely available for metal complexes. It was demonstrated that the major interaction site for RAPTA-C is His33, whereas the primary binding site for platinum complexes (cisplatin, oxaliplatin, *etc.*) is Met65. Top-down mass spectrometry, more precisely, MS/MS experiments using collision-induced dissociation (CID) were used for the identification of binding sites of cisplatin, transplatin, oxaliplatin and several organometallic ruthenium complexes on Ub.^{70,87}

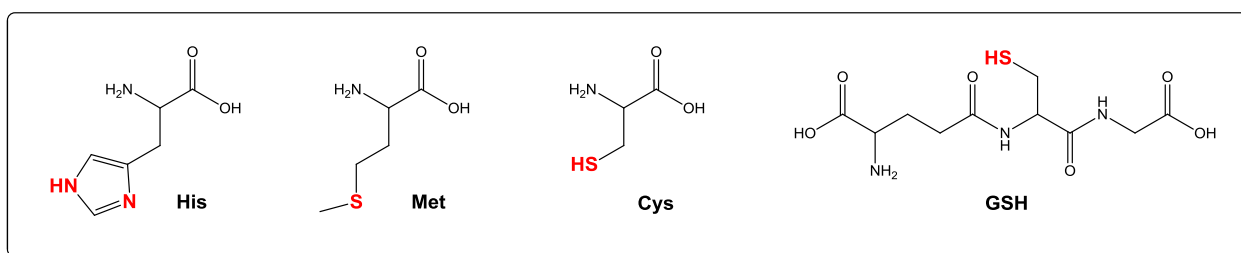


Figure 12. Chemical structures of histidine (His), methionine (Met), cysteine (Cys) and glutathione (GSH).

The observed trends of the RAPTA complexes' reactivity with proteins might be explained in terms of the accessibility of metal-binding sites. It was shown that metallodrugs target Met1 and His68 of ubiquitin (structures are shown in Figure 12). These amino acids are exposed on the surface of ubiquitin, and therefore, metal complexes can approach them easier than nucleophilic sites of cytochrome c (see Figure 13).

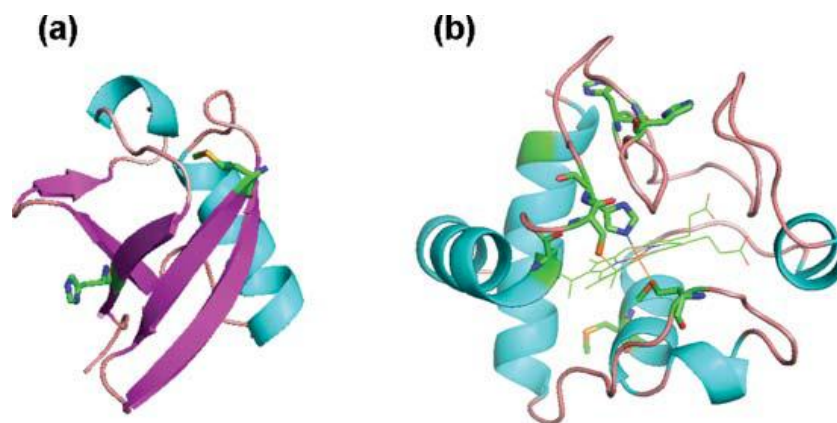


Figure 13. Molecular structures of (left) ubiquitin and (right) cytochrome C with His, Met and Cys residues highlighted as stick graphics (PyMOL v0.98, (c) DeLano Scientific LLC). The figure was reproduced with a kind permission of authors from reference ⁶³.

Clearly, comparison of the complexes with different substituents would reveal different reactivity trends, as the presence of bulky sterically demanding substituents would dramatically decrease reactivity of the complexes with biomolecules.

4.3.5 Glutathione (GSH)

Following the initial success of the MS studies on the identification of molecular species formed between RAPTA complexes and single biomolecules, selectivity of binding and further reactions after adduct formation were monitored. Hartinger *et al.* investigated the ability of glutathione to destroy RAPTA-ubiquitin adducts by removing the ruthenium moiety from the protein.⁹⁰

Glutathione (GSH) is a natural tripeptide (γ -L-Glu-L-Cys-Gly, the structures of Cys and GSH are shown in Figure 12) and the most abundant non-protein molecule in the cell. Another form of GSH which can be found in cells is a conjugate with proteins formed *via* a disulfide bond. Glutathione has a number of physiological roles in the body. For example, it is the major cellular antioxidant and detoxificant. As a result, glutathione metabolism plays an intrinsic role in cancer. It detoxifies carcinogens and subsequently

removes them from the body. In cancer cells it is present in relatively high concentrations (0.5-10 mM) and protects tumors by removing chemotherapeutic agents. The increased level of GSH is often associated with increased resistance to anticancer drugs.⁹¹

As GSH is a high affinity metal binder, it may induce release of metallodrugs from their conjugates with biological targets. Therefore, studies on the formation of RAPTA-GSH and RAPTA-Ub-GSH conjugates were performed and subsequent release of a metal fragment was monitored. RAPTA-C quickly reacted with glutathione resulting in the formation of RAPTA-GSH adducts, such as $[(\eta^6\text{-cymene})\text{Ru}(\text{GS})]^+$, $[(\eta^6\text{-cymene})\text{Ru}(\text{PTA})(\text{GS})]^+$ and $[(\eta^6\text{-cymene})\text{Ru}(\text{PTA})(\text{GS})_2+\text{H}]^+$. After 24 h only minor ruthenated species were detected. Most importantly, GSH was shown to slowly remove RAPTA moiety from the RAPTA-Ub adducts compared with cisplatin.⁹⁰ It is worth noting that the formation of ternary complexes was not observed.

Consequently, some important conclusions about the possible fate of RAPTA complexes within the body can be drawn. As soon as RAPTA compounds are intravenously injected into the body, they meet proteins, their first binding partners. Blood proteins may act as reservoirs and deliver compounds to cells, slowly releasing small portions of active agents. Such conjugates may be cleaved by glutathione (or other chelators) and the metal moieties react with other intracellular targets.

4.3.6 Metallothioneins (MTs)

Similar experiments were also performed with metallothioneins, since this class of proteins is also thought to be responsible for drug resistance. Casini *et al.* demonstrated high affinity of RAPTA-C towards metallothioneins and showed that adding metallothioneins to the conjugates of RAPTA with other proteins leads to the removal of RAPTA fragments and its detoxification.⁷⁷

Metallothioneins (MTs) are a class of small (7 kD) proteins with cysteine residues binding a high number of metal ions. They have high affinity to transition metals of groups Ib and IIb, especially zinc and MT is the major zinc binding intracellular thiol. However, under physiological conditions zinc ions are readily displaceable by other metal ions, such as Cu^+ or Cd^{2+} . In mammals there are four different subgroups of metallothioneins (MT-1, MT-2, MT-3 and MT-4) which are concentrated in different tissues and subsequently serve different biological functions. The primary biological role

of MTs has yet to be identified but due to their high affinity to metal ions these proteins are essential in the homeostasis of essential metals and detoxification of heavy metals.⁹² Moreover, MTs are involved in the regulation of cell cycle and apoptosis, and are overexpressed in a number of tumor types. The overexpression of MTs serves as a marker for tumor progression and metallodrug resistance.⁹³ It was shown that due to the high affinity of Pt^{II} to sulfur atoms, MT-2 acts as an effective intracellular scavenger of platinum(II) drugs by forming stable MT-Pt^{II} conjugates.⁹⁴ Interestingly, even when the Pt^{II} moiety was already bound to DNA, MTs were still able to interfere and form stable ternary complexes.

The interactions between RAPTA complexes, ubiquitin and MT-2 were monitored by ESI-MS and ICP-AES and subsequently compared with cisplatin.⁷⁷ The adducts observed after reaction with other proteins were also seen after the incubation of RAPTA-C with MT-2 in water for 48 h, namely monoruthenated $[(\eta^6\text{-cymene})\text{Ru}]$ -MT species with or without PTA ligand. In contrast to cisplatin-MT-2 adducts, no bi-, tri- or tetrametallated species of RAPTA complexes were detected. This is in agreement with the results from previous experiments with RAPTA-C and other biologically relevant molecules. It was demonstrated that RAPTA-C displaced zinc ions upon binding to metallothionein demonstrating its high affinity towards Cys. The number of released Zn^{II} ions was even higher in case of cisplatin, probably due to the retained $\eta^6\text{-p-cymene}$ ligand of RAPTA-C. Metallothioneins trigger the release of a RAPTA moiety from RAPTA-ubiquitin adducts, which is significantly faster than the release triggered by glutathione. A similar correlation between GSH and MT-2 release was described for platinum compounds; nevertheless, in comparison with RAPTA-C the kinetics of platinum release was significantly faster with both biomolecules revealing different binding affinities of ruthenium- and platinum-based complexes. This is a very important observation, since metallothioneins are not able to completely cleave the RAPTA complex from its targets which may play an important role in overcoming drug resistance in patients.

4.3.7 Poly(adenosine diphosphate (ADP)-ribose) polymerases (PARPs)

Another essential class of proteins involved in cancer resistance to chemotherapies is the class of **poly(adenosine diphosphate (ADP)-ribose) polymerases (PARPs)** which are called “the guardian angels” of DNA. This family of proteins is involved in the processes of DNA repair and apoptosis. Thus, cells trigger PARP activation immediately

after ssDNA breaks occur. PARPs detect single-stranded DNA breaks, bind to them and start repair. Once the repair is over, PARPs degrade. Severe DNA damages might induce hyperactivation of PARPs, which consequently leads to apoptosis. The PARP family comprises 17 members, where each member has a different function in a cell. PARP-1, which is the most studied member of the PARP family, functions as a tumor-suppressor protein in cells. PARP inhibitors prevent the repair of DNA strand breaks, leading to the death of cells. Normal cells survive the inhibition of PARP, since they do not replicate DNA to the same extent as cancer cells and do not contain mutated BRCA genes. The activity of PARP upon cisplatin treatment is not yet clearly understood, however, it is known that platinated DNA adducts can be PARP-repaired. Ruthenium complexes, in turn, might act as potential PARP1 inhibitors. Since PARP1 contains two zinc-finger (ZF) motifs in its structure, RAPTA-T might compete with zinc for a binding site of the ZF, thus altering its structure.

RAPTA-T indeed maintained PARP1 inhibition activity. However, it was significantly less pronounced than of cisplatin or NAMI-A, indicating the importance of other protein targets in the mode of action of the RAPTA family.⁷⁶ It should be noted that cisplatin co-administered with RAPTA-T resulted in a synergistic effect of cytotoxicity. This effect might be a consequence of the reduced repair of DNA-cisplatin adducts due to partial PARP-1 inhibition by ruthenium complexes. Adducts which formed between RAPTA-T and apo-ZF-PARP were monitored by FT-ICR MS. It was shown that RAPTA-T retained both arene and PTA ligands as with other proteins. The addition of RAPTA-T to the physiological ZF-motif (holo-ZF-PARP) resulted in the standard adduct types maintaining Zn^{II} ion, possibly indicating that RAPTA-T coordinates amino acids which are not involved in the structure of zinc finger motifs.

4.3.8 Human serum albumin (HSA) and human serum transferrin (Tf)

Human serum transferrin (Tf) and **human serum albumin (HSA)** are two proteins that play significant roles in the modes of action of anticancer metallodrugs. Both are considered essential for the transport, delivery or storage of metallodrugs. The main roles of albumin are maintenance of the osmotic pressure in blood and deactivation of free radicals. It constitutes 52% of the total serum protein content thus being the most abundant protein in serum. As a result, it binds to a wide range of drugs immediately after their intravenous application.⁹⁵ On the one hand, this binding affinity represents a challenge in drug development, as HSA restricts a free active form of a drug. On the

other hand, such properties can be used for the development of specific drug delivery systems.⁹⁶

Human serum transferrin (Tf) is an iron-binding blood plasma glycoprotein responsible for controlling the level of free iron in biological fluids.⁹⁷ The iron affinity of protein is extremely high; however, it decreases at low pH. When transferrin does not contain iron atoms, it is called apotransferrin. The role of transferrin in the body is vital, since all cells require iron for the cell growth and division, and transferrin transports iron among the sites of absorption, utilization, storage and hemoglobin degradation. Due to the overexpression of endogenous transferrin receptors on tumor cells, they might be potential markers for cancers. Therefore, transferrin is an attractive molecule for targeted cancer therapy.

Nowadays, the delivery of ruthenium antiproliferative complexes to tumor cells by transferrin and albumin is such a commonly exploited hypothesis that it turned from a hypothesis to a fact. However, it is essential to show that under *physiological conditions* metallodrugs indeed form adducts with transferrin and albumin. From the results of the experiment, where a complex of NAMI-A with transferrin was incubated with cancer cells, it was not possible to draw any useful conclusion in favor of transferrin transportation inside the cells. Mass spectrometric analysis of transferrin and albumin drug adducts is hampered by the molecular mass of the investigated proteins (albumin is 67 kDa, transferrin is 80 kDa). One of the strategies to overcome this problem is to use model low weight peptides mimicking the active site of albumin and transferrin residues. Groessl *et al.* investigated the binding of RAPTA-T to apo-Tf and a small peptide which contains His249 involved in the iron binding on transferrin and some other putative binding partners.⁷⁵ After the incubation of the metal complex with transferrin at a 5:1 ratio, standard protein-RAPTA adducts formed, namely, monoruthenated $[(\eta^6\text{-arene})\text{Ru}]$ -apo-Tf species. The MS interpretation of the RAPTA-model peptide adducts gave an insight into the exact binding mode of the complex and the nature of the formed species. One histidine residue was found to be the major binding partner. As expected, cysteine was also involved in the binding, although to a smaller extent. It should be noted that in similar experiments cisplatin was less reactive and less selective, which matches the results of previously described experiments.

Driven by the demand of molecular biology and proteomics for special techniques capable of determination of metallodrug behavior in biological systems, highly sensitive and accurate bioanalytical techniques were developed. Nowadays ESI-MS techniques

described above are immensely popular; however, inductively coupled plasma mass spectrometry (ICP-MS) which is capable to detect elements at sub-ppt concentrations has become the method of choice for a number of metallomics experiments. ICP-MS can be coupled to various separation techniques, such as liquid chromatography (LC-ICP-MS) or capillary zone electrophoresis (CZE-ICP-MS). Due to the high separation power, compatibility with physiological conditions and possibility to quantify the amount of protein-bound metal complex, the latter method was employed in the studies of hydrolytic stability of RAPTA-C as well as its binding properties toward dGMP (see Chapters 4.1.2 and 4.2).⁴³ ICP-MS coupled online to size-exclusion chromatography (SEC-ICP-MS) can be used for separation of proteins on the basis of their molecular weight and consequently, the molecular weight distribution of the metal-binding partners can be determined.⁷⁸

Using this approach, Groessl *et al.* collected information on the affinity of RAPTA-T and cisplatin for albumin and transferrin.⁷⁵ It was indicated that RAPTA-T revealed a significantly higher activity to all proteins compared to cisplatin. Furthermore, the influence of hydrolysis on protein binding was investigated. Two parallel sets of experiments were performed, where metal complexes were either incubated with proteins for 1 h or first pre-incubated for 24 h prior to addition of proteins. As expected, the hydrolyzed product was more reactive due to the presence of labile aqua ligands. It was demonstrated that RAPTA complexes bind with a higher affinity to holo-transferrin in comparison with apo-transferrin and albumin, whereas cisplatin was non-selective and had a similar affinity to all the proteins used in the study.

4.3.9 Subcellular localization

ICP-MS was also used for the determination of cellular uptake of RAPTA-T and its subcellular localization.⁹⁸ It was demonstrated that the uptake of RAPTA-T is dependent on the cell type. It was accumulated in cisplatin-resistant cells to a higher extent than in cisplatin-sensitive cells. This result indicates that RAPTA-T uptake is not influenced by cisplatin-resistance mechanisms, since the concentration of platinum is significantly reduced in cisplatin-resistant cell lines after 24 hours. Moreover, the absolute metal content in cisplatin-resistant cell lines is much higher after treatment with RAPTA than with cisplatin under similar conditions.

The overview of the subcellular localization of a drug is important, since the knowledge about the distribution of RAPTA complexes in different organelles might give an insight into its dynamic distribution and potential biomolecular targets. After successful separation of a cell into fractions, each component was subsequently analyzed by different techniques. The metal content is typically determined by ICP-MS. Studies on the subcellular distribution of cisplatin in A549 cells revealed that the cytosol fraction (fluid with organelles) contained more than 70% of the metal complex, whereas membrane, nucleus and cytoskeletal fractions contained approximately 17%, 9% and 4%, correspondingly.⁹⁹ Notably, in cisplatin-resistant cells, the highest accumulation of cisplatin was observed in the particulate fraction. In contrast, RAPTA-T demonstrated a high preference for the particulate fraction containing organelles, *i.e.* mitochondria, endoplasmic reticulum, Golgi apparatus, lysosomes. In cisplatin-resistant cell line this preference is reduced and shifted towards nucleus and cytosol.⁹⁸ Notably, the amount of RAPTA-T in mitochondria is significantly higher than the amount of cisplatin in both cisplatin-sensitive and resistant cells, whereas no platinum was detected in cisplatin-resistant cells. Differences in biodistribution patterns indicate different metabolization pathways of cisplatin and RAPTA-T.

The interaction of RAPTA complexes with the cytoskeleton is of special interest, since cytoskeletal proteins are crucial for metastatic processes and RAPTA complexes are known to be active against metastases. As expected, ruthenium was detected in cytoskeletal and membranes fraction, revealing the interactions of metallodrug with structural cell components.

As a next step, each fraction was analyzed by SEC-ICP-MS in order to reveal high or low molecular binding partners of RAPTA-T in each component. Ru was found in the cytosolic fraction bound to high and low molecular weight biomolecules, whereas in the particulate and nuclear fractions binding to small biomolecules was preferential. Possibly, high and low molecular weight adducts in the cytosolic fraction represent adducts of RAPTA complexes with albumin and small biomolecules (amino acids, glutathione, buffer components), correspondingly. Low molecular weight components in the nucleus might result from the adduct formation of RAPTA-T with small detoxifying molecules or also histones.

4.3.10 Nucleosome core particle (NCP)

The preference of RAPTA complexes to proteins in presence of DNA was for the first time demonstrated by Wu *et al.* An X-ray structure of a **nucleosome core particle (NCP)** with RAPTA complexes showed exclusive binding to protein sites rather than DNA.¹⁰⁰

X-ray diffraction analysis is an important technique with respect to the investigation of metallodrug-biomolecule interactions. The advantage of this method is the structural information about adducts on the atomic level. Therefore, X-ray structure answers questions about binding type, stoichiometry of interactions and preferred binding partners. However, this method requires formation of a single crystal of a molecule of interest, which is not always possible to obtain. Moreover, some crystals poorly diffract and as a result, reliable structural information is not available. It should be noted that this method represents only the situation in solid state, which might not resemble the behavior of molecules in solution. Two commonly used methods to crystallize proteins with metallodrugs are co-crystallization of protein crystals with the metal complex or soaking of proteins with a high concentration of the metal complex. The latter was used for obtaining crystal structures of NCP with RAPTA-C but also cisplatin¹⁰¹.

The nucleosome core (NCP) consists of a double-stranded DNA segment which is wrapped around an 8 histone protein core. Therefore, both DNA and protein parts reside in close proximity to each other. The unusual structure of NCP is a result of the packing of large eukaryotic genomes into a nucleus while ensuring appropriate access to genomes. The described structural organization of the genome in nucleosomes ensures correct gene expression and plays a vital role in gene transcription, repair, replication and recombination. As a result, approximately 83% of genomic DNA is found in nucleosomes. Recently, nucleosomes have been also shown to act as apoptotic markers in various cancers.¹⁰²

A previous crystallographic study of the interactions of NCP and cisplatin or oxaliplatin revealed that both platinum complexes bound exclusively to DNA despite its lower accessibility in the particle.¹⁰³ Perhaps, the coordination of platinum complexes to histones results in the inhibition of platinum adduct repair. Contrary to platinum-based drugs, RAPTA complexes demonstrated selective binding to the protein rather than the double helix of the DNA fragment (see Figure 14).¹⁰⁰

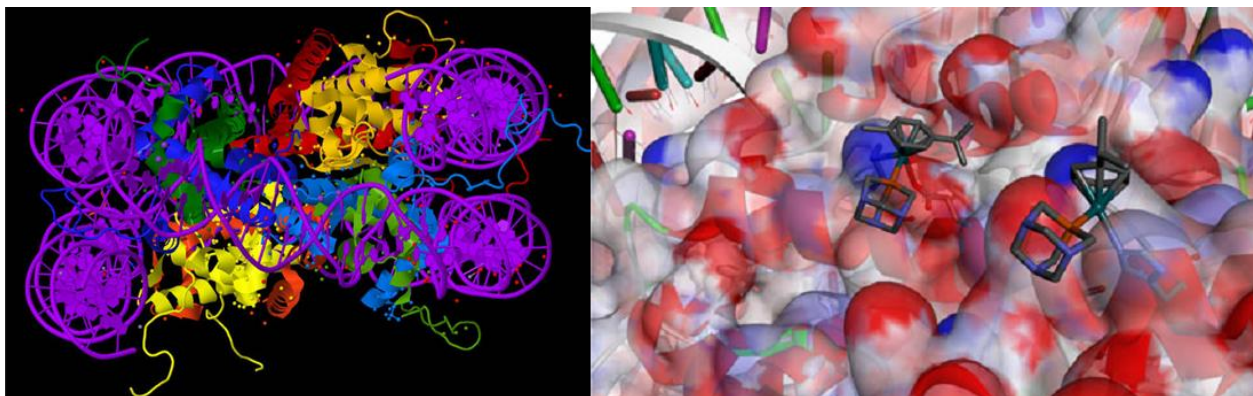


Figure 14. The crystal structure of nucleosome core particle (to the left) and RAPTA-C binding sites (to the right). The picture was taken from a reference ¹⁰⁰.

X-ray diffraction analysis revealed 3 well defined histone binding sites preferential for RAPTA-C coordination. Preferential coordination of histones was confirmed in solution by analysis with SEC-ICP-MS. More than 85% of ruthenium adducts were associated with histone proteins and approximately 5% of the intracellular ruthenium content was detected at chromatin, which supports that nucleosome might be a possible target for RAPTA complexes. The important conclusion is that **chromatin (nucleosome) binding** might be associated with the mode of action of RAPTA-C.

4.4 Advanced proteins era. The role of proteomics in metallodrug research

In order to understand the mode of action of chemotherapeutics, the importance of identification of protein/enzyme targets is undeniable. The routine screening of putative RAPTA-protein interactions is very time-consuming, considering that there is an infinite number of potential biomolecular targets. To find “the needle in the haystack” – the one protein in the cell’s proteome, more advanced analytical and molecular biology techniques should be exploited. Within the last years, metallomics techniques gained popularity to comprehend metallodrug behavior in biological systems. Modern “omics” approaches allow the identification of the target profile of a drug which provides information about its molecular mechanism of action, side effects, fate in biological systems, *etc.* The identification of new targets can potentially lead to unexpected novel therapeutic applications. Contrary to the metal-focused nature of metallomics techniques, the main goal of proteomics is the global analysis of proteins, i.e. their identification, characterization, quantification and comparison. Proteomics methods in

combination with bioinformatic analysis offer a possibility to detect changes in the whole proteome induced by a metallodrug and unravel its molecular mechanisms in the body.

Recently, Messori *et al.* and Wolters *et al.* independently demonstrated the importance of proteomics and metallomics in the evaluation of cancer cell response to RAPTA-T treatment on the protein level.^{98,104}

4.4.1 Protein targets determined by 2D-DIGE

Messori *et al.* used a highly sensitive and advanced technique, namely, **two-dimensional difference in gel electrophoresis (2D-DIGE)** to monitor changes in the expression of intracellular proteins upon cancer cell exposure.¹⁰⁴ 2D-DIGE is a modern highly sensitive proteomics method, which is an advanced version of classical two-dimensional polyacrylamide gel electrophoresis (2D-PAGE). Separation of proteins in 2D-DIGE is performed the same way as in 2D-PAGE; however, different protein samples are labeled with different fluorescent dyes and then mixed together prior to separation. As a result, each protein sample in a mixture can be monitored separately, since different dyes are detected at different wavelengths. The advantage of this method over traditional 2D gel separation is the direct comparison of various samples (healthy/diseased, treated/untreated) in the same gel.

According to the 2D-DIGE method, cancer cells treated with RAPTA-T or NAMI-A were labeled with a cyanine dye and subsequently mixed with control untreated cells labeled with another cyanine dye. After two-dimensional protein separation 2500 protein spots were detected. However, only a small number of protein spots and demonstrated significant up- or down-regulation (the change of spot volume not less than 1.3-fold). Notably, RAPTA-T did not induce significant changes in protein expression profiles. From these experimental results it is evident that cell respond differently to treatment with cisplatin or RAPTA-C in terms of protein expression. Even though in a number of studies both compound classes were shown to have affinity for the same binding sites in proteins, they bind different proteins. As a result, their modes of action are markedly different. Remarkably, contrary to cisplatin, NAMI-A and RAPTA-T shared several protein targets, revealing similarities in their molecular mechanisms.

After the treatment with RAPTA-T, DNA polymerase epsilon subunit 3 (POLE3) was profoundly downregulated, whereas several proteins were significantly upregulated:

- 1) acetyl-CoA acetyltransferase, cytosolic (ACAT2)
- 2) deoxyuridine 5'-triphosphate nucleotidohydrolase, mitochondrial (DUT)
- 3) ubiquitin-conjugating enzyme E2 G1
- 4) omega-amidase (NIT2)
- 5) thymidylate kinase (TMK)
- 6) histidine triad nucleotide-binding protein 1 (HINT1)
- 7) prefoldin subunit 3 (PFD3).

POLE3 is a histone-fold protein which interacts with other histone proteins to bind DNA; in turn, these proteins combine within larger enzymatic complexes for DNA transcription and replication. Possibly, detrimental reduction of POLE3 expression affects DNA replication processes.¹⁰⁵

Deoxyuridine 5'-triphosphate nucleotidohydrolase (DUT) is an essential enzyme for the nucleotide metabolism; it serves as a catalyst for hydrolysis of deoxyuridine triphosphate (dUTP) to pyrophosphate and deoxyuridine monophosphate (dUMP), where the latter is an important prerequisite for DNA replication. The upregulation of this enzyme triggers an increased incorporation of uracyl into DNA which results in an increased excision repair of DNA.

DUT is closely connected with the thymidylate metabolism, since thymidylate synthase (TS) catalyzes dUMP to form thymidylate (TMP). The inhibition of TS leads to the accumulation of dUTP pools, which causes detrimental repair of DNA and consequently, cell death. **Thymidylate kinase (TMK)** is a protein responsible for the conversion of deoxythymidine triphosphate (dTTP) to deoxythymidine diphosphate (dTDP). Overexpression of TMK induces an increase in the cellular dTTP pool. It was shown that downregulation of dTTP during mitosis and the G1 phase is essential for maintaining genetic stability. Therefore, its upregulation caused by RAPTA-T treatment might result in the disruption of mitosis processes.

One of the most interesting hits is **histidine triad nucleotide-binding protein 1 (HINT1)**, since it is involved in the regulation of apoptotic processes and closely associated with p53 expression. RAPTA-C was shown to induce p53 expression upregulation.⁶⁸ This upregulation of HINT1 induced by RAPTA-T treatment once again demonstrates that this compound might interfere with apoptotic pathways of cancer cells.

Omega amidase (NIT2) is a protein, which removes potentially toxic intermediates from cells. Overexpression of a gene leads to cell cycle arrest in the G2 phase.¹⁰⁵

PFD3 has been identified as a binding protein to von Hippel-Lindau gene product (VHL) which acts as a tumor suppressor. It is a chaperone protein involved in folding and unfolding of other proteins. Many chaperones are heat shock proteins which are upregulated as a response to the stress.

To conclude, RAPTA-T did not induce significant modifications of protein expression profile but several proteomic alterations were detected to be substantially different from those caused by cisplatin and similar to those caused by NAMI-A. Clearly, RAPTA-T interferes with metabolic pathways in cells.

4.4.2 Protein targets determined by MudPIT

In order to get further insight on the mode of action of RAPTA complexes, Wolters *et al.* implemented multidimensional protein identification technology (MudPIT).⁹⁸ MudPIT is a bottom-up mass spectrometry approach (for the difference between top-down and bottom-up approach, see Chapter 4.3.4), a non-gel based technique for the separation and identification of individual components in complex protein and peptide mixtures. The separation is established *via* 2D liquid chromatography (reversed-phase and strong cation-exchange) which is hyphenated with ESI tandem mass spectrometry. In comparison with two-dimensional (2D) gel electrophoresis, MudPIT allows greater separation of proteins with high resolution and maximum sensitivity. MudPIT was successfully used for the identification of the binding sites of cisplatin in albumin, transferrin and other abundant serum proteins.⁷⁸ It was found that platinum preferentially coordinated sulfur-containing aminoacids in serum proteins, such as cysteine or methionine. In addition, it coordinated carboxyl and hydroxyl-containing aminoacids. MudPIT enabled detection of platinated tryptic peptides after cisplatin was incubated with *E. coli*. Consequently, highly abundant proteins and enzymes, such as ribosomal proteins, were platinum-enriched. However, several low abundance proteins, which contained platinum, were also detected and assigned to efflux proteins, redox regulators, DNA mismatch repair protein mutS, DNA helicase II and topoisomerase I.¹⁰⁶

Similar experiments were performed with RAPTA-T and 414 proteins localized in various organelles were identified. Consequently, 74 proteins were quantified and 25 of the quantified proteins demonstrated profound up- or down-regulation upon treatment with RAPTA-T. More precisely, proteins were found in endoplasmic reticulum (16), intermediate filament (24) and mitochondria (34), nucleus (88) and cytoskeleton (43). It is worth noting that most identified cytoskeletal proteins serve as constructive elements of cell junctions. This might be one of the reasons for the antimetastatic activity of RAPTA complexes, since the disruption of cell-cell interactions is closely related with metastasis.

It is worth discussing the functions of proteins, which were targeted by RAPTA-T. 87 proteins play a structural role in the organization of the cytoskeleton, namely, in actine crosslink formation or in the cytoskeleton-dependent intracellular transport. 63 proteins are heat shock proteins with 19 of them acting as chaperons. Therefore, they are involved in cellular stress response. 33 proteins are ribonucleoproteins regulating mRNA processes, where two of the proteins are known to act as tumor suppressors (heterogeneous nuclear ribonucleoproteins G). Histones constitute a substantial number of proteins observed in the MudPIT experiment. Markedly, 14 of them were down-regulated upon RAPTA-T treatment, which is an indication of DNA damage signaling. Interestingly, in terms of apoptosis observed results are contradictory, since 11 of the identified proteins contribute to apoptosis, whereas 5 proteins play an anti-apoptotic role. However, none of these proteins were significantly up- or down-regulated. Nucleoprotein TPR (P12270), tropomyosin alpha-3 chain (P06753) and other tropomyosin analogues (B2RDE1, B4DTB1 and B4DVY2) are of particular interest, since these proteins act as proto-oncogenes.

Three up-regulated proteins (ATP synthase subunit beta and its fragment (ATP5B), ATP synthase subunit alpha (ATP5A1)) belong to the group of proteins which serve as structural components of ATP synthase. Their up-regulation might be explained by a high demand of ATP under stress conditions. As it was mentioned above, the majority of the down-regulated proteins belong to the group of histones. The most significant down-regulation upon RAPTA-T treatment was however observed for vimentin proteins (VIM). These proteins belong to a group of cytoskeletal proteins indicating cytoskeleton changes.

A substantial number of proteins was found metallated but was not identified and their functions and localization are unknown. There is a very insignificant overlap of RAPTA-T protein hits with proteins affected by cisplatin yet both metallodrugs share several proteins, such as heterogeneous nuclear ribonucleoproteins C1/C2 (P07910), beta-actin-like protein 2 (Q562R1) and phosphoglycerate kinase (B7Z7A9).

4.5 Modern times. Towards targeted therapy with RAPTA complexes

The results described above show that the mechanism of action of RAPTA compounds is not simple and cannot be explained by the interaction with one particular biomolecule (protein, DNA, enzyme, *etc.*). In order to enhance the selectivity of the complexes, they can be modified with functional groups specific for a chosen biological target. The usual strategy for the development of compounds for a targeted therapeutic is the following: 1) a biological target is chosen, 2) a specific substrate for this target is found, 3) a drug is modified with this substrate and the resulting compound is checked by standard tests (MTT, kinase inhibition activity, *etc.*) to ensure that the modification does not significantly alter its biological activity in comparison with the parent unmodified compounds. After all these steps are accomplished, the studies on the interaction of a novel compound with the biological target are performed.

Modification of each structural moiety of RAPTA complexes has an impact on its biological activity (see Chapter 4.1.3). It appears that the modification of the η^6 -coordinated arene is the most promising for the development of the novel targeted RAPTA complexes. However, a serious drawback of this method is the laborious synthesis of functionalized cyclic dienes, which are common precursors for arene ligands.

4.5.1 Targeting DNA

The X-ray structure of nucleosome core particle evidenced that RAPTA complexes have a strong preference towards proteins over DNA; therefore, the focus of the research implicitly shifted from DNA. Recently the interest on DNA with respect to RAPTA complexes was recovered, when RAPTA complexes were derivatized with a fluorescent naphthalimide moiety capable of intercalating with DNA (see Figure 15).¹⁰⁷ The ligand

was attached to the ruthenium fragment *via* the arene ring; in addition, an imidazole derivative in place of PTA was prepared.

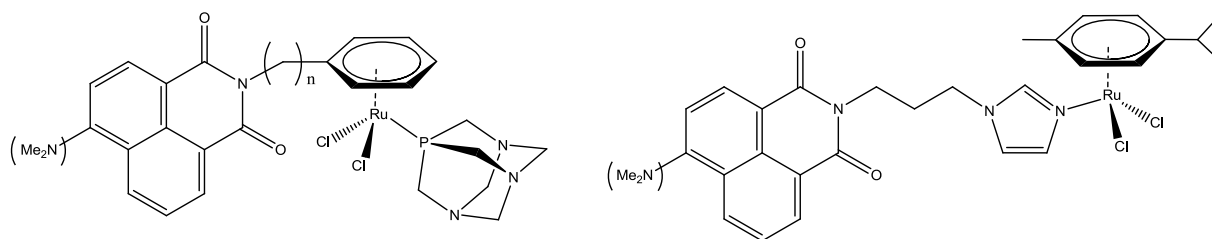


Figure 15. Naphtalimide-tagged RAPTA complex and its imidazole analogue.

The cytotoxicity of the complexes was evaluated with the MTT assay towards standard cisplatin-sensitive and cisplatin-resistant cell lines A2780 and A2780R ovarian carcinoma and compared to RAPTA-C. Human embryonic kidney cells were chosen as a model for healthy cells. All complexes were significantly more active (up to 40 times) than RAPTA-C, however, they were also profoundly toxic. Complexes with the naphthalimide moiety attached to imidazole in place of PTA were nonselective (IC_{50} values of $28.1 \pm 0.8 \mu\text{M}$, $36 \pm 3 \mu\text{M}$ and $36 \pm 3 \mu\text{M}$ for A2780, A2780R and HEK, respectively), whereas complexes with functionalized arene ring were selective to some extent (IC_{50} values = $8.53 \pm 1.41 \mu\text{M}$, $6.89 \pm 1.49 \mu\text{M}$ and $16.61 \pm 1.13 \mu\text{M}$ for A2780, A2780R and HEK, respectively). This indicates that PTA is at list to some degree responsible for the selectivity of the complexes.

It was reported that naphthalene monoimides with amino substituents enhanced the intercalation with DNA.¹⁰⁸ Therefore, one series of RAPTA-naphthalimide conjugates with $-NMe_2$ moieties was prepared, whereas another series comprised RAPTA complexes with an unmodified naphthalimide group. The latter series was markedly less active (up to 3 times), which is in agreement with the intercalation of the naphthalimide fragment of the complexes into DNA. NMR, circular dichroism and UV-vis spectroscopic studies revealed the interaction of the complexes with DNA. It was not possible to confirm DNA intercalation and, most probably, noncovalent interactions dominated over Ru-DNA binding interactions. Upon incubation of ruthenium complexes with an excess of guanosine, Ru-guanosine adducts were also detected by ESI-MS, but to a much smaller extent than for unmodified RAPTA-C. Additionally, the binding of novel complexes to model protein ubiquitin (Ub) was tested by ESI-MS and adducts “Ub + $[(\eta^6\text{-arene})Ru]$ ”, where naphthalimide moiety remained coordinated to ruthenium center, were readily detected. In conclusion, novel naphthalimide-modified complexes were demonstrated to

simultaneously bind to proteins (similarly to other members of RAPTA family) and DNA *via* intercalation.

4.5.2 Targeting glutathione-S-transferase (GST)

Glutathione-S-transferases (GSTs) represent a major group of enzymes responsible for the detoxification of cells from toxic compounds.¹⁰⁹ The key role of glutathione-S-transferases is the catalysis of the thioether bond formation between a reduced form of glutathione and electrophilic xenobiotic substrates for the purpose of their detoxification. The binding site for glutathione called G-site is almost similar in all enzymes of the family. Structural differences occur at the binding site for hydrophobic co-substrate of glutathione (H-site). Increased levels of glutathione are always associated with increased resistance to anticancer drugs. Despite several reported exceptions, high levels of GST are frequently associated with a malignant phenotype and overexpression of this enzyme might be also connected to drug resistance. So far, there is no straightforward evidence in the correlation between participation of GST in detoxification reactions and its role in anticancer drug resistance. Nevertheless, glutathione-S-transferase has been widely exploited as a target for various anticancer drugs, such as ethacrynic acid which is a known GST inhibitor competing for binding to the H-site.

The idea to develop a GST inhibitor based on a RAPTA complex was supported by the fact that ruthenium tends to coordinate cysteine residues of proteins and they are easily accessible on the surface of GST enzymes (*e.g.*, Cys47 and Cys101 in GST P1-1). As a result, the RAPTA fragment was tethered to ethacrynic acid *via* its α -acetic functionality so that the phenolic fragment mainly responsible for its inhibitory activity could assess the H-site and ruthenium could simultaneously coordinate Cys residues. A series of RAPTA-ethacrynic acid complexes was prepared, where an acid was attached either to the arene ring or through imidazole coordinated to the ruthenium center instead of a PTA ligand (see Figure 16).^{18,110} Their anticancer activity was evaluated in A2780 and A2780cisR ovarian carcinoma cell lines. Ruthenium complexes were highly efficient in inhibiting the growth of both cell lines and about 5-times more potent than ethacrynic acid.

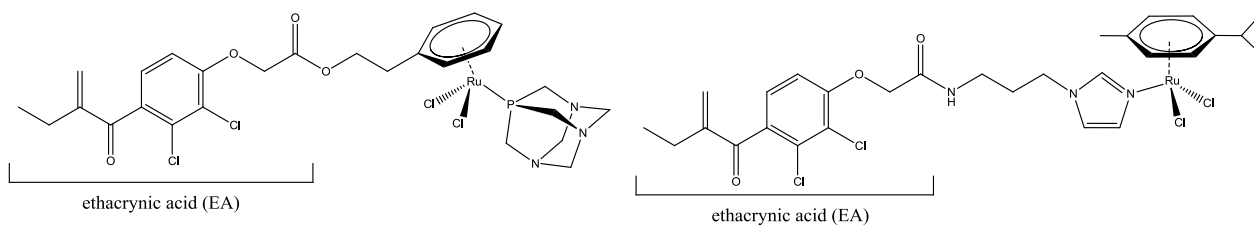


Figure 16. RAPTA-ethacrynic acid conjugate and its imidazole analogue.

Furthermore, the enzyme inhibitory activity of the novel complexes was measured using GST P1-1 and its cysteine-modified mutants. Whereas unmodified RAPTA complexes did not show any inhibitory effect, RAPTA-EA conjugates were similarly potent to uncoordinated ethacrynic acid. However, in contrast to ethacrynic acid, treatment with the modified RAPTA complex caused almost complete inhibition of GST P1-1 activity (residual activity less than 5% contrary to 20% residual activity for EA) under the same experimental conditions. Moreover, the inhibition of glutathione-S-transferase by RAPTA-EA conjugates (1.6 min) was significantly more rapid than by an uncoordinated EA (12 min). To prove that Ru center increases the inhibitory activity by coordinating cysteine residues exposed on the surface of the enzyme, similar experiments were performed with GST P1-1 mutants, where cysteine residues were replaced with serines. As expected, the inhibitory activity of the complexes diminished up to 4.5 times. This is an important finding, since it evidences the involvement of Cys101 and Cys47 in the activity of the enzyme and the effect of these enzyme fragments on RAPTA complexes. The nature of RAPTA-GST adducts was determined by ESI-QToF-MS. It was shown that upon incubation multiple covalent products formed with a retained or cleaved EA ligand. Both ethacrynic acid and its RAPTA conjugate disclosed preference for Cys47 rather than Cys101. Additionally, competitive inhibition experiments were performed using GST P1-1 wild type, which revealed that the complexes are non-competitive towards GSH. This result, which was also supported by a crystal structure,¹¹¹ indicates the preferential binding of the complexes at the catalytic H-site rather than G-site. There was also excellent correlation between the ability of novel complexes to inhibit cancer cell growth and GST activity and therefore, GST might indeed be a potential intracellular target of the modified RAPTA complexes.

4.5.3 Targeting human serum albumin (HSA). Exploiting the EPR effect.

The idea of developing drugs targeting HSA originates from the fact that such macromolecules may penetrate tumor tissue due to the **enhanced permeability and retention (EPR) effect**.¹¹² It is also known that macro-molecular substances are

retained in solid tumors, whereas low-molecular-weight compounds are returned back to circulating blood by diffusion. The EPR effect is a phenomenon which results from the unique characteristics of solid tumors, such as extensive, but defective angiogenesis, damaged lymphatic drainage/recovery system and increased number of permeability receptors. The EPR effect provides great opportunities for selective targeting of macromolecule-conjugated drugs.

One of the possibilities to target a certain protein is to involve its amino functionalities, such as lysine residues or N-terminal amino acids. However, such targeting will be non-specific, since most of the proteins generally carry a significant number of these functions. An attractive alternative is a highly nucleophilic thiol group of cysteines, which are not frequently detected in the free state but HSA features such a group with Cys34.

One group of reagents known to specifically target cysteines with the formation of stable thioether bonds is a group of various N-substituted maleimides. Therefore, numerous metal-based drugs were modified with a maleimide group.¹¹³ Subsequently, RAPTA complexes with maleimide moiety were prepared and its anticancer activity was tested against human cancer cell lines and compared to RAPTA-C (see Figure 17).¹¹⁴ The derivatization did not markedly alter the activity of the complex in the SW480 cell line but a 2.5-fold increase of cytotoxicity on the chemosensitive CH1 cell line was observed. It was shown that biomolecules, such as cysteine and glutathione (a cysteine-rich biomolecule) were selective towards the maleimide functionality and binding was not influenced by hydrolysis of the ruthenium center. The reaction with HSA by means of SEC-ICP-MS was studied and after 72 hours the majority of ruthenium was found in the HSA-containing fraction. Albumin reactivity was profoundly lower compared to small molecules; however, it should be noted that RAPTA-C also reacted to HSA to a smaller extent than to other serum proteins.⁷⁵

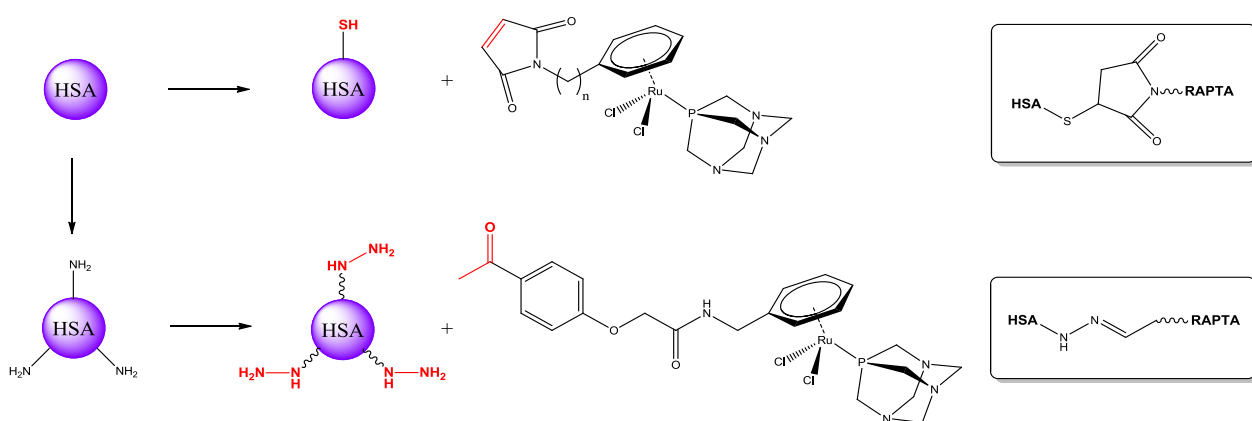


Figure 17. Strategy for tagging RAPTA complexes to human serum albumin (HSA) via

the formation of thioether bond (upper box) or hydrazone bond (lower box). Functional groups involved in derivatization are marked in red.

Another possible strategy to attach RAPTA to HSA is to form hydrazone bonds using an aldehyde and hydrazine.⁹⁶ The advantage of this approach is the high lability of hydrazone bonds under acidic conditions, and hence, a selective release of the bioactive moiety in the acidic environment of cancer cells. HSA contains numerous lysine residues, which can be modified with hydrazine functionalities *via* standard coupling procedures (e.g., using succinyl HCl terephthalic hydrazine linker). The RAPTA fragment was modified with an aldehyde group and subsequently incubated with HSA-hydrazine. It was determined by means of MALDI-ToF MS that each molecule of modified human serum albumin contains up to four RAPTA moieties. Notably, a remarkable improvement of the biological activity was observed, since an HSA-RAPTA conjugate was markedly cytotoxic in A2780 ovarian carcinoma cells with the IC₅₀ values being more than 20-times lower than for the parent RAPTA complex (11 and >300 μM, respectively). It is worth noting that conjugation of the protein and metal-based complex *via* ester bonds may not result in a similar improvement of cytotoxicity, since this bond can be hydrolyzed before cellular uptake.

4.5.4 Metallodendrimers. Further exploiting the EPR effect.

Attachment of metal complexes to dendritic scaffolds is another possibility to take advantage of the EPR effect. Metallodendrimers are multinuclear and highly branched molecules with a central core and well-defined molecular structure. Another advantage of dendrimer-drug conjugates is their multivalency, which might possibly lead to enhanced interactions with biological targets. A number of organic drugs were derivatized with various dendritic and polymeric structures, which significantly enhanced the uptake of drugs into tumor cells and increased their cytotoxicity. Numerous studies on the modification of cisplatin with dendritic structures have also been reported.^{115,116} Consequently, the effect of the attachment of dendrimers to arene complexes (iridium, rhodium, platinum, *etc.*) on their biological properties was investigated.¹¹⁷⁻¹²⁰ However, till recently the examples of metallodendrimers based on ruthenium(II) and osmium(II) arene fragments were scarce. Smith *et al.* investigated the formation of conjugates of dendrimers with ruthenium and osmium arene complexes (including RAPTA complexes), *i.e.* prepared several series of half-sandwich complexes with functionalized

poly(propyleneimine) dendrimer scaffolds and evaluated their antiproliferative properties (see Figure 18).¹²⁰⁻¹²²

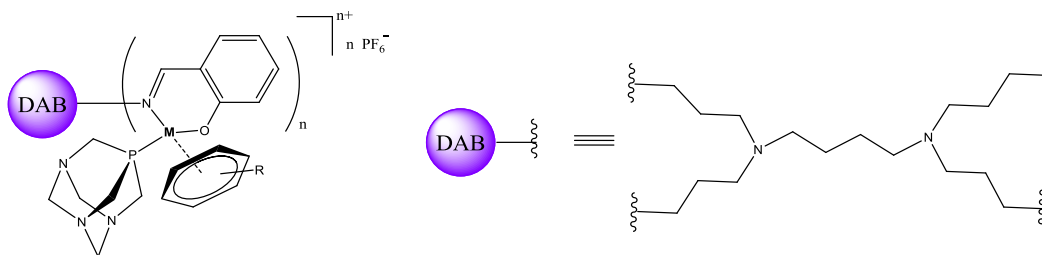


Figure 18. Example of metallodendrimers with PTA moiety (DAB = 1,4-diaminobutane dendrimer; M =Ru, Os; n= 4, 8, 16, 32).

All complexes showed a clear correlation between their size and cytotoxicity, with the cytotoxicity increasing with the size of the dendrimer. Mononuclear ruthenium and osmium compounds were significantly less cytotoxic than their structurally similar dendritic analogues, and the highest cytotoxicity was observed for the fourth generation metallodendrimers, containing 32 peripheral Ru(arene)(PTA) fragments. Some of the complexes were more cytotoxic than cisplatin in cisplatin-sensitive cells and significantly more cytotoxic than cisplatin in the cisplatin-resistant variant, which indicates that their modes of action do not overlap. The nature or the metal did not influence the cytotoxicity significantly but the presence of a PTA ligand is important, since it brings some selectivity toward tumor cells relative to healthy HEK cells, which is in agreement with previously described structure-activity relationships. The binding of different metallodendrimers to plasmid DNA was studied by gel electrophoresis. Cationic metallodendrimers displayed higher cytotoxicity and reactivity towards DNA than neutral compounds, probably due to enhanced electrostatic interactions between complexes and negatively charged phosphate groups of DNA. Notably, in contrast to mononuclear ruthenium complexes which did not interact with DNA, some ruthenium metallodendrimers bound to DNA even more effectively than cisplatin,¹²² probably, due to the close proximity of metal centers and their cumulative effect. However, this hypothesis has to be further validated.

4.5.5 RAPTA complexes with thermomorphic properties.

RAPTA complexes with triphenylphosphine ligands functionalized with perfluorinated chains $[\text{Ru}(\eta^6\text{-arene})(\text{PTA})(\text{PR}_3)\text{Cl}]\text{BF}_4$ were investigated for their thermomorphic properties, that is, these complexes were expected to change their properties (e.g.

solubility) in heated tumors.¹²³ In course of thermotherapy, a tumor undergoes local heating, which results in the disordered structure and subsequent damage of tumor cells, whereas healthy highly organized cells dissipate the heat.¹²⁴ Thermotherapy can be used in combination with thermoresponsive compounds which can aggregate only in the heated tumors resulting in a higher accumulation of drugs in cancer cells.

Phosphines of the general formula $\text{PPh}_x\text{R}_{3-x}$ ($x= 0-3$), where R is $p\text{-C}_6\text{H}_4\text{C}_2\text{H}_4\text{C}_8\text{F}_{17}$, are well-known thermomorphing compounds, since their solubility significantly increases upon heating. It was demonstrated that the solubility of several modified RAPTA complexes was indeed temperature-dependent, since it increased 4-times upon heating from 37 °C to 42 °C. The new complexes were more cytotoxic than RAPTA-C and interestingly, a PTA ligand only slightly affected the cytotoxicity, whereas the nature of the fluorophosphine ligand appeared to be important. The antiproliferative activity of the complex with one perfluorinated chain ($\text{PPh}_2(p\text{-C}_6\text{H}_4\text{C}_2\text{H}_4\text{C}_8\text{F}_{17})$) was 6 μM , whereas the corresponding free ligand was inactive. Moreover, it was not released by the complex in aqueous solution. Presumably, the observed effect might be related to the increased uptake of the lipophilic fluorinated ligand by cells. The complexes, which were poorly soluble at 37 °C revealed a higher activity at elevated temperature (42 °C) due to the increased solubility and subsequent facilitated uptake within the cell medium and in the cell itself. To the best of our knowledge, this is the first example of specifically designed metal-based compounds with thermomorphing properties.

4.5.6 Fluorescent postlabeling.

Recently, Ang *et al.* developed a water-soluble acetal-functionalized RAPTA-probe for selective postlabeling.¹²⁵ The method is based on the specific properties of diacetal compounds, which are able to converse into aldehydes under mild conditions and subsequently react with hydroxylamines *via* oxime coupling. According to the proposed workflow, cells treated with diethylacetal-RAPTA are fixed and activated by aqueous HCl solution, and consequently formed aldehyde species are conjugated with a hydroxylamine-functionalized fluorophore (see Figure 19). Consequently, HEK cells incubated with the RAPTA probe were visualized with AlexaFluor488 hydroxylamine fluorophore. It was demonstrated that the metal complex was successfully taken up into cells.

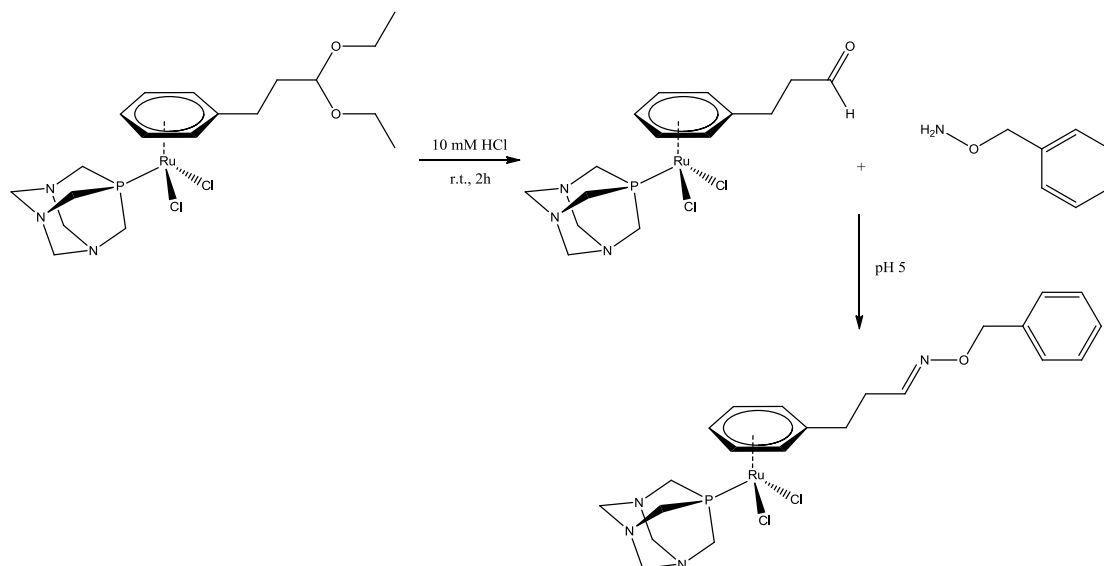


Figure 19. Example of postlabeling of a RAPTA probe with fluorescent *o*-benzylhydroxylamine.

4.5.7 Metallacages. Multifunctional drugs.

The group of Therrien *et al.* proposed a very elegant solution for the targeted delivery and subsequent release of active compounds to diseased cells.¹²⁶⁻¹²⁸ They encapsulated pyrenyl-functionalized RAPTA complexes in the water-soluble ruthenium metallacage $[\text{Ru}_6(\eta^6\text{-}p\text{-cymene})_6(\text{tpt})_2(\text{donq})_3]^{6+}$, where $\text{tpt} = 2,4,6\text{-tri-(pyridine-4-yl)-1,3,5-triazine}$; $\text{donq} = 5,8\text{-dioxido-1,4-naphthoquinolate}$ (see Figure 20).¹²⁸ The advantage of this approach is a combination of multiple factors comprising simultaneous interaction with DNA and proteins, improved delivery of the cages through the EPR effect and subsequent release of drugs once inside the cells.

The derivatization of RAPTA complexes with a pyrenyl derivative has a similar effect as their modification with a naphthalimide moiety (see section “Targeting DNA”, Chapter 4.5.1). These moieties intercalate between DNA base pairs and interfere with transcription processes. Therefore, in addition to the protein binding, a RAPTA complex modified with a pyrenyl functionality is able to simultaneously interact with DNA. The pyrenyl fragment was attached to the RAPTA moiety *via* amide, ester or ether bonds, which have different stability in tumor cells and therefore might have an effect on the cytotoxicity of the complexes. Notably, the most stable ether derivative showed the highest activity with reference to RAPTA-C.

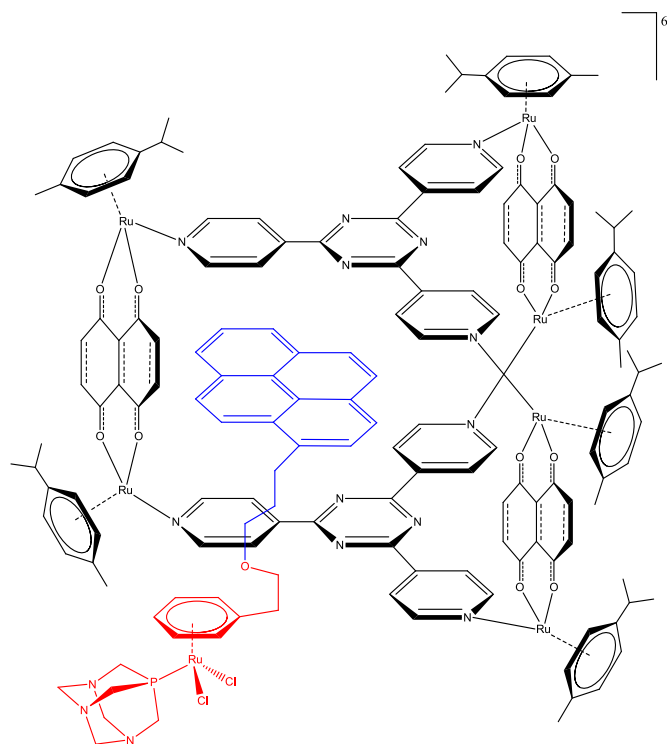


Figure 21. RAPTA derivative encapsulated in the ruthenium metallacage.

It was shown that loaded cages were similarly cytotoxic to free cages which is significantly higher than that of free RAPTA complexes (in A2780 cell line, the IC_{50} values for the pyrenyl-amide-RAPTA complex, empty and loaded cages were $>25 \mu\text{M}$, $3.4 \pm 0.6 \mu\text{M}$ and $3.1 \pm 1.0 \mu\text{M}$, correspondingly). In order to deduce the correlation between the activity of the complexes and their intracellular accumulation, cellular uptake studies were performed by means of fluorescent measurements in HeLa cervix cancer cells. It is known that compounds containing a pyrenyl moiety are highly fluorescent. Upon encapsulation into the cage the fluorescence was quenched.^{127,128} After incubation of cells with a pyrenyl-RAPTA complex, an empty and a loaded cage, interesting results were observed. Whereas cells incubated with the empty cage presented marginal fluorescence to be detected, cells with the complex or loaded cage displayed intense fluorescence. The signal for the loaded cage was stronger than for the complex itself, suggesting a higher uptake of the loaded cage by HeLa cells. Notably, the fluorescence signal of the cells incubated with a loaded cage revealed the same intensity as in the case of an empty cage. However, in the course of time the fluorescence intensity markedly increased, indicating the successful release of a guest compound. In conclusion, it was demonstrated that water-soluble metallacages serve as molecular missiles, which selectively deliver and release RAPTA complexes into cancer cells.

4.6 New era. Conclusions. What comes next?

More than one decade passed since 2001 when the first communication about RAPTA-C was published. However, till now the interest in RAPTA compounds has not faded and keeps growing. One of the most promising compounds of this family, which will possibly enter clinical trials, is a RAPTA complex functionalized with ethacrynic acid acting as an effective inhibitor of glutathione-S-transferase.

From the results described above it is clear that RAPTA complexes display a number of advantages over traditional drugs, *e.g.* cisplatin. The main drawbacks of cisplatin are severe toxicity and resistance in a number of cells which result from the lack of discrimination between cancer and healthy cells and appear connected with DNA binding. Ruthenium complexes are in general significantly less toxic than platinum complexes, since they are more selectively delivered to cancer cells and preferentially bind to proteins. One possible explanation for the low toxicity of RAPTA complexes is their rapid binding to serum proteins upon their administration and subsequent slow release to cells in small portions; however, this hypothesis requires additional investigations.

Notably, it was demonstrated that RAPTA complexes were active in cisplatin-resistant cell lines indicating that the mechanisms of action of the two classes of compounds are different. RAPTA complexes might overcome cisplatin resistance of cancer cells through a number of mechanisms:

- 1) It is believed that the interactions with mitochondrial proteins are essential for the activity of cisplatin, since blocking of release of mitochondrial proteins into cytosol is closely associated with cisplatin resistance (Chapter 3.2).⁷ However, in mitochondria of cisplatin-resistant cells, platinum was not detected. In contrast, the incubation of RAPTA complexes with cisplatin-resistant cells resulted in ruthenium accumulation in mitochondria (Chapter 4.3.9).⁹⁸
- 2) One of the reasons for drug resistance is the avoidance of drug-triggered apoptosis established by over-expression of bcl-2 or decreased expression of bax and p21, mediated by p53. The treatment of cancer cells with RAPTA complexes resulted in the decrease of bcl-2 with a simultaneous increase of bax and p21 levels.⁶⁸ Additionally, RAPTA-C significantly up-regulated the tumor suppression protein p53 (Chapter 4.1.4).

- 3) Another reason for drug resistance is the inactivation of the drugs by cellular defense mechanisms. It was shown that both RAPTA complexes and cisplatin react with glutathione and metallothioneins but RAPTA complexes react with metallothioneins to a much smaller extent and its release from adducts with glutathione and metallothioneins is much slower (Chapter 4.3.6).^{90 77}

The antimetastatic activity of RAPTA complexes might be associated with

- 1) Antiangiogenic properties. An important component of the metastatic pathway is angiogenesis, since new blood vessels formed during the process of angiogenesis provide possibilities for cancer cells to leave the primary tumor and enter the blood- or lymphstream (Figure 2). RAPTA complexes were demonstrated to be effective angiogenesis inhibitors (Chapter 4.1.4).⁶⁹
- 2) Matrix metalloproteinases (MMP). MMP inhibitors inhibit cell migration, which is closely related to metastasis. It was shown that RAPTA-T caused significantly down-regulation of MMP (Chapter 4.1.4).⁶⁷
- 3) Cytoskeletal proteins. Cytoskeletal proteins are essential for metastatic processes, since they regulate the motility of cells.⁹⁸ Upon incubation of RAPTA complexes with cancer cells, ruthenium was detected in cytoskeletal and membranes fraction, revealing interactions with structural cell components (Chapter 4.3.9).
- 4) Cathepsin B. Inhibition of cat B results in reduced cell mobility and diminished invasiveness *in vitro*. It was demonstrated that RAPTA compounds are effective inhibitors of cat B in the low micromolar range (Chapter 4.3.2).⁵⁶

Despite the extensive research on RAPTA compounds, as well as on other metal-based drugs with antiproliferative activity, their molecular targets often remain elusive, which limits the design of next-generation targeted derivatives. A more complete picture of the interactions of metallodrugs with cellular targets would help to improve the understanding of their modes of action. Therefore, it was aimed within this PhD project to develop a test system which allows for determination of the 'natural' target profile of metallodrugs, *i.e.*, the identification of selective binding partners of metallodrugs in a mixture of potential targets.

Secondly, despite several approaches towards targeted therapy with RAPTA complexes (Chapter 4.5), the role of vitamin receptors had not been investigated yet. Therefore,

RAPTA complexes with biotin ligands were developed to specifically target cancer cells with an overexpressed level of the sodium multivitamin transporter.

Finally, since Ru^{II}(arene) complexes interact with a wide range of proteins in a non-specific way (Chapter 4.4, 4.4), structure-activity relationships were established for novel non-specifically targeting ruthenium compounds, namely Ru^{II}(arene) complexes with am(m)ine ligands. In the course of investigations of interactions of Ru^{II}(am(m)ine) complexes with proteins by means of mass spectrometry, we discovered that the efficiency of detecting adducts was dependent on the mass analyzer of the mass spectrometer. Therefore, the impact of the mass analyzer on the adduct formation of metallodrugs towards proteins was explored.

5. References

- [1] L. Pecorino, *Molecular biology of cancer: mechanisms, targets, and therapeutics*, third ed., Oxford University Press, Oxford, 2012.
- [2] D. Lobo, *Biology of cancer*, Second ed., Pearson, 2012.
- [3] D. Hanahan, R. A. Weinberg, *Cell (Cambridge, MA, U. S.)* 2011, 144, 646-674.
- [4] R. M. Bremnes, K. Andersen, E. A. Wist, *Eur J Cancer* 1995, 31A, 1955-1959.
- [5] G. F. Weber, *Cancer Lett* 2013, 328, 207-211.
- [6] P. Heffeter, U. Jungwirth, M. Jakupec, C. Hartinger, M. Galanski, L. Elbling, M. Micksche, B. Keppler, W. Berger, *Drug Resistance Updates* 2008, 11, 1-16.
- [7] X. Yang, J. Wang, Y. Zhou, Y. Wang, S. Wang, W. Zhang, *Cancer Lett. (N. Y., NY, U. S.)* 2012, 321, 137-143.
- [8] B. Serli, E. Zangrando, T. Gianferrara, C. Scolaro, P. J. Dyson, A. Bergamo, E. Alessio, *Eur. J. Inorg. Chem.* 2005, 3423-3434.
- [9] aD. C. Ware, W. R. Wilson, W. A. Denny, C. E. F. Richard, *J. Chem. Soc., Chem. Commun.* 1991, 1171-1173; bJ. Y.-C. Chang, G.-L. Lu, R. J. Stevenson, P. J. Brothers, G. R. Clark, K. J. Botting, D. M. Ferry, M. Tercel, W. R. Wilson, W. A. Denny, D. C. Ware, *Inorg. Chem.* 2013, 52, 7688-7698.
- [10] aW. H. Ang, I. Khalaila, C. S. Allardyce, L. Juillerat-Jeanneret, P. J. Dyson, *J. Am. Chem. Soc.* 2005, 127, 1382-1383; bH. Baruah, C. G. Barry, U. Bierbach, *Curr. Top. Med. Chem. (Sharjah, United Arab Emirates)* 2004, 4, 1537-1549.
- [11] aH. Hagen, P. Marzenell, E. Jentzsch, F. Wenz, M. R. Veldwijk, A. Mokhir, *J. Med. Chem.* 2012, 55, 924-934; bP. Marzenell, H. Hagen, L. Sellner, T. Zenz, R. Grinyte, V. Pavlov, S. Daum, A. Mokhir, *J. Med. Chem.* 2013, 56, 6935-6944; cA. Mokhir, H. Hagen, P. Marzenell, E. Jentzsch, M. Veldwijk, Ruprecht-Karls-Universitaet Heidelberg, Germany . 2012, p. 45pp.
- [12] T. W. Failes, C. Cullinane, C. I. Diakos, N. Yamamoto, J. G. Lyons, T. W. Hambley, *Chem. - Eur. J.* 2007, 13, 2974-2982.
- [13] E. Meggers, G. E. Atilla-Gokcumen, H. Bregman, J. Maksimoska, S. P. Mulcahy, N. Pagano, D. S. Williams, *Synlett* 2007, 1177-1189.
- [14] A. L. Harris, X. Yang, A. Hegmans, L. Povirk, J. J. Ryan, L. Kelland, N. P. Farrell, *Inorg. Chem.* 2005, 44, 9598-9600.
- [15] A. Nguyen, A. Vessieres, E. A. Hillard, S. Top, P. Pigeon, G. Jaouen, *Chimia* 2007, 61, 716-724.
- [16] S. J. Dougan, A. Habtemariam, S. E. McHale, S. Parsons, P. J. Sadler, *Proc. Natl. Acad. Sci. U. S. A.* 2008, 105, 11628-11633.
- [17] J. J. Soldevila-Barreda, P. C. A. Bruijninx, A. Habtemariam, G. J. Clarkson, R. J. Deeth, P. J. Sadler, *Organometallics* 2012, 31, 5958-5967.
- [18] M. C. DeRosa, R. J. Crutchley, *Coord. Chem. Rev.* 2002, 233-234, 351-371.
- [19] J.-P. Lecomte, A. Kirsch-De Mesmaeker, M. M. Feeney, J. M. Kelly, *Inorg. Chem.* 1995, 34, 6481-6491.
- [20] aC. Lottner, K.-C. Bart, G. Bernhardt, H. Brunner, *J. Med. Chem.* 2002, 45, 2064-2078; bC. Lottner, K.-C. Bart, G. Bernhardt, H. Brunner, *J. Med. Chem.* 2002, 45, 2079-2089.
- [21] S. Dhar, S. J. Lippard, Wiley-VCH Verlag GmbH & Co. KGaA, 2011, pp. 79-95.
- [22] Y. K. Yan, M. Melchart, A. Habtemariam, P. J. Sadler, *Chem. Commun. (Cambridge, U. K.)* 2005, 4764-4776.
- [23] aC. G. Hartinger, M. A. Jakupec, S. Zorbas-Seifried, M. Groessler, A. Egger, W. Berger, H. Zorbas, P. J. Dyson, B. K. Keppler, *Chemistry & Biodiversity* 2008, 5, 2140-2155; bC. G. Hartinger, S. Zorbas-Seifried, M. A. Jakupec, B. Kynast, H. Zorbas, B. K. Keppler, *Journal of Inorganic Biochemistry* 2006, 100, 891-904.
- [24] E. Alessio, G. Mestroni, A. Bergamo, G. Sava, *Curr. Top. Med. Chem. (Sharjah, United Arab Emirates)* 2004, 4, 1525-1535.
- [25] aW. H. Ang, *Chimia* 2007, 61, 140-142; bW.-H. Ang, A. Casini, G. Sava, P. J. Dyson, *J. Organomet. Chem.* 2011, 696, 989-998.
- [26] aM. A. Jakupec, B. K. Keppler, *Curr. Top. Med. Chem. (Sharjah, United Arab Emirates)* 2004, 4, 1575-1583; bM. A. Jakupec, B. K. Keppler, *Met Ions Biol Syst* 2004, 42, 425-462; cA. R. Timerbaev, *Metallomics* 2009, 1, 193-198.
- [27] N. P. E. Barry, P. J. Sadler, *Chem. Commun. (Cambridge, U. K.)* 2013, 49, 5106-5131.
- [28] T. Gianferrara, I. Bratsos, E. Alessio, *Dalton Trans.* 2009, 7588-7598.
- [29] A. A. Adeniyi, P. A. Ajibade, *J. Mol. Model.* 2013, 19, 1325-1338.
- [30] S. Bolano, G. Ciancaleoni, J. Bravo, L. Gonsalvi, A. Macchioni, M. Peruzzini, *Organometallics* 2008, 27, 1649-1652.
- [31] C. S. Allardyce, P. J. Dyson, D. J. Ellis, S. L. Heath, *Chemical Communications (Cambridge)* 2001, 1396-1397.

- [32] C. S. Allardyce, P. J. Dyson, D. J. Ellis, P. A. Salter, R. Scopelliti, *J. Organomet. Chem.* 2003, 668, 35-42.
- [33] Y. Zhang, Z. Guo, X.-Z. You, *J. Am. Chem. Soc.* 2001, 123, 9378-9387.
- [34] M. Groessl, C. G. Hartinger, P. J. Dyson, B. K. Keppler, *J. Inorg. Biochem.* 2008, 102, 1060-1065.
- [35] F. Wang, H. Chen, S. Parsons, I. D. H. Oswald, J. E. Davidson, P. J. Sadler, *Chem. - Eur. J.* 2003, 9, 5810-5820.
- [36] aC. Scolaro, A. Bergamo, L. Brescacin, R. Delfino, M. Cocchietto, G. Laurency, T. J. Geldbach, G. Sava, P. J. Dyson, *J. Med. Chem.* 2005, 48, 4161-4171; bC. Scolaro, C. G. Hartinger, C. S. Allardyce, B. K. Keppler, P. J. Dyson, *J. Inorg. Biochem.* 2008, 102, 1743-1748.
- [37] C. Gossens, A. Dorcier, P. J. Dyson, U. Rothlisberger, *Organometallics* 2007, 26, 3969-3975.
- [38] A. E. Egger, C. G. Hartinger, A. K. Renfrew, P. J. Dyson, *JBIC, J. Biol. Inorg. Chem.* 2010, 15, 919-927.
- [39] C. Gossens, I. Tavernelli, U. Rothlisberger, *J. Am. Chem. Soc.* 2008, 130, 10921-10928.
- [40] A. K. Renfrew, A. D. Phillips, E. Tapavicza, R. Scopelliti, U. Rothlisberger, P. J. Dyson, *Organometallics* 2009, 28, 5061-5071.
- [41] aB. Dutta, C. Scolaro, R. Scopelliti, P. J. Dyson, K. Severin, *Organometallics* 2008, 27, 1355-1357; bA. Romerosa, T. Campos-Malpartida, C. Lidrissi, M. Saoud, M. Serrano-Ruiz, M. Peruzzini, J. A. Garrido-Cardenas, F. Garcia-Maroto, *Inorg. Chem.* 2006, 45, 1289-1298.
- [42] aA. Dorcier, W. H. Ang, S. Bolano, L. Gonsalvi, L. Juillerat-Jeannerat, G. Laurency, M. Peruzzini, A. D. Phillips, F. Zanolini, P. J. Dyson, *Organometallics* 2006, 25, 4090-4096; bA. Dorcier, P. J. Dyson, C. Gossens, U. Rothlisberger, R. Scopelliti, I. Tavernelli, *Organometallics* 2005, 24, 2114-2123; cA. K. Renfrew, A. D. Phillips, A. E. Egger, C. G. Hartinger, S. S. Bosquain, A. A. Nazarov, B. K. Keppler, L. Gonsalvi, M. Peruzzini, P. J. Dyson, *Organometallics* 2009, 28, 1165-1172; dA. Casini, C. Gabbiani, F. Sorrentino, M. P. Rigobello, A. Bindoli, T. J. Geldbach, A. Marrone, N. Re, C. G. Hartinger, P. J. Dyson, L. Messori, *J. Med. Chem.* 2008, 51, 6773-6781.
- [43] aA. Casini, F. Edefe, M. Erlandsson, L. Gonsalvi, A. Ciancetta, N. Re, A. Ienco, L. Messori, M. Peruzzini, P. J. Dyson, *Dalton Trans.* 2010, 39, 5556-5563; bA. Dorcier, C. G. Hartinger, R. Scopelliti, R. H. Fish, B. K. Keppler, P. J. Dyson, *Journal of Inorganic Biochemistry* 2008, 102, 1066-1076.
- [44] C. Scolaro, T. J. Geldbach, S. Rochat, A. Dorcier, C. Gossens, A. Bergamo, M. Cocchietto, I. Tavernelli, G. Sava, U. Rothlisberger, P. J. Dyson, *Organometallics* 2006, 25, 756-765.
- [45] D. N. Akbayeva, L. Gonsalvi, W. Oberhauser, M. Peruzzini, F. Vizza, P. Brueggeller, A. Romerosa, G. Sava, A. Bergamo, *Chem. Commun. (Cambridge, U. K.)* 2003, 264-265.
- [46] W. H. Ang, E. Daldini, C. Scolaro, R. Scopelliti, L. Juillerat-Jeannerat, P. J. Dyson, *Inorg. Chem.* 2006, 45, 9006-9013.
- [47] C. A. Vock, A. K. Renfrew, R. Scopelliti, L. Juillerat-Jeanneret, P. J. Dyson, *European Journal of Inorganic Chemistry* 2008, 1661-1671.
- [48] C. Scolaro, A. B. Chaplin, C. G. Hartinger, A. Bergamo, M. Cocchietto, B. K. Keppler, G. Sava, P. J. Dyson, *Dalton Trans.* 2007, 5065-5072.
- [49] A. K. Renfrew, A. E. Egger, R. Scopelliti, C. G. Hartinger, P. J. Dyson, *C. R. Chim.* 2010, 13, 1144-1150.
- [50] I. Berger, M. Hanif, A. A. Nazarov, C. G. Hartinger, R. O. John, M. L. Kuznetsov, M. Groessl, F. Schmitt, O. Zava, F. Biba, V. B. Arion, M. Galanski, M. A. Jakupc, L. Juillerat-Jeanneret, P. J. Dyson, B. K. Keppler, *Chemistry--A European Journal* 2008, 14, 9046-9057.
- [51] A. A. Nazarov, J. Risse, W. H. Ang, F. Schmitt, O. Zava, A. Ruggi, M. Groessl, R. Scopelliti, L. Juillerat-Jeanneret, C. G. Hartinger, P. J. Dyson, *Inorg. Chem.* 2012, 51, 3633-3639.
- [52] A. Bergamo, A. Masi, P. J. Dyson, G. Sava, *Int. J. Oncol.* 2008, 33, 1281-1289.
- [53] S. Chatterjee, S. Kundu, A. Bhattacharyya, C. G. Hartinger, P. J. Dyson, *JBIC, J. Biol. Inorg. Chem.* 2008, 13, 1149-1155.
- [54] P. Nowak-Sliwinska, B. J. R. van, A. Casini, A. A. Nazarov, G. Wagnieres, d. B. H. van, P. J. Dyson, A. W. Griffioen, *J. Med. Chem.* 2011, 54, 3895-3902.
- [55] M. Groessl, Y. O. Tsybin, C. G. Hartinger, B. K. Keppler, P. J. Dyson, *JBIC, J. Biol. Inorg. Chem.* 2010, 15, 677-688.
- [56] A. Ratanaphan, P. Temboot, P. J. Dyson, *Chem. Biodiversity* 2010, 7, 1290-1302.
- [57] P. J. Dyson, G. Sava, *Dalton Trans.* 2006, 1929-1933.
- [58] A. Casini, G. Mastrobuoni, W. H. Ang, C. Gabbiani, G. Pieraccini, G. Moneti, P. J. Dyson, L. Messori, *ChemMedChem* 2007, 2, 631-635.
- [59] A. Casini, C. Gabbiani, E. Michelucci, G. Pieraccini, G. Moneti, P. J. Dyson, L. Messori, *JBIC, J. Biol. Inorg. Chem.* 2009, 14, 761-770.
- [60] M. Groessl, M. Terenghi, A. Casini, L. Elviri, R. Lobinski, P. J. Dyson, *J. Anal. At. Spectrom.* 2010, 25, 305-313.
- [61] F. Mendes, M. Groessl, A. A. Nazarov, Y. O. Tsybin, G. Sava, I. Santos, P. J. Dyson, A. Casini, *J. Med. Chem.* 2011, 54, 2196-2206.
- [62] A. Casini, A. Karotki, C. Gabbiani, F. Rugi, M. Vasak, L. Messori, P. J. Dyson, *Metallomics* 2009, 1, 434-441.

- [63] M. Groessl, C. G. Hartinger, *Analytical and Bioanalytical Chemistry* 2013, 405, 1791-1808.
- [64] S. Gromer, S. Urig, K. Becker, *Med Res Rev* 2004, 24, 40-89.
- [65] aA. Casini, C. Gabbiani, G. Mastrobuoni, L. Messori, G. Moneti, G. Pieraccini, *ChemMedChem* 2006, 1, 413-417; bF. Wang, J. Bella, J. A. Parkinson, P. J. Sadler, *JBIC, J. Biol. Inorg. Chem.* 2005, 10, 147-155.
- [66] A. Mani, E. P. Gelmann, *J. Clin. Oncol.* 2005, 23, 4776-4789.
- [67] E. C. Ledgerwood, I. M. Morison, *Clin. Cancer Res.* 2009, 15, 420-424.
- [68] L. W. Oberley, G. R. Buettner, *Cancer Res.* 1979, 39, 1141-1149.
- [69] aS. M. Meier, Y. O. Tsybin, P. J. Dyson, B. K. Keppler, C. G. Hartinger, *Analytical and Bioanalytical Chemistry* 2012, 402, 2655-2662; bS. M. Meier, M. Novak, W. Kandjoller, M. A. Jakupec, V. B. Arion, N. Metzler-Nolte, B. K. Keppler, C. G. Hartinger, *Chem. - Eur. J.* 2013, 19, 9297-9307; cC. G. Hartinger, Y. O. Tsybin, J. Fuchser, P. J. Dyson, *Inorg. Chem.* 2008, 47, 17-19; dT. Peleg-Shulman, D. Gibson, *J. Am. Chem. Soc.* 2001, 123, 3171-3172; eT. Peleg-Shulman, Y. Najajreh, D. Gibson, *J. Inorg. Biochem.* 2002, 91, 306-311.
- [70] C. G. Hartinger, A. Casini, C. Duhot, Y. O. Tsybin, L. Messori, P. J. Dyson, *J. Inorg. Biochem.* 2008, 102, 2136-2141.
- [71] G. K. Balendiran, R. Dabur, D. Fraser, *Cell Biochem. Funct.* 2004, 22, 343-352.
- [72] A. T. Miles, G. M. Hawksworth, J. H. Beattie, V. Rodilla, *Crit. Rev. Biochem. Mol. Biol.* 2000, 35, 35-70.
- [73] M. Knipp, *Curr. Med. Chem.* 2009, 16, 522-537.
- [74] M. Knipp, A. V. Karotki, S. Chesnov, G. Natile, P. J. Sadler, V. Brabec, M. Vasak, *J. Med. Chem.* 2007, 50, 4075-4086.
- [75] J. Ghuman, P. A. Zunszain, I. Petitpas, A. A. Bhattacharya, M. Otagiri, S. Curry, *J. Mol. Biol.* 2005, 353, 38-52.
- [76] W. H. Ang, E. Daldini, L. Juillerat-Jeanneret, P. J. Dyson, *Inorg. Chem.* 2007, 46, 9048-9050.
- [77] M. C. M. Chung, *Biochem. Educ.* 1984, 12, 146-154.
- [78] D. A. Wolters, M. Stefanopoulou, P. J. Dyson, M. Groessl, *Metallomics* 2012, 4, 1185-1196.
- [79] A. Zayed, T. Shoeib, S. E. Taylor, G. D. D. Jones, A. L. Thomas, J. P. Wood, H. J. Reid, B. L. Sharp, *Int. J. Mass Spectrom.* 2011, 307, 70-78.
- [80] B. Wu, M. S. Ong, M. Groessl, Z. Adhireskan, C. G. Hartinger, P. J. Dyson, C. A. Davey, *Chem. - Eur. J.* 2011, 17, 3562-3566.
- [81] B. Wu, P. Droege, C. A. Davey, *Nat. Chem. Biol.* 2008, 4, 110-112.
- [82] J. M. Al-Shuneigat, S. S. Mahgoub, F. Huq, *J Biomed Sci* 2011, 18, 50.
- [83] B. Wu, C. A. Davey, *Chem. Biol. (Cambridge, MA, U. S.)* 2008, 15, 1023-1028.
- [84] F. Guidi, A. Modesti, I. Landini, S. Nobili, E. Mini, L. Bini, M. Puglia, A. Casini, P. J. Dyson, C. Gabbiani, L. Messori, *J. Inorg. Biochem.* 2013, 118, 94-99.
- [85]
- [86] J. Will, W. S. Sheldrick, D. Wolters, *JBIC, J. Biol. Inorg. Chem.* 2008, 13, 421-434.
- [87] K. J. Kilpin, C. M. Clavel, F. Edefe, P. J. Dyson, *Organometallics* 2012, 31, 7031-7039.
- [88] K. A. Stevenson, S. F. Yen, N. C. Yang, D. W. Boykin, W. D. Wilson, *J. Med. Chem.* 1984, 27, 1677-1682.
- [89] K. D. Tew, Y. Manevich, C. Grek, Y. Xiong, J. Uys, D. M. Townsend, *Free Radical Biol. Med.* 2011, 51, 299-313.
- [90] W. H. Ang, L. A. De, C. Chapuis-Bernasconi, L. Juillerat-Jeanneret, B. M. Lo, P. J. Dyson, *ChemMedChem* 2007, 2, 1799-1806.
- [91] W. H. Ang, L. J. Parker, L. A. De, L. Juillerat-Jeanneret, C. J. Morton, B. M. Lo, M. W. Parker, P. J. Dyson, *Angew. Chem., Int. Ed.* 2009, 48, 3854-3857.
- [92] H. Maeda, J. Wu, T. Sawa, Y. Matsumura, K. Hori, *J. Controlled Release* 2000, 65, 271-284.
- [93] P. Haquette, M. Salmain, K. Svedlung, A. Martel, B. Rudolf, J. Zakrzewski, S. Cordier, T. Roisnel, C. Fosse, G. Jaouen, *ChemBioChem* 2007, 8, 224-231.
- [94] M. Hanif, A. A. Nazarov, A. Legin, M. Groessl, V. B. Arion, M. A. Jakupec, Y. O. Tsybin, P. J. Dyson, B. K. Keppler, C. G. Hartinger, *Chem. Commun. (Cambridge, U. K.)* 2012, 48, 1475-1477.
- [95] aV. K. Yellepeddi, A. Kumar, D. M. Maher, S. C. Chauhan, K. K. Vangara, S. Palakurthi, *Anticancer Res.* 2011, 31, 897-906; bB. A. Howell, *ACS Symp. Ser.* 2010, 1053, 161-179.
- [96] aP. Chellan, K. M. Land, A. Shokar, A. Au, S. H. An, D. Taylor, P. J. Smith, T. Riedel, P. J. Dyson, K. Chibale, G. S. Smith, *Dalton Trans* 2013, 43, 513-526; bR. Payne, P. Govender, B. Therrien, C. M. Clavel, P. J. Dyson, G. S. Smith, *J. Organomet. Chem.* 2013, 729, 20-27; cP. Chellan, K. M. Land, A. Shokar, A. Au, S. H. An, D. Taylor, P. J. Smith, T. Riedel, P. J. Dyson, K. Chibale, G. S. Smith, *Dalton Trans.* 2014, 43, 513-526; dP. Govender, F. Edefe, B. C. E. Makhubela, P. J. Dyson, B. Therrien, G. S. Smith, *Inorg. Chim. Acta* 2014, 409, 112-120.
- [97] aP. Govender, N. C. Antonels, J. Mattsson, A. K. Renfrew, P. J. Dyson, J. R. Moss, B. Therrien, G. S. Smith, *J. Organomet. Chem.* 2009, 694, 3470-3476; bP. Govender, A. K. Renfrew, C. M. Clavel, P. J. Dyson, B. Therrien, G. S. Smith, *Dalton Trans.* 2011, 40, 1158-1167.
- [98] A. K. Renfrew, R. Scopelliti, P. J. Dyson, *Inorg. Chem.* 2010, 49, 2239-2246.

- [99] M. K. Bakht, M. Sadeghi, M. Pourbaghi-Masouleh, C. Tenreiro, *Curr. Cancer Drug Targets* 2012, 12, 998-1015.
- [100] Y. Q. Tan, P. J. Dyson, W. H. Ang, *Organometallics* 2011, 30, 5965-5971.
- [101] aF. Schmitt, J. Freudenreich, N. P. E. Barry, L. Juillerat-Jeanneret, G. Suss-Fink, B. Therrien, *J. Am. Chem. Soc.* 2012, 134, 754-757; bO. Zava, J. Mattsson, B. Therrien, P. J. Dyson, *Chem. - Eur. J.* 2010, 16, 1428-1431; cM. A. Furrer, F. Schmitt, M. Wiederkehr, L. Juillerat-Jeanneret, B. Therrien, *Dalton Trans.* 2012, 41, 7201-7211.

II. Results

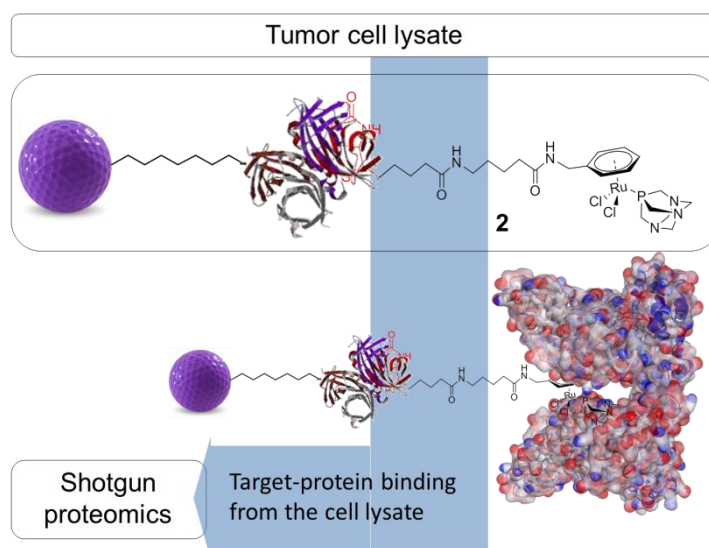
*“If you’re not failing every now and again, it’s a sign
you’re not doing anything very innovative”*

Woody Allen

1. Target profiling of RAPTA-drugs by chemical proteomics

Maria V. Babak, Samuel M. Meier, Kilian Huber, Jóhannes Reynisson, Anton A. Legin, Michael A. Jakupec, Alexander Roller, Alexey Stukalov, Manuela Gridling, Keiryn L. Bennett, Jacques Colinge, Walter Berger, Paul J. Dyson, Giulio Superti-Furga, Bernhard K. Keppler, Christian G. Hartinger

Submitted to *JACS*, 2014



The molecular targets of metal-based anticancer agents are often elusive. Herein, we describe a drug pull-down approach for RAPTA derivatives. Our data suggest that this compound binds to a wide variety of intracellular proteins, some of which are cancer-related.

Target Profiling of RAPTA Anticancer Agents by Chemical Proteomics

Maria V. Babak,^{†‡} Samuel M. Meier,[‡] Kilian Huber,[§] Jóhannes Reynisson,[†] Anton A. Legin,[‡] Michael A. Jakupec,[‡] Alexander Roller,[‡] Alexey Stukalov,[§] Manuela Gridling,[§] Keiryn L. Bennett,[§] Jacques Colinge,[§] Walter Berger,[⊥] Paul J. Dyson,[∇] Giulio Superti-Furga,[§] Bernhard K. Keppler,[‡] Christian G. Hartinger^{*†,‡}

[†] School of Chemical Sciences, University of Auckland, Private Bag 92019, Auckland 1142, New Zealand

[‡] Institute of Inorganic Chemistry, University of Vienna, Waehringer Str. 42, A-1090 Vienna, Austria

[§] CeMM Research Center for Molecular Medicine, Lazarettgasse 14, AKH BT 25.3, A-1090 Vienna, Austria

[⊥] Department of Medicine I, Institute of Cancer Research, Medical University Vienna, Borschkegasse 8a, A-1090 Vienna, Austria

[∇] Institut des Sciences et Ingénierie Chimiques, Ecole Polytechnique Fédérale de Lausanne, CH-1015 Lausanne, Switzerland

KEYWORDS. Biotin/streptavidin; Metallodrug pull-down; Protein target; RAPTA; Ru(arene)

ABSTRACT: The molecular targets of anticancer metallodrugs are often elusive which limits the design of next-generation targeted derivatives. In order to establish the molecular target profile of a class of the antimetastatic ruthenium (RAPTA) complexes, a drug pull-down approach was developed. This approach is based on a combination of the design of a pharmacophore derivative with similar biological properties as the parent compound, drug affinity purification of cancer cell lysates with subsequent high-end mass spectrometry and bioinformatics. The comparison of data sets obtained for cell lysates from cancer cells and after pretreatment with a competitive binder suggests that the compound type binds to a wide variety of intracellular proteins including key cancer related proteins.

INTRODUCTION

The modes of action of organometallic anticancer ruthenium complexes, which are substantially different from commonly used platinum-based chemotherapeutics, account for the growing interest in this compound class.¹⁻⁴ RAPTA compounds have the general formula [Ru(arene)(PTA)X₂] (Figure 1), where PTA = 1,3,5-triaza-7-phosphatricyclo-[3.3.1.1]decane and X = halogenide or biscarboxylate, and are a promising class of organometallic Ru^{II} compounds which are not cytotoxic against cancer cells *in vitro*, but exhibit pronounced antimetastatic activity *in vivo*.^{5,6} With their cis-configured halogenido ligands resembling the cisplatin structure, DNA was initially considered to be the target.⁷⁻⁹ However, in recent years the focus of mode-of-action studies has shifted from investigations of RAPTA-DNA to RAPTA-protein interactions.¹⁰⁻¹² It has been demonstrated that RAPTA compounds preferentially bind to proteins even in the presence of DNA, as shown from crystallographic and bioanalytical studies with the nucleosome core particle.^{13,14} Notably the selection of the ligands determines the reactivity of organoruthenium compounds to biological targets. In contrast to

the RAPTA derivatives, Ru(arene) complexes with a chelating ethylenediamine ligand bind preferentially to DNA.¹⁴ In addition, adduct formation of RAPTA with a range of isolated proteins has been demonstrated, and in some cases enzyme inhibition has been observed.^{10-12,15-18} In comparison to platinum compounds RAPTA complexes tend to be more reactive towards proteins, but also display greater selectivity, even though both compound classes react with the same binding sites in proteins.¹⁵

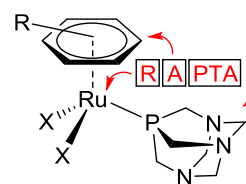


Figure 1. Schematic representation of the components of the RAPTA framework.

A more complete picture of the interactions of RAPTA compounds with cellular targets would help to improve understanding of their mode of action. The screening of putative RAPTA-protein interactions is laborious because

of the enormous number of potential biomolecular targets in cells. Moreover, with these *ex vivo* studies there is a high probability that binding to amino acid side chain donor atoms will occur if any isolated protein is incubated with the metal complex and also do not reflect competitive binding events, highly likely in studies in living organisms. Therefore, a more complex test system more closely reflecting the real situation is required, which, however, necessitates more advanced analytical and molecular biology approaches to identify a selective binding partner in a mixture of potential targets.¹⁹ Recently, Messori *et al.* and Wolters *et al.* demonstrated the importance of using proteomic studies in evaluation of cancer cell response to RAPTA-T, [Ru(η^6 -toluene)(PTA)Cl₂], treatment on the protein level.^{20,21} Wolters *et al.* employed multidimensional protein identification technology and identified 414 proteins out of which 74 proteins were further analyzed on their regulation profile,²⁰ and histones were suggested to play an important role in the mode of action of RAPTA complex.¹³ Messori *et al.* used 2-dimensional difference gel electrophoresis to monitor the changes in the expression of intracellular proteins upon exposure of cancer cells to RAPTA-T. In comparison to the control experiment, RAPTA-T did not induce significant modifications of protein expression profiles although a small number of up- and down-regulated proteins were detected.²¹ It is worth noting that in both cases substantial differences in the proteome profiles of cells treated with RAPTA compounds and those treated with platinum complexes were observed, highlighting their different modes of action.

In this paper, we describe the development of a chemical proteomics method, involving affinity chromatography, using a solid phase functionalized with a RAPTA derivative that was especially designed for this purpose, shotgun proteomics and bioinformatics.

EXPERIMENTAL SECTION

Materials and Methods. Materials from chemical suppliers were used as received and all the reactions were carried out under argon atmosphere in anhydrous solvents. RuCl₃·3H₂O was purchased from Johnson Matthey. [(η^6 -Benzylammonium)RuCl₂]₂Cl₂ (**a**),²² 1,4-cyclohexadiene-1-methanamine (**b**),²³ and 1,3,5-triaza-7-phosphaadamantane (PTA)²⁴ were prepared according to literature procedures. Methanol was dried and distilled over Mg under an argon atmosphere. D-Biotin and 6-biotinylamino-hexanoic acid-N-hydroxysuccinimidyl ester were purchased from Iris Biotech GMBH, triethylamine (99%) and dimethylsulfoxide (p.a) from Acros, acetic anhydride ($\geq 99.0\%$) and ethanolamine (p.a) from Fluka, N,N-dimethyl formamide (absolute, over molecular sieves, $\geq 99.5\%$) from Aldrich, sodium dodecyl sulphate ($\geq 98.5\%$), HEPES (99.5%), ubiquitin (from bovine erythrocytes) and horse heart cytochrome-c were from Sigma and tetramethylammonium acetate ($>98\%$) from TCI. The isolation of products was conducted without any special precautions. Elemental analyses were performed by the

Microanalytical Laboratory of the Faculty of Chemistry of the University of Vienna. Electrospray ionization mass spectrometry was carried out with a Bruker Esquire 3000 instrument (Bruker Daltonics, Bremen, Germany), MilliQ water (18.2 M Ω ; Millipore Synergy 185 UV Ultrapure Water System; Molsheim, France) and methanol (VWR Int., HiPerSolv, CHROMANORM) were used as solvents for ESI-MS studies. The ¹H and ³¹P NMR spectra were recorded at 500.10 and 202.44 MHz on a Bruker FT-NMR spectrometer Avance IITM 500 MHz. ¹H NMR kinetic experiments were measured at 500.32 MHz on a Bruker DPX500 (Ultrasield Magnet). Chemical shifts are given in ppm relative to the residual solvent peak.

X-ray Diffraction Analysis. X-ray diffraction measurements were performed on a Bruker X8 APEX II CCD diffractometer at 100 K. Single crystals were positioned at 35 mm from the detector, and 1112 and 2123 frames were measured, each for 60 and 20 s over 1° scan width for 1 and 3, respectively. The data were processed using SAINT software.²⁵ Crystal data, data collection parameters, and structure refinement details for 1 and 3 are given in Table S1 and key bond lengths and angles in Table S2. The structures were solved by direct methods and refined by full-matrix least-squares techniques. Non-hydrogen atoms were refined with anisotropic displacement parameters. H atoms were placed at calculated positions and refined as riding atoms in the subsequent least squares model refinements. The isotropic thermal parameters were estimated to be 1.2 times the values of the equivalent isotropic thermal parameters of the non-hydrogen atoms to which hydrogen atoms are bonded. The following computer programs, equipment and tables were used: structure solution, SHELXS-97; refinement, SHELXL-2013,²⁶ OLEX2;²⁷ molecular diagrams, Mercury 3.0.

Cell Lines and Culture Conditions. The human cancer cell lines CH1 (ovarian carcinoma), A549 (non-small cell lung cancer) and SW480 (colon carcinoma) were grown in 75 cm² culture flasks (CytoOne, Starlab, UK) as adherent monolayer cultures in complete medium [i.e., Minimal Essential Medium (MEM) supplemented with 10% heat-inactivated fetal bovine serum, 1 mM sodium pyruvate, 4 mM L-glutamine, and 1% from 100x nonessential amino acids ready-to-use stock (all purchased from Sigma-Aldrich Austria)]. Cell cultures were incubated at 37 °C in a moist atmosphere containing 5% CO₂.

Cytotoxicity Tests in Cancer Cell Lines. The cytotoxicity of the compounds was determined by means of colorimetric microculture assay (MTT assay, MTT = 3-(4,5-dimethyl-2-thiazolyl)-2,5-diphenyl-2H-tetrazolium bromide). The cells were harvested from culture flasks by trypsinization and seeded into 96-well microculture plates (CytoOne, Starlab, UK) in densities of 1×10³ cells per well (for CH1), 2.5×10³ cells per well (for SW480) and 3×10³ cells per well (for A549). After 24 h preincubation of the cells, the test compounds were dissolved in complete medium and then added in aliquots of 100 μ L per well. After continuous exposure for 96 h, solutions of the compounds were replaced with 86 μ L RPMI 1640 medium (supplemented with 10% heat-inactivated fetal bovine

serum and 2 mM L-glutamine) plus 14 μL MTT solution in phosphate-buffered saline (5 mg/mL). After incubation for 4 h, the medium/MTT mixtures were removed, and the formazan crystals formed by viable cells were dissolved in 150 μL of DMSO per well. Optical densities at 550 nm were measured with a microplate reader (ELx808 Absorbance Microplate Reader, Bio-Tek, USA), using a reference wavelength of 690 nm to correct for unspecific absorption. The quantity of viable cells was expressed in terms of T/C values by comparison to untreated control microcultures, and 50% inhibitory concentrations (IC_{50}) were calculated from concentration-effect curves by interpolation. Evaluation is based on means from at least three independent experiments, each comprising three replicates per concentration level.

Stability Studies. Stability studies for **1** were performed on an AmaZon SL ion trap mass spectrometer using ESI Compass 1.3 software (Bruker Daltonics GmbH, Bremen, Germany). The samples were introduced by direct infusion at a flow rate of 180 $\mu\text{L}/\text{h}$. Compound **1** was dissolved in dimethylsulfoxide or dry *N,N*-dimethylformamide, respectively, and was incubated for the appropriate time. The sample was diluted with water : methanol (1 : 1) to a final concentration of 5 μM prior to injection into the instrument. Typical instrument parameters were as follows: average accumulation time ~1500 μs , dry gas 6.0 L/min, dry temperature 100 $^{\circ}\text{C}$, end plate offset -500 V, HV capillary -3.5 kV, nebulizer 8 psi, RF Level 63%, trap drive 55.2. The Data Analysis 4.0 software package (Bruker Daltonics GmbH, Bremen, Germany) was used for processing of the raw data. Stability studies in aqueous solution were carried out as described below.

Protein Binding Studies. Compound **1** or **3** (400 μM) and ubiquitin or cytochrome-c (400 μM) were dissolved in water and tetramethylammonium acetate (20 mM). These stock solutions were mixed to obtain a 2 : 1 metal-to-ubiquitin and a 3 : 1 metal-to-cytochrome-c molar ratio. The final protein concentration was 50 μM and the mixtures were incubated at 37 $^{\circ}\text{C}$ in the dark using a thermomixer at 400 rpm (Ditabis, Pforzheim, Germany, HLC). References containing only **1** or **3** (50 μM) were incubated in parallel. Mass spectra of the incubation solutions were recorded after 2, 6, 24 and 48 h. The samples were analyzed using a MaXis Q-ToF mass spectrometer (Bruker Daltonics, Bremen, Germany) equipped with a Triversa nanomate (Advion Biosystems Inc., Ithaca, New York, USA) using ChipSoft 8.3 (Advion Biosystems Inc.) to control the nanomate. The general parameters were as follows: HV capillary -1.8 kV, gas flow 0.1 psi, dry temperature 180 $^{\circ}\text{C}$, 200 Vpp funnel RF, 3 eV quadrupole ion energy, 150 μs ion cooler transfer time and 15 $^{\circ}\text{C}$ nanomate sample plate temperature. The samples were diluted before injection to 1–3 μM using water : methanol : formic acid (50 : 50 : 0.2). The spectra were recorded in positive ion mode over 0.5 min and averaged. The Data Analysis 4.0 software package was used for processing and maximum entropy deconvolution (automatic data point spacing and 30000 instrument resolving power) was applied.

Docking Experiments. The structures were docked to a streptavidin crystal structure (3RY2, resolution 0.95 \AA),²⁸ which was obtained from the Protein Data Bank (PDB).^{29,30} The Scigress Ultraversion 7.7.0.47 program³¹ was used to prepare the crystal structure for docking, i.e. hydrogen atoms were added, the co-crystallized ligand (biotin) was removed as well as crystallographic water molecules. The Scigress software suite was also used to build the compounds and the MM2³² force field was used to optimize the structures. The centre of the binding pocket was defined as the oxygen atom on the bicyclic system ($x = 27.048$, $y = 10.773$, $z = 12.293$) in biotin with 10 \AA radius. Fifty docking runs were allowed for each ligand with default search efficiency (100%). The basic amino acids lysine and arginine were defined as protonated. Furthermore, aspartic and glutamic acids were assumed to be deprotonated. All the bonds to the metal centre were fixed for the docking runs. The GoldScore (GS),³³ ChemScore (CS),^{34,35} ChemPLP³⁶ and ASP³⁷ algorithms in the GOLD v5.1 software suite were implemented to predict binding modes and relative energies of the ligands.

Drug Pull-Down. Per experiment, 100 μL streptavidin bead slurry (UltraLink Immobilized Streptavidin Plus, 50% in 20% ethanol, Pierce) was distributed in Eppendorf tubes, centrifuged, and the supernatant removed. After washing with lysis buffer (3 \times 1 mL), 50 mmol of biotin-conjugated compound **3** was added (prepared as described below) and incubated on a roto-shaker for 30 min at 4 $^{\circ}\text{C}$. After centrifugation and one additional wash step, beads were resuspended in CH1 lysates (10 mg per pull-down) and incubated on a roto-shaker for 2 h at 4 $^{\circ}\text{C}$. For competition experiments, lysates were preincubated with 20 μM of **2**, respectively, for 20 min at 4 $^{\circ}\text{C}$. After centrifugation, beads were transferred to spin columns (MoBiTec) and washed with lysis buffer (5 mL) and HEPES (2.5 mL), respectively. To elute bound proteins, beads were treated with 250 μL elution buffer (50% urea, 50% formic acid) and eluates collected in glass vials.

Liquid chromatography mass spectrometry. Mass spectrometry was performed on a hybrid LTQ Orbitrap Velos mass spectrometer (ThermoFisher Scientific, Waltham, MA, USA) using Xcalibur version 2.1.0 SP1.1160 coupled to an Agilent 1200 HPLC nanoflow system (dual pump with one precolumn and one analytical column) (Agilent Biotechnologies, Palo Alto, CA, USA) via a nano-electrospray ion source using liquid junction (Proxeon, Odense, Denmark). Solvents for HPLC separation of peptides were as follows: solvent A consisted of 0.4% formic acid (FA) in water and solvent B consisted of an aqueous solution of 0.4% FA in 70% methanol and 20% isopropanol. From a thermostatted microautosampler, 8 μL of the tryptic peptide mixture was automatically loaded onto a trap column (Zorbax 300SB-C18 5 μm , 5 \times 0.3 mm, Agilent Biotechnologies, Palo Alto, CA, USA) with a binary pump at a flow rate of 45 $\mu\text{L}/\text{min}$. 0.1% trifluoroacetic acid (TFA) used for loading and washing the precolumn. After washing, the peptides were eluted by back-flushing onto a 16 cm fused silica analytical column with an inner diameter of 50 μm packed with C18 reversed phase material

(ReproSil-Pur 120 C18-AQ, 3 μm , Dr. Maisch GmbH, Ammerbuch-Entringen, Germany). The peptides were eluted from the analytical column with a 27 min gradient ranging from 3 to 30% solvent B, followed by a 25 min gradient from 30 to 70% solvent B and, finally, a 7 min gradient from 70 to 100% solvent B at a constant flow rate of 100 nL/min.³⁸ The analyses were performed in a data-dependent acquisition mode and dynamic exclusion for selected ions was 60 s. A top 15 collision-induced dissociation (CID) method was used, and a single lock mass at m/z 445.120024 ($\text{Si}(\text{CH}_3)_2\text{O}_6$) was employed.^{39,40} Maximal ion accumulation time allowed in CID mode was 50 ms for MS^n in the LTQ and 500 ms in the C-trap. Automatic gain control was used to prevent overfilling of the ion traps and was set to 5,000 in MS^n mode for the LTQ and 10^6 ions for a full FTMS scan. Intact peptides were detected in the Orbitrap Velos at 60000 resolution at m/z 400. All samples were analyzed as biochemical and technical duplicates.

Data analysis. The acquired raw MS data files were processed with msconvert (ProteoWizard Library v2.1.2708) and converted into MASCOT generic format (mgf) files. The resultant peak lists were searched against the human SwissProt database version v2012.05_20120529 (36898 sequences, respectively, including isoforms, as obtained from varsplic.pl) with the search engines MASCOT (v2.3.02, MatrixScience, London, UK) and Phenyx (v2.5.14, GeneBio, Geneva, Switzerland).³⁹ Submission to the search engines was via a Perl script that performs an initial search with relatively broad mass tolerances (MASCOT only) on both the precursor and fragment ions (± 10 ppm and ± 0.6 Da, respectively). High-confidence peptide identifications were used to recalibrate all precursor and fragment ion masses prior to a second search with narrower mass tolerances (± 4 ppm and ± 0.3 Da). One missed tryptic cleavage site was allowed. Carbamidomethyl cysteine was set as a fixed modification and oxidized methionine was set as a variable modification. To validate the proteins, MASCOT and Phenyx output files were processed by internally-developed parsers. Proteins with ≥ 2 unique peptides above a threshold score T_1 , or with a single peptide above a score T_2 were selected as unambiguous identifications. Additional peptides for these validated proteins with score $> T_3$ were also accepted. For MASCOT and Phenyx, T_1 , T_2 and T_3 peptide scores were equal to 16, 40, 10 and 5.5, 9.5, 3.5, respectively (P-value < 0.001). The validated proteins retrieved by the two algorithms were merged, any spectral conflicts discarded and grouped according to shared peptides. A false positive detection rate (FDR) of $< 1\%$ and $< 0.1\%$ (including the peptides exported with lower scores) was determined for proteins and peptides, respectively, by applying the same procedure against a reversed database.

Synthesis of η^6 -(benzylammonium chloride) $\text{RuCl}_2(\text{PTA})$ (1). [η^6 -Benzylammonium chloride] RuCl_2 (a) (0.35 mmol, 221 mg) and PTA (0.98 mmol, 157 mg) were suspended in dry DMF (30 ml) and the mixture was stirred for 4 h. An orange precipitate

formed, which was collected by filtration, washed with dichloromethane and diethyl ether and dried *in vacuo* to give 208 mg of the target product (yield: 63%). Crystals suitable for X-ray diffraction analysis (red needles) were grown by slow diffusion of diethyl ether into an absolute methanol solution. Calc. for $\text{C}_{13}\text{H}_{22}\text{Cl}_3\text{N}_4\text{PRu}$ (472.74 g/mol): C, 33.03; H, 4.69; N, 11.85. Found: C, 33.02; H, 4.53; N, 11.47%. nESI-Q-TOF MS pos. mode: m/z 401.0230 [$\text{RuCl}(\eta^6\text{-C}_6\text{H}_5(\text{CH}_2)\text{NH}_2)(\text{PTA})$] $^+$, 436.9987 [$\text{RuCl}_2(\eta^6\text{-C}_6\text{H}_5(\text{CH}_2)\text{NH}_2)(\text{PTA}) + \text{H}$] $^+$; found 401.0230 (< 1 ppm), 436.9994 (2 ppm). ^1H NMR (500.10 MHz, $\text{DMSO-}d_6$): 8.39 (brs, 3H, NH_3), 5.98 (brs, 4H, η^6 -phenyl-H), 5.49 (brs, 1H, η^6 -phenyl-H), 4.46 (s, 6H, PTA-CH_2), 4.23 (s, 6H, PTA-CH_2), 3.73 (brs, 2H, $-\text{CH}_2\text{-NH}$). $^{31}\text{P}\{^1\text{H}\}$ NMR (202.44 MHz; $\text{DMSO-}d_6$): -30.8 (s) ppm.

Synthesis of biotin derivative (2). Compound 1 (4.72 mg, 0.01 mmol) and 6-biotinylamino-hexanoic acid-*N*-hydroxysuccinimidyl ester (4.55 mg, 0.01 mmol) were suspended in dry DMF (2 ml). After addition of triethylamine (500 μl) and subsequent sonication the mixture was stirred for 24 h, which resulted in a clear red-brown solution. The solution was freeze-dried and *in situ* incubated with the beads. nESI-Q-TOF MS pos. mode: m/z 704.2047 [$\text{Ru}\{\eta^6\text{-C}_6\text{H}_5(\text{CH}_2)\text{NH}(\text{linker-biotin})\}(\text{PTA}) - \text{H}$] $^+$, 722.2146 [$\text{Ru}\{\eta^6\text{-C}_6\text{H}_5(\text{CH}_2)\text{NH}(\text{linker-biotin})\}(\text{PTA}) + \text{OH}$] $^+$, 740.1821 [$\text{RuCl}\{\eta^6\text{-C}_6\text{H}_5(\text{CH}_2)\text{NH}(\text{linker-biotin})\}(\text{PTA})$] $^+$, 776.1580 [$\text{RuCl}_2\{\eta^6\text{-C}_6\text{H}_5(\text{CH}_2)\text{NH}(\text{linker-biotin})\}(\text{PTA}) + \text{H}$] $^+$; found 704.2087 (6 ppm), 722.2193 (7 ppm), 740.1851 (4 ppm), 776.1615 (5 ppm).

Synthesis of N -(cyclohexa-1,4-dienylmethyl)acetamide (c). The synthetic method was adapted from a reported procedure.⁴¹ Upon addition of sodium dodecyl sulfate (47 mg, 0.163 mmol) to a stirred heterogeneous suspension of 1-methylamine-1,4-cyclohexadiene (b) (1472 mg, 13.5 mmol) in water (30 ml), a turbid colorless solution formed. Acetic anhydride (1652 mg, 1.52 ml, 16.2 mmol) was added dropwise to the solution over a period of 40 min. It was left at 0 $^\circ\text{C}$ overnight and a white precipitate formed which was collected by filtration, washed with a minimal amount of diethyl ether and dried *in vacuo*. The solution was extracted with ethyl acetate (2 \times 30 ml) and the combined organic extracts were dried with Na_2SO_4 . The solvent was removed on a rotary evaporator under reduced pressure resulting in a yellow oil. It was washed with a minimal amount of diethyl ether and dried *in vacuo* to yield 1182 mg of the target product as a white powder (yield: 58%). The product was used without additional purification. ^1H NMR (500.10 MHz, CDCl_3): 5.73 (m, 2H, cyclohexadiene- $\text{CH}=\text{}$), 5.61 (brs, 1H, cyclohexadiene- $\text{CH}=\text{}$), 5.46 (m, 1H, $-\text{CONH}$), 3.80 (d, 2H, $-\text{CH}_2\text{-NH}$, $^3J_{\text{H,H}} = 5.8$ Hz), 2.72 (m, 2H, cyclohexadiene- CH_2), 2.64 (m, 2H, cyclohexadiene- CH_2), 2.03 (s, 3H, $-\text{CH}_3$).

Synthesis of [η^6 -(*N*-benzylacetamide) RuCl_2] (d). $\text{RuCl}_3 \cdot 3\text{H}_2\text{O}$ (863 mg, 4.15 mmol) was refluxed in dry methanol (50 ml) for 40 minutes. To the clear red-brown solution *N*-(cyclohexa-1,4-dienylmethyl)acetamide (c) (1104 mg, 7.26 mmol) was added and the mixture was re-

fluxed for 18 h at 80 °C. The dark brown solution turned initially bright green and then light orange, and eventually a brown-orange precipitate formed. The solution was filtered, washed with dichloromethane and diethyl ether and dried *in vacuo* to afford 1172 mg of an orange powder (yield: 88%). The product was used without additional purification. ¹H NMR (500.10 MHz, DMSO-*d*⁶): 8.34 (t, 1H, -CONH, ³J_{H,H} = 5.9 Hz), 6.05 (d, 2H, η⁶-phenyl-H, ³J_{H,H} = 5.9 Hz), 5.80 (t, 2H, η⁶-phenyl-H, ³J_{H,H} = 5.6 Hz), 5.33 (t, 2H, η⁶-phenyl-H, ³J_{H,H} = 5.6 Hz), 4.12 (d, 2H, -CH₂-NH, ³J_{H,H} = 5.9 Hz), 1.88 (s, 3H, -CH₃).

Synthesis of η⁶-(*N*-benzylacetamide)RuCl₂(PTA) (3). The synthetic method was adapted from a reported procedure.⁹ [η⁶-(*N*-Benzylacetamide)RuCl₂]₂ (d) (64 mg, 0.1 mmol) and PTA (47 mg, 0.3 mmol) were suspended in dry DMF (30 ml) and the mixture was stirred for 3 h. The resulting red-brown solution was filtered and the solvent was subsequently removed *in vacuo*. The remaining solid was washed with dichloromethane and diethyl ether and dried *in vacuo* to give 96 mg of the target product (yield: 47%). Crystals suitable for X-ray diffraction analysis (red needles) were grown by slow diffusion of diethyl ether into an absolute methanol solution. Calc. for C₁₅H₂₃Cl₂N₄PORu (478.32 g/mol): C, 37.67; H, 4.85; N, 11.71. Found: C, 37.39; H, 4.49; N, 11.33%. nESI-Q-TOF MS pos. mode:

<i>m/z</i>	443.0331	[RuCl(η ⁶ -C ₆ H ₅ (CH ₂)NHCOCH ₃)(PTA)] ⁺	479.0090	[RuCl ₂ (η ⁶ -C ₆ H ₅ (CH ₂)NHCOCH ₃)(PTA) + H] ⁺
1 ppm				
2 ppm				

¹H NMR (500.10 MHz, DMSO-*d*⁶): 8.30 (t, 1H, -CONH, ³J_{H,H} = 5.9 Hz), 5.87 (ddd, 2H, η⁶-phenyl-H, ³J_{H,H} = 5.9 Hz, 5.6 Hz, 2.1 Hz), 5.67 (d, 2H, η⁶-phenyl-H, ³J_{H,H} = 5.9 Hz), 5.33 (t, 2H, η⁶-phenyl-H, ³J_{H,H} = 5.6 Hz), 4.44 (s, 6H, PTA-CH₂), 4.21 (s, 6H, PTA-CH₂), 3.97 (d, 2H, -CH₂-NH, ³J_{H,H} = 5.9 Hz), 1.88 (s, 3H, -CH₃). ³¹P{¹H} NMR (202.44 MHz; DMSO-*d*⁶): -31.4 (s) ppm.

RESULTS AND DISCUSSION

Experimental design. In order to establish the ‘natural’ target profile of RAPTA anticancer agents, we used a combination of drug affinity purification with subsequent high-end mass spectrometry and bioinformatics. This approach is termed drug pull-down and for the work-flow used see Figure 2.⁴² Such chemical proteomics method identifies drug-binding proteins from whole cell extracts, after the pharmacophore **1** was immobilized on a solid support. The natural state and environment of proteins in these extracts, such as level of abundance, post-translational modifications, natural binding partners, *etc.*, are preserved,⁴³ which is crucial for global analysis.

By employing two routes of analysis, *i.e.*, the non-competitive (data set 1) and competitive pathways (data set 2), high-affinity binders can be identified (Figure 2). To obtain data set 1 in a non-competitive experiment, the beads modified with the pharmacophore **2** are exposed to the cell extract. In contrast in the competitive experiment, the pharmacophore on the beads is in competition with a free drug analogue for the preferred protein target.

A traditional drug pull-down experiment involves covalent attachment of drug molecules or fragments to matrices such as *N*-hydroxysuccinimidyl-sepharose and requires extensive cleansing to block unreacted beads.⁴³ Such cleansing is not possible with reactive metallodrugs as they are likely to undergo undesirable side reactions during the workflow. Since the RAPTA fragment reacts with electron donors to form coordinative bonds to biological targets,^{10,11,13,17} the arene ligand was functionalized with a primary amine to load the organometallic RAPTA fragment onto beads without modifying the site essential for binding to its biological target and, hence, for its biological activity. In this way, the Ru^{II} center, which reacts with donor atoms to form covalent bonds to biological targets,^{10,11,13,17} is maintained.

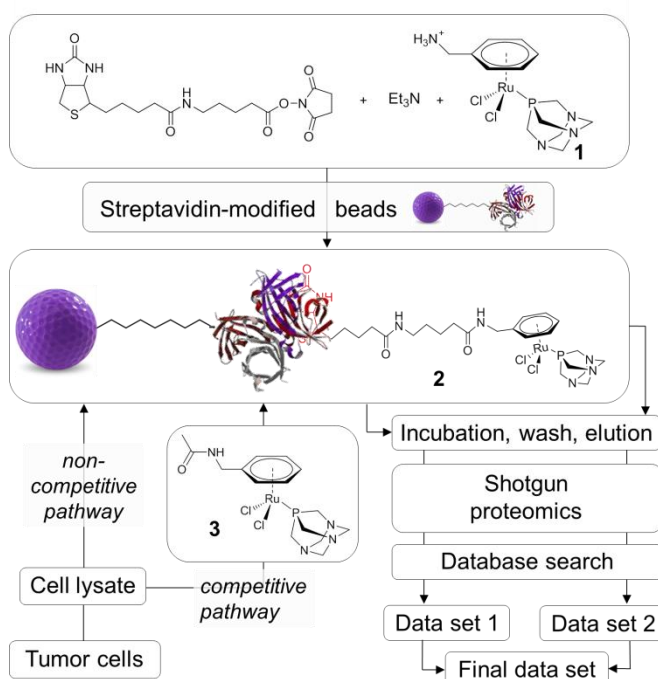


Figure 2. Schematic representation of the work-flow used in the metallodrug pull-down experiments. In the non-competitive pathway (data set 1) proteins can bind only to modified beads, whereas in the competitive pathway (data set 2) proteins can bind to modified beads and a non-bound RAPTA analogue **3**. The golf ball represents the beads and was used with the permission of LogoBallz.com.

To avoid decomposition of the organometallic complex during immobilization onto the matrix, we employed a biotin/streptavidin approach, which draws on one of the largest known binding constants of $K \sim 10^{14} \text{ M}^{-1}$ and has been used in biocatalysis.⁴⁴ This self-assembly approach should result in near quantitative functionalization of the beads with the RAPTA moiety, requiring minimal purification that could potentially deactivate the complex.

Functionalization of the pharmacophore. Based on the considerations outlined before, the synthetic strategy depicted in Figure 2 was followed: functionalization of the arene ring of the ruthenium complex with a primary amine group (**1**) allowed subsequent reaction with biotin-

6-aminohexanoic acid-*N*-hydroxysuccinimide ester to yield **2**. This compound was immobilized on streptavidin-modified beads *in situ*. By employing 6-aminohexanoic acid as a linker, the distance between streptavidin and the reactive metal center was extended to allow sufficient flexibility and low steric demand for reactions with target proteins.

Molecular Structures. In order to perform competition experiments (competitive pathway in Figure 2), **1** was converted into the acetyl derivative **3** and the molecular structures of **1** and **3** were established by X-ray diffraction analysis (Figure 4). Analysis of the bond lengths and angles confirmed structural similarity to RAPTA-C, [Ru(η^6 -*p*-cymene)(PTA)Cl₂] (Supporting Information)⁴⁵ and indicates that these derivatives can be used as suitable structural models for drug pull-down experiments.

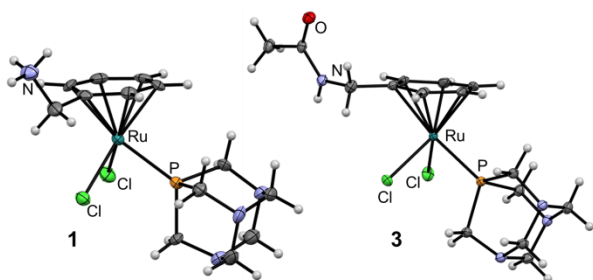


Figure 4. Molecular structures of **1** and of one of two independent molecules of **3** shown at the 50% probability level. Ru – cyan, C – grey, H – white, Cl – green, P – yellow and O – red. For bond lengths and angles see Supporting Information.

Binding of Biotin Derivatives to Streptavidin. Molecular modeling was used to evaluate the binding ability of the functionalized biotin into the target pocket of streptavidin. The docking scaffold was based on a biotin/streptavidin crystal structure (pdb 3RY2). The four scoring functions included in the GOLD software suite reproduced the experimental binding conformation well with a low root-mean-square deviation (e.g. goldscore (GS) gave 0.30 Å).

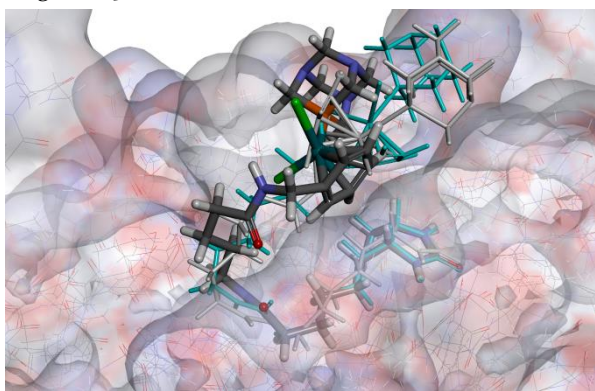


Figure 3. Docked configurations of ruthenium derivative **2** in the binding site of streptavidin for the three highest scoring GS runs overlaid.

In a second step, the ligand without the metal moiety was used as a model system, followed by addition of the Ru-PTA fragment to the functionalized arene. GS was the only scoring function able to treat the metal fragment. The biotin moieties of all the docked compounds showed good overlap with the co-crystallized biotin, reproducing also the hydrogen bonding pattern. The best scoring GS values of 82.0 for the organic fragment and 75.7 for **2** indicate that the binding energy of all the molecules is similar or slightly higher than that of biotin (70.7). Moreover, comparing a variety of highly scoring docking configurations allows concluding that the ruthenium moiety is flexible and accessible on the protein surface and the biotin scaffold is stable in the binding pocket, as shown in Figure 3. Both compounds are characterized by negligible adduct formation within 24 h in buffered solution, whereas in aqueous solution the reactivity of the organometallics towards biomolecules is enhanced. The compounds form low-abundance adducts, such as a [Ru(arene)(PTA)] fragment coordinated to ubiquitin in the case of **3** (Supporting Information).

Cytotoxicity. A suitable cell line and conditions for the metallodrug pull-down assay were chosen based on cytotoxicity studies (see Table 1). Ideally the functionalized derivatives show similar activity profiles as the parent compound to resemble the same target profile in cells. Therefore, the efficacy of **1–3** to inhibit cancer cell growth in the ovarian cancer CH1, colon carcinoma SW480 and non-small cell lung cancer A549 cell lines was tested by using the MTT assay (Table 1) and compared to that of RAPTA-C, as the prototype RAPTA derivative. The compounds were not cytotoxic in the rather chemoresistant A549 cell line, but displayed modest activity against SW480 cells, and reasonable cytotoxicity in the CH1 cell line. Consequently, CH1 cell lysates were chosen for the drug pull-down experiment as these cell lysates are mostly likely to contain detectable and relevant drug-target interactions.

Table 1. *In vitro* anticancer activity of compounds 1–3 and RAPTA-C in the human cancer cell lines CH1, SW480 and A549 after 96 h.

Compound	IC ₅₀ / μM		
	CH1	SW480	A549
1	9.6 ± 1.2	358 ± 19	> 500
2	74 ± 6	216 ± 81	> 500
3	13 ± 1	357 ± 79	> 500
RAPTA-C	65 ± 15	170 ± 60	> 500

Stability Studies. The choice of suitable solvents for the incubation of *in situ*-prepared **2** with cell lysate obtained from CH1 cells for the metallodrug pull-down experiment is crucial for maintaining the organometallic fragment without comprising the solubility of the modified molecule. DMSO, which is typically used for the reaction of organic molecules in pull-down experiments with beads, was replaced by DMF, as incubation of **1** and **3** in

DMSO results in loss of the arene moiety (see Supplementary Information). In DMF, however, the arene moiety of the RAPTA complex is sufficiently stable. The drug pull-down experiments were conducted in DMF as outlined in Figure 2.

Competition Experiments. To reduce the signal-to-noise ratio without reducing the sensitivity of the pull-down protocol, competition experiments with the acetylated RAPTA analogue **3**, which mimics the conjugated complex **1**, were included in the workflow. For competition experiments, cell lysates were pre-incubated with **3** before incubation with the affinity matrix. Complex **3** and immobilized **2** compete for the same set of proteins, which results in a significantly reduced abundance of high-affinity binders and their interactors in the purified sample, as characterized by MS. Comparison of the two independent MS data sets provides the cross-section of both experiments, as indicated by lower spectral counts for high-abundance proteins, whereas spectral counts for low-affinity proteins remain constant. This method is sensitive and reliable with the limitation that high abundance proteins can also be specific targets of the drug.⁴⁶

Data analysis. In these experiments, on average more than 300 proteins were observed per pull-down. To identify specific binders for the RAPTA derivatives, competitive and regular pull-downs were compared applying a threshold of a 1.5-fold increase in spectral counts (*i.e.*, the number of mass spectra recorded for a peptide as a part of a protein sequence) to be considered significant (see Table 2 and Supporting Information). In general, the spectral counts for enriched proteins were low compared to the overall counts and sequence coverage for those proteins was less than 10% in most cases.

Table 2. List of selected cancer-related proteins identified by chemical proteomics. Numbers indicate spectral counts.

Protein	Drug pull-down (data set 1)	Competition experiment (data set 2)
RRP1B ^a	4	1
Midkine	6	2
Protein FAM32A	4	0

^a Ribosomal RNA processing protein 1 homolog B

Even though there are exceptions to the latter, many proteins that appear to be enriched (e.g. ribosomal proteins) are ‘frequent hitters’, *i.e.* are most likely non-specific binders that are observed in many pull-down experiments (a selection of cancer-related proteins with significantly higher counts observed in the pull-down experiment compared to the competition experiment is given in Table 2).

SUMMARY AND CONCLUSIONS

Identification of cellular target proteins is a major challenge in drug development. With the exception of the DNA targeting platinum complexes, the targets of metal-

based anticancer agents are widely unknown. Herein, we describe an approach that can be widely employed for a variety of metallodrugs, once the sites that are not crucial for target protein interaction have been identified. We have demonstrated this for the RAPTA family, a class of anticancer drug candidates. By functionalizing the arene ligand for coupling with a biotin derivative that can be loaded on streptavidin-modified beads for a drug affinity chromatography experiment, mass spectrometry and bioinformatics showed that the complex reacts with a range of proteins. Some of the hits are proteins that have been proposed earlier as potential targets in complementary experiments, such as histone proteins (compare Table S3),^{13,14} which confirms the suitability of the approach. This study also shows that RAPTA compounds are able to interact with a wide range of different proteins, as expected for a relatively simple metal complex undergoing ligand exchange reactions with nucleophilic amino acid donor atoms. This broad action is, nonetheless, important, as it leads to a widespread modification of cellular proteins and helps to overcome resistance to established drugs or to sensitize cells to cytotoxic agents when used in combination, as has been demonstrated in biological experiments for the compound class.

AUTHOR INFORMATION

Corresponding Author

c.hartinger@auckland.ac.nz

Author Contributions

All authors have given approval to the final version of the manuscript.

Funding Sources

Genome Research Program Austria (GEN-AU, BMWF-70.081/0018-II/1a/2008)

ACKNOWLEDGMENTS

This work was supported by the Platform Austria for Chemical Biology of the Genome Research Program Austria (GEN-AU, BMWF-70.081/0018-II/1a/2008), and COST CM1105. We gratefully acknowledge Prof. Vladimir Arion for the refinement of X-ray diffraction data and Prof. Markus Galanski for recording the 2D NMR spectra.

ABBREVIATIONS

CCR2, CC chemokine receptor 2; CCL2, CC chemokine ligand 2; CCR5, CC chemokine receptor 5; TLC, thin layer chromatography.

REFERENCES

- (1) Hillard, E. A.; Jaouen, G. *Organometallics* **2011**, *30*, 20.
- (2) Gasser, G.; Ott, I.; Metzler-Nolte, N. *J. Med. Chem.* **2011**, *54*, 3.
- (3) Sava, G.; Jaouen, G.; Hillard, E. A.; Bergamo, A. *Dalton Trans.* **2012**, *41*, 8226.
- (4) Hartinger, C. G.; Metzler-Nolte, N.; Dyson, P. J. *Organometallics* **2012**, *31*, 5677.
- (5) Scolaro, C.; Bergamo, A.; Brescacin, L.; Delfino, R.; Cocchietto, M.; Laurenczy, G.; Geldbach, T. J.; Sava, G.; Dyson, P. J. *J. Med. Chem.* **2005**, *48*, 4161.

- (6) Bergamo, A.; Masi, A.; Dyson, P. J.; Sava, G. *Int. J. Oncol.* **2008**, *33*, 1281.
- (7) Dorcier, A.; Dyson, P. J.; Gossens, C.; Rothlisberger, U.; Scopelliti, R.; Tavernelli, I. *Organometallics* **2005**, *24*, 2114.
- (8) Dorcier, A.; Ang, W. H.; Bolano, S.; Gonsalvi, L.; Juillerat-Jeanerret, L.; Laurency, G.; Peruzzini, M.; Phillips, A. D.; Zanobini, F.; Dyson, P. J. *Organometallics* **2006**, *25*, 4090.
- (9) Scolaro, C.; Geldbach, T. J.; Rochat, S.; Dorcier, A.; Gossens, C.; Bergamo, A.; Cocchietto, M.; Tavernelli, I.; Sava, G.; Rothlisberger, U.; Dyson, P. J. *Organometallics* **2006**, *25*, 756.
- (10) Scolaro, C.; Chaplin, A. B.; Hartinger, C. G.; Bergamo, A.; Cocchietto, M.; Keppler, B. K.; Sava, G.; Dyson, P. J. *Dalton Trans.* **2007**, 5065.
- (11) Casini, A.; Mastrobuoni, G.; Ang, W. H.; Gabbiani, C.; Pieraccini, G.; Moneti, G.; Dyson, P. J.; Messori, L. *ChemMedChem* **2007**, *2*, 631.
- (12) Casini, A.; Gabbiani, C.; Sorrentino, F.; Rigobello, M. P.; Bindoli, A.; Geldbach, T. J.; Marrone, A.; Re, N.; Hartinger, C. G.; Dyson, P. J.; Messori, L. *J. Med. Chem.* **2008**, *51*, 6773.
- (13) Wu, B.; Ong, M. S.; Groessl, M.; Adhireksan, Z.; Hartinger, C. G.; Dyson, P. J.; Davey, C. A. *Chem. Eur. J.* **2011**, *17*, 3562.
- (14) Adhireksan, Z.; Davey, G. E.; Campomanes, P.; Groessl, M.; Clavel, C. M.; Yu, H.; Nazarov, A. A.; Yeo, C. H. F.; Ang, W. H.; Dröge, P.; Rothlisberger, U.; Dyson, P. J.; Davey, C. A. *Nat Commun* **2014**, *5*.
- (15) Casini, A.; Gabbiani, C.; Michelucci, E.; Pieraccini, G.; Moneti, G.; Dyson, P. J.; Messori, L. *J. Biol. Inorg. Chem.* **2009**, *14*, 761.
- (16) Casini, A.; Karotki, A.; Gabbiani, C.; Rugi, F.; Vasak, M.; Messori, L.; Dyson, P. J. *Metallomics* **2009**, *1*, 434.
- (17) Groessl, M.; Terenghi, M.; Casini, A.; Elvirri, L.; Lobinski, R.; Dyson, P. J. *J. Anal. At. Spectrom.* **2010**, *25*, 305.
- (18) Mendes, F.; Groessl, M.; Nazarov, A. A.; Tsybin, Y. O.; Sava, G.; Santos, I.; Dyson, P. J.; Casini, A. *J. Med. Chem.* **2011**, *54*, 2196.
- (19) Groessl, M.; Hartinger, C. G. *Anal. Bioanal. Chem.* **2013**, *405*, 1791.
- (20) Wolters, D. A.; Stefanopoulou, M.; Dyson, P. J.; Groessl, M. *Metallomics* **2012**, *4*, 1185.
- (21) Guidi, F.; Modesti, A.; Landini, I.; Nobili, S.; Mini, E.; Bini, L.; Puglia, M.; Casini, A.; Dyson, P. J.; Gabbiani, C.; Messori, L. *J. Inorg. Biochem.* **2013**, *118*, 94.
- (22) Cheung, F. K.; Lin, C.; Minissi, F.; Crivillé, A. L.; Graham, M. A.; Fox, D. J.; Wills, M. *Org. Lett.* **2007**, *9*, 4659.
- (23) Ang, W. H.; Daldini, E.; Juillerat-Jeanerret, L.; Dyson, P. J. *Inorg. Chem.* **2007**, *46*, 9048.
- (24) Daigle, D. J.; Pepperman, A. B.; Vail, S. L. *J. Heterocycl. Chem.* **1974**, *11*, 407.
- (25) Pressprich, M. R.; Chambers, J.; Bruker Analytical X-ray systems: Madison, 2004.
- (26) Sheldrick, G. M. *Acta Crystallogr., Sect. A: Found. Crystallogr.* **2008**, *A64*, 112.
- (27) Dolomanov, O. V.; Bourhis, L. J.; Gildea, R. J.; Howard, J. A. K.; Puschmann, H. *J. Appl. Crystallogr.* **2009**, *42*, 339.
- (28) Le Trong, I.; Wang, Z.; Hyre, D. E.; Lybrand, T. P.; Stayton, P. S.; Stenkamp, R. E. *Acta Crystallogr. Sect. D* **2011**, *67*, 813.
- (29) Berman, H. M.; Westbrook, J.; Feng, Z.; Gilliland, G.; Bhat, T. N.; Weissig, H.; Shindyalov, I. N.; Bourne, P. E. *Nuc. Acids Res.* **2000**, *28*, 235.
- (30) Berman, H.; Henrick, K.; Nakamura, H. *Nat. Struct. Biol.* **2003**, *10*, 980.
- (31) Fijitsu Limited: 2000 - 2007.
- (32) Allinger, N. L. *J. Am. Chem. Soc.* **1977**, *99*, 8127.
- (33) Jones, G.; Willet, P.; Glen, R. C.; Leach, A. R.; Taylor, R. *J. Mol. Biol.* **1997**, *267*, 727.
- (34) Eldridge, M. D.; Murray, C.; Auton, T. R.; Paolini, G. V.; Mee, P. M. *J. Comp. Aid. Mol. Design* **1997**, *11*, 425.
- (35) Verdonk, M. L.; Cole, J. C.; Hartshorn, M. J.; Murray, C. W.; Taylor, R. D. *Proteins* **2003**, *52*, 609.
- (36) Korb, O.; Stutzle, T.; Exner, T. E. *J. Chem. Inf. Model.* **2009**, *49*, 84.
- (37) Mooij, W. T. M.; Verdonk, M. L. *Proteins* **2005**, *61*, 272.
- (38) Bennett, K. L.; Funk, M.; Tschermutter, M.; Breitwieser, F. P.; Planyavsky, M.; Mohien, C. U.; Muller, A.; Trajanoski, Z.; Colinge, J.; Superti-Furga, G.; Schmidt-Erfurth, U. *J. Proteomics* **2011**, *74*, 151.
- (39) Colinge, J.; Masselot, A.; Giron, M.; Dessingy, T.; Magnin, J. *Proteomics* **2003**, *3*, 1454.
- (40) Olsen, J. V.; de Godoy, L. M. F.; Li, G. Q.; Macek, B.; Mortensen, P.; Pesch, R.; Makarov, A.; Lange, O.; Horning, S.; Mann, M. *Mol. Cell Proteomics* **2005**, *4*, 2010.
- (41) Naik, S.; Bhattacharjya, G.; Talukdar, B.; Patel, Bhisma K. *Eur. J. Org. Chem.* **2004**, *2004*, 1254.
- (42) Superti-Furga, G.; Huber, K.; Winter, G. In *Designing Multi-Target Drugs*; Morphy, J. R., Harris, C. J., Eds.; The Royal Society of Chemistry: Cambridge, UK, 2012; Vol. 21, p 94.
- (43) Rix, U.; Gridling, M.; Superti-Furga, G. *Methods Mol. Biol.* **2012**, *803*, 25.
- (44) Letondor, C.; Pordea, A.; Humbert, N.; Ivanova, A.; Mazurek, S.; Novic, M.; Ward, T. R. *J. Am. Chem. Soc.* **2006**, *128*, 8320.
- (45) Allardyce, C. S.; Dyson, P. J.; Ellis, D. J.; Heath, S. L. *Chem. Commun.* **2001**, 1396.
- (46) Fadden, P.; Huang, K. H.; Veal, J. M.; Steed, P. M.; Barabasz, A. F.; Foley, B.; Hu, M.; Partridge, J. M.; Rice, J.; Scott, A.; Dubois, L. G.; Freed, T. A.; Rehder, S. M. A.; Barta, T. E.; Hughes, P. F.; Ommen, A.; Ma, W.; Smith, E. D.; Woodward, S. A.; Eaves, J.; Hanson, G. J.; Hinkley, L.; Jenks, M.; Lewis, M.; Otto, J.; Pronk, G. J.; Verleysen, K.; Haystead, T. A.; Hall, S. E. *Chem. Biol.* **2010**, *17*, 686.

Supporting Information

to

Target Profiling of RAPTA Drugs by Chemical Proteomics

Maria V. Babak,^{a,b} Samuel M. Meier,^b Kilian Huber,^c Jóhannes Reynisson,^a Anton A. Legin,^b
Michael A. Jakupec,^b Alexander Roller,^b Alexey Stukalov,^c Manuela Gridling,^c Keiryn L.
Bennett,^c Jacques Colinge,^c Walter Berger,^d Paul J. Dyson,^e Giulio Superti-Furga,^c Bernhard K.
Keppler,^b Christian G. Hartinger^{a,b,*}

^a School of Chemical Sciences, The University of Auckland, Private Bag 92019, Auckland 1142, New Zealand

^b Institute of Inorganic Chemistry, University of Vienna, Waehringer Str. 42, A-1090 Vienna, Austria

^c CeMM Research Center for Molecular Medicine, Lazarettgasse 14, AKH BT 25.3, A-1090 Vienna, Austria

^d Department of Medicine I, Institute of Cancer Research, Medical University Vienna, Borschkegasse 8a, A-1090 Vienna, Austria

^e Institut des Sciences et Ingénierie Chimiques, Ecole Polytechnique Fédérale de Lausanne, CH-1015 Lausanne, Switzerland

Table of Contents

Crystal data and details of data collection for **1** and **3**

Key bond lengths and angles observed in the molecular structures of **1**, **3^b** and RAPTA-C

Concentration–effect curves of complexes **1–3** in the human ovarian cancer cell line CH1

Deconvoluted mass spectra of ubiquitin and **1** or **3** after incubation for 24 h

Deconvoluted mass spectra of cytochrome C and **1** or **3** after incubation for 24 h

ESI-IT mass spectra of **1** in dimethylsulfoxide

ESI-IT tandem mass spectrometric analysis of the signal at m/z 527.81 from the solution of **1** in dimethylsulfoxide after 24 h

Time-dependent ¹H NMR study on the stability of **1** in dimethylsulfoxide-*d*⁶

ESI-IT mass spectrum of **1** in dry dimethylformamide after 24 h

nESI-Q-TOF mass spectra of **1** in water after 2 and 48 hours

Experimental isotopic distributions and simulations of the mass signals of **1,2,3** in water

List of proteins identified by chemical proteomics. Numbers indicate spectral counts.

Table S1. Crystal data and details of data collection for **1** and **3**.

Complex	1	3
CCDC no.	972667	972668
Empirical formula	C ₁₄ H ₂₆ Cl ₃ N ₄ OPRu	C ₁₅ H ₂₃ Cl ₂ N ₄ OPRu
Fw	504.78	478.31
Crystal system	monoclinic	triclinic
Space group	<i>P</i> 2 ₁ / <i>n</i>	<i>P</i> -1
<i>a</i> , Å	6.9163(14)	10.5379(5)
<i>b</i> , Å	23.660(4)	12.8283(6)
<i>c</i> , Å	11.8396(19)	13.7451(7)
α , deg	90	100.766(2)
β , deg	97.078(9)	97.279(2)
γ , deg	90	91.491(2)
<i>V</i> , Å ³	1922.6(6)	1808.34(15)
<i>Z</i>	4	4
λ , Å	0.71073	0.71073
ρ_{calcd} , g cm ⁻³	1.740	1.757
Crystal size, mm ³	0.30 × 0.05 × 0.02	0.20 × 0.08 × 0.03
<i>T</i> , K	100(2)	100(2)
μ , cm ⁻¹	1.326	1.262
Reflns collected/unique	46451/3479	80118/10580
[<i>R</i> _{int}]	0.2078	0.0489
<i>R</i> 1 ^a	0.0548	0.0203
<i>wR</i> 2 ^b	0.1242	0.0505
GOF ^c	0.979	1.036

^a $R_1 = \Sigma||F_o| - F_c|/\Sigma|F_o|$, ^b $wR_2 = \{\Sigma w(F_o^2 - F_c^2)^2/\Sigma w(F_o^2)^2\}^{1/2}$. ^c GOF = $\{\Sigma[w(F_o^2 - F_c^2)^2]/(n - p)\}^{1/2}$, where *n* is the number of reflections and *p* is the total number of parameters refined.

Table S2. Key bond lengths and angles observed in the molecular structures of **1**, **3**^b and RAPTA-C.

Bond lengths (Å) and angles (°)	1	3	RAPTA-C ^a
Ru–arene _{centroid} / Å	1.700	1.699	1.692
Ru–C _{substituted} / Å	2.198(6)	2.2834(14)	2.207(10) 2.194(10)
Ru–C _{unsubstituted} / Å	2.189(6)	2.168(2)	2.179(9)
	2.195(6)	2.175(2)	2.182(10)
	2.201(7)	2.181(2)	2.210(10)
	2.213(7)	2.187(2)	2.240(10)
	2.267(6)	2.2659(14)	
Ru–Cl1 / Å	2.432(2)	2.3966(4)	2.412(3)
Ru–Cl2 / Å	2.414(2)	2.4291(4)	2.429(2)
Ru–P1 / Å	2.307(2)	2.2916(4)	2.296(2)
P1–Ru–Cl1 / °	82.28(6)	87.477(13)	87.09(9)
P1–Ru–Cl2 / °	84.60(6)	82.730(13)	83.42(8)
Cl1–Ru–Cl2 / °	88.55(6)	88.068(13)	87.25(8)

^a taken from Cambridge Structural Database, CCDC no. 161466

^b data for one of two independent molecules is given.

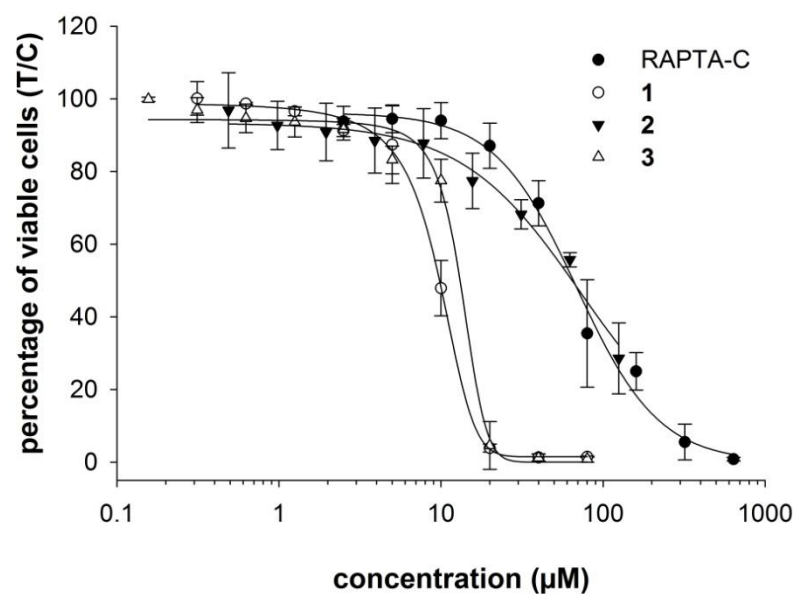


Figure S1. Concentration–effect curves of complexes **1–3** in the human ovarian cancer cell line CH1. Values were obtained by the MTT assay and are means \pm standard deviations from at least three independent experiments using exposure times of 96 h.

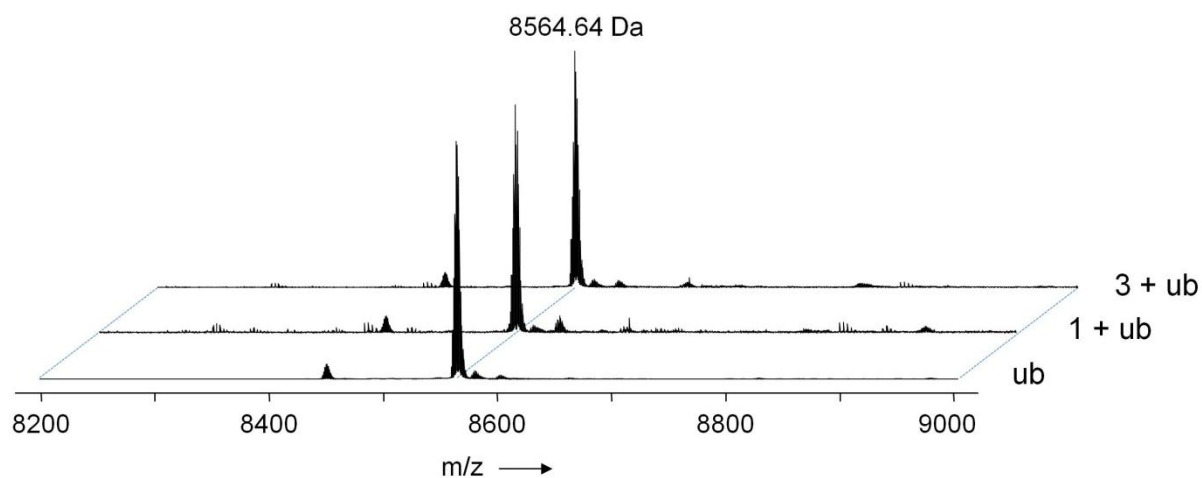


Figure S2. Deconvoluted mass spectra of ubiquitin and **1** or **3** after incubation for 24 h. The mixture was incubated at a 2 : 1 metal-to-protein ratio in buffer (pH 7.7).

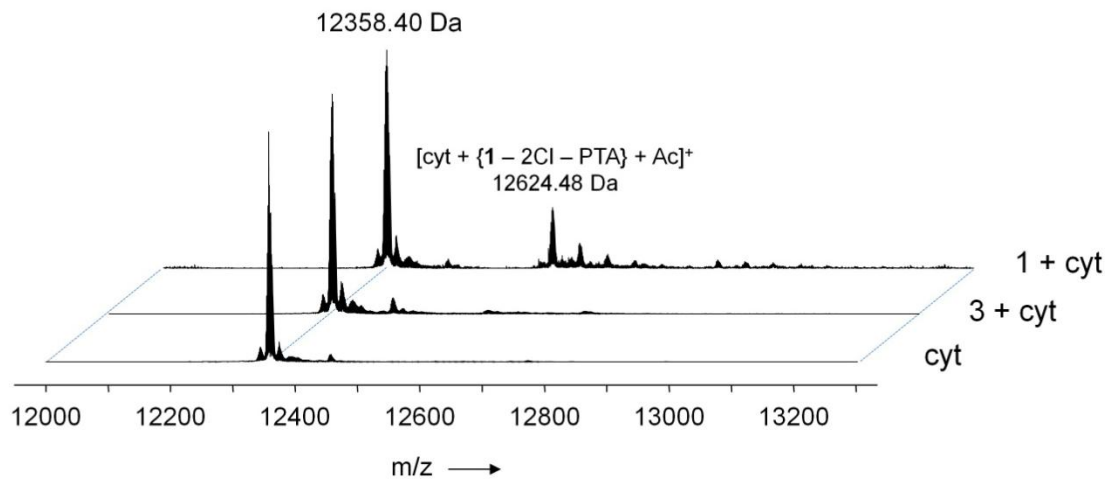


Figure S3. Deconvoluted mass spectra of cytochrome C and **1** or **3** after incubation for 24 h. The mixture was incubated at a 3 : 1 metal-to-protein ratio in buffer (pH 7.7).

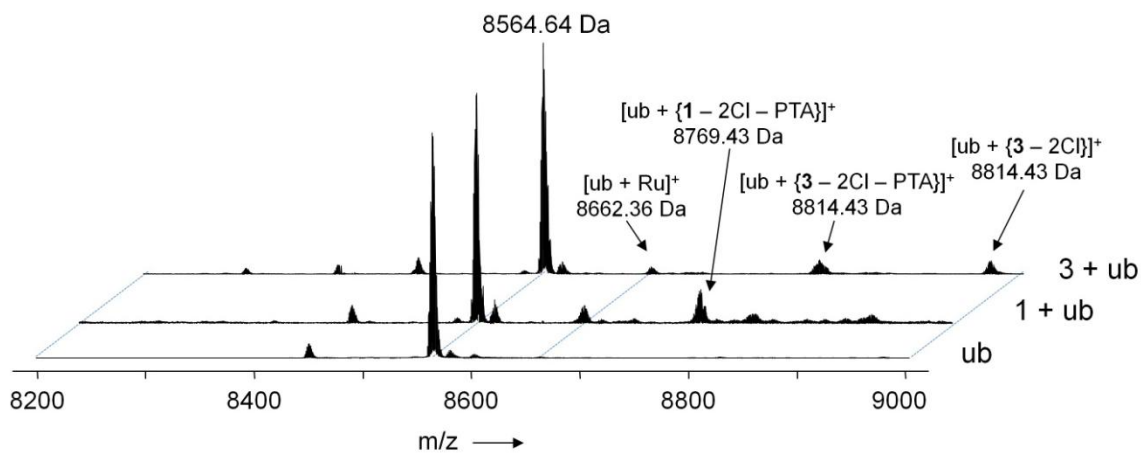


Figure S4. Deconvoluted mass spectra of ubiquitin and **1** or **3** after incubation for 48 h. The mixture was incubated at a 2 : 1 metal-to-protein ratio in water (pH 6.0).

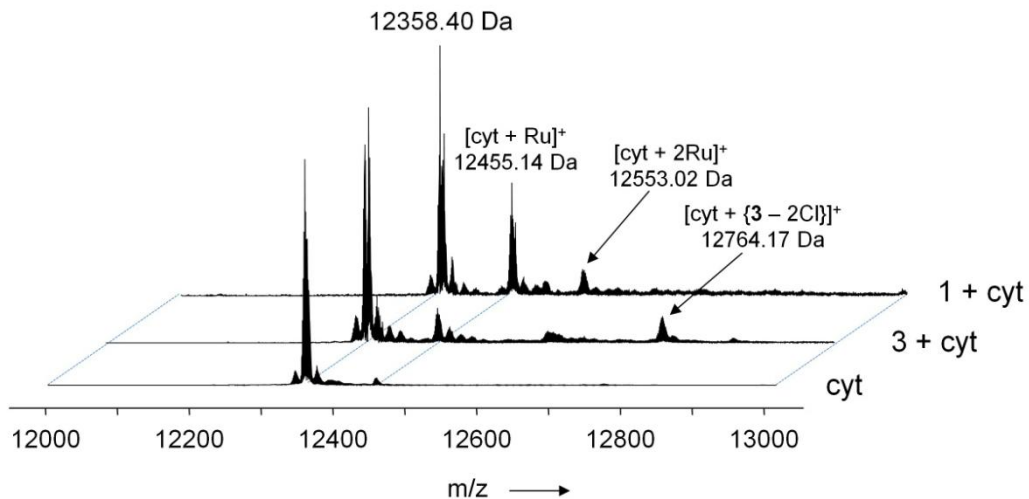


Figure S5. Deconvoluted mass spectra cytochrome C and **1** or **3** after incubation for 48 h. The mixture was incubated at a 3 : 1 metal-to-protein ratio in water (pH 6.0).

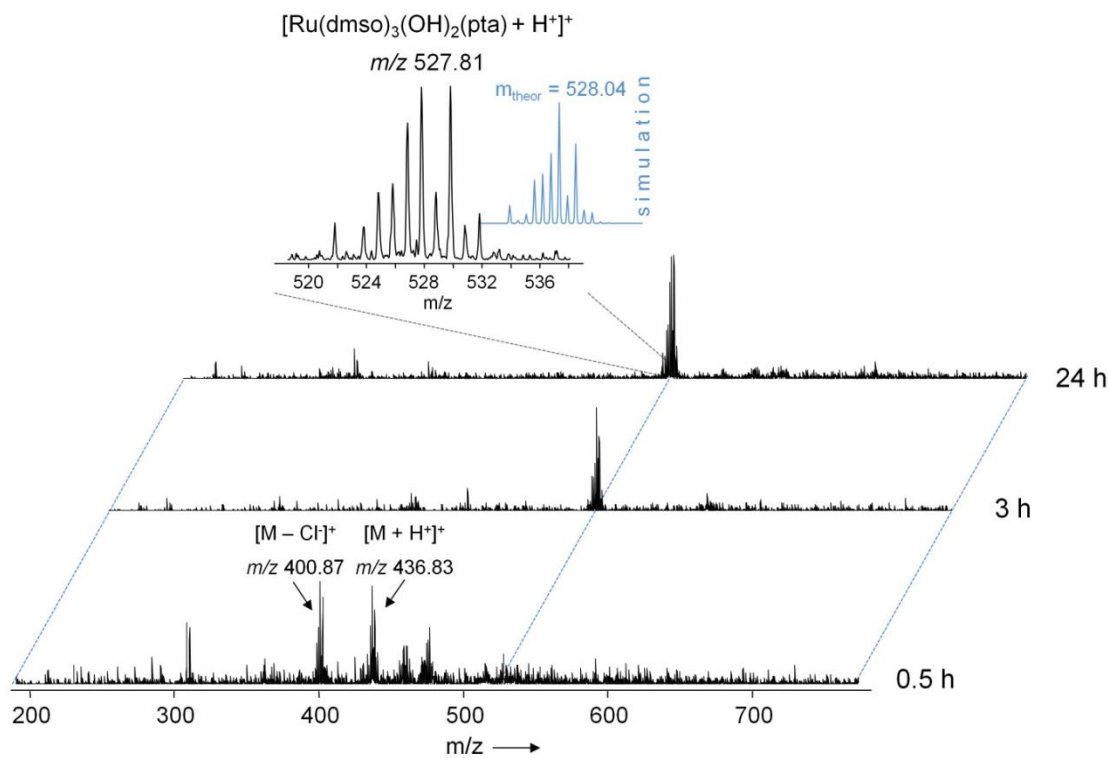


Figure S6. ESI-IT mass spectra of **1** in dimethylsulfoxide. The solution was diluted with water : methanol (1 : 1) prior to injection into the mass spectrometer.

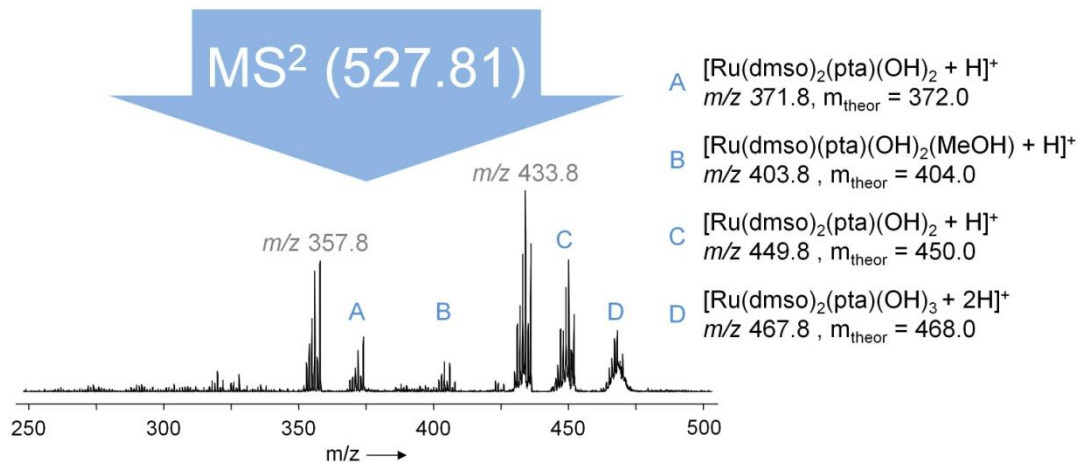


Figure S7. ESI-IT tandem mass spectrometric analysis of the signal at m/z 527.81 from the solution of **1** in dimethylsulfoxide after 24 h.

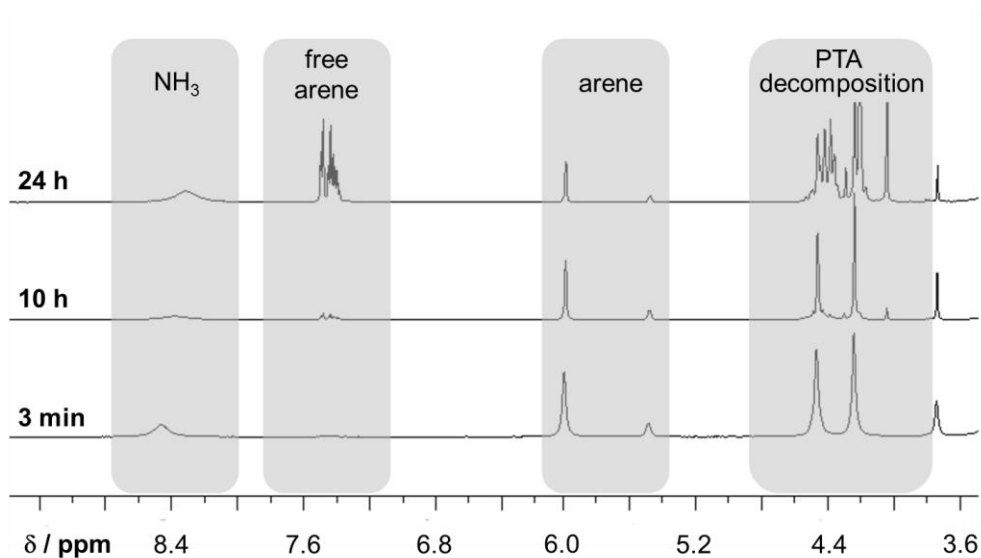


Figure S8. Time-dependent ^1H NMR study on the stability of **1** in dimethylsulfoxide- d^6 .

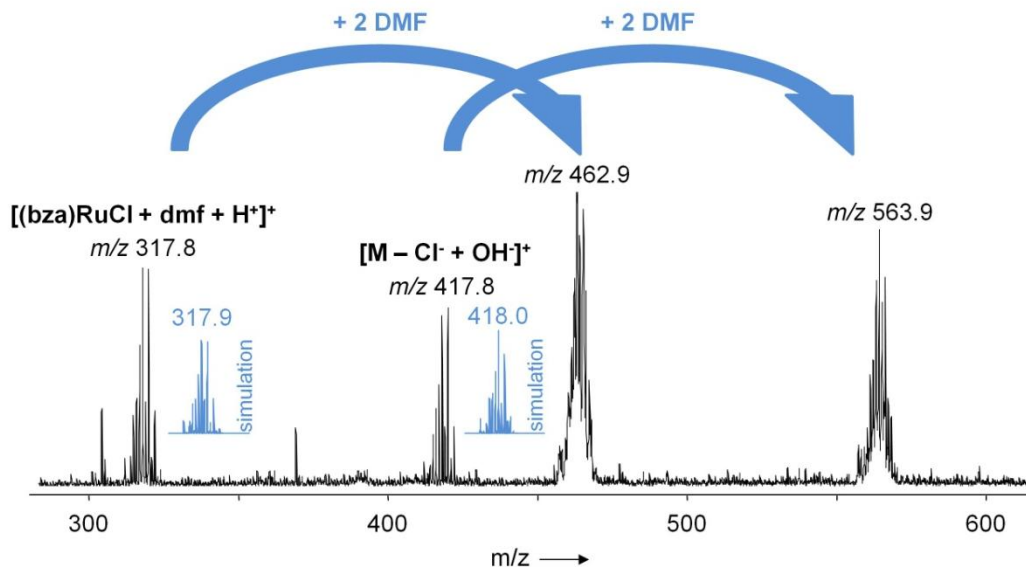


Figure S9. ESI-IT mass spectrum of **1** in dry dimethylformamide after 24 h. The solution was diluted with water : methanol (1 : 1) prior to injection into the mass spectrometer.

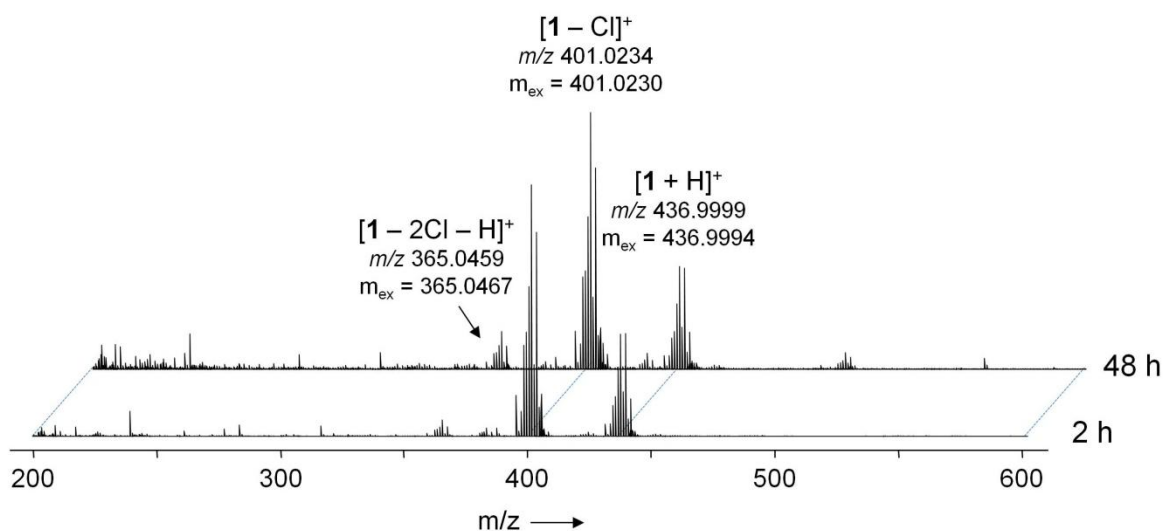


Figure S10. nESI-Q-TOF mass spectra of **1** in water after 2 and 48 hours. The solution was diluted with water prior to injection into the mass spectrometer.

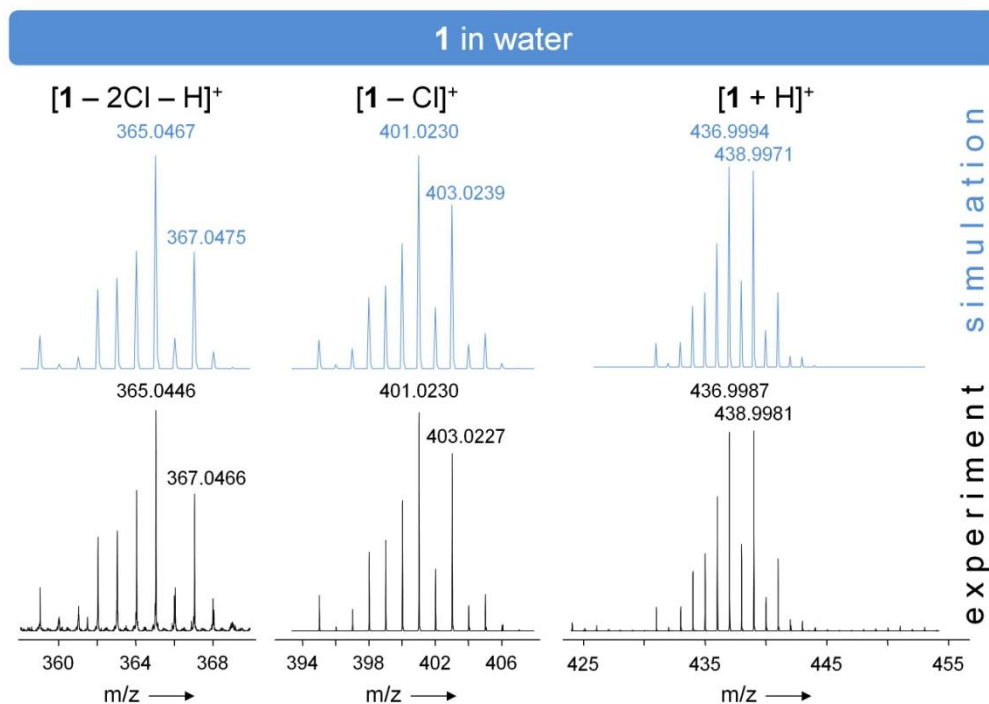


Figure S11. Experimental isotopic distributions and simulations of the mass signals of **1** in water.

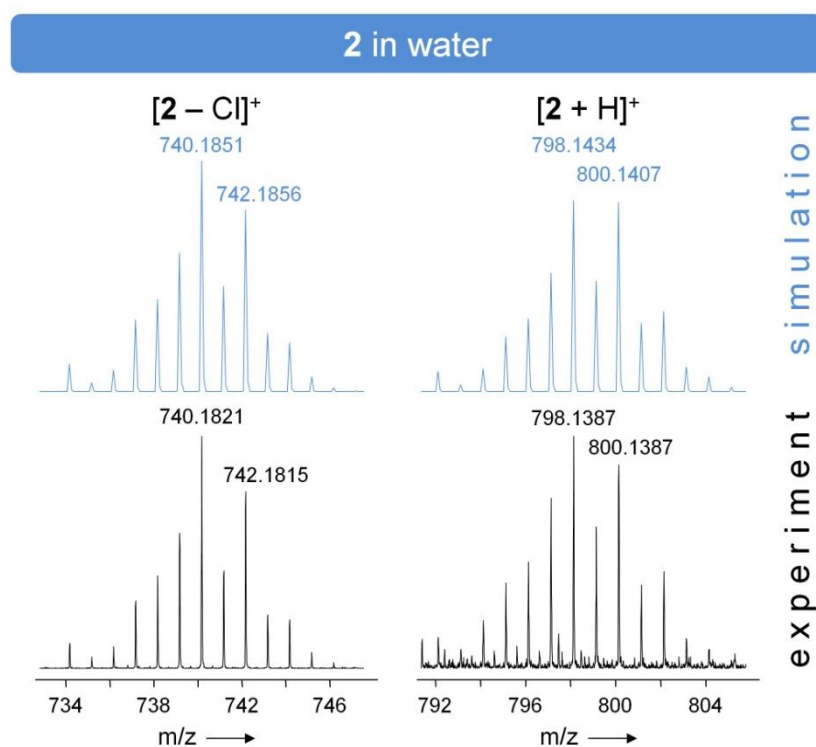


Figure S12. Experimental isotopic distributions and simulations of the mass signals of **2** in water.

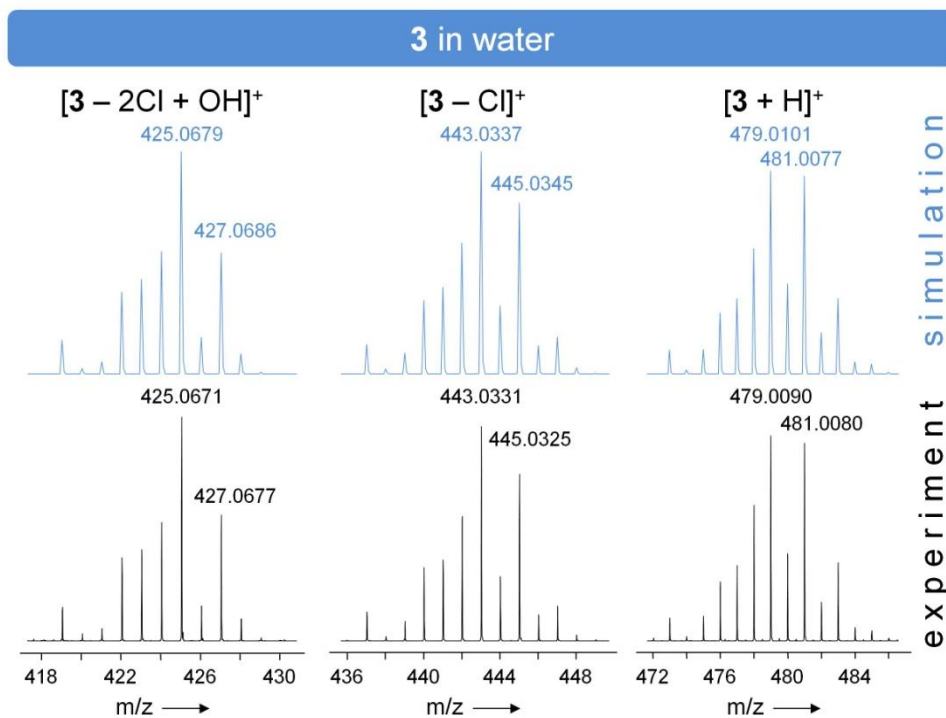


Figure S13. Experimental isotopic distributions and simulations of the mass signals of **3** in water.

Table S3. List of proteins identified by chemical proteomics. Numbers indicate spectral counts.

Protein ID	Description	Drug	Competition
RL23_HUMAN	60S ribosomal protein L23	14	14
IKBL1_HUMAN	NF-kappa-B inhibitor-like protein 1	3	7
RL29_HUMAN	60S ribosomal protein L29	13	10
ZN768_HUMAN	Zinc finger protein 768	5	2
NUMA1_HUMAN	Nuclear mitotic apparatus protein 1	10	12
HSP76_HUMAN	Heat shock 70 kDa protein 6	4	5
CLAP1_HUMAN	CLIP-associating protein 1	3	6
CMS1_HUMAN	Protein CMSS1	3	5
KIF1B_HUMAN	Kinesin-like protein KIF1B	6	6
BCD1_HUMAN	Box C/D snoRNA protein 1	4	3
SETX_HUMAN	Probable helicase senataxin	5	5
DBPA_HUMAN	DNA-binding protein A	4	5
ZEB2_HUMAN	Zinc finger E-box-binding homeobox 2	4	4
RL18_HUMAN	60S ribosomal protein L18	4	6
VIR_HUMAN	Protein virilizer homolog	3	0
RM34_HUMAN	39S ribosomal protein L34, mitochondrial	4	5
RRP1B_HUMAN	Ribosomal RNA processing protein 1 homolog B	4	1
RL27_HUMAN	60S ribosomal protein L27	5	6
H15_HUMAN	Histone H1.5	5	3
PTH_HUMAN	Probable peptidyl-tRNA hydrolase	5	4
NXF1_HUMAN	Nuclear RNA export factor 1	0	5
RIF1_HUMAN	Telomere-associated protein RIF1	4	4
HSP71_HUMAN	Heat shock 70 kDa protein 1A/1B	4	5
MK_HUMAN	Midkine	6	2
TIF1B_HUMAN	Transcription intermediary factor 1-beta	0	5
TB10B_HUMAN	TBC1 domain family member 10B	4	2
T2FA_HUMAN	General transcription factor IIF subunit 1	8	9
LS14B_HUMAN	Protein LSM14 homolog B	5	6
ZN625_HUMAN	Zinc finger protein 625	4	6
RS16_HUMAN	40S ribosomal protein S16	5	4
ZN589_HUMAN	Zinc finger protein 589	4	5
NOM1_HUMAN	Nucleolar MIF4G domain-containing protein 1	5	2
PESC_HUMAN	Pescadillo homolog	3	5
PTRF_HUMAN	Polymerase I and transcript release factor	11	11
RS19_HUMAN	40S ribosomal protein S19	6	4
RM36_HUMAN	39S ribosomal protein L36, mitochondrial	7	8
UTP11_HUMAN	Probable U3 small nucleolar RNA-associated protein 11	3	0
MET17_HUMAN	Methyltransferase-like protein 17, mitochondrial	2	6
AGRIN_HUMAN	Agtrin	5	4
ZN281_HUMAN	Zinc finger protein 281	5	5
IF2G_HUMAN	Eukaryotic translation initiation factor 2 subunit 3	0	4
OZF_HUMAN	Zinc finger protein OZF	5	5
PSB5_HUMAN	Proteasome subunit beta type-5	0	6
TCP4_HUMAN	Activated RNA polymerase II transcriptional coactivator p15	4	5
FA32A_HUMAN	Protein FAM32A	4	0
H31_HUMAN	Histone H3.1	4	1
BLM_HUMAN	Bloom syndrome protein	0	2
UBP37_HUMAN	Ubiquitin carboxyl-terminal hydrolase 37	1	4
RM15_HUMAN	39S ribosomal protein L15, mitochondrial	0	2

Table S3. continued

RUFY2_HUMAN	RUN and FYVE domain-containing protein 2	2	0
DDX47_HUMAN	Probable ATP-dependent RNA helicase DDX47	2	5
SPT5H_HUMAN	Transcription elongation factor SPT5	2	4
RL21_HUMAN	60S ribosomal protein L21	0	2
SRFB1_HUMAN	Serum response factor-binding protein 1	4	2
RAM_HUMAN	RNMT-activating mini protein	0	2
MET15_HUMAN	Probable methyltransferase-like protein 15	2	4
NOP2_HUMAN	Putative ribosomal RNA methyltransferase NOP2	0	2
AFG32_HUMAN	AFG3-like protein 2	0	2
JPH1_HUMAN	Junctophilin-1	2	2
MYL6B_HUMAN	Myosin light chain 6B	0	2
SAMD1_HUMAN	Atherin	5	5
DDX49_HUMAN	Probable ATP-dependent RNA helicase DDX49	0	2
C2D1A_HUMAN	Coiled-coil and C2 domain-containing protein 1A	2	2
ZN248_HUMAN	Zinc finger protein 248	2	2
ZC3H3_HUMAN	Zinc finger CCCH domain-containing protein 3	0	2
SNUT2_HUMAN	U4/U6.U5 tri-snRNP-associated protein 2	1	2
SC24A_HUMAN	Protein transport protein Sec24A	2	5
NOG1_HUMAN	Nucleolar GTP-binding protein 1	0	2
HXA5_HUMAN	Homeobox protein Hox-A5	3	3
PLK1_HUMAN	Serine/threonine-protein kinase PLK1	0	2
SNUT1_HUMAN	U4/U6.U5 tri-snRNP-associated protein 1	4	6
RL19_HUMAN	60S ribosomal protein L19	4	4
ALKB2_HUMAN	Alpha-ketoglutarate-dependent dioxygenase alkB homolog 2	0	2
GTPBA_HUMAN	GTP-binding protein 10	0	3
FOXK1_HUMAN	Forkhead box protein K1	2	0
ATPO_HUMAN	ATP synthase subunit O, mitochondrial	1	3
HSPB1_HUMAN	Heat shock protein beta-1	1	4
GRP75_HUMAN	Stress-70 protein, mitochondrial	2	3
CLAP2_HUMAN	CLIP-associating protein 2	3	5
TAOK2_HUMAN	Serine/threonine-protein kinase TAO2	0	2
PHF6_HUMAN	PHD finger protein 6	2	4
UIF_HUMAN	UAP56-interacting factor	4	2
CC124_HUMAN	Coiled-coil domain-containing protein 124	4	4
CDK13_HUMAN	Cyclin-dependent kinase 13	0	3
NEUA_HUMAN	N-acetylneuraminase cytidylyltransferase	1	2
CHD7_HUMAN	Chromodomain-helicase-DNA-binding protein 7	4	3
MAP2_HUMAN	Microtubule-associated protein 2	1	4
CGBP1_HUMAN	CGG triplet repeat-binding protein 1	2	0
FGFP3_HUMAN	Fibroblast growth factor-binding protein 3	2	0
RS17_HUMAN	40S ribosomal protein S17	4	0
CR021_HUMAN	UPF0711 protein C18orf21	2	4
FBRL_HUMAN	rRNA 2'-O-methyltransferase fibrillarin	2	0
HMGA2_HUMAN	High mobility group protein HMGI-C	0	2
PTN_HUMAN	Pleiotrophin	5	3
RL39_HUMAN	60S ribosomal protein L39	21	15
MO4L2_HUMAN	Mortality factor 4-like protein 2	2	2
SPT2_HUMAN	Protein SPT2 homolog	4	2
KLF12_HUMAN	Krueppel-like factor 12	2	4
MBB1A_HUMAN	Myb-binding protein 1A	3	3
CENPV_HUMAN	Centromere protein V	6	6
THAP4_HUMAN	THAP domain-containing protein 4	4	4
HUTU_HUMAN	Urocanate hydratase	2	0
T53I2_HUMAN	Tumor protein p53-inducible nuclear protein 2	2	2
CHM4B_HUMAN	Charged multivesicular body protein 4b	2	0

Table S3. continued

SOX15_HUMAN	Protein SOX-15	0	2
MA7D3_HUMAN	MAP7 domain-containing protein 3	2	0
GNL3_HUMAN	Guanine nucleotide-binding protein-like 3	2	0
H2A1B_HUMAN	Histone H2A type 1-B/E	2	4
ZN644_HUMAN	Zinc finger protein 644	0	2
TR112_HUMAN	tRNA methyltransferase 112 homolog	4	4
CC152_HUMAN	Coiled-coil domain-containing protein 152	2	3
CE152_HUMAN	Centrosomal protein of 152 kDa	0	2
CD11B_HUMAN	Cyclin-dependent kinase 11B	0	3
CENPV_HUMAN	Centromere protein V	7	6
PLCD3_HUMAN	1-phosphatidylinositol 4,5-bisphosphate phosphodiesterase delta-3	0	2
ETV3_HUMAN	ETS translocation variant 3	0	2
RL18A_HUMAN	60S ribosomal protein L18a	2	4
ZN771_HUMAN	Zinc finger protein 771	0	4
ZN182_HUMAN	Zinc finger protein 182	0	2
ARH40_HUMAN	Rho guanine nucleotide exchange factor 40	0	3
RBM42_HUMAN	RNA-binding protein 42	2	3
PIAS2_HUMAN	E3 SUMO-protein ligase PIAS2	2	3
TSR1_HUMAN	Pre-rRNA-processing protein TSR1 homolog	1	3
RS20_HUMAN	40S ribosomal protein S20	2	0
ARRD1_HUMAN	Arrestin domain-containing protein 1	1	0
GFAP_HUMAN	Glial fibrillary acidic protein	2	1
SALL4_HUMAN	Sal-like protein 4	4	4
CHM2B_HUMAN	Charged multivesicular body protein 2b	2	1
NACA_HUMAN	Nascent polypeptide-associated complex subunit alpha	3	3
ZFY27_HUMAN	Protrudin	2	2
RM22_HUMAN	39S ribosomal protein L22, mitochondrial	2	1
RT14_HUMAN	28S ribosomal protein S14, mitochondrial	0	2
ZN664_HUMAN	Zinc finger protein 664	1	2
CP087_HUMAN	UPF0547 protein C16orf87	1	1
FGF2_HUMAN	Fibroblast growth factor 2	2	2
IF2A_HUMAN	Eukaryotic translation initiation factor 2 subunit 1	1	1
ARHG2_HUMAN	Rho guanine nucleotide exchange factor 2	2	2
SHRM3_HUMAN	Protein Shroom3	2	2
SAS10_HUMAN	Something about silencing protein 10	2	2
GNA12_HUMAN	Guanine nucleotide-binding protein subunit alpha-12	0	1
PHC2_HUMAN	Polyhomeotic-like protein 2	0	1
SOST_HUMAN	Sclerostin	1	2
SPS2L_HUMAN	SPATS2-like protein	1	1
GTPB6_HUMAN	Putative GTP-binding protein 6	0	1
DDX54_HUMAN	ATP-dependent RNA helicase DDX54	1	1
AROS_HUMAN	Active regulator of SIRT1	2	2
LN28A_HUMAN	Protein lin-28 homolog A	1	0
PDIA1_HUMAN	Protein disulfide-isomerase	0	2
SP9_HUMAN	Transcription factor Sp9	1	0
RMTL1_HUMAN	RNA methyltransferase-like protein 1	1	0
ZN655_HUMAN	Zinc finger protein 655	1	0
CDC42_HUMAN	Cell division control protein 42 homolog	2	2
TAF6L_HUMAN	TAF6-like RNA polymerase II p300/CBP-associated factor-associated factor 65 kDa subunit 6L	1	0
SIR7_HUMAN	NAD-dependent protein deacetylase sirtuin-7	0	1
TCF7_HUMAN	Transcription factor 7	1	1
RS29_HUMAN	40S ribosomal protein S29	1	0

Table S3. continued

CHTOP_HUMAN	Chromatin target of PRMT1 protein	0	1
DDX3X_HUMAN	ATP-dependent RNA helicase DDX3X	2	2
TSNA1_HUMAN	t-SNARE domain-containing protein 1	1	0
FCF1_HUMAN	rRNA-processing protein FCF1 homolog	1	2
ZN581_HUMAN	Zinc finger protein 581	1	2
LRC41_HUMAN	Leucine-rich repeat-containing protein 41	1	0
CCDC8_HUMAN	Coiled-coil domain-containing protein 8	0	1
HMGN1_HUMAN	Non-histone chromosomal protein HMG-14	1	0
CA174_HUMAN	UPF0688 protein C1orf174	2	3
PRPK_HUMAN	TP53-regulating kinase	0	2
NEP1_HUMAN	Ribosomal RNA small subunit methyltransferase NEP1	2	1
OTUD4_HUMAN	OTU domain-containing protein 4	2	0
NACC2_HUMAN	Nucleus accumbens-associated protein 2	0	2
MCES_HUMAN	mRNA cap guanine-N7 methyltransferase	0	1
RT23_HUMAN	28S ribosomal protein S23, mitochondrial	1	1
RL13A_HUMAN	60S ribosomal protein L13a	1	1
IMA2_HUMAN	Importin subunit alpha-2	0	1
SERF2_HUMAN	Small EDRK-rich factor 2	0	1
RT09_HUMAN	28S ribosomal protein S9, mitochondrial	0	1
RLA2_HUMAN	60S acidic ribosomal protein P2	1	1
PLEC_HUMAN	Plectin	1	2
PTMS_HUMAN	Parathyrosin	0	1
IRS2_HUMAN	Insulin receptor substrate 2	0	2
ZNF8_HUMAN	Zinc finger protein 8	0	1
ERI1_HUMAN	3'-5' exoribonuclease 1	0	1
ANKZ1_HUMAN	Ankyrin repeat and zinc finger domain-containing protein 1	2	1
GULP1_HUMAN	PTB domain-containing engulfment adapter protein 1	1	2
BPTF_HUMAN	Nucleosome-remodeling factor subunit BPTF	1	0

2. Half-sandwich ruthenium(II) biotin-conjugates as biological vectors to cancer cells

Maria V. Babak, Damian Plazuk, Samuel M. Meier, John Arabshahi, Jóhannes Reynisson, Błażej Rychlik, Andrzej Błaż, Muhammad Hanif, Sebastian Ströbl, Bernhard K. Keppler, Christian G. Hartinger

Manuscript to be submitted to *Chem. Eur. J.*, **2014**

Half-sandwich Ruthenium(II) Biotin Conjugates as Biological Vectors to Cancer Cells

Maria V. Babak,^[a, b, c] Damian Plazuk,^[e] Samuel M. Meier,^[c, d] Homayon John Arabshahi,^[b] Jóhannes Reynisson,^[b] Błażej Rychlik,^[f] Andrzej Błaż,^[f] Katarzyna Szulc,^[f] Muhammad Hanif,^[b] Sebastian Strobl,^[a] Alexander Roller,^[a] Bernhard K. Keppler,^[a, c] and Christian G. Hartinger*^[a, b, c]

^[a] Institute of Inorganic Chemistry, University of Vienna, Waehringer Str. 42, 1090 Vienna, Austria

^[b] School of Chemical Sciences, University of Auckland, Private Bag 92019, Auckland 1142, New Zealand

^[c] Research Platform “Translational Cancer Therapy Research” University of Vienna, Waehringer Str. 42, 1090 Vienna, Austria

^[d] Institute of Analytical Chemistry, University of Vienna, Waehringer Str. 38, 1090 Vienna, Austria

^[e] Department of Organic Chemistry, Faculty of Chemistry, University of Łódź, Tamka 12, 91-403 Łódź, Poland

^[f] Cytometry Lab, Department of Molecular Biophysics, Faculty of Biology and Environmental Protection, University of Łódź, 12/16 Banacha St., 90-237 Łódź, Poland

Correspondence should be addressed to:

Prof. C. G. Hartinger

School of Chemical Sciences, University of Auckland

Private Bag 92019, Auckland 1142, New Zealand

Fax: (+64)9 373 7599 ext 87422

E-mail: c.hartinger@auckland.ac.nz

Homepage: <http://hartinger.wordpress.fos.auckland.ac.nz/>

Abstract

Ruthenium(II)-arene complexes with biotin-containing ligands were prepared in order to develop a novel drug delivery system based on tumor-specific vitamin-receptor mediated endocytosis. Complexes were characterized by spectroscopic methods and their *in vitro* anticancer activity in cancer cell lines with various levels of biotin receptors (COLO205, HCT116 and SW620 cells) was tested in comparison with free ligands. In all cases, coordination of ruthenium resulted in significantly enhanced cytotoxicity. The affinity of Ru^{II}(biotin) complexes to avidin was investigated and was lower than that of unmodified biotin. High values of Hill coefficients (2.012–2.851) suggest strong positive cooperation between complexes and the protein. In order to estimate the likelihood of binding to the SMVT transporter, docking studies with avidin and streptavidin were conducted. The results of the docking experiments explain to some extent the *in vitro* anticancer activity data. These novel half-sandwich ruthenium(II) biotin conjugates may act as biological vectors to cancer cells.

Keywords: cancer, arene ligands, sodium multivitamin transporter (SMVT), biotin-avidin interactions, docking

Introduction

The most frequently used chemotherapeutic agents target cells depending on the speed of their division. However, they cannot distinguish between cancer cells and rapidly dividing epithelial cells, which leads to low selectivity and severe side effects, such as nausea, loss of hair, and development of ulcers. As a result, a number of patients refuse or stop adjuvant chemotherapy.^[1,2] Therefore, a key feature of new chemotherapeutic agents is selectivity for cancerous cells over healthy tissue. This can be achieved by exploiting intrinsic differences between healthy and tumor cells. One strategy is to take advantage of the fact that cancerous cells over-express various receptors on the surface of tumor cells which are found to a lower extent for healthy cells. If an anticancer agent can selectively interact with one of those receptors, a cytotoxin may be accumulated more effectively in affected cells. Consequently, the therapeutic effect will be enhanced and adverse effects will be reduced.

Cancer cells require a significant amount of vitamins to sustain their rapid growth. Moreover, there is a strong correlation between the level of over-expression of vitamin receptors and the stage of tumor growth with the highest levels for stage IV.^[3] The attachment of vitamins, such as vitamin B12, folic acid, and biotin to anticancer prodrugs is therefore a worthwhile strategy to enhance tumor targeting.^[4] Various cancer cell types express higher levels of biotin receptors than of folate or vitamin B12 receptors and consequently display higher uptake of biotin-modified molecules. It was reported that biotin derivatives were also more effective in killing cancer cells, which makes biotin a particularly promising vector.^[5]

The main biotin uptake system in human intestinal epithelial cells is the sodium-dependent multivitamin transporter (hSMVT) system. SMVT is a protein (635 amino acids) encoded by the *SLC5A6* gene, which was found to be activated in various aggressive cancer cell lines.^[6,7] Consequently, biotinylation of compounds converts them into biological vectors to SMVT-overexpressing cells. This has been the subject of numerous studies with organic drugs and drug candidates (camptothecin,^[8] methotrexate,^[5,9] doxorubicin,^[5] paclitaxel,^[10-12] gemcitabine,^[13,14] polyamidoamine dendrimers (PAMAM),^[15-17] and TAT peptides^[18,19]). However, the targeted delivery of analogous metal-based compounds remains largely unexplored. Although a number of metal-based biotin compounds has been reported, only a few have been tested for their biological properties in living cells. Lo and coworkers evaluated the anticancer activity of Re,^[20,21] Ir,^[22,23] and Rh^[23] complexes with a range of polyaromatic diimine ligands with a

differing number of attached biotin moieties. The cytotoxicity of the complexes was strongly dependent on the number of biotin pendants, with lower IC₅₀ values corresponding to a lower number of biotin residues.^[21] However, non-biotinylated analogues with a similar structure exhibited the same order of cytotoxicity as the biotinylated derivatives. Similarly, the cytotoxicity of a biotin-appended RAPTA complex was not higher than of non-modified RAPTA-C ([Ru(η^6 -*p*-cymene)Cl₂(PTA)], where PTA is 1,3,5-triaza-7-phosphaadamantane).^[24] In contrast, biotin-ferrocene conjugates^[25] and biotinylated cisplatin-loaded nanoparticles^[15] showed a significant increase of cytotoxicity compared with the respective non-biotinylated derivatives. However, much of the data was collected on different cell lines with different affinity and capacity of the hSMVT transporter.^[26]

Herein, we present the systematic investigation of novel biotin-conjugated half-sandwich Ru(II) compounds in terms of their antiproliferative activity in cancer cells. We have, in particular, aimed to evaluate the correlation between the cytotoxicity and the *SLC5A6* gene (hSMVT) expression, as this is an important parameter if biotin functions as a vector. These studies were complemented by the determination of the binding affinity of the biotin derivatives to avidin and molecular docking experiments.

Experimental

Materials and methods

Materials from chemical suppliers were used as received, and all ruthenium complexes were synthesized under argon atmosphere in anhydrous solvents. Biotin *N*-hydroxysuccinimidyl ester, biotinyl-(*N*- ϵ -amidocaproic) acid, *N*-hydroxysuccinimidyl ester, biotinamidohexanoic acid,^[27] $[\{(\eta^6\text{-}p\text{-cymene})\text{-RuCl}_2\}_2]$,^[28] and $[\text{Ru}(\eta^6\text{-}p\text{-cymene})\text{Cl}_2(\text{pyridine})]$ (**6**)^[29] were prepared according to literature procedures. Methanol was dried and distilled over Mg under argon atmosphere, tetrahydrofuran was distilled over Na under argon atmosphere or purchased from Acros (99.5%, extra dry over molecular sieve, stabilized, AcroSeal), and toluene was distilled under argon atmosphere. *N,N*-Dimethylformamide (99.8%, extra dry over molecular sieve, stabilized, AcroSeal) was purchased from Acros and $\text{RuCl}_3\cdot 3\text{H}_2\text{O}$ was from Johnson Matthey. D-Biotin was obtained from Iris Biotech GmbH, *N*-hydroxysuccinimide ($\geq 97\%$), dicyclohexylcarbodiimide (99%), 6-aminocaproic acid ($\geq 99\%$), 6-cyano-1*H*-indazole (95%), 4-(aminomethyl)pyridine (98%) and indazole (98%) from Aldrich, 1-methyl-2-pyrrolidinone (99%), lithium aluminium hydride (95%) and triethylamine (99%) from Acros. MilliQ water (18.2 M Ω ; Millipore Advantage A10, 185 UV Ultrapure Water System, Molsheim, France) was used for ESI-IT MS studies.

Elemental analyses were performed by the Microanalytical Laboratory of the Faculty of Chemistry of the University of Vienna. The ^1H , $^{13}\text{C}\{^1\text{H}\}$ and $^{19}\text{F}\{^1\text{H}\}$ NMR spectra were recorded at 500.10, 125.75 and 470.56 MHz on a Bruker FT NMR spectrometer Avance II 500 MHz. Two-dimensional ^1H - ^1H COSY, ^1H - ^1H NOESY, ^1H - ^{13}C HSQC NMR spectra were recorded on a Bruker Avance III 500 MHz NMR spectrometer at 500.32 (^1H) and 125.81 (^{13}C). Chemical shifts are given in parts per million (ppm) relative to the residual solvent peak.

Preparative RP-HPLC was performed on an Agilent 1200 Series system controlled by Chemstation software at a flow rate 17.00 ml/min. The experimental conditions were as follows: silica-based C18 gel as stationary phase (XBridge BEH C18 OBD Prep Column, 130Å, 5 μm , 19 mm x 250 mm), $\text{H}_2\text{O}/\text{MeOH}/0.1\% \text{CF}_3\text{COOH}$ mobile phases, 5–7 ml injection volume, column temperature of 25 °C, UV-vis detection at 225, 250 and 275 nm. Analytical RP-HPLC analysis was carried out with a Dionex Summit system

controlled by Dionex Chromeleon 6.60 software at a flow rate of 1 mL/min. The experimental conditions were as follows: a silica-based C18 gel as stationary phase (Agilent Zorbax Eclipse, 4.6 × 250 mm), H₂O/MeOH/0.1% HCOOH mobile phases, UV-vis detection at 225, 250, 275, and 330 nm, column temperature of 25 °C. A concentration of 0.25 mM was used for the investigated complexes and 0.1 mM KI solution as the internal standard (injection volume 25 µL). Solvent gradients were equal for analytical and preparative HPLC: from 5-95% MeOH within 20 minutes.

X-ray diffraction measurement was performed on a Bruker X8 APEX II CCD diffractometer at 100 K. Crystals were obtained by slow diffusion of diethyl ether into dichloromethane (orange needles). A single crystal was positioned 40 mm from the detector, and 771 frames were measured, each for 10 s over 1° scan width. The data were processed with SAINT software.^[30] Crystal data, data collection parameters and structure refinement details for **6** are given in Table S1 of the Supporting Information and selected bond lengths and angles are listed in the caption to Figure 3. The structure was solved by direct methods and refined by full-matrix least-squares techniques. Non-hydrogen atoms were refined with anisotropic displacement parameters. Hydrogen atoms were placed at calculated positions and refined as riding atoms in the subsequent least squares model refinements. The isotropic thermal parameters were estimated to be 1.2-times the values of the equivalent isotropic thermal parameters of the non-hydrogen atoms to which hydrogen atoms are bonded. The following computer programs were used: structure solution, SHELXS-97; refinement, SHELXL-97;^[31] molecular diagrams, Mercury 3.0.

Stability tests with ESI-IT MS

The reactions of [Ru(η^6 -*p*-cymene)Cl₂]₂ with 2 equivalents of the ligands **2–5** in DMF were investigated using electrospray AmaZon SL ionization-ion trap mass spectrometry (ESI-IT MS, Bruker Daltonics GmbH, Bremen, Germany). The mixtures were analyzed after 3, 6 and 24 hours. Additionally, the reaction mixtures were freeze-dried, redissolved and analyzed again for compound integrity. Experiments were performed by direct infusion at a flow rate of 4 µL/min after diluting the solution 1:1'000 to final concentration of approx. 4 µM. Positive and negative ionization modes were acquired. Typical instrument parameters were as follows: average accumulation time 72 µs (ICC target 50'000), dry gas 8 L/min, dry temperature 200 °C, HV capillary –4.5 kV, HV end plate offset –0.5kV, nebulizer 8 psi, RF level 77%, trap drive 64.8. Mass spectra were

acquired and processed using Compass 1.3 and Data Analysis 4.0 (Bruker Daltonics GmbH, Bremen, Germany).

Docking studies

The structures were docked to a streptavidin crystal structure (3RY2, resolution 0.95 Å),^[32] which was obtained from the Protein Data Bank (PDB).^[33,34] The Scigress Ultraversion 7.7.0.47 program^[35] was used to prepare the crystal structure for docking, *i.e.*, hydrogen atoms were added, the co-crystallized ligand (biotin) was removed as well as crystallographic water molecules. The Scigress software suite was also used to build the compounds and the MM2^[36] force field was used to optimize the structures. The center of the binding pocket was defined as the oxygen atom on the bicyclic system ($x = 27.048$, $y = 10.773$, $z = 12.293$) in biotin with a 10 Å radius. Fifty docking runs were allowed for each ligand with default search efficiency (100%). The basic amino acids lysine and arginine were defined as protonated. Furthermore, aspartic and glutamic acids were assumed to be deprotonated. All the bonds to the metal center were fixed for the docking runs. The GoldScore (GS),^[37] ChemScore (CS),^[38,39] ChemPLP^[40] and ASP^[41] algorithms in the GOLD v5.1 software suite were implemented to predict binding modes and relative energies of the ligands.

Cell lines

The cell lines COLO 205 (human colon adenocarcinoma), HCT116 (human colorectal carcinoma) and SW620 (human colorectal adenocarcinoma) were purchased from the American Tissue and Cell Collection (ATCC) and were routinely tested every 3 months for *Mycoplasma* contamination. The cells were grown on RPMI1640 medium (biotin-free medium) with addition of Glutamax-I[®] (Gibco brand, Life Technologies Corporation) supplemented with 10% fetal bovine serum (Life Technologies Corporation). They were cultured in standard cell culture conditions (37 °C, 5% CO₂, 100% relative humidity).

Cytotoxicity tests in cancer cell lines

The cell line sensitivity to the compounds was determined according to a modified MTT-reduction assay.^[42] Cells suspended in 100 µl of medium were seeded on 96-well plates at a density of 10000/well. The cells were allowed to attach for 24 h and then the test compound was added at the desired concentration. Stock solutions were prepared in DMSO and the solvent concentration was kept constant in all wells including the controls. The final DMSO concentration did not exceed 0.01% v/v and was non-toxic to the cells. The cytotoxicity of the compounds was tested within the range of 3 nM – 30

μM . After 70 h of incubation, MTT was added to the medium to a final concentration of 1.1 mM. After further 2 h the medium was removed and the formazan crystals were dissolved in 100 μl of DMSO. The absorbance was measured at 580 nm analytical wavelength and 720 nm reference wavelength. The results were turned into percentage of controls and the IC_{50} values for each cell line and substance were calculated with the GraphPad Prism 5.02 software (GraphPad Inc.) using a sigmoidal dose-response variable slope fit.

Interactions with avidin

Relative affinity towards avidin was determined using Biotective™ Green reagent which is a fluorescent derivative of avidin in a complex with 2-(4'-hydroxyazobenzene)benzoic acid as a quencher^[43] included in the FluoReporter® Biotin Quantitation Assay Kit (Life Technologies Corporation). Briefly, at least three independent stock solutions of the biotinylated compounds were prepared in DMSO and then a series of dilutions in phosphate-buffered saline was made. 50 μL aliquots were transferred into wells of 96-well black PP plate and 50 μL of Biotective™ Green reagent solution was added. The mixture was incubated in the dark for 15 min at room temperature and the fluorescence was measured with an EnVision 2104 fluorescence microplate reader (Perkin Elmer) using 492/8 filter for excitation and 530/10 for emission. The fluorescence intensity is proportional to the amount of biotinylated compound bound to avidin and was plotted against the concentration of the test compound in GraphPad Prism 5.02 software (GraphPad Inc.). The apparent equilibrium dissociation constant as a measure of the affinity and the Hill coefficient as a measure of the co-operativity between biotin-binding sites of an avidin molecule were determined from these plots using equation (1).

$$B = (B_{\text{max}} \times C^H) / (K_d^H + C^H) \quad (1)$$

B is the amount of bound compound, B_{max} is maximum amount of bound compound, C is the compound concentration, H is the Hill coefficient and K_d is the apparent equilibrium dissociation constant.

Synthesis

6-(Methylamino)-indazole (**1**)

LiAlH₄ (12 mmol, 456 mg) was suspended in 80 ml of anhydrous THF at 0 °C under argon. A solution of 6-cyano-1*H*-indazole (3 mmol, 430 mg) in anhydrous THF under argon atmosphere was cautiously added to this suspension at 0 °C. After the color of the reaction mixture changed from light yellow to dark brown, it was allowed to warm to room temperature and refluxed for 4 hours. The solution turned almost colorless and a light yellow precipitate formed. The reaction mixture was cooled down to 0 °C and a minimum amount of water was added in 50 µl aliquots with the last aliquot following the termination of gas evaluation. The suspension was filtered and the pale yellow solution was evaporated to dryness and dried *in vacuo*. The crude product was purified by reversed-phase HPLC (H₂O/MeOH/0.1% CF₃COOH, gradient 5–95% MeOH, 20 min) followed by evaporation under reduced pressure to result in **1** as a white solid (243 mg, 54%). The purity was controlled by analytical HPLC (retention time 11.6 min). MS (ESI+): *m/z* 130.8 [M – NH₂]⁺, 148.4 [M + H]⁺. ¹H NMR (500.10 MHz; [D₆]DMSO): δ = 13.24 (s, 1H, *NH*-indazole), 8.22 (brs, 3H, NH₃⁺), 8.11 (s, 1H, H_u), 7.82 (d, 1H, ³J_{HH} = 8.4 Hz, H_s), 7.66 (s, 1H, H_w), 7.20 (d, 1H, ³J_{HH} = 8.4 Hz, H_r), 4.19 (s, 2H, H_p).

Biotin-(6-methylamido)-indazole (**2**)

Biotin *N*-hydroxysuccinimidyl ester (240 mg, 0.7 mmol) and 6-(Methylamino)-indazole (**1**, 103 mg, 0.7 mmol) were dissolved in a minimum amount of dimethylformamide (*ca.* 10 ml). Triethylamine (292 µl, 212 mg, 2.1 mmol) was added to the solution and the color changed to light yellow. The reaction mixture was stirred overnight at room temperature. Dimethylformamide was removed under reduced pressure and the residue was dissolved in a minimum amount of methanol and filtered. Diethyl ether (50 ml) and petroleum ether (50 ml) were added to the filtrate. The formed precipitate was collected by filtration, washed with petroleum ether and dried *in vacuo* to give a pale yellow powder. The crude product was purified by reversed-phase HPLC (H₂O/MeOH/0.1% CF₃COOH, gradient 5–95% MeOH, 20 min) followed by evaporation under reduced pressure to obtain **2** as a white solid (191 mg, 73%). The purity of the product was confirmed by analytical HPLC (retention time 17.8 min).

Elemental analysis (%) calcd for C₁₈H₂₃N₅O₂S·1.25 CF₃COOH (516.00 g mol⁻¹): C 47.72, H 4.74, N 13.57, S 6.21; found: C 47.58, H 4.89, N 13.58, S 6.42%; MS (ESI+): *m/z* 374.45 [M + H]⁺ (*m*_{theor} = 374.16). ¹H NMR (500.10 MHz; [D₆]DMSO): δ = 12.97 (s, 1H, *NH*-indazole), 8.36 (t, 1H, ³J_{HH} = 6.1 Hz, *NH*), 8.02 (1H, s, H_u), 7.69 (d, 1H, ³J_{HH} = 8.4 Hz, H_s), 7.38 (s, 1H, H_w), 7.01 (d, 1H, ³J_{HH} = 8.4 Hz, H_r), 6.41 (s, 1H, *NH*-biotin), 6.36 (s, 1H, *NH*-biotin), 4.39 (d, 2H, ³J_{HH} = 6.0 Hz, H_p), 4.31 (m, 1H, H_g), 4.13 (m, 1H, H_f), 3.10

(m, 1H, H_e), 2.83 (dd, 1H, ²J_{HH} = 12.5 Hz, ³J_{HH} = 5.0 Hz, H_h), 2.59 (d, 1H, ²J_{HH} = 12.6 Hz, H_{h'}), 2.17 (t, 2H, ³J_{HH} = 7.4 Hz, H_a), 1.68 – 1.28 (m, 6H, H_{b,c,d}). ¹³C NMR (125.75 MHz; [D₆]DMSO) δ = 172.5 (C_i), 163.2 (C_x), 140.6 (C_v), 138.4 (C_q), 133.7 (C_u), 122.3 (C_t), 120.8 (C_r), 120.8 (C_s), 108.5 (C_w), 61.5 (C_f), 59.7 (C_g), 55.9 (C_e), 40.4 (overlap with DMSO) (C_{h,h'}), 42.8 (C_p), 35.7 (C_a), 28.7 (C_{b/c/d}), 28.5 (C_{b/c/d}), 25.8 (C_{b/c/d}). ¹⁹F NMR (470.56 MHz; [D₆]DMSO): δ = -76.0 ppm (s, CF₃COOH).

Biotin-(4-methylamido)-pyridine (3)

Biotin *N*-hydroxysuccinimidyl ester (512 mg, 1.5 mmol) and 4-(aminomethyl)pyridine (243 mg, 2.25 mmol) were dissolved in a minimum amount of dimethylformamide (ca. 10 ml). Triethylamine (418 μl, 303 mg, 3 mmol) addition to the solution caused a color change to light yellow. The reaction mixture was stirred overnight at room temperature. Dimethylformamide was removed under reduced pressure and the residue was subsequently washed with ether. Then it was dissolved in a minimum amount of methanol and filtered. Diethyl ether (50 ml) and petroleum ether (50 ml) were added to a filtrate, and precipitate was removed by filtration, washed with petroleum ether and dried *in vacuo* to give a pale yellow powder. The crude product was purified by reversed phase HPLC (H₂O/MeOH/0.1% CF₃COOH, gradient 5–95% MeOH, 20 min) followed by evaporation under reduced pressure to result in **3** as a white solid (331 mg, 66%). The purity of the product was confirmed by the analytical HPLC (retention time 12.8 min).

Elemental analysis (%) calcd for C₁₆H₂₂N₄O₂S·1.1 H₂O (354.25 g mol⁻¹): C 54.25, H 6.89, N 15.82, S 9.05; found: C 54.47, H 6.52, N 15.55, S 8.89%; MS (ESI+): m/z 335.14 [M + H]⁺ (m_{theor} = 335.15). ¹H NMR (500.10 MHz; [D₆]DMSO): δ = 8.50 (dd, 2H, ³J_{HH} = 4.4 Hz, ⁴J_{HH} = 1.6 Hz, H_{v,s}), 8.41 (t, 1H, ³J_{HH} = 5.9 Hz, NH), 7.24 (dd, 2H, ³J_{HH} = 4.4 Hz, ⁴J_{HH} = 1.5 Hz, H_{w,r}), 6.43 (s, 1H, NH-biotin), 6.37 (s, 1H, NH-biotin), 4.32 (m, 1H, H_g), 4.29 (d, 2H, ³J_{HH} = 5.9 Hz, H_p), 4.14 (m, 1H, H_f), 3.12 (m, 1H, H_e), 2.84 (dd, 1H, ²J_{HH} = 12.6 Hz, ³J_{HH} = 5.1 Hz, H_h), 2.59 (d, 1H, ²J_{HH} = 12.5 Hz, H_{h'}), 2.19 (t, 2H, ³J_{HH} = 7.4 Hz, H_a), 1.68 – 1.28 (m, 6H, H_{b,c,d}). ¹³C NMR (125.75 MHz; [D₆]DMSO) δ = 172.9 (C_i), 163.2 (C_x), 150.0 (C_{s,v}), 149.2 (C_q), 122.5 (C_{r,w}), 61.5 (C_f), 59.7 (C_g), 55.9 (C_e), 41.5 (C_p), 40.4 (overlap with DMSO) (C_{h,h'}), 35.6 (C_a), 28.7 (C_{b/c/d}), 28.5 (C_{b/c/d}), 25.7 (C_{b/c/d}).

Biotinyl-(N-ε-amidocaproic)-(6-methylamido)-indazole (4)

Biotinamidohexanoic acid *N*-hydroxysuccinimidyl ester (**3**, 545 mg, 1.2 mmol) was dissolved in a minimum amount of dimethylformamide (ca. 20 ml). Triethylamine (334 μl, 2.4 mmol, 242 mg) and (1H-indazol-6-yl)methanamine (**1**; 176 mg, 1.2 mmol) in 10 ml of

dimethylformamide were added. The mixture was stirred for 20 h at room temperature, filtered and evaporated under reduced pressure. The residue was dissolved in a minimum amount of methanol and filtered. Diethyl ether (50 mL) was added to the filtrate, and the precipitate was removed by filtration, washed with diethyl ether and dried *in vacuo* to give pale yellow solid. The crude product was purified by reversed phase HPLC (H₂O/MeOH/0.1% CF₃COOH, gradient 5–95% MeOH, 20 min) followed by evaporation under reduced pressure to result in **4** as a white solid (128 mg, 22%). The purity of the product was confirmed by the analytical HPLC (retention time 18.7 min).

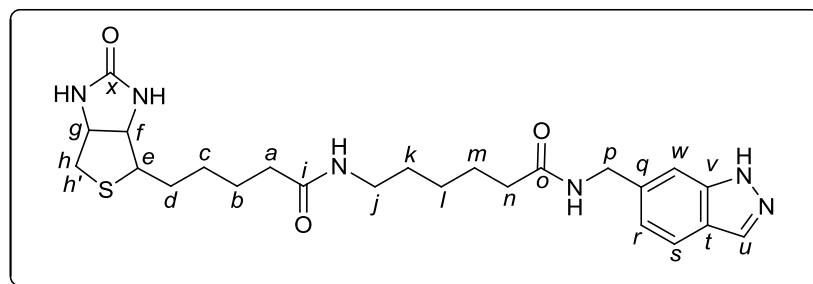


Figure 1. NMR numbering scheme used for **4**.

Elemental analysis (%) calcd for C₂₄H₃₄N₆O₃S·0.3 CF₃COOH·H₂O (538.85 g mol⁻¹): C 54.83, H 6.79, N 15.60, S 5.95; found: C 54.51, H 6.90, N 15.91, S 5.76%; MS (ESI+): m/z 486.93 [M+H]⁺ (m_{theor} = 487.25). ¹H NMR (500.10 MHz; [D₆]DMSO): δ = 12.98 (s, 1H, NH-indazole), 8.36 (t, 1H, ³J_{HH} = 5.9 Hz, NH), 8.02 (1H, m, H_u), 7.76 (t, 1H, ³J_{HH} = 5.6 Hz, NH), 7.69 (d, 1H, ³J_{HH} = 8.3 Hz, H_s), 7.37 (s, 1H, H_w), 7.01 (d, 1H, ³J_{HH} = 8.3 Hz, H_r), 6.41 (s, 1H, NH-biotin), 6.35 (s, 1H, NH-biotin), 4.39 (d, 2H, ³J_{HH} = 5.9 Hz, H_p), 4.31 (m, 1H, H_g), 4.13 (m, 1H, H_f), 3.40 (m, 1H, H_e), 3.02 (dd, 2H, ³J_{HH} = 12.8 Hz, ³J_{HH} = 6.8 Hz, H_j), 2.82 (dd, 1H, ²J_{HH} = 12.4 Hz, ³J_{HH} = 5.0 Hz, H_h), 2.58 (d, 1H, ²J_{HH} = 12.4 Hz, H_{h'}), 2.16 (t, 2H, ³J_{HH} = 7.4 Hz, H_a), 2.05 (t, 2H, ³J_{HH} = 7.4 Hz, H_n), 1.67 – 1.28 (m, 12H, H_{b,c,d,m,l,k}). ¹³C NMR (125.75 MHz; [D₆]DMSO) δ = 172.6 (C_o), 172.4 (C_i), 163.2 (C_x), 140.6 (C_v), 138.4 (C_q), 133.7 (C_u), 122.3 (C_t), 120.8 (C_r), 120.8 (C_s), 108.4 (C_w), 61.5 (C_f), 59.7 (C_g), 55.9 (C_e), 40.4 (overlap with DMSO) (C_{h,h'}), 42.7 (C_p), 38.8 (C_j), 35.8 (C_a), 35.7 (C_n), 29.5 (C_{b/c/d/m/l/k}), 28.7 (C_{b/c/d/m/l/k}), 28.5 (C_{b/c/d/m/l/k}), 26.6 (C_{b/c/d/m/l/k}), 25.8 (C_{b/c/d/m/l/k}), 25.6 (C_{b/c/d/m/l/k}). ¹⁹F NMR (470.56 MHz; [D₆]DMSO): δ = -75.2 ppm (s, CF₃COOH).

Biotinyl-(N-ε-amidocaproic)-(4-methylamido)-pyridine (5)

The procedure of Lo *et al.* was used with additional purification steps.^[44] Biotinamidohexanoic acid *N*-hydroxysuccinimidyl ester (182 mg, 0.4 mmol) was

dissolved in a minimum amount of dimethylformamide (ca. 5 ml). Triethylamine (226 μ l, 164 mg, 1.6 mmol) and a solution of 4-(aminomethyl)-pyridine (65 mg, 0.6 mmol) in 5 ml of dimethylformamide were added. The mixture was stirred overnight at room temperature and evaporated to dryness under reduced pressure to give pale yellow oil. It was suspended in methanol and insoluble residue was removed by filtration. The filtrate was concentrated under reduced pressure and dichloromethane (7 ml) and diethyl ether (50 ml) were added. The precipitate was removed by filtration, washed with dichloromethane and diethyl ether, and dried *in vacuo* to give off-white solid. The crude product was purified by reversed phase HPLC (H₂O/MeOH/0.1% CF₃COOH, gradient 5–95% MeOH, 20 min) followed by evaporation under reduced pressure to result in **5** as a white solid (66 mg, 37%). The purity of the product was confirmed by the analytical HPLC (retention time 17.8 min).

Elemental analysis (%) calcd for C₂₂H₃₃N₅O₃S·0.9 CF₃COOH (550.22 g mol⁻¹): C 51.95, H 6.21, N 12.73, S 5.83, O 13.96; found: C 51.86, H 6.50, N 12.81, S 5.56, O 14.31%; MS (ESI+): m/z 448.20 [M+H]⁺ (m_{theor} = 448.24). ¹H NMR (500.10 MHz; [D₆]DMSO): δ = 8.59 (dd, 2H, ³J_{HH} = 6.0 Hz, ⁴J_{HH} = 1.4 Hz, H_{v,s}), 8.46 (t, 1H, ³J_{HH} = 5.8 Hz, NH), 7.74 (t, 1H, ³J_{HH} = 5.6 Hz, NH), 7.39 (dd, 2H, ³J_{HH} = 6.1 Hz, ⁴J_{HH} = 1.4 Hz, H_{w,r}), 6.42 (s, 1H, NH-biotin), 6.36 (s, 1H, NH-biotin), 4.35 (d, 2H, ³J_{HH} = 6.0 Hz, H_p), 4.31 (m, 1H, H_g), 4.14 (m, 1H, H_f), 3.11 (m, 1H, H_e), 3.02 (dd, 2H, ³J_{HH} = 12.8 Hz, ³J_{HH} = 6.9 Hz, H_j), 2.83 (dd, 1H, ²J_{HH} = 12.5 Hz, ³J_{HH} = 5.1 Hz, H_h), 2.59 (d, 1H, ²J_{HH} = 12.5 Hz, H_r), 2.19 (t, 2H, ³J_{HH} = 7.5 Hz, H_a), 2.05 (t, 2H, ³J_{HH} = 7.4 Hz, H_n), 1.67 – 1.28 (m, 12H, H_{b,c,d,m,l,k}). ¹³C NMR (125.75 MHz; [D₆]DMSO) δ = 173.0 (C_o), 172.3 (C_i), 163.2 (C_x), 152.3 (C_q), 147.9 (C_{s,v}), 123.2 (C_{r,w}), 61.5 (C_f), 59.7 (C_g), 55.9 (C_e), 41.7 (C_p), 40.4 (overlap with DMSO) (C_{h,h'}), 38.8 (C_j), 35.7 (C_a), 35.7 (C_n), 29.5 (C_{b/c/d/m/l/k}), 28.7 (C_{b/c/d/m/l/k}), 28.5 (C_{b/c/d/m/l/k}), 26.6 (C_{b/c/d/m/l/k}), 25.8 (C_{b/c/d/m/l/k}), 25.6 (C_{b/c/d/m/l/k}). ¹⁹F NMR (470.56 MHz; [D₆]DMSO): δ = -75.15 ppm (s, CF₃COOH).

[Ru(η^6 -*p*-cymene)Cl₂(κ N2-*H*1-indazole)] (**9**)

The synthetic method was adapted from a literature procedure.^[29] Indazole (35 mg, 0.3 mmol, 2 equiv.) was added to a suspension of [Ru(η^6 -*p*-cymene)Cl₂]₂ (92 mg, 0.15 mmol) in toluene (15 ml) at room temperature. Orange precipitate formed immediately. The resulting mixture was heated to reflux for 3 h. After the mixture was cooled, the precipitate was filtered, washed with petroleum ether (3 × 10 mL) and ether, dried *in vacuo*, affording 93 mg of an orange microcrystalline solid (yield 73%). Elemental analysis (%) calcd for C₁₇H₂₀Cl₂N₂Ru (424.33 g mol⁻¹): C 48.12, H 4.75, N 6.60; found: C 48.19, H 4.69, N 6.54%; ¹H NMR (500.10 MHz; CDCl₃): δ = 11.78 (s, 1H, NH-indazole),

8.41 (s, 1H, H_u), 7.71 (d, 1H, ³J_{HH} = 8.4 Hz, H_s), 7.41 (m, 2H, H_{r,w}), 7.19 (m, 1H, H_q), 5.59 (d, 2H, ³J_{HH} = 6.0 Hz, CH_{cym}), 5.41 (d, 2H, ³J_{HH} = 6.0 Hz, CH_{cym}), 3.00 (sept, 1H, ³J_{HH} = 7.0 Hz, CHMe₂), 2.28 (s, 3H, C₆H₄(CH₃)), 1.29 (d, 6H, ³J_{HH} = 7.0 Hz, CH(CH₃)₂) ppm.

General procedure for preparation of the complexes 7, 8, 10, 11

[Ru(η^6 -*p*-cymene)Cl₂]₂ (4.72 mg, 0.01 mmol) and **2–5** (2 equiv, 0.02 mmol) were dissolved in anhydrous DMF (2 ml). The reaction mixture was stirred for 3 hours, freeze-dried and *in situ* incubated with the cancer cells.

[Ru(η^6 -*p*-cymene)(biotin-(4-methylamido)- κ N1-pyridine)Cl₂] (**7**):

ESI-IT MS, pos. mode: *m/z* 285.06 [M – 2Cl]²⁺ (*m*_{theor} = 285.08), *m/z* 605.12 [M – Cl]⁺ (*m*_{theor} = 605.13).

[Ru(η^6 -*p*-cymene)(biotinyl-(*N*- ϵ -amidocaproic)-(4-methylamido)- κ N1-pyridine)Cl₂] (**8**)

ESI-IT MS, pos. mode: *m/z* 341.58 [M – 2Cl]²⁺ (*m*_{theor} = 341.62), *m/z* 682.20 [M – 2Cl – H]²⁺ (*m*_{theor} = 682.24), *m/z* 718.14 [M – Cl]⁺ (*m*_{theor} = 718.21).

[Ru(η^6 -*p*-cymene)(biotin-(6-methylamido)- κ N2-H1-indazole)Cl₂] (**10**)

ESI-IT MS, pos. mode: *m/z* 608.25 [M – 2Cl – H]²⁺ (*m*_{theor} = 608.16), *m/z* 644.31 [M – Cl]⁺ (*m*_{theor} = 644.14).

[Ru(η^6 -*p*-cymene)(biotinyl-(*N*- ϵ -amidocaproic)-(6-methylamido)- κ N2-H1-indazole)Cl₂] (**11**)

ESI-IT MS, pos. mode: *m/z* 360.33 [M – 2Cl]²⁺ (*m*_{theor} = 360.62), *m/z* 721.40 [M – 2Cl – H]²⁺ (*m*_{theor} = 721.25), *m/z* 757.35 [M – Cl]⁺ (*m*_{theor} = 757.22).

Results and Discussion

Synthesis

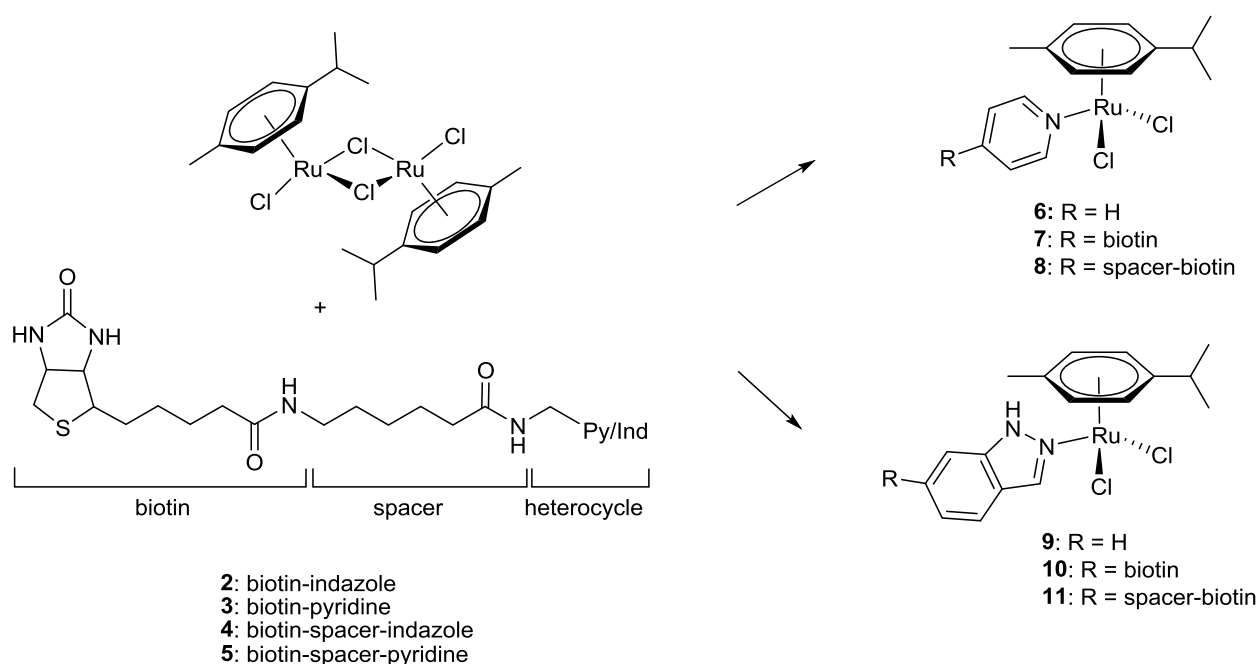
In order to test the effect of ruthenium-biotin conjugates on the viability of cancer cells and its correlation with the level of *SLC5A6* gene expression, we synthesized the biotin-containing ligands **2–5**, the corresponding half-sandwich ruthenium(II) complexes **7–10** and the structurally similar non-biotinylated ruthenium(II) analogues **6** and **11**. The SMVT transporter can recognize biotin, if the thiophane and keto fragments of biotin are

not modified.^[25,45] Therefore, these moieties remained unaltered, and the valeric carboxylic acid residue of biotin was used for further derivatization. Consequently, **2** and **3** were prepared by standard amide coupling of the biotin targeting unit with primary amino groups of *N*-heterocycles to allow coordination to the metal center. 4-Aminopyridine and 6-aminoindazole were found to be inappropriate for such coupling and therefore commercially available 4-(aminomethyl)pyridine and 6-(aminomethyl)indazole from the reduction of 6-cyano-1*H*-indazole with LiAlH₄ were used. For comparison purposes, the structurally similar ligands **4** and **5** with an incorporated aminohexanoyl linker were prepared. In the literature, the data on the effect of the spacer between the active component and targeting moiety on the biological activity of compounds is controversial. An aminohexanoyl spacer between biotin and a ferrocene complex displayed a detrimental effect on the cytotoxicity.^[25] Other studies revealed that such spacers dramatically increase the stability of Ru^{II}(polypyridine)–biotin complexes and their interactions with cell membranes.^[46] Moreover, it was demonstrated that spatial separation between biotin and the metal-based complex is vital for biorecognition of both units.^[47]

Compounds of the biotin–linker–*N*-heterocycle type such as **2–5** have been extensively used for various purposes and their syntheses are well established. In order to synthesize ruthenium complexes with these ligands, it is essential that they do not contain any trace of unreacted precursors which could also coordinate to the ruthenium fragment. Therefore, all ligands were additionally purified by reversed phase HPLC, and their purity was confirmed by analytical HPLC and elemental analysis. However, this resulted in low yield of the target compounds. 6-(Methylamino)-indazole can be used for coupling with biotin derivatives without HPLC purification. All ligands were characterized by ¹H and ¹³C{¹H} NMR (the atom numbering scheme is shown in Figure 1) as well as ESI-MS and elemental analysis.

In order to coordinate the biotin ligands to the Ru center, we adapted the procedure of Vock *et al.*, who developed the synthesis of half-sandwich Ru(II) complexes with a number of *N*-heterocyclic ligands.^[29] Following this method, the non-biotinylated Ru^{II}(cymene) complexes with pyridine (**6**) and indazole (**9**) ligands were obtained by refluxing [Ru(η⁶-*p*-cymene)Cl₂]₂ with the corresponding ligand in anhydrous toluene for 3 h. However, the analogous synthesis of Ru(II) biotin conjugates was seriously limited by the solubility of the biotin derivatives and the stability of the corresponding complexes. Ligands **2–5** were moderately soluble in ethanol and well soluble only in

dimethylformamide and dimethylsulfoxide. We have recently discovered that incubation of half-sandwich arene Ru(II) complexes in dimethylsulfoxide resulted in loss of the arene moiety.^[24] Therefore, we investigated the reactions of $[\text{Ru}(\eta^6\text{-}p\text{-cymene})\text{Cl}_2]_2$ with 2 equiv. of the ligands **2–5** in ethanol or dimethylformamide by means of ESI-MS. In the present study, ethanol was a less suitable solvent for such complexation reactions due to the marked formation of dinuclear Ru species, especially for **10** (for the mass spectrum see Figure 2) and **11** (Figure S7). The formation of the ruthenium complexes **7**, **8**, **10** and **11** was more selective in dimethylformamide although either dimeric hydrolysis products or DMF adducts accompanied by ligand release were detected for the complexes without aminohexanoic spacers, *i.e.*, **7** and **10**, respectively (Figure 2). It is known that the detection of coordinated mono-dentate *N*-donor ligands can be challenging with ESI-MS and indicates a limited complex stability under the ESI spraying conditions.^[48-50] However, this does not reflect the situation in solution. Interestingly, such species were not observed for the complexes with aminohexanoic spacers, *i.e.*, **8** and **11**. These findings suggest that once the ligand is coordinated to the ruthenium center, the spacer has a beneficial role on the stability of the resulting complexes. Consequently, the complex stability increases when the ligand contains indazole and/or a spacer.



Scheme 1. Biotinylation of half-sandwich Ru^{II} complexes (anhydrous DMF, Ru dimer : ligand = 1:2, 3 hours, RT)

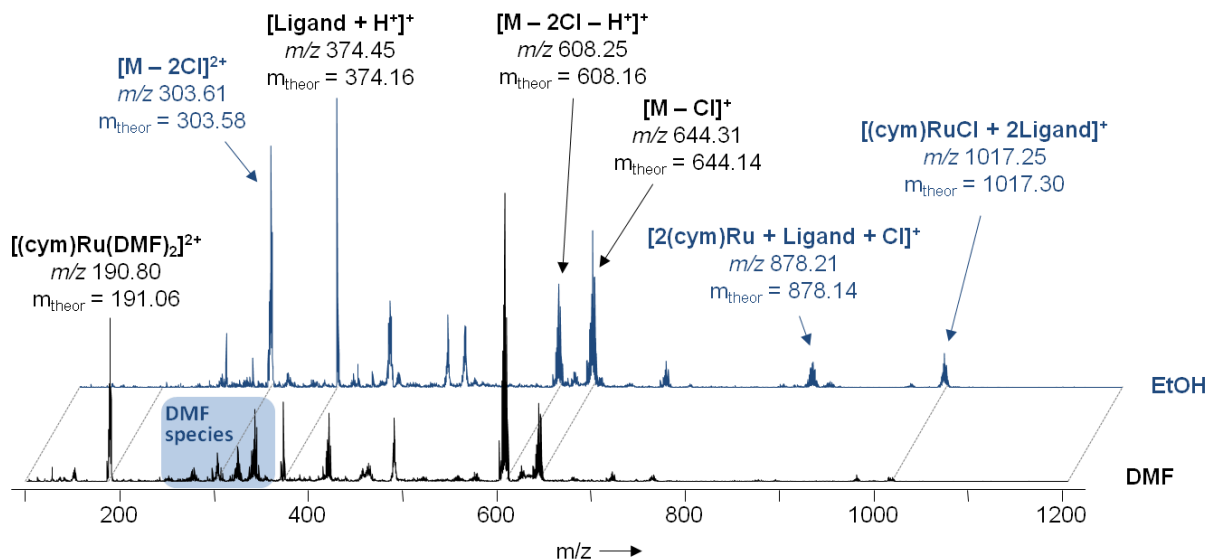


Figure 2. Full ESI-IT mass spectra of the reaction mixture yielding compound **10** after 3 h. The reactions were carried out in dimethylformamide (DMF) and ethanol (EtOH). The reaction using DMF as a solvent leads to a more selective formation of **10**.

The reactions were analyzed by ESI-MS after 3, 6 and 24 hours. Whereas **8**, **10** and **11** did not reveal any changes within 24 hours of incubation (Figure S4-S6), complex **7** was significantly less stable and started to decompose after 6 h (Scheme S2). Based on the results of the ESI-MS experiments, we modified the procedure of Vock *et al.* to stirring a mixture of $[Ru(\eta^6\text{-}p\text{-cymene})Cl_2]_2$ with the corresponding ligand in anhydrous dimethylformamide at room temperature for 3 h with subsequent removal of dimethylformamide by freeze-drying. This generic method was used for the synthesis of the biotinylated complexes **7**, **8**, **10** and **11** (Scheme 1). Non-biotinylated complex **6** was also obtained by this method and its characterization data was in agreement with published data.^[29] We assumed that lyophilization of the products did not affect their integrity, since no changes in ESI-MS spectra of lyophilized complexes were revealed. The novel complexes **7**, **8**, **10** and **11** were highly hygroscopic and moisture-sensitive, and their prolonged exposure to air resulted in their decomposition. Therefore, for subsequent biological studies the lyophilized complexes were *in situ* incubated with cell extracts. It was previously reported that addition of more than one biotin moiety to the substrate resulted in decreased cytotoxicity^[21] and an aggravated SMVT transporter recognition.^[19] Accordingly, only one biotin-functionalized ligand was coordinated to the ruthenium center.

The molecular structure of **6** was in addition determined by X-ray diffraction analysis (Figure 3; for crystallographic data see Table S1). Single crystals were grown by slow diffusion of diethyl ether into a saturated dichloromethane solution at 277 K. The *p*-

cymene ring is coordinated to the ruthenium center in a η^6 -manner. The rest of the coordination sphere is filled with two chlorido and a pyridine ligand. The geometrical parameters of the complex are in agreement with previously determined structures of compounds, which vary just in the nature of the *N*-donor ligands.^[51,52] The average Ru–C bond length in **6** is 2.186 Å, whereas Ru–Cl1, Ru–Cl2 and Ru–N distances are 2.4194(4), 2.4026(4) and 2.1368(12) Å, respectively (in comparison, Ru–C_{av} 2.170(8), Ru–Cl1 2.4157(6), Ru–Cl2 2.4157(6), and Ru–N 2.130(3) Å for [Ru(η^6 -*p*-cymene)Cl₂(NH₃)].^[52] The crystal structure of **6** was employed as the starting point for subsequent docking studies.

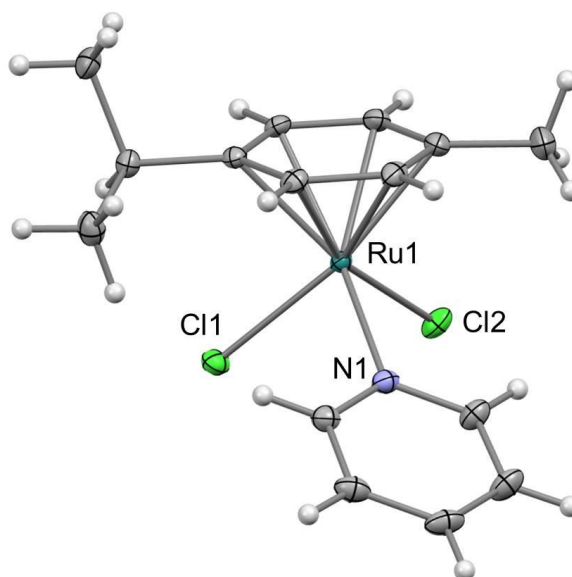


Figure 3. Molecular structure of the neutral complex [(η^6 -*p*-cymene)Ru(pyridine)Cl₂] **6**. Selected bond lengths [Å] and angles [°]: Ru1–C(1–6)_{av} 2.186, Ru1–N1 2.1368(12), Ru1–Cl1 2.4194(4), Ru1–Cl2 2.4026(4); N1–Ru1–Cl1 85.94(3), N1–Ru1–Cl2 86.81(4), Cl1–Ru1–Cl2 87.328(14).

Cytotoxicity

The *in vitro* anticancer activity of the ruthenium complexes and ligands was determined in COLO205, SW620 and HCT116 colon carcinoma cells by means of the colorimetric MTT assay with an exposure time of 70 h (see Table 1 for the IC₅₀ values; concentration-effect curves are shown in Figure S11). These cell lines were chosen due their different *SLC5A6* gene expression levels coding for SMVT. Therefore, the response of cancer cells to the Ru–biotin conjugates may be correlated with the relative level of SMVT expression. *SLC5A6* mRNA is most abundant in SW620 cells, and almost 3-times higher than in COLO-205 and HCT116 cells, which have comparable *SLC5A6* gene expression levels.^[25]

Table 1. Cytotoxicity of the Ru complexes **6–11** in COLO205 (colon adenocarcinoma), HCT116 (colon carcinoma) and SW620 (colon adenocarcinoma) cells, determined by means of the MTT assay. Calculations are based on results of three independent experiments. 95%-confidence intervals are given in parentheses to enable better comparison of the results.

Compound		IC ₅₀ [μM]		
		COLO205 SMVT (low)	HCT116 SMVT (low)	SW620 SMVT (high)
pyridine	6	≥ 100	3.4 (2.2–5.1)	4.1 (2.3–5.5)
	7	4.6 (2.1–10.2)	6.7 (4.6–9.6)	1.1 (0.8–1.7)
	8	17 (9–36)	2.5 (1.4–4.5)	2.1 (1.3–3.4)
indazole	9	23 (18–31)	33 (18–60)*	14 (12–17)
	10	≥ 100	≥ 100	19 (15–24)
	11	≥ 100	6.7 (4.6–9.7)	29 (22–37)

* denotes extrapolated values

With the exception of **7**, COLO205 cells were markedly less chemosensitive to complexes **6–11** than HCT116 and SW620 (Table 1). Complex **6** was reported to be inactive in TS/A murine adenocarcinoma cells (IC₅₀ = 757 μM).^[29] It was significantly more active in the human cell lines HCT116 and SW620 with IC₅₀ values of 3.4 and 4.1 μM, respectively, although different conditions were used in the experiments. In general, the cancer cells were more sensitive towards the pyridine complexes (**6–8**) than their indazole analogues (**9–11**). Whereas the activity of **6** and **8** was almost similar in cell lines with high and low levels of SMVT expression, complexes **7** and **10** were significantly more active in the SMVT-overexpressing SW620 cell line. In contrast, **11** was 4-times more active in the cell line with a low level of SMVT expression (6.7 and 29 μM in HCT116 and SW620, respectively). Interestingly, the biotin derivatives with pyridine were more potent in the SW620 cell line (IC₅₀ = 1.1 μM and 2.1 μM for **7** and **8**, respectively) than the parent non-biotinylated compound **6** (IC₅₀ = 4.1 μM). However, biotin complexes with an indazole fragment were less active in SW620 cells than their non-biotinylated analogue **9**. From these results no clear correlations between the cytotoxicity, the SLC5A6 expression levels and the structures of the complexes can be drawn. Notably, none of the corresponding ligands was toxic in the investigated concentration range.

Interactions with avidin

The relative affinity of compounds **7**, **8**, **10** and **11** with avidin was determined using Biotective™ Green reagent, a fluorescent derivative of avidin complexed with 2-(4'-hydroxyazobenzene)benzoic acid as a quencher. The apparent equilibrium dissociation constants for the investigated compounds with avidin were found to be higher than for biotin, which was used as a reference. Accordingly, the affinity of all test compounds towards avidin was significantly lower than for the natural ligand. The affinity for pyridine derivatives was higher than for the indazole analogues. Hill coefficients in the range of 2.012–2.851 indicate positive cooperativity in the binding event. The values do not differ significantly among the compounds tested. This suggests no major steric hindrance introduced by any of the investigated compounds as interactions among biotin-binding sites remain unchanged. The recognition of biotin-appended complexes by avidin and SMVT transporter indicates that thiophane and keto fragments of biotin ligands were not modified upon complexation.^[25,45]

Table 2. Apparent equilibrium dissociation constants and Hill coefficients for investigated compounds. Calculations were based on results of at least three independent experiments. 95%-confidence intervals are given in parentheses to enable better comparison of the results.

Compound		K _d [nM]	Hill coefficient
biotin		680 (610–751)	2.752 (1.985–3.520)
pyridine	7	895 (823–967)	2.851 (2.257–3.445)
	8	1124 (1050–1198)	2.785 (2.390–3.179)
indazole	10	1194 (1112–1275)	2.371 (2.085–2.658)
	11	1980 (1144–2816)	2.012 (1.030–2.994)

Docking studies with (strept)avidin

In order to explain the findings from the cytotoxicity assays and estimate the likelihood of binding to the SMVT transporter, docking studies with avidin and a crystal structure of streptavidin (PDB: 3RY2) were conducted. Gold Score (GS) was the only scoring function able to treat the metal complexes. Initial docking studies were conducted with avidin. However, the biotin moiety was not placed in the binding pocket of avidin, thus giving no reason to suggest any binding between the ligand and protein. Since the results are based on the use of a homology model rather than a crystal structure the impact is difficult to estimate. As the docking experiments of biotin with the crystal

structure of streptavidin gave a good overlap of modeled biotin and co-crystallized biotin (GS 71), this was used as a model system. GS gives arbitrary numbers with higher values predicting better binding.

The docking of the pyridine derivatives **6–8** to streptavidin was compared with that of biotin. The biotin moieties of **7** and **8** showed good overlap with the co-crystallized biotin in the streptavidin crystal structure, reproducing also the hydrogen bonding pattern. The top three results for **7** all had scores of 70 ± 2 (Figure 4). This is comparable with the scoring of biotin. The results indicate that the binding energy of **7** is similar compared to that of biotin. Compound **8** gave top scores of 80 ± 1 , predicting higher binding than for **7** and biotin. This may be related to the increase in the molecules size. The addition of the linker provides greater flexibility to the ruthenium moiety, whereas the biotin was anchored deep in the pocket. In contrast the GS for the pyridine complex **6** was only 36 ± 1 and was found in the binding pocket where biotin would normally be positioned (Figure S8). The low score coupled with no hydrogen bonding suggests that the complex binding in the pocket may not be favored. In addition a model compound with the $\text{Ru}(\eta^6\text{-}p\text{-cymene})\text{Cl}_2$ fragment coordinated to the biotin-sulfur atom was studied (Figure S9) and a score of 55 ± 2 was obtained. The biotin moiety of the top three docking results showed some overlap with the co-crystallized biotin, resulting in a partial reproduction of the hydrogen bonding pattern. The top three hits also showed good overlap with each other.

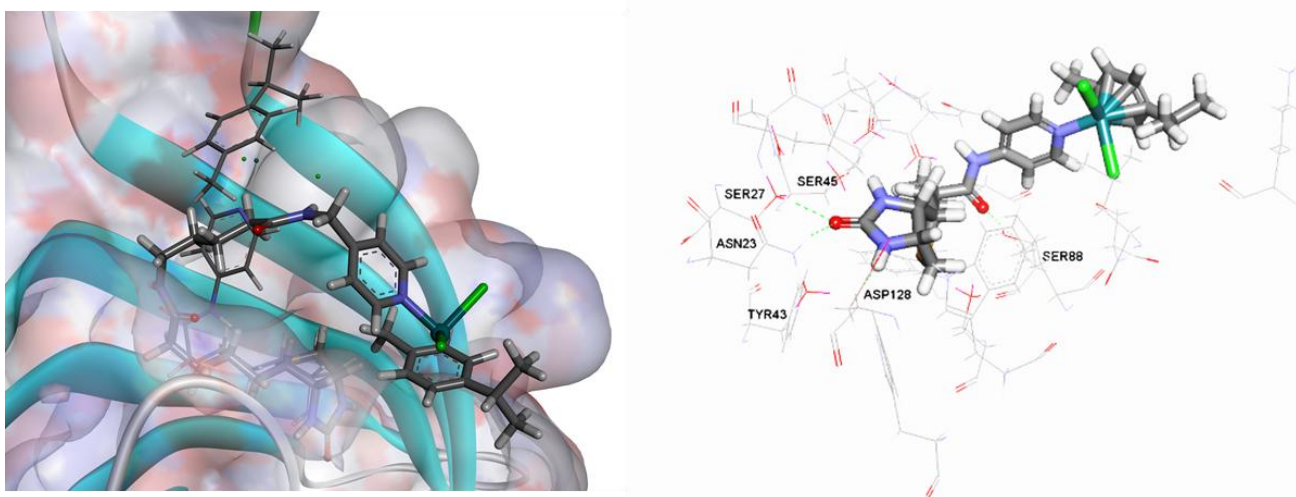


Figure 4. (left) Overlay of the docking results of **7** and **8** in the binding site of streptavidin indicating overlap of the biotin moieties of both molecules and (right) the hydrogen bonds between the biotin moiety of **7** and streptavidin depicted as green lines between the pyridine-biotin complex and the amino acids Asp128, Asn23, Ser27, Tyr43, Ser45 (not shown in green).

The same set of experiments was conducted with the indazole-substituted biotin derivatives. For **10**, the top three hits showed overlap between each other, but not in the expected position, resulting in no overlap with the co-crystallized biotin (Figure S10). The biotin head of the docked compounds was positioned outside the binding pocket. The scoring for these molecules was 57 ± 1 suggesting less favorable binding in comparison to biotin or analogous **7**. Even more surprising was the result of the docking studies feature **11**. The top three scores from the screening showed no overlap at all. Due to the high level of flexibility the molecules were spread out in various positions. Similarly to **6**, complex **9** occupied the binding pocket without any hydrogen bonding. The scores for the top three compounds were 40 ± 1 , slightly higher than that of **6**.

The results of the docking experiments explain to some extent the *in vitro* anticancer activity data. Compounds **9–11** showed much lower scores than especially **7** and **8** in the streptavidin docking experiments and this is consistent with the higher *in vitro* activity of the latter derivatives in the SMVT-high cell line SW620. The same set of compounds showed much lower activity in the SMVT-low cells and therefore in this case the (strept)avidin binding ability may be indicative of an SMVT-mediated mode of action. On the other hand, the indazole derivatives also show significant cytotoxicity in some of the cell lines, which may be explained with a mode of action not involving the SMVT transporter. The favorable interaction of the indazole derivatives with the SMVT in the *in vitro* experiment may be related to the extended π -system of indazole rather than the biotin moiety.

Conclusions

Because of the high demand of tumors for vitamin H (biotin) to sustain their rapid growth, they overexpress biotin-specific receptors (SMVT) on the tumor cell surface. This provides an option to selectively accumulate chemotherapeutics with high affinity for SMVT by designing novel drug delivery systems. We have linked an SMVT targeting moiety through a spacer to a biologically active metal fragment. Biotin derivatives featuring the natural binding moiety to SMVT were used as the basis for the vector to exploit tumor-specific vitamin-receptor mediated endocytosis. As a proof of concept, a series of half-sandwich ruthenium(II) complexes with ligands functionalized with biotin were prepared. Their biological activity was confirmed by cytotoxicity assays in cell lines with differing SMVT expression profiles. Whereas the ligands were not toxic in the investigated concentration range, the complexes revealed a marked cytotoxicity and cell-specificity based on the level of SMVT expression. The relative binding affinity of the

complexes to avidin was determined and it was shown that all complexes were recognized by avidin, although to a lower extent than biotin. This indicates that the structural component of biotin essential for recognition was not altered upon complexation. The interactions of the complexes with (strept)avidin were investigated by docking studies. Overall, a good correlation with the antiproliferative activity of the complexes was revealed and the likelihood of binding of the complexes to SMVT transporter was confirmed. The data suggest that the complexes obtained may be viable vectors to improve the tumor accumulation of cytotoxic moieties and thereby improve the selectivity of cancer chemotherapy.

References

- [1] R. M. Bremnes, K. Andersen, E. A. Wist, *Eur. J. Cancer* **1995**, 31A, 1955-1959.
- [2] M. L. Slevin, L. Stubbs, H. J. Plant, P. Wilson, W. M. Gregory, P. J. Armes, S. M. Downer, *Brit. Med. J.* **1990**, 300, 1458-1460.
- [3] J. A. Reddy, P. S. Low, *Crit. Rev. Ther. Drug Carrier Syst.* **1998**, 15, 587-627.
- [4] L. Bildstein, C. Dubernet, P. Couvreur, *Adv. Drug Delivery Rev.* **2011**, 63, 3-23.
- [5] G. Russell-Jones, K. McTavish, J. McEwan, J. Rice, D. Nowotnik, *J. Inorg. Biochem.* **2004**, 98, 1625-1633.
- [6] H. M. Said, *J. Nutr.* **2009**, 139, 158-162.
- [7] H. Wang, W. Huang, Y. J. Fei, H. Xia, T. L. Yang-Feng, F. H. Leibach, L. D. Devoe, V. Ganapathy, P. D. Prasad, *J. Biol. Chem.* **1999**, 274, 14875-14883.
- [8] T. Minko, P. V. Paranjpe, B. Qiu, A. Laloo, R. Won, S. Stein, P. J. Sinko, *Cancer Chemother. Pharmacol.* **2002**, 50, 143-150.
- [9] K. Na, T. B. Lee, K.-H. Park, E.-K. Shin, Y.-B. Lee, H.-K. Choi, *Eur. J. Pharm. Sci.* **2003**, 18, 165-173.
- [10] S. Chen, X. Zhao, J. Chen, J. Chen, L. Kuznetsova, S. S. Wong, I. Ojima, *Bioconjugate Chem.* **2010**, 21, 979-987.
- [11] I. Ojima, *Acc. Chem. Res.* **2008**, 41, 108-119.
- [12] S. Lin, K. Fang, M. Hashimoto, K. Nakanishi, I. Ojima, *Tetrahedron Lett.* **2000**, 41, 4287-4290.
- [13] S. Bhuniya, M. H. Lee, H. M. Jeon, J. H. Han, J. H. Lee, N. Park, S. Maiti, C. Kang, J. S. Kim, *Chem. Commun.* **2013**, 49, 7141-7143.
- [14] S. Maiti, N. Park, J. H. Han, H. M. Jeon, J. H. Lee, S. Bhuniya, C. Kang, J. S. Kim, *J. Am. Chem. Soc.* **2013**, 135, 4567-4572.
- [15] V. K. Yellepeddi, A. Kumar, D. M. Maher, S. C. Chauhan, K. K. Vangara, S. Palakurthi, *Anticancer Res.* **2011**, 31, 897-906.
- [16] V. K. Yellepeddi, A. Kumar, S. Palakurthi, *Anticancer Res.* **2009**, 29, 2933-2943.
- [17] W. Yang, Y. Cheng, T. Xu, X. Wang, L.-p. Wen, *Eur. J. Med. Chem.* **2009**, 44, 862-868.
- [18] S. Ramanathan, S. Pooyan, S. Stein, P. D. Prasad, J. Wang, M. J. Leibowitz, V. Ganapathy, P. J. Sinko, *Pharm. Res.* **2001**, 18, 950-956.
- [19] S. Ramanathan, B. Qiu, S. Pooyan, G. Zhang, S. Stein, M. J. Leibowitz, P. J. Sinko, *J. Controlled Release* **2001**, 77, 199-212.
- [20] K. K.-W. Lo, M.-W. Louie, K.-S. Sze, J. S.-Y. Lau, *Inorg. Chem.* **2008**, 47, 602-611.

- [21] M.-W. Louie, M. H.-C. Lam, K. K.-W. Lo, *Eur. J. Inorg. Chem.* **2009**, 4265-4273.
- [22] K. Y. Zhang, K. K.-W. Lo, *Inorg. Chem.* **2009**, *48*, 6011-6025.
- [23] S.-K. Leung, K. Y. Kwok, K. Y. Zhang, K. K.-W. Lo, *Inorg. Chem.* **2010**, *49*, 4984-4995.
- [24] M. V. Babak, S. M. Meier, K. Huber, J. Reynisson, A. A. Legin, M. A. Jakupec, A. Roller, A. Stukalov, M. Gridling, K. L. Bennett, J. Colinge, W. Berger, P. J. Dyson, G. Superti-Furga, B. K. Keppler, C. G. Hartinger, **2014**, unpublished data.
- [25] D. Plazuk, J. Zakrzewski, M. Salmain, A. Blauz, B. Rychlik, P. Strzelczyk, A. Bujacz, G. Bujacz, *Organometallics* **2013**, *32*, 5774-5783.
- [26] A. D. Vadlapudi, R. K. Vadlapatla, A. K. Mitra, *Curr. Drug Targets* **2012**, *13*, 994-1003.
- [27] M. Wilchek, E. A. Bayer, *Methods Enzymol.* **1990**, *184*, 123-138.
- [28] M. A. Bennett, A. K. Smith, *J. Chem. Soc., Dalton Trans.* **1974**, 233-241.
- [29] C. A. Vock, C. Scolaro, A. D. Phillips, R. Scopelliti, G. Sava, P. J. Dyson, *J. Med. Chem.* **2006**, *49*, 5552-5561.
- [30] M. R. Pressprich, J. Chambers, *SAINT + Integration Engine, Program for Crystal Structure Integration*, Bruker Analytical X-ray systems, Madison, **2004**.
- [31] G. M. Sheldrick, *Acta Crystallographica, Section A: Foundations of Crystallography* **2008**, *A64*, 112-122.
- [32] I. Le Trong, Z. Wang, D. E. Hyre, T. P. Lybrand, P. S. Stayton, R. E. Stenkamp, *Acta Crystallogr. Sect. D* **2011**, *67*, 813-821
- [33] H. M. Berman, J. Westbrook, Z. Feng, G. Gilliland, T. N. Bhat, H. Weissig, I. N. Shindyalov, P. E. Bourne, *Nuc.Acids Res.* **2000**, *28*, 235-242.
- [34] H. Berman, K. Henrick, H. Nakamura, *Nat. Struct. Biol.* **2003**, *10*, 980.
- [35] *Scigress Explorer Ultra Version 7.7.0.47*, Fijitsu Limited, **2000 - 2007**.
- [36] N. L. Allinger, *J. Am. Chem. Soc.* **1977**, *99*, 8127-8134.
- [37] G. Jones, P. Willet, R. C. Glen, A. R. Leach, R. Taylor, *J.Mol.Biol.* **1997**, *267*, 727-748.
- [38] M. D. Eldridge, C. Murray, T. R. Auton, G. V. Paolini, P. M. Mee, *J. Comp. Aid. Mol. Design* **1997**, *11*, 425-445.
- [39] M. L. Verdonk, J. C. Cole, M. J. Hartshorn, C. W. Murray, R. D. Taylor, *Proteins* **2003**, *52*, 609-623.
- [40] O. Korb, T. Stütze, T. E. Exner, *J. Chem. Inf. Model.* **2009**, *49*, 84-96.
- [41] W. T. M. Mooij, M. L. Verdonk, *Proteins* **2005**, *61*, 272-287.
- [42] J. Carmichael, W. G. DeGraff, A. F. Gazdar, J. D. Minna, J. B. Mitchell, *Cancer Res.* **1987**, *47*, 936-942.

- [43] R. H. Batchelor, A. Sarkez, W. G. Cox, I. Johnson, *BioTechniques* **2007**, *43*, 503-507.
- [44] K. K.-W. Lo, W.-K. Hui, *Inorg. Chem.* **2005**, *44*, 1992-2002.
- [45] A. D. Vadlapudi, R. K. Vadlapatla, D. Pal, A. K. Mitra, *Int. J. Pharm. (Amsterdam, Neth.)* **2013**, *441*, 535-543.
- [46] K. K.-W. Lo, T. K.-M. Lee, *Inorg. Chem.* **2004**, *43*, 5275-5282.
- [47] M. Slim, N. Durisic, P. Grutter, H. F. Sleiman, *ChemBioChem* **2007**, *8*, 804-812.
- [48] W. Kandioller, C. G. Hartinger, A. A. Nazarov, M. L. Kuznetsov, R. O. John, C. Bartel, M. A. Jakupec, V. B. Arion, B. K. Keppler, *Organometallics* **2009**, *28*, 4249-4251.
- [49] W. Kandioller, C. G. Hartinger, A. A. Nazarov, C. Bartel, M. Skocic, M. A. Jakupec, V. B. Arion, B. K. Keppler, *Chem. Eur. J.* **2009**, *15*, 12283-12291.
- [50] M. V. Babak, S. M. Meier, A. A. Legin, M. S. A. Razavi, A. Roller, M. A. Jakupec, B. K. Keppler, C. G. Hartinger, *Chem. Eur. J.* **2013**, *19*, 4308-4318.
- [51] S. Betanzos-Lara, A. Habtemariam, G. J. Clarkson, P. J. Sadler, *Eur. J. Inorg. Chem.* **2011**, *2011*, 3257-3264.
- [52] M. V. Babak, S. M. Meier, A. A. Legin, M. S. Adib Razavi, A. Roller, M. A. Jakupec, B. K. Keppler, C. G. Hartinger, *Chem. - Eur. J.* **2013**, *19*, 4308-4318.

Supporting Information

to

Half-sandwich Ruthenium(II) Biotin Conjugates as Biological Vectors to Cancer Cells

Maria V. Babak,^[a, b, c] Damian Plazuk,^[e] Samuel M. Meier,^[c, d] Homayon John Arabshahi,^[b] Jóhannes Reynisson,^[b] Błażej Rychlik,^[f] Andrzej Błaż, ^[f] Katarzyna Szulc,^[f] Muhammad Hanif,^[b] Sebastian Strobl,^[a] Alexander Roller, ^[a] Bernhard K. Keppler,^[a, c] and Christian G. Hartinger*^[a, b, c]

^[a] Institute of Inorganic Chemistry, University of Vienna, Waehringer Str. 42, 1090 Vienna, Austria

^[b] School of Chemical Sciences, University of Auckland, Private Bag 92019, Auckland 1142, New Zealand

^[c] Research Platform “Translational Cancer Therapy Research” University of Vienna, Waehringer Str. 42, 1090 Vienna, Austria

^[d] Institute of Analytical Chemistry, University of Vienna, Waehringer Str. 38, 1090 Vienna, Austria

^[e] Department of Organic Chemistry, Faculty of Chemistry, University of Łódź, Tamka 12, 91-403 Łódź, Poland

^[f] Cytometry Lab, Department of Molecular Biophysics, Faculty of Biology and Environmental Protection, University of Łódź, 12/16 Banacha St., 90-237 Łódź, Poland

Table of Contents

Crystallographic data and measurement parameters

Mass spectra for the *in situ* preparation of the complexes with biotin-functionalized ligands

Results of docking experiments with Ru complexes to streptavidin

Dose-response curves of **6–11** in human colon cancer cell lines.

Table S1. Crystal data and details of data collection for **6**.

Compound	6
Empirical formula	C ₁₅ H ₁₉ Cl ₂ NRu
Fw	385.28
Crystal system	monoclinic
Space group	P2 ₁ /c
<i>a</i> , Å	9.9304(6)
<i>b</i> , Å	7.8751(5)
<i>c</i> , Å	20.0044(11)
α [°]	90
β [°]	103.3950(10)
γ [°]	90
<i>V</i> , Å ³	1521.84(16)
<i>Z</i>	4
λ , Å	0.71073
ρ_{calcd} , g cm ⁻³	1.682
Crystal size, mm ³	0.20 × 0.14 × 0.12
<i>T</i> , K	100(2)
μ , mm ⁻¹	1.367
Reflections collected/unique	21326 / 4494
[<i>R</i> _{int}]	0.0295
<i>R</i> ₁ ^[a]	0.0194
<i>wR</i> ₂ ^[b]	0.0471
GOF ^[c]	1.037

^a $R_1 = \Sigma ||F_o| - F_c| / \Sigma |F_o|$, ^b $wR_2 = \{\Sigma w(F_o^2 - F_c^2)^2 / \Sigma w(F_o^2)\}^{1/2}$. ^c $GOF = \{\Sigma [w(F_o^2 - F_c^2)^2] / (n - p)\}^{1/2}$, where *n* is the number of reflections and *p* is the total number of parameters refined.

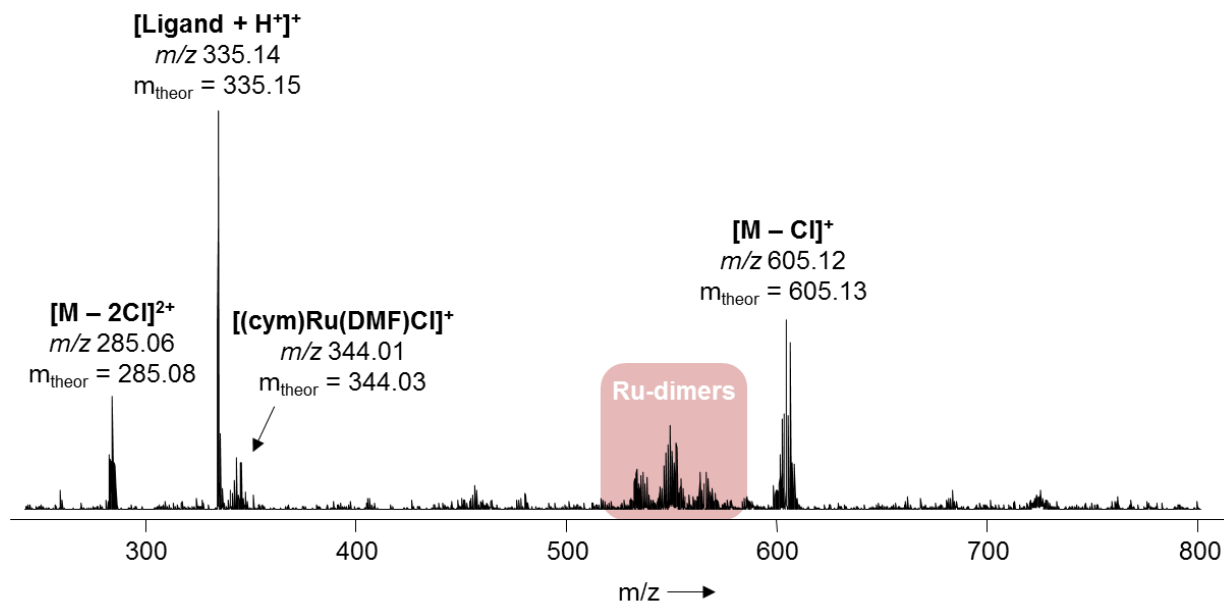


Figure S1. Full mass spectrum of **7** obtained by the reaction between $[\text{Ru}(\eta^6\text{-}p\text{-cymene})\text{Cl}_2]_2$ and 2 equivalents of **3**. Representative mass spectrum for reaction times 3-6 h. Ru-dimers denote dimeric hydrolysis products resulting from chloride and biotin ligand release.

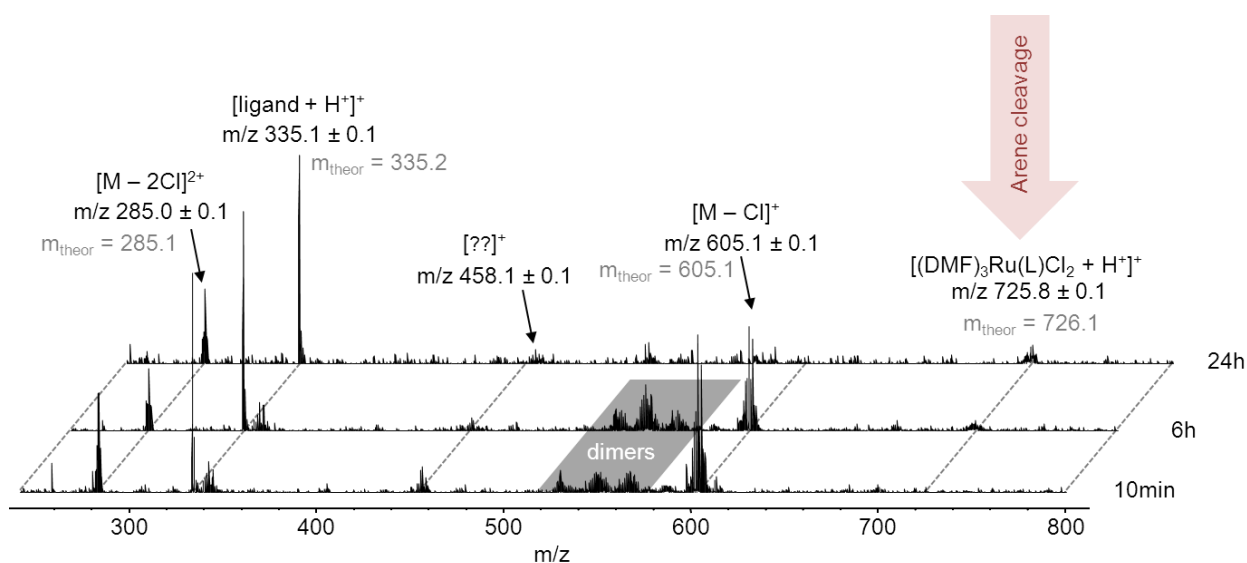


Figure S2. Mass spectrum of **7** obtained by the reaction between $[\text{Ru}(\eta^6\text{-}p\text{-cymene})\text{Cl}_2]_2$ and 2 equivalents of **3**. Representative mass spectrum for reaction times of 10 min, 6 and 24 h. Substantial arene cleavage was observed after more than 6 h of incubation.

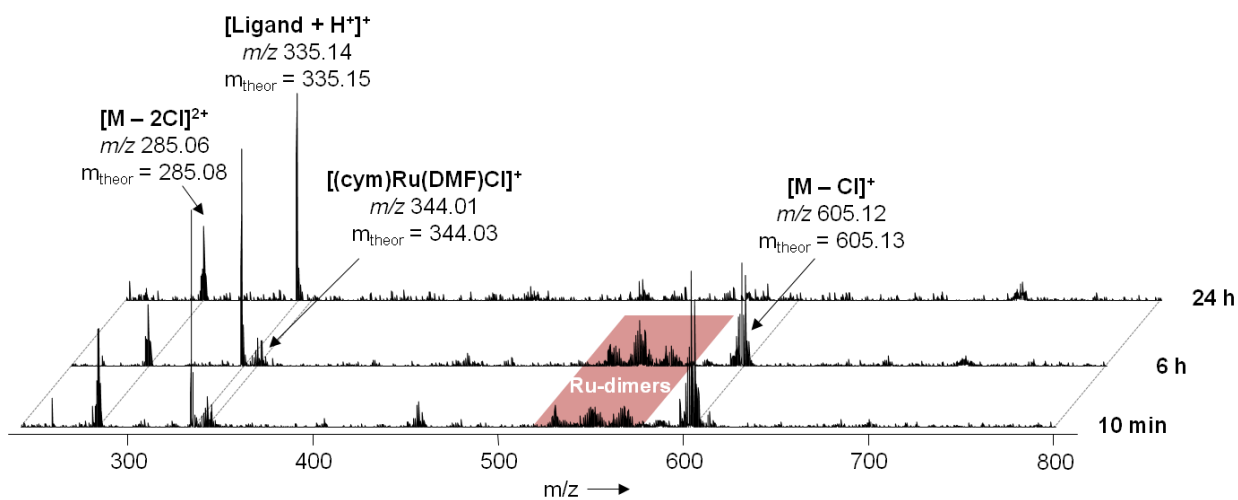


Figure S3. Full mass spectra of the reaction products obtained by the reaction between $[\text{Ru}(\eta^6\text{-}p\text{-cymene})\text{Cl}_2]_2$ and 2 equivalents of **3**, after 10 min, 3 h and 24 h. Ru-dimers denote dimeric hydrolysis products resulting from chloride and biotin ligand release.

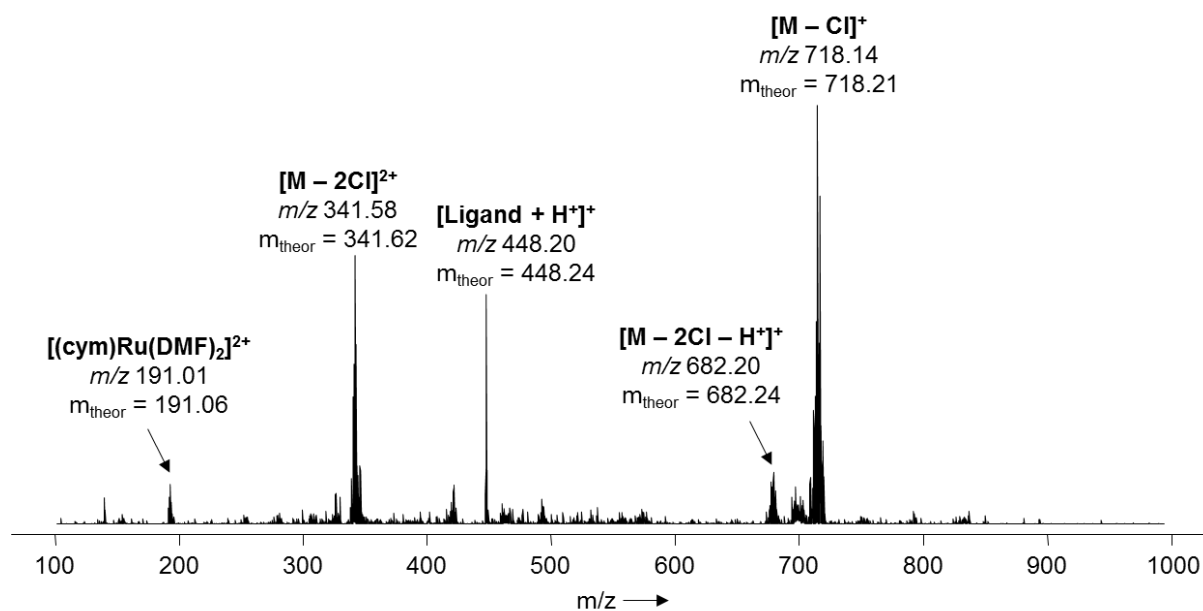


Figure S4. Full mass spectrum of **8** obtained by the reaction between $[\text{Ru}(\eta^6\text{-}p\text{-cymene})\text{Cl}_2]_2$ and 2 equivalents of **5**. Representative mass spectrum for reaction times 3-24 h.

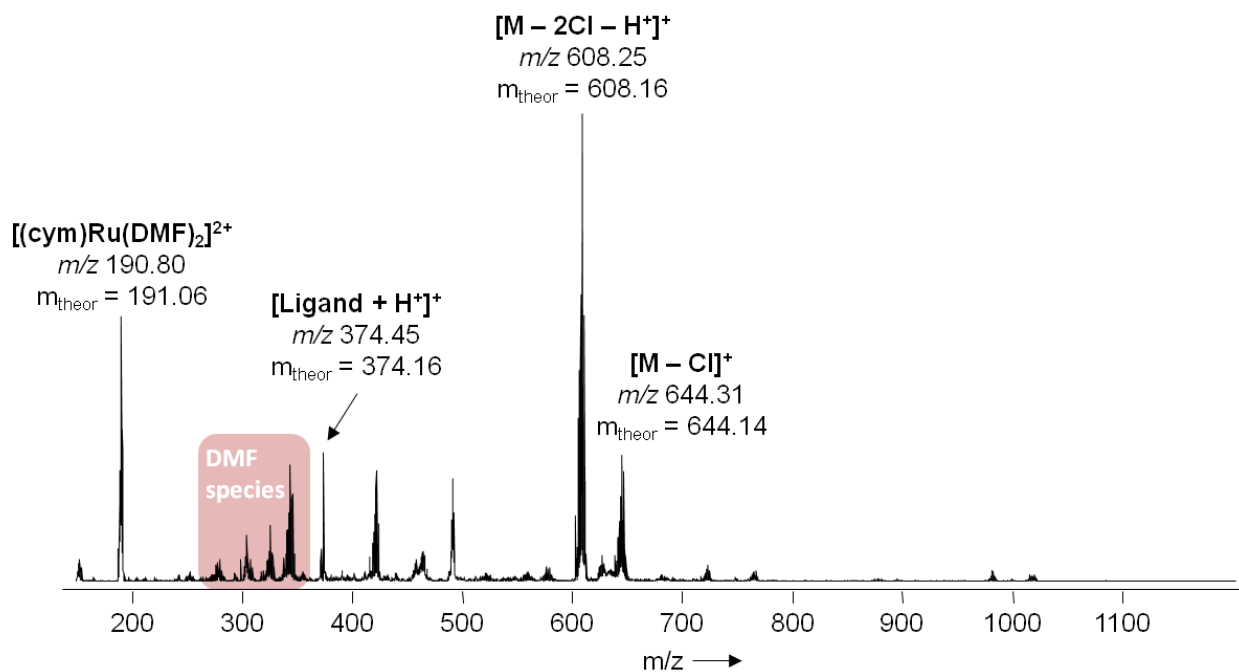


Figure S5. Full mass spectrum of **10** obtained by the reaction between $[\text{Ru}(\eta^6\text{-}p\text{-cymene})\text{Cl}_2]_2$ and 2 equivalents of **2**. Representative mass spectrum for reaction times 3-24 h. DMF species are Ru(cym) adducts with DMF, which was the solvent used for the reaction.

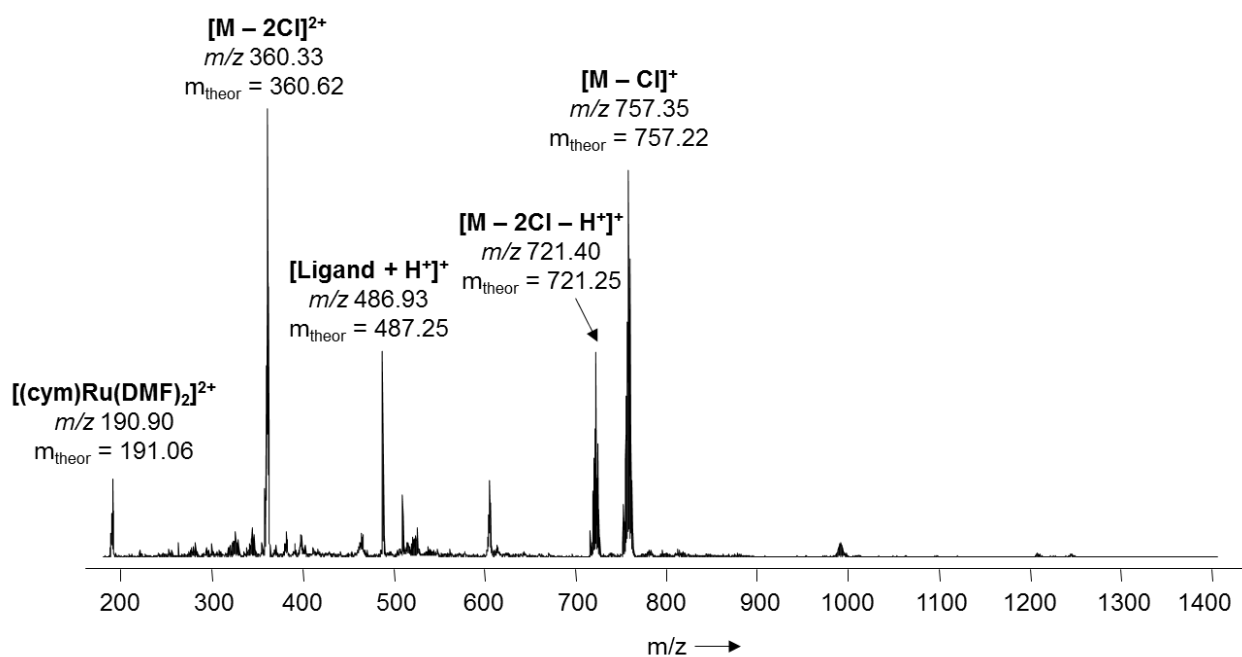


Figure S6. Full mass spectrum of **11** obtained by the reaction between $[\text{Ru}(\eta^6\text{-}p\text{-cymene})\text{Cl}_2]_2$ and 2 equivalents of **4**. Representative mass spectrum for reaction times 3-24 h.

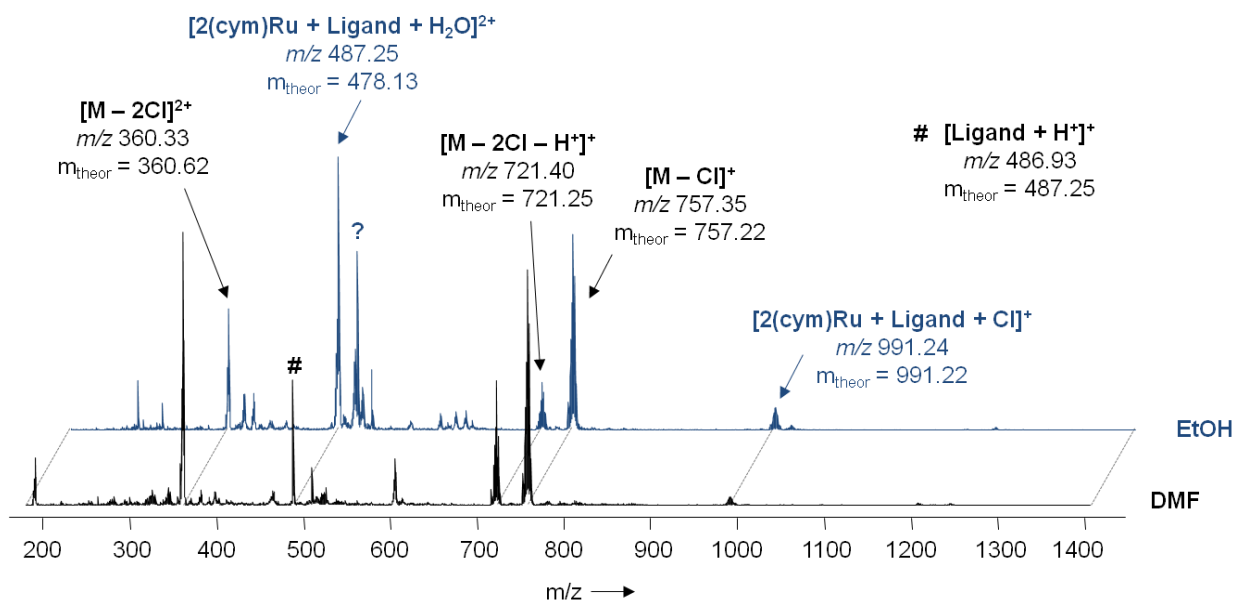


Figure S7. ESI-IT mass spectra of the reaction mixture yielding compound **11** after 3 h. The reactions were carried out in dimethylformamide (DMF) and ethanol (EtOH). The reaction using DMF as a solvent leads to a more selective formation of **11**.

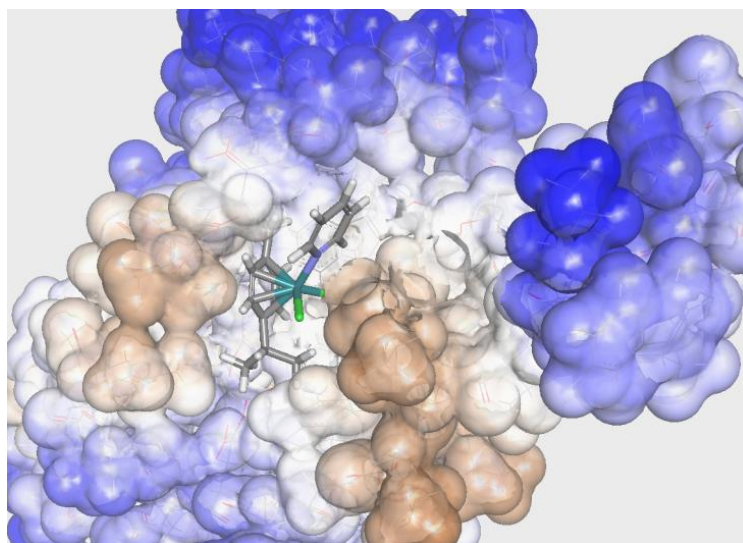


Figure S8. The docked configuration of the pyridine complex **6** in the binding site of streptavidin.

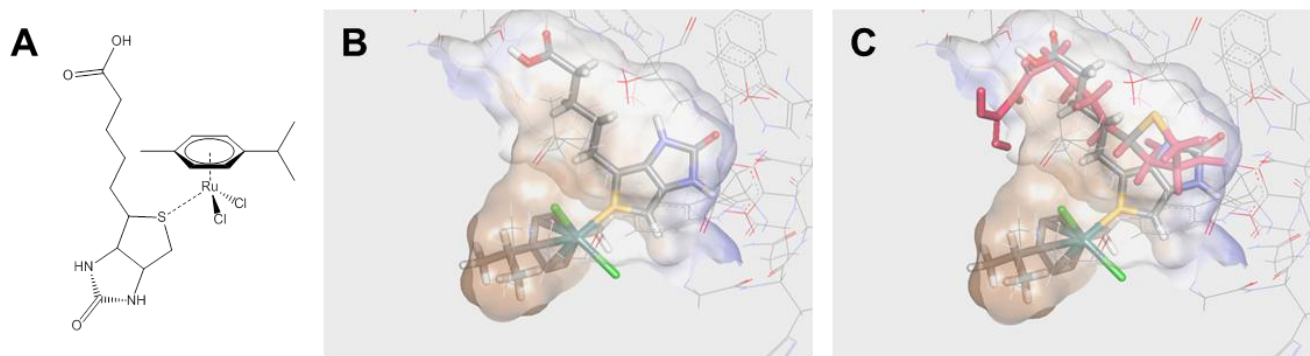


Figure S9. The docked configuration of the model complex with biotin coordinated to Ru through its S atom in the binding site of streptavidin. (A) Proposed structure of the complex. (B) The molecule binding only featured hydrogen bonding to Asp128 and Ser88. The ruthenium complex is positioned outside the pocket. (C) Overlap of a biotin head moiety (pink) and the compound showing the variation of sulfur positioning.

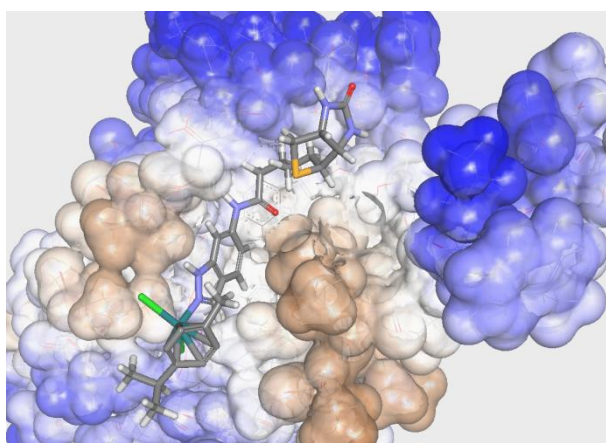


Figure S10. The docked configuration of the indazole complex **10** in the binding site of streptavidin.

The top three ligands showed overlap between each other, but not in the expected position, resulting in no overlap with the co-crystallized biotin. The biotin head of the docked compounds was positioned outside the binding pocket. The scoring for these molecules was 56.5 ± 1 suggesting less favourable binding in comparison to biotin or compound 8.

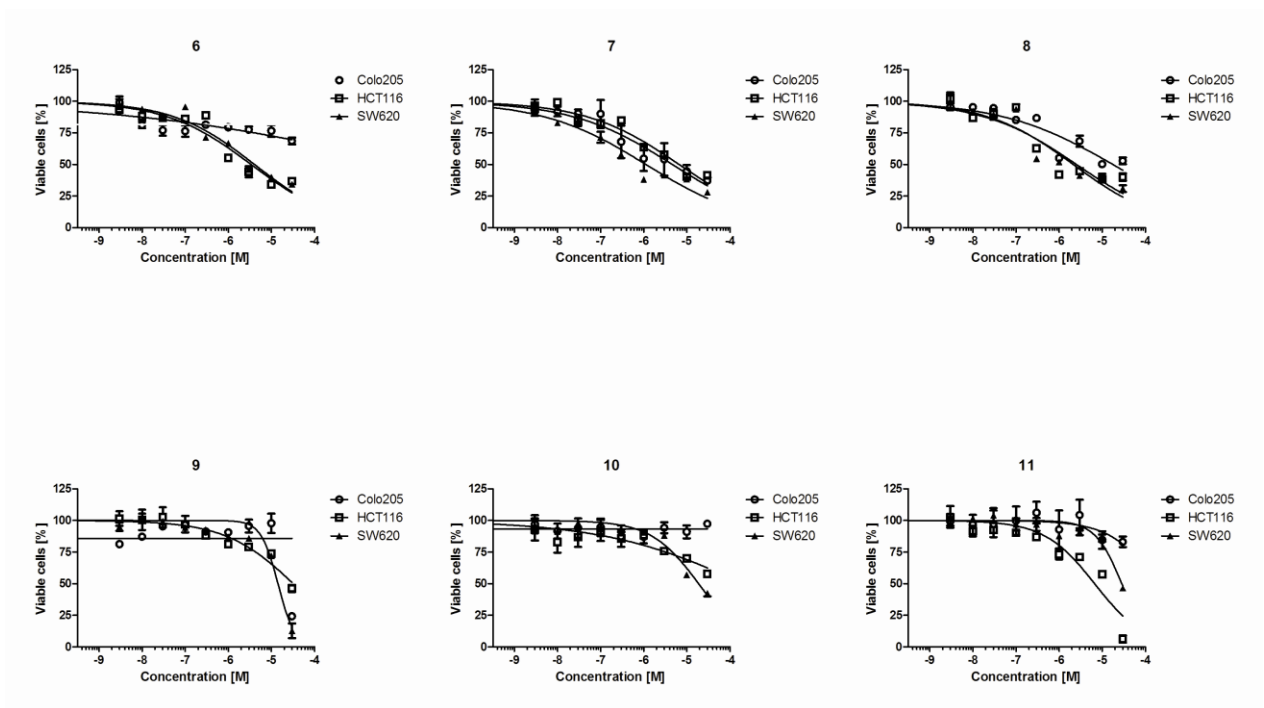
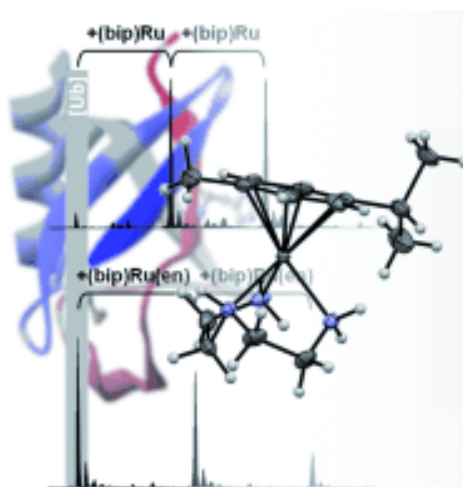


Figure S11. Concentration–effect curves of compounds **6–11** in the human colon cancer cell lines. Values were obtained by the MTT assay and are means \pm SEM values from at least three independent experiments using exposure times of 96 h.

3. Am(m)ines make the difference: organoruthenium am(m)ine complexes and their chemistry in anticancer drug development

Maria V. Babak, Samuel M. Meier, Alexander Roller, Anton A. Legin, Michael A. Jacupec, Bernhard K. Keppler, Christian G. Hartinger

Chem. Eur. J., 19(13), 4308-18, **2013**, DOI: 10.1002/chem.201202657



Ruthenium(II) arene complexes bearing ammine, ethylenediamine (en), or diethylenetriamine (dien) ligands, such as the depicted $[(\eta^6\text{-}p\text{-cymene})\text{Ru}^{\text{II}}(\text{dien})]^{2+}$, were studied. For this class of compounds, activity in anticancer assays is found when they are stable in aqueous solution and have low rates of hydrolysis and binding to proteins. Mass spectrometric studies revealed formation of mono- and bis-adducts between Ru biphenyl (bip) complexes and ubiquitin (see figure).

Am(m)ines Make the Difference: Organoruthenium Am(m)ine Complexes and Their Chemistry in Anticancer Drug Development

Maria V. Babak,^[a] Samuel M. Meier,^[a, b] Anton A. Legin,^[a] Mahsa S. Adib Razavi,^[a] Alexander Roller,^[a] Michael A. Jakupec,^[a, b] Bernhard K. Keppler,^[a, b] and Christian G. Hartinger ^{*[a, b, c]}

Abstract: With the aim of systematically studying fundamental structure–activity relationships as a basis for the development of Ru^{II} arene complexes (arene = *p*-cymene or biphenyl) bearing mono-, bi-, or tridentate am(m)ine ligands as anticancer agents, a series of ammine, ethylenediamine, and diethylenetriamine complexes were prepared by different synthetic routes. Especially the synthesis of mono-, di-, and triammine complexes was found to be highly dependent on the reaction conditions, such as stoichiometry, temperature, and time. Hydrolysis and pro-

tein-binding studies were performed to determine the reactivity of the compounds, and only those containing chlorido ligands undergo aquation or form protein adducts. These properties correlate well with in vitro tumor-inhibiting potency of the compounds. The complexes were found to be active in anticancer assays when meeting the following criteria: stability in aqueous

solution and low rates of hydrolysis and binding to proteins. Therefore, the complexes least reactive to proteins were found to be the most cytotoxic in cancer cells. In general, complexes with biphenyl as arene ligand inhibited the growth of tumor cells more effectively than the cymene analogues, consistent with the increase in lipophilicity. This study highlights the importance of finding a proper balance between reactivity and stability in the development of organometallic anticancer agents.

Keywords: arene ligands • cancer • N ligands • ruthenium • structure–activity relationships

Introduction

The discovery of the anticancer activity of cisplatin by Rosenberg et al.^[1] has broadened the range of routinely applied chemotherapeutics from organic drugs to metal-based compounds. Complexes based on titanium,^[2] arsenic, and ruthenium^[2a,3] succeeded cisplatin in clinical trials, and especially Ru anticancer agents show promising results.^[4] The unique properties of Ru compounds are thought to be related to an enhanced degree of selectivity compared to many

other metallodrugs due to binding to proteins in the blood stream and activation by reduction (Ru^{III/II}) once inside the tumor.^[4b,5] As cisplatin consists of a Pt^{II} core with two ammine and two chlorido ligands, researchers focused initially on analogous multichlorido ruthenium complexes with ammine ligands. Two mixed-valent ruthenium complexes, namely, [(NH₃)₃Ru^{III}ORu^{IV}(NH₃)₄ORu^{III}(NH₃)₅]⁶⁺ (ruthenium red) and [Cl(NH₃)₄Ru^{III}ORu^{IV}(NH₃)₄(OH)]³⁺ (Ru360), which have been used as cytological stains,^[6] were found to be inhibitors of the mitochondrial uniporter (Ca²⁺ uptake)^[7] and, like other ruthenium compounds, such as [Ru^{III}(py)(NH₃)₅]³⁺ (py = pyridine), *cis*-[Ru^{III}(Him)₂(NH₃)₄] (Him = imidazole), they show remarkable immunosuppressant activity.^[3a,8] The extensive work of Clarke and colleagues demonstrated that am(m)ine coordination complexes of Ru^{III} and Ru^{II} are active antitumor agents (e.g., *cis*-[Ru^{III}Cl₂(NH₃)₄]⁺,^[9] *fac*-[Ru^{III}Cl₃(NH₃)₃],^[10] [Ru^{III}(O₂CCH₂CH₃)(NH₃)₅]²⁺,^[3a] [Ru^{II}(H₂O)(NH₃)₅]²⁺,^[11] etc.).^[3a,12] Other studies indicated the potential of mixed-ligand ruthenium(II) complexes with ethylenediamine and its derivatives.^[13] In contrast to cisplatin, which is known to form preferably intrastrand cross-links between adjacent guanine residues of DNA,^[14] ruthenium am(m)ine complexes favor interstrand cross-link formation, probably due to the steric hindrance of the octahedrally configured ruthenium center as opposed to the less crowded square-planar coordination geometry of Pt^{II}.^[3a] Although the complexes exhibited very good anticancer activity in primary tumors, low solubility prevented

[a] M. V. Babak, S. M. Meier, A. A. Legin, M. S. Adib Razavi, A. Roller, Dr. M. A. Jakupec, Prof. Dr. B. K. Keppler, Prof. Dr. C. G. Hartinger
Institute of Inorganic Chemistry
University of Vienna
Währinger Strasse 42, 1090 Vienna (Austria)

[b] S. M. Meier, Dr. M. A. Jakupec, Prof. Dr. B. K. Keppler, Prof. Dr. C. G. Hartinger
Research Platform “Translational Cancer Therapy Research”
University of Vienna
Währinger Strasse 42, 1090 Vienna (Austria)

[c] Prof. Dr. C. G. Hartinger
School of Chemical Sciences
The University of Auckland
Private Bag 92019, Auckland 1142 (New Zealand)
Fax: (+64)9-3737-599 ext. 87422
E-mail: c.hartinger@auckland.ac.nz

 Supporting information for this article is available on the WWW under <http://dx.doi.org/10.1002/chem.201202657>.

their further development. However, complexes with simple nitrogen-containing ligands (NH₃, 1,2-ethylenediamine, pyridine) other than indazole and imidazole proved to have potential in anticancer drug development.

More recently, Ru^{II} arene compounds made an appearance in medicinal chemistry, and their biological activity is significantly dependent on the nature of the coligands.^[3b,15] Complexes of the type [(η⁶-arene)Ru(en)X]⁺ with bidentate ethylenediamine (en) and chloride as a leaving group (X) exhibited excellent cytotoxicity against primary tumors which was in good correlation with their DNA binding ability.^[16] Surprisingly, recently published neutral half-sandwich ruthenium complexes [(η⁶-arene)Ru(NH₃)Cl₂] (arene = *p*-cymene or biphenyl) do not inhibit the growth of tumor cells in an in vitro setting, probably due to their low aqueous stability and high reactivity in cell culture medium.^[17] Similar observations were also made with other Ru(arene) complexes, the cytotoxicity of which greatly depends on their reactivity.^[18] To control interactions with the wide variety of biomolecules present in the cell, the choice of the type of ligands (chelating/nonchelating), arene (more/less lipophilic), and the presence of a leaving group (inert/labile to aquation as an activation step) is of high importance. With the aim of weaving together all of the disparate threads running through the development of half-sandwich Ru^{II} complexes bearing various am(m)ine ligands, we present a systematic investigation including their synthesis, spectroscopic properties, crystal structures, behavior in aqueous solution, and studies on their antiproliferative activity in cancer cells and interactions with biomolecules.

Experimental Section

Materials and methods: Materials from chemical suppliers were used as received, and all reactions were carried out under argon atmosphere in anhydrous solvents if not otherwise stated. RuCl₃·3H₂O was purchased from Johnson Matthey. [(η⁶-*p*-cymene)Ru^{II}(ethylenediamine)Cl]PF₆ (**7a**), [(η⁶-biphenyl)Ru^{II}(ethylenediamine)Cl]PF₆ (**7b**),^[19] [(η⁶-*p*-cymene)RuCl₂] (**A**), and [(η⁶-biphenyl)RuCl₂] (**B**)^[20] were prepared according to literature procedures. Methanol was dried and distilled over Mg under argon atmosphere. Ethylenediamine was distilled over Na prior to use or was purchased from Aldrich (purified by redistillation, >99.5%). NH₄OH (25% solution in water) and formic acid (98%) were obtained from Fluka; NH₄PF₆ (>95%), AgPF₆ (98%), diethylenetriamine (97%) from Aldrich; and ubiquitin (from bovine erythrocytes) and horse heart cytochrome c from Sigma. Dimethyl sulfoxide was obtained from Acros, and 9-ethylguanine (EtG) from Sigma. Products were isolated without taking any special precautions, but anhydrous solvents were used for isolation of **2a**, **2b**, **5a**, **5b**, **6a**, **7a**, and **7b**.

Elemental analyses were performed by the Microanalytical Laboratory of the Faculty of Chemistry of the University of Vienna. Electrospray ionization mass spectrometry was carried out with a Bruker Esquire 3000 instrument (Bruker Daltonics, Bremen, Germany), MilliQ water (18.2 MΩ; Millipore Synergy 185 UV Ultrapure Water System; Molsheim, France) and methanol (VWR Int., HiPerSolv, CHROMANORM) were used as solvents for ESI-MS studies. The ¹H and ³¹P NMR spectra were recorded at 500.10 and 202.44 MHz on a Bruker FT NMR spectrometer Avance II 500 MHz. ¹H NMR kinetic experiments were performed at 500.32 MHz on a Bruker DPX500 (Ultraschield Magnet). Chemical shifts are given in parts per million (ppm) relative to the resid-

ual solvent peak. NaOD (40% in D₂O, Fluka) was used for H/D-exchange NMR experiments.

X-ray diffraction measurements were performed on a Bruker X8 APEX II CCD diffractometer at 100 (**2b**, **6a**), 150 (**4b**), or 296 K (**3a**). Single crystals were positioned 40, 35, 35, and 35 mm from the detector, and 1468, 2295, 2780 and 823 frames were measured, each for 10, 30, 10 and 10 s over 1° scan width for **2b**, **3a**, **4b**, and **6a**, respectively. The data were processed with SAINT software.^[21] Crystal data, data collection parameters, and structure refinement details for **2b**, **3a**, **4b**, and **6a** are given in Table S1 of the Supporting Information and key bond lengths and angles in Table S2. The structures were solved by direct methods and refined by full-matrix least-squares techniques. Non-hydrogen atoms were refined with anisotropic displacement parameters. Hydrogen atoms were placed at calculated positions and refined as riding atoms in the subsequent least squares model refinements. The isotropic thermal parameters were estimated to be 1.2 times the values of the equivalent isotropic thermal parameters of the non-hydrogen atoms to which hydrogen atoms are bonded. Severe disorder of the hexafluorophosphate anion in **3a**, modeled with two positions for P1, resulted in relatively high residual electron density. The following computer programs, equipment and tables were used: structure solution, SHELXS-97; refinement, SHELXL-97;^[22] molecular diagrams, Mercury 3.0.

Cell lines and culture conditions: The human cancer cell line CH1 (ovarian carcinoma) was provided by Lloyd R. Kelland (CRC Centre for Cancer Therapeutics, Institute of Cancer Research, Sutton, UK). A549 (non-small cell lung cancer) and SW480 (colon carcinoma) cells were supplied by Brigitte Marian (Institute of Cancer Research, Department of Medicine I, Medical University of Vienna, Austria). Adherent cell cultures were grown in 75 cm² culture flasks (Iwaki/Asahi Technoglass, Gyouda, Japan) in complete medium [i.e., minimal essential medium (MEM) supplemented with 10% heat-inactivated fetal bovine serum, 1 mM sodium pyruvate, 4 mM L-glutamine, and 1% v/v nonessential amino acids from 100× ready-to-use stock (all purchased from Sigma-Aldrich, Austria)]. Cell cultures were incubated at 37°C in a moist atmosphere containing 5% CO₂.

Cytotoxicity test in cancer cell lines: The cytotoxicity of the compounds was determined by means of a colorimetric microculture assay (MTT assay). The cells were harvested from culture flasks by trypsinization and seeded into 96-well microculture plates (Iwaki/Asahi Technoglass, Gyouda, Japan) in densities of 1×10³ cells per well (for CH1), 2.5×10³ cells per well (for SW480), and 3×10³ cells per well (for A549). After the cells were allowed to resume exponential growth for 24 h, the test compounds were dissolved in complete medium and 100 μL of serial dilution was added per well. After exposure for 96 h, drug solutions were replaced with 100 μL of RPMI 1640 culture medium (supplemented with 10% heat-inactivated fetal bovine serum and 2 mM of L-glutamine) plus 20 μL of MTT solution in phosphate-buffered saline (5 mg mL⁻¹). After incubation for 4 h, the RPMI/MTT mixtures were removed, and the formazan crystals formed in viable cells were dissolved in 150 μL of DMSO per well. Optical densities were measured at 550 nm with a microplate reader (Tecan Spectra Classic), by using a reference wavelength of 690 nm to correct for unspecific absorption. The quantity of viable cells was expressed in terms of treated/control (T/C) values by comparison to untreated control microcultures, and 50% inhibitory concentrations (IC₅₀) were calculated from concentration–effect curves by interpolation. Evaluation was based on means from at least three independent experiments, each comprising three replicates per concentration level.

Protein-binding studies: The metal compounds (400 μM) were dissolved in 1% aqueous dimethyl sulfoxide, and the proteins ubiquitin and cytochrome c (200 μM) in water. These stock solutions were mixed to obtain 2:1 metal-to-protein molar ratios and then kept at 37°C in the dark. Mass spectra of the incubation solutions were recorded after 0, 3, 6, 24, and 48 h. Furthermore, the compounds were incubated under comparable conditions with an ubiquitin–cytochrome c mixture to yield a molar ratio of 1:1:1.

The samples were analyzed by using a MaXis ESI-Q-ToF mass spectrometer (Bruker Daltonics, Bremen, Germany) with the following parameters: capillary –4.5 kV, gas flow 8 psi, dry gas 6 L min⁻¹, dry temperature

150 °C, 400 V_{pp} funnel RF, 4 eV quadrupole ion energy and 100 μs transfer time. The samples were diluted to 2 μM with water/methanol/formic acid (50:50:0.2) and thereafter injected into the mass spectrometer by direct infusion at a flow rate of 180 μL h⁻¹. The spectra were recorded in positive-ion mode over 0.5 min and averaged. The Data Analysis 4.0 software package (Bruker Daltonics, Bremen, Germany) was used for processing, and maximum entropy deconvolution (automatic data point spacing and 30000 instrument resolving power) was applied.

Binding to the DNA model 9-ethylguanine: Compounds **2b**, **5b**, and **7b** (400 μM) were dissolved in 1% dimethyl sulfoxide aqueous solution. EtG (800 μM) was dissolved in water. The compounds and EtG were incubated at 1:2 molar ratio at metal-to-complex concentrations of 50–100 μM for 3, 6, 24, and 48 h at 37 °C. Samples were diluted with water/methanol (1:1) to final concentrations of 5–10 μM and immediately introduced into the mass spectrometer. ESI-IT mass spectra were recorded on an AmaZon Ion Trap mass spectrometer (Bruker Daltonics, Bremen Germany) by direct infusion at a flow rate of 180 μL h⁻¹. The following parameters were employed: capillary –2.5 kV, gas flow 9 psi, dry gas 6 L min⁻¹, dry temperature 200 °C, and trap drive 55.1. The Data Analysis 4.0 software package (Bruker Daltonics, Bremen, Germany) was used for processing the raw data.

Synthesis of complexes

[(η⁶-p-cymene)Ru^{II}(NH₃)₃](PF₆)₂ (1a**):** Method 1: [(η⁶-p-cymene)RuCl₂]₂ (0.3 mmol, 0.184 g) was stirred for 10 min in dry methanol (10 mL). Ammonia gas was bubbled through the solution, which caused significant warming of the reaction mixture and was accompanied by a fast change of the color from red-orange to light yellow. After the solution had cooled down, the gas supply was stopped and the reaction mixture was stirred for 30 min. The yellow solution was concentrated by rotary evaporation under reduced pressure to 1 mL, and a saturated solution of NH₄PF₆ in methanol (2–4 mL) was added. The resulting solution was filtered and diethyl ether (15 mL) added. The light yellow precipitate was collected by filtration, washed with diethyl ether (3 × 5 mL), and dried in vacuo to yield 286 mg (90%) of the target complex.

Method 2: Ammonia (2 mL, 25% aqueous solution) was added to a suspension of [(η⁶-p-cymene)RuCl₂]₂ (0.2 mmol, 0.122 g) in dry methanol (10 mL). The reaction mixture was heated to reflux for 1 h at 85 °C. The resulting yellow solution was concentrated by rotary evaporation under reduced pressure to 1 mL and a saturated solution of NH₄PF₆ in methanol (2–4 mL) was added. The resulting solution was filtered and diethyl ether (15 mL) was added. The yellow precipitate was collected by filtration, washed with diethyl ether (3 × 5 mL), and dried in vacuo to yield 152 mg (64%) of the target complex.

Elemental analysis (%) calcd for C₁₀H₂₂RuN₃P₂F₁₂·0.1 NH₄PF₆ (592.61 g mol⁻¹): C 20.26, H 3.98, N 7.33; found: C 20.01, H 3.82, N 7.23%; MS (ESI+): *m/z* 270.1 [(η⁶-p-cymene)Ru(NH₃)₂-H]⁺ + [(η⁶-p-cymene)Ru(NH₃)₂]⁺; found: 270.0; MS (ESI-): *m/z* 145.0 [PF₆]⁻; found: 144.5; ¹H NMR (500.10 MHz; [D₆]DMSO): δ = 1.19 (d, 6H, ³J_{HH} = 7.0 Hz, CH(CH₃)₂), 2.12 (s, 3H, C₆H₄(CH₃)), 2.81 (sept, 1H, ³J_{HH} = 6.9 Hz, CHMe₂), 3.41 (s, 9H, NH₃), 5.41 (d, 2H, ³J_{HH} = 6.0 Hz, CH_{cym}), 5.70 ppm (d, 2H, ³J_{HH} = 6.0 Hz, CH_{cym}); ³¹P NMR (202.44 MHz; [D₆]DMSO): δ = -144.10 ppm (sept, 1P, ¹J_{PF} = 727.7 Hz, PF₆).

[(η⁶-biphenyl)Ru^{II}(NH₃)₃](PF₆)₂ (1b**):** Method 1: [(η⁶-biphenyl)RuCl₂]₂ (0.2 mmol, 0.130 g) was stirred for 10 min in dry methanol (10 mL). Ammonia gas was bubbled through the solution, which caused significant warming of the reaction mixture and changed the black-brown suspension to a light yellow solution. After the solution had cooled, the gas supply was stopped and the reaction mixture was stirred for 1 h. The yellow solution was filtered and concentrated by rotary evaporation under reduced pressure to 1 mL, and saturated solution of NH₄PF₆ in water (2–4 mL) was added. A light yellow precipitate formed immediately, which was collected by filtration, washed with water (2 × 2 mL) and diethyl ether (3 × 15 mL), and dried in vacuo to yield 175 mg (70%) of the target complex.

Method 2: Ammonia (2 mL of 25% aqueous solution) was added to a suspension of [(η⁶-biphenyl)RuCl₂]₂ (0.2 mmol, 0.130 g) in dry methanol (15 mL) and the reaction mixture was heated to reflux for 1 h at 85 °C. Then it was filtered, the resulting light-orange solution concentrated by

rotary evaporation under reduced pressure to 1 mL, and a saturated solution of NH₄PF₆ in water (2–4 mL) added. The orange-yellow precipitate was collected by filtration, washed with water (1 × 2 mL) and diethyl ether (3 × 15 mL), and dried in vacuo to give 160 mg (64%) of the target product.

Elemental analysis (%) calcd for C₁₂H₁₉RuN₃P₂F₁₂·0.2 NH₄PF₆ (628.90 g mol⁻¹): C 22.92, H 3.17, N 7.13; found: C 22.77, H 3.24, N 6.86%; MS (ESI+): *m/z* 290.0 [(η⁶-biphenyl)Ru(NH₃)₂-H]⁺ + [(η⁶-biphenyl)Ru(NH₃)₂]⁺; found: 290.0; MS (ESI-): *m/z* 145.0 [PF₆]⁻; found: 144.5; ¹H NMR (500.10 MHz; [D₆]DMSO): δ = 3.51 (s, 9H, NH₃), 5.87 (m, 3H, CH_{phen}), 6.17 (m, 2H, CH_{phen}), 7.57 (m, 3H, RuCH_{phen}), 7.78 ppm (m, 2H, RuCH_{phen}); ³¹P NMR (202.44 MHz; [D₆]DMSO): δ = -144.13 ppm (sept, 1P, ¹J_{PF} = 720.5 Hz, PF₆).

[(η⁶-p-cymene)Ru^{II}(NH₃)₂Cl]PF₆ (2a**):** Ammonia (150 μL of 25% aqueous solution) was added to a suspension of [(η⁶-p-cymene)RuCl₂]₂ (0.2 mmol, 0.122 g) in dry methanol (10 mL) and the reaction mixture was heated to reflux for 1 h at 85 °C. The resulting orange solution was concentrated by rotary evaporation under reduced pressure to 1 mL and a saturated solution of NH₄PF₆ in methanol (2–4 mL) was added. The resulting bright orange solution was filtered and diethyl ether (15 mL) was added. The yellow precipitate was collected by filtration, washed with diethyl ether (3 × 5 mL) and dried in vacuo to yield 88 mg (49%) of the target complex.

Elemental analysis (%) calcd for C₁₀H₂₀RuN₂PF₆Cl (449.77 g mol⁻¹): C 26.70, H 4.48, N 6.23; found: C 26.68, H 4.33, N 6.04%; MS (ESI+): *m/z* 288.0 [(η⁶-p-cymene)Ru(NH₃)Cl]⁺; found: 288.4; MS (ESI-): *m/z* 145.0 [PF₆]⁻; found: 144.9; ¹H NMR (500.10 MHz; [D₆]DMSO): δ = 1.21 (d, ³J_{HH} = 7.0 Hz, 6H, CH(CH₃)₂), 2.12 (s, 3H, C₆H₄(CH₃)), 2.81 (sept, 1H, ³J_{HH} = 6.9 Hz, CHMe₂), 3.37 (s, 6H, NH₃), 5.37 (d, 2H, ³J_{HH} = 6.0 Hz, CH_{cym}), 5.61 ppm (d, 2H, ³J_{HH} = 6.1 Hz, CH_{cym}); ³¹P NMR (202.44 MHz; [D₆]DMSO): δ = -144.15 ppm (sept, 1P, ¹J_{PF} = 702.7 Hz, PF₆).

[(η⁶-biphenyl)Ru^{II}(NH₃)₂Cl]PF₆ (2b**):** Ammonia (150 μL of 25% aqueous solution) was added to a suspension of [(η⁶-biphenyl)RuCl₂]₂ (0.2 mmol, 0.130 g) in dry methanol (15 mL) and the reaction mixture was heated to reflux for 1 h at 85 °C. Then it was filtered, the resulting orange solution concentrated by rotary evaporation under reduced pressure to 1 mL, and a saturated solution of NH₄PF₆ in methanol (2–4 mL) was added. The yellow-ochre precipitate that formed immediately was collected by filtration, washed with water (1 × 2 mL) and diethyl ether (3 × 15 mL), and dried in vacuo. The ochre solid was redissolved in the minimum amount of methanol, and diethyl ether was added to precipitate 65 mg of the target complex as a yellow powder. The orange aqueous supernatant was left to stand at 0 °C for 8 h and orange microcrystals of the complex formed (15 mg, overall yield 43%). Crystals suitable for X-ray diffraction analysis (orange needles) were grown by slow diffusion of diethyl ether into a methanol solution.

Elemental analysis (%) calcd for C₁₂H₁₆RuN₂PF₆Cl (469.76 g mol⁻¹): C 30.68, H 3.43, N 5.96; found: C 30.90, H 3.14, N 5.86%; MS (ESI+): *m/z* 308.0 [(η⁶-biphenyl)Ru(NH₃)Cl]⁺; found: 308.4; MS (ESI-): *m/z* 145.0 [PF₆]⁻; found: 144.5; ¹H NMR (500.10 MHz; [D₆]DMSO): δ = 3.49 (s, 6H, NH₃), 5.82 (m, 3H, CH_{phen}), 6.11 (m, 2H, CH_{phen}), 7.51 (m, 3H, RuCH_{phen}), 7.80 ppm (m, 2H, RuCH_{phen}); ³¹P NMR (202.44 MHz; [D₆]DMSO): δ = -144.24 ppm (sept, 1P, ¹J_{PF} = 711.7 Hz, PF₆).

[(η⁶-p-cymene)Ru^{II}(diethylenetriamine)Cl]PF₆ (3a**):** Diethylenetriamine (27 μL, 0.25 mmol) was added to a suspension of [(η⁶-p-cymene)RuCl₂]₂ (0.09 mmol, 0.056 g) in dry methanol (15 mL). The reaction mixture immediately turned into a light yellow solution, which was stirred for 1.5 h, filtered, and concentrated by rotary evaporation under reduced pressure to 1 mL, after which a saturated solution of NH₄PF₆ in methanol (2–4 mL) was added. The solution was filtered and diethyl ether (15 mL) added. The mixture was allowed to stand at 0 °C for 8 h, and the yellow precipitate was collected by filtration, washed with diethyl ether (3 × 15 mL), and dried in vacuo to yield 70 mg (75%) of the target complex. Crystals suitable for X-ray diffraction analysis were grown by slow diffusion of diethyl ether into a methanol solution.

Elemental analysis (%) calcd for C₁₄H₂₇RuN₃PF₆Cl (518.87 g mol⁻¹): C 32.41, H 5.24, N 8.10; found: C 32.21, H 4.95, N 8.21%; MS (ESI+): *m/z* 338.1 [(η⁶-p-cymene)Ru(diethylenetriamine)-H]⁺; found: 337.9; MS

(ESI⁻): 145.0 [PF₆]⁻; found: 144.8; ¹H NMR (500.10 MHz; [D₆]DMSO): δ = 1.21 (d, 6H, ³J_{HH} = 6.9 Hz, CH(CH₃)₂), 2.25 (s, 3H, C₆H₄(CH₃)), 2.48–2.55 (m, 4H, C₂H₄), 2.61 (m, 2H, C₂H₄), 2.76 (m, 2H, C₂H₄), 2.96 (sept, 1H, ³J_{HH} = 6.9 Hz, CHMe₂), 5.14 (m, 2H, NH₂), 5.61 (d, 2H, ³J_{HH} = 6.2 Hz, CH_{cym}), 5.73 (d, 2H, ³J_{HH} = 6.2 Hz, CH_{cym}), 6.48 (m, 2H, NH₂), 7.92 ppm (m, 1H, NH); ³¹P NMR (202.44 MHz; [D₆]DMSO): δ = -144.22 ppm (sept, 1P, ¹J_{PF} = 720.6 Hz, PF₆).

[(η^6 -biphenyl)Ru^{II}(diethylenetriamine)](PF₆)₂ (**3b**): [(η^6 -biphenyl)RuCl₂]₂ (0.14 mmol, 0.091 g) was heated to reflux in water/methanol (10:1) at 85 °C for 2 h and then cooled to 55 °C. Diethylenetriamine (38 μ L, 0.35 mmol) was added to this suspension, which turned from red-brown to yellow-greenish. This was then slowly heated to reflux again for another 1.5 h and filtered while hot. The resulting yellow solution was then concentrated by rotary evaporation under reduced pressure to 1 mL, and a saturated solution of NH₄PF₆ in water (2–4 mL) was added. The flask was briefly shaken, and a light-yellow precipitate immediately formed. The mixture was allowed to stand at 0 °C for 8 h, the precipitate was collected by filtration, washed with water (2 \times 2 mL) and diethyl ether (3 \times 15 mL), and dried in vacuo to yield 98 mg (54 %) of the target complex.

Elemental analysis (%) calcd for C₁₆H₂₃RuN₃P₂F₁₂ (648.37 g mol⁻¹): C 29.64, H 3.58, N 6.48; found: C 29.54, H 3.20, N 6.25 %; MS (ESI⁺): *m/z* 358.1 [(η^6 -biphenyl)Ru(diethylenetriamine)-H]⁺; found: 357.9; MS (ESI⁻): 145.0 [PF₆]⁻; found: 144.8; ¹H NMR (500.10 MHz; [D₆]DMSO): δ = 2.41–2.60 (m, 4H, C₂H₄), 2.72 (m, 4H, C₂H₄), 4.31 (m, 2H, NH₂), 5.92 (t, 2H, ³J_{HH} = 6.0 Hz, CH_{phen}), 6.04 (t, 1H, ³J_{HH} = 5.7 Hz, CH_{phen}), 6.30 (d, 2H, ³J_{HH} = 6.0 Hz, CH_{phen}), 5.92 (m, 2H, NH₂), 7.55 (m, 3H, RuCH_{phen}), 7.80 (m, 2H, RuCH_{phen}), 8.32 ppm (m, 1H, NH); ³¹P NMR (202.44 MHz; [D₆]DMSO): δ = -144.19 ppm (sept, 1P, ¹J_{PF} = 711.3 Hz, PF₆).

[(η^6 -biphenyl)Ru^{II}(ethylenediamine)(NH₃)](PF₆)₂ (**4b**): A solution of AgPF₆ (0.11 mmol, 0.028 g) in methanol (2 mL) was added to a solution of [(η^6 -biphenyl)Ru(ethylenediamine)Cl]PF₆ (0.1 mmol, 0.050 g) in dry methanol (7 mL) and the mixture stirred for 2 h. A white precipitate of AgCl was quickly filtered off under aerobic conditions and the resulting solution was flushed with Ar. Ammonia gas was bubbled through the solution, which caused significant warming of the reaction mixture with no color change. After the clear solution had cooled the gas supply was stopped and the reaction mixture was stirred for 1 h. The yellow solution was filtered, concentrated to 1 mL by rotary evaporation under reduced pressure, and a saturated solution of NH₄PF₆ in water (2–4 mL) was added. A green-yellow precipitate formed immediately, which was collected by filtration, washed with water (2 \times 2 mL) and diethyl ether (3 \times 15 mL) and dried in vacuo to yield 21 mg (33 %) of the target complex. Crystals suitable for X-ray diffraction analysis were grown by slow diffusion of diethyl ether into a methanol solution.

Elemental analysis (%) calcd for C₁₄H₂₁RuN₃P₂F₁₂·0.5 CH₃OH (638.36 g mol⁻¹): C 27.28, H 3.63, N 6.58; found: C 27.59, H 3.89, N 6.59 %; MS (ESI⁺): *m/z* 315.0 [(η^6 -biphenyl)Ru(diethylenediamine)-H]⁺; found: 315.1; MS (ESI⁻): *m/z* 145.0 [PF₆]⁻; found: 144.9; ¹H NMR (500.10 MHz; [D₆]DMSO): δ = 2.18 (m, 2H, CH₂), 2.34 (m, 2H, CH₂), 3.51 (s, 3H, NH₃), 4.30 (m, 2H, NH₂), 5.89 (t, 2H, ³J_{HH} = 6.0 Hz, CH_{phen}), 5.97 (t, 1H, ³J_{HH} = 5.6 Hz, CH_{phen}), 6.23 (d, 2H, ³J_{HH} = 6.1 Hz, CH_{phen}), 6.41 (m, 2H, NH₂), 7.57 (m, 3H, RuCH_{phen}), 7.76 ppm (m, 2H, RuCH_{phen}); ³¹P NMR (202.44 MHz; [D₆]DMSO): δ = -143.18 ppm (sept, 1P, ¹J_{PF} = 720.5 Hz, PF₆).

[(η^6 -p-cymene)Ru^{II}(NH₃)Cl₂][(dmbaH)(PF₆)] (**5a**): The procedure of Betanzos-Lara et al.^[17] was used after minor modification. In brief, *N,N*-dimethylbenzylamine (dmba, 0.098 mL, 0.65 mmol) and NH₄PF₆ (0.106 g, 0.65 mmol) were added to a suspension of [(η^6 -p-cymene)RuCl₂]₂ (0.32 g, 0.2 mmol) in dry methanol (15 mL) and the reaction mixture was stirred for 18 h at room temperature. Then it was filtered and the resulting orange solution evaporated to dryness. The oily residue was redissolved in the minimum amount of CH₂Cl₂ and diethyl ether (30 mL) added. The flask was briefly shaken, and a light yellow precipitate immediately formed. The mixture was allowed to stand at 0 °C for 8 h, and the precipitate was collected by filtration, washed with diethyl ether (3 \times 15 mL), and dried in vacuo to yield 155 mg (64 %) of the target complex.

Elemental analysis (%) calcd for C₁₉H₃₁RuN₂Cl₂PF₆ (604.40 g mol⁻¹): C 37.75, H 5.17, N 4.63; found: C 37.58, H 5.46, N 4.96 %; MS (ESI⁺): *m/z* 136.1 [dmba+H]⁺, 289.0 [(η^6 -p-cymene)Ru(NH₃)Cl]⁺ + [(η^6 -p-cymene)Ru(NH₃)Cl+H]⁺; found: 136.6, 289.3; MS (ESI⁻): *m/z* 145.0 [PF₆]⁻; found: 144.5; ¹H NMR (500.10 MHz; CD₃NO₂): δ = 1.31 (d, 6H, ³J_{HH} = 7.0 Hz, CH(CH₃)₂), 2.10 (s, 3H, C₆H₄(CH₃)), 2.90 (sept, 1H, ³J_{HH} = 7.0 Hz, CHMe₂), 2.74 (s, 3H, NH₃), 2.94 (s, 6H, N(CH₃)₂), 4.38 (s, 2H, CH₂), 5.35 (d, 2H, ³J_{HH} = 6.0 Hz, CH_{cym}), 5.56 (d, 2H, ³J_{HH} = 6.0 Hz, CH_{cym}), 7.53 (m, 3H, CH_{dmba}), 7.58 ppm (m, 2H, CH_{dmba}); ³¹P NMR (202.44 MHz; CD₃NO₂): δ = -146.53 ppm (sept, 1P, ¹J_{PF} = 734.1 Hz, PF₆).

[(η^6 -biphenyl)Ru^{II}(NH₃)Cl₂][(dmbaH)(PF₆)] (**5b**): [(η^6 -biphenyl)RuCl₂]₂ (0.3 mmol, 0.196 g) was heated to reflux in methanol (80 mL) at 85 °C for 2 h and then cooled to room temperature. *N,N*-Dimethylbenzylamine (0.09 mL, 0.6 mmol) and NH₄PF₆ (0.98 g, 0.6 mmol) were added to the brown solution and the reaction mixture was stirred for 18 h at ambient temperature while no color change occurred. The solution was filtered and the orange-brown filtrate was evaporated to dryness. The oily residue was redissolved in a minimum amount of CH₂Cl₂ and 30 mL of diethyl ether was added. The precipitate was collected by filtration, washed with diethyl ether (3 \times 15 mL), and dried in vacuo to yield 123 mg (33 %) of the target complex.

Elemental analysis (%) calcd for C₂₁H₂₇RuN₂Cl₂PF₆ (624.39 g mol⁻¹): C 40.40, H 4.36, N 4.49; found: C 40.22, H 4.46, N 4.50 %; MS (ESI⁺): *m/z* 136.1 [dmba+H]⁺, 308.0 [(η^6 -biphenyl)Ru(NH₃)Cl]⁺; found: 136.3, 308.3; MS (ESI⁻): *m/z* 145.0 [PF₆]⁻; found: 144.6; ¹H NMR (500.10 MHz; CD₃NO₂): δ = 2.18 (br, 3H, NH₃), 2.88 (s, 6H, N(CH₃)₂), 4.14 (s, 2H, CH₂), 5.97 (m, 2H, CH_{phen}), 5.76 (m, 2H, CH_{phen}), 7.51 (m, 3H, RuCH_{phen}), 7.58 (m, 5H, CH_{dmba}), 7.79 ppm (m, 2H, RuCH_{phen}); ³¹P NMR (202.44 MHz; [D₆]DMSO): δ = -144.15 ppm (sept, 1P, ¹J_{PF} = 746.7 Hz, PF₆).

[(η^6 -p-cymene)Ru^{II}(NH₃)Cl₂][(Et₃NH)(PF₆)] (**6a**): Triethylamine (0.090 mL, 0.65 mmol) and NH₄PF₆ (0.106 g, 0.65 mmol) were added to a suspension of [(η^6 -p-cymene)RuCl₂]₂ (0.32 g, 0.2 mmol) in dry methanol (15 mL) and the reaction mixture was stirred for 18 h at room temperature. Then it was filtered and the resulting orange solution was concentrated to 2 mL, whereby it turned dark brown. The solution was filtered again and crystals suitable for X-ray diffraction analysis (long brown needles) were grown by slow diffusion of diethyl ether into a dichloromethane solution. The crystals were manually separated from the brown residue and washed with diethyl ether (5 \times 15 mL) to give 80 mg (35 %) of the target product.

Elemental analysis (%) calcd for C₁₆H₃₃RuN₂Cl₂PF₆ (570.39 g mol⁻¹): C 33.69, H 5.83, N 4.91; found: C 33.40, H 6.20, N 4.86 %; MS (ESI⁺): *m/z* 102.2 [Et₃N+H]⁺, 270.7 [(η^6 -p-cymene)RuCl]⁺, 289.0 [(η^6 -cymene)Ru(NH₃)Cl]⁺ + [(η^6 -p-cymene)Ru(NH₃)Cl+H]⁺; found: 102.6, 271.1, 289.1; MS (ESI⁻): *m/z* 145.0 [PF₆]⁻; found: 144.5; ¹H NMR (500.10 MHz; CD₃NO₂): δ = 1.30 (d, 6H, ³J_{HH} = 7.0 Hz, CH(CH₃)₂), 1.37 (t, 9H, ³J_{HH} = 7.3 Hz, CH₃), 2.19 (s, 3H, C₆H₄(CH₃)), 2.88 (sept, 1H, ³J_{HH} = 6.9 Hz, CHMe₂), 2.71 (s, 3H, NH₃), 3.34 (m, 6H, CH₂), 5.31 (d, 2H, ³J_{HH} = 5.9 Hz, CH_{cym}), 5.53 ppm (d, 2H, ³J_{HH} = 5.9 Hz, CH_{cym}); ³¹P NMR (202.44 MHz; CD₃NO₂): δ = -146.53 ppm (sept, 1P, ¹J_{PF} = 737.0 Hz, PF₆).

Results and Discussion

Synthesis of organoruthenium(II) am(m)ine complexes: Numerous studies on Ru^{II} η^6 -arene complexes with different numbers of coordinated ammine ligands have been published^[17,23] since the first report of the synthesis of [(η^6 -benzene)Ru(NH₃)₂Cl](PF₆)₃·NH₄PF₆ in 1978^[23b] until the most recent publications.^[17,23g] Despite the variety of synthetic pathways, some of them are contradictory.^[23a,c,d] We found that the type of products, that is, with two ammine ligands in [(η^6 -arene)Ru(NH₃)₂Cl](PF₆) or three in [(η^6 -arene)Ru(NH₃)₃](PF₆)₂, and their yields strictly depend on

the reaction conditions, such as temperature and reaction time, concentration of the reactants, and quality of the solvents.

All of the complexes were synthesized from the ruthenium precursors $[(\eta^6\text{-arene})\text{RuCl}_2]_2$ (**A**: arene = *p*-cymene; **B**: arene = biphenyl). Dimeric complex **B** has low solubility in most commonly used solvents. Therefore, in general, reactions involving the η^6 -biphenyl fragment require longer reaction times and additional purification steps and resulted in lower yields in comparison to η^6 -*p*-cymene complexes. The metal species formed during the reaction are highly reactive and can be stabilized by coordination of solvent molecules which are quickly substituted by nitrogen ligands with higher affinity to ruthenium. It was reported that solvents of medium polarity, such as methanol and nitromethane, yield the target complexes in higher yields,^[17] a fact also observed in our studies. The generated compounds with labile chlorido ligands can be easily hydrolyzed, and therefore synthesis and isolation were performed in absolute solvents.

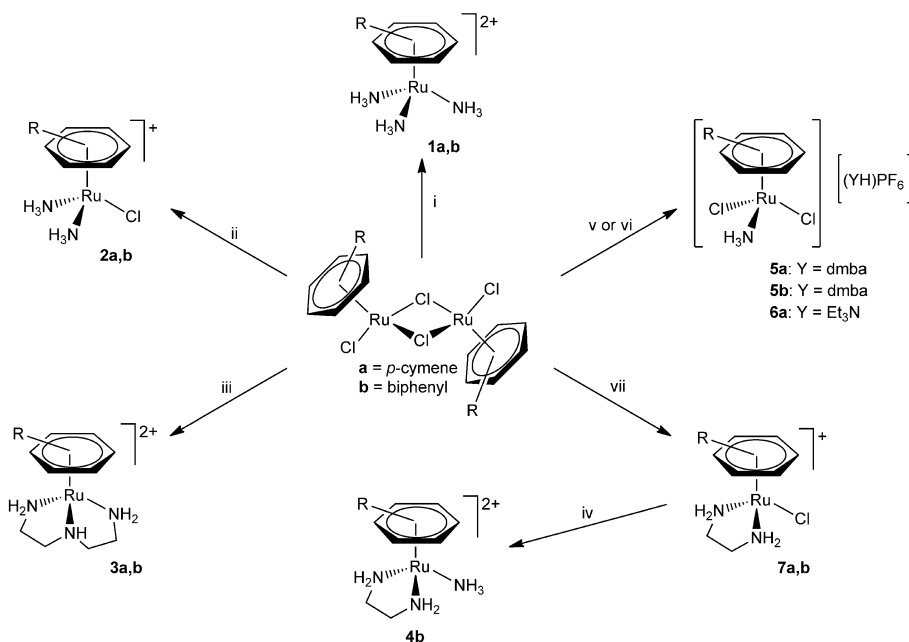
It was recently reported that the reaction of **A** and **B** with aqueous ammonia results in a mixture of products.^[23g] However, by treating **A** and **B** with a large excess of 25% aqueous ammonia in refluxing methanol we obtained ruthenium complexes **1a** and **1b** with three ammonia ligands, which were unambiguously characterized by NMR spectroscopy and mass spectrometry. The reaction time does not affect the type of product, but the yield of the reaction. Indeed, a series of experiments was performed with refluxing or stirring the reagents for 1 or 24 h, and it was found that the maximum yield can be obtained after 1 h of reflux (64%) or 24 h of stirring (60%), while the yields after 1 h of stirring and 24 h of reflux were unsatisfactory (37 and 22%). Low or moderate yields of the reaction prompted the use of alternative sources of ammonia. Commercially available solutions of NH_3 in dioxane or ethanol were found to be inappropriate for preparing the desired compounds. However, reaction with ammonia gas bubbled through the reaction mixture yielded the target complexes in good yields (90 and 70% for **1a** and **1b**, respectively).

When ruthenium precursors **A** and **B** were heated to reflux with a slight excess of 25% aqueous ammonia for one hour, complexes with two ammonia and one chlorido ligand were formed in moderate yields (49 and 43% for **2a** and **2b**; Scheme 1). The optimal reaction time was found to be 1–3 h. However, the same reac-

tion but with an equimolar amount of NH_3 did not lead to the target products **5a** and **5b** featuring one ammonia and two chlorido ligands. These complexes were successfully prepared by in situ generation of NH_3 from stoichiometric amounts of base (e.g. dimethylbenzylamine or triethylamine) and NH_4PF_6 and were always isolated as adducts of the complexes with the base.

Complexes **7a** and **7b** with bidentate ethylenediamine (en) ligand were synthesized according to a literature procedure.^[19] Complex **4b** can be obtained in a single step from **7b** by removal of the chlorido ligand with silver salts and subsequent reaction with ammonia gas bubbled through the solution (yield: 33%). We also investigated the reactions of **A** and **B** with various tridentate ligands. Although osmium complexes with tridentate macrocycles such as 1,4,7-trimethyl-1,4,7-triazacyclononane and 1,4,7-triazacyclononane are known,^[23f,24] similar reactions with the ruthenium precursors resulted in fast darkening of the solution and decomposition. However, we succeeded in the synthesis of ruthenium complexes with the tridentate ligand diethylenetriamine (dien), which readily forms a complex with dimer **A** on stirring for 1.5 h with an excess of the ligand (yield: 75%). The reaction of biphenyl precursor **B** under the same conditions resulted in the formation of **3b** in low yield. However, **3b** was obtained in 54% yield when **B** was heated to reflux for 2 h in water/methanol before an excess of dien was added, followed by stirring for 1.5 h at 55 °C.

All complexes were characterized by ^1H and ^{31}P NMR spectroscopy as well as ESI-MS and elemental analysis. The NH_3 protons of $[(\eta^6\text{-}p\text{-cymene})\text{Ru}(\text{NH}_3)_3](\text{PF}_6)_2$ (**1a**), $[(\eta^6\text{-biphenyl})\text{Ru}(\text{NH}_3)_3](\text{PF}_6)_2$ (**1b**), $[(\eta^6\text{-}p\text{-cymene})\text{Ru}(\text{NH}_3)_2\text{Cl}](\text{PF}_6)$ (**2a**), and $[(\eta^6\text{-biphenyl})\text{Ru}(\text{NH}_3)_2\text{Cl}](\text{PF}_6)$



Scheme 1. Synthesis of Ru^{II} arene complexes with am(m)ine ligands. i) MeOH, NH_3 , NH_4PF_6 /MeOH or 25% NH_4OH excess, NH_4PF_6 ; ii) MeOH, 25% NH_4OH , NH_4PF_6 ; iii) MeOH, dien, NH_4PF_6 ; iv) MeOH, en, NH_3 , AgPF_6 , NH_4PF_6 ; v) MeOH, dmbs, NH_4PF_6 ; vi) MeOH, Et_3N , NH_4PF_6 ; vii) MeOH, en, NH_4PF_6 .^[19]

(**2b**) appear as a broad singlet. The NH₃ proton resonances of *cymene* complexes are detected at a higher field (3.36 ppm) than those of biphenyl derivatives (3.49 ppm) because of the higher electron density at the Ru^{II} centers caused by the weaker π -accepting and stronger π -donating capability of *p*-cymene. The NH₃ signal has approximately the same chemical shift in [(η^6 -biphenyl)Ru(NH₃)₃](PF₆)₂ (**1b**), [(η^6 -biphenyl)Ru(NH₃)₂Cl](PF₆) (**2b**), and [(η^6 -biphenyl)Ru(ethylenediamine)(NH₃)](PF₆)₂ (**4b**).

The ¹H NMR spectrum of the free dien ligand was recorded in a variety of solvents (see Table S3 in the Supporting Information). The methylene protons gave rise to two sharp multiplets in all solvents, whereas NH and NH₂ protons appeared as sharp singlets at δ = 1.06 and 4.83 ppm in CDCl₃ and CD₃OD, and as a broad singlet at δ = 1.44 ppm in [D₆]DMSO. In D₂O, NH/NH₂ signals were not observed due to H/D exchange. On coordination to the metal center, the proton spectra undergo drastic changes, and the NH₂/NH protons are detected as three significantly downshifted signals (see Table S2 in the Supporting Information), indicating electron donation by the diethylenetriamine ligand to the Ru^{II} center. The NMR spectra of [(η^6 -*p*-cymene)Ru(dien)]-

(PF₆)₂ (**3a**) and [(η^6 -biphenyl)Ru(dien)](PF₆)₂ (**3b**) were also recorded in various solvents, but no significant differences were found for the resonances of the arene rings. Methyl and methylene proton resonances were also insensitive to the nature of the solvent, unlike those of the amino groups. In both complexes, the NH/NH₂ proton resonances of coordinated diethylenetriamine recorded in [D₆]DMSO lie downfield ($\Delta\delta$ = 1.06 and 0.57 ppm for **3a** and **3b**, respectively) with respect to those recorded in CD₃OD and D₂O. The NH/NH₂ protons of the diethylenetriamine ligand in **3a** and **3b** undergo slow H/D exchange in protic solvents (>48 h), but it can be accelerated by addition of NaOD to be complete within several minutes. The protons of the ammine ligands in **1a**, **1b**, **2a**, **2b**, and **4b** undergo fast H/D exchange (see Figure S1 in the Supporting Information), which results in the disappearance of the corresponding signals in the ¹H NMR spectra within several hours. Therefore, coordination of chelating triethylenetriamine results in a more pronounced reduction of the rate of H/D exchange in protic solvent compared to monodentate ammine ligands.

X-ray structure determination: The molecular structures of

[(η^6 -biphenyl)Ru^{II}(NH₃)₂Cl](PF₆) (**2b**), [(η^6 -*p*-cymene)Ru^{II}(dien)](PF₆)(Cl) (**3a**), [(η^6 -biphenyl)Ru^{II}(en)(NH₃)](PF₆)₂ (**4b**), and [(η^6 -*p*-cymene)Ru^{II}(NH₃)Cl₂][(Et₃NH)(PF₆)] (**6a**) were determined by X-ray diffraction analysis (Figures 1 and 2, see Tables S1 and S2 in the Supporting Information for crystallographic data, bond lengths, and bond angles). Single crystals of the complexes were grown by slow diffusion of diethyl ether into saturated methanol solutions at 277 K.

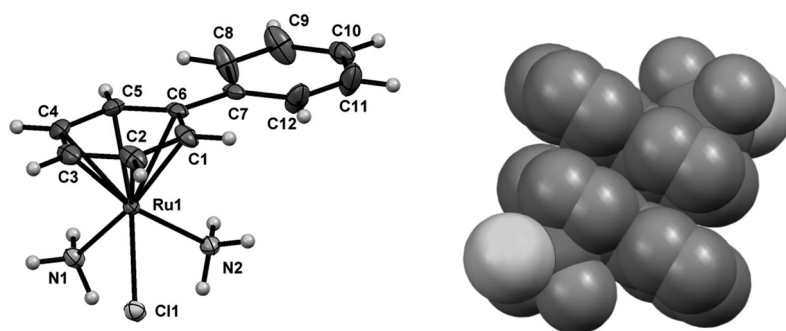


Figure 1. Molecular structure of [(η^6 -biphenyl)Ru^{II}(NH₃)₂Cl](PF₆) (**2b**, left) and space-filling model (right) showing π - π stacking interactions between the phenyl rings of two molecules. The PF₆⁻ anion has been omitted for clarity. Selected bond lengths [Å] and angles [°]: Ru1-C(1-6)_{av} 2.1826(35), Ru1-C11 2.4125(4), Ru1-N1 2.1417(14), Ru1-N2 2.1324(14); N1-Ru1-C11 83.53(4), N2-Ru1-C11 83.36(4), N1-Ru1-N2 82.88(6).

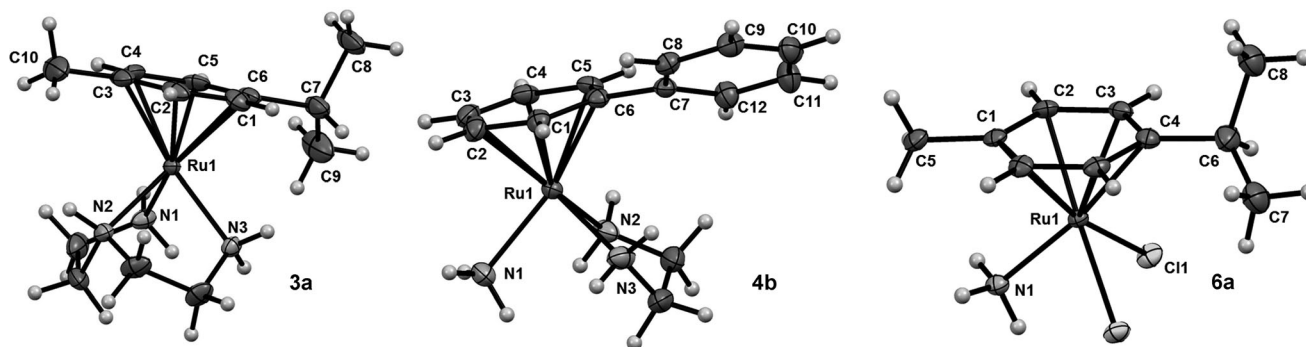


Figure 2. Molecular structures of dicationic [(η^6 -*p*-cymene)Ru^{II}(dien)](PF₆)₂ (**3a**, left) and [(η^6 -biphenyl)Ru^{II}(en)(NH₃)](PF₆)₂ (**4b**, center) and neutral [(η^6 -*p*-cymene)Ru^{II}(NH₃)Cl₂][(Et₃NH)(PF₆)] (**6a**, right). The PF₆⁻ anions and Et₃NH⁺ were omitted for clarity. Selected bond lengths [Å] and angles [°] for **3a**: Ru1-C(1-6)_{av} 2.190(1), Ru1-N1 2.120(5), Ru1-N2 2.127(5), Ru1-N3 2.130(5); N1-Ru1-N2 79.4(2), N3-Ru1-N1 88.39(19), N2-Ru1-N3 77.61(19). For **4b**: Ru1-C(1-6)_{av} 2.1937(52), Ru1-N1 2.1515(17), Ru1-N2 2.1324(17), Ru1-N3 2.1388(17), N1-Ru1-N2 84.79(7), N3-Ru1-N1 88.35(7), N2-Ru1-N3 79.39(7). For **6a**: The complex cation contains a reflection plane passing through Ru1, N1, C1, C4, C5, and C6; Ru1-C(1-6)_{av} 2.170(8), Ru1-C11 2.4157(6), Ru1-C12 2.4157(6), Ru1-N1 2.130(3); N1-Ru1-C11 83.26(6), N1-Ru1-C12 83.26(6), C11-Ru1-C12 85.10.

The pseudo-octahedral coordination environment of the Ru^{II} center consists of Cl⁻ (**2b**, **6a**), and NH₃ (**2b**, **4b**, **6a**) or chelating ligands (**3a**, **4b**) and the η⁶-arene ring. The unit cell of **6a** also contains a triethylammonium hexafluorophosphate ion pair.

In general, the geometrical parameters of all complexes are very similar. The Ru–Cl bond length does not vary significantly with the coordinated arene [2.4125(4) Å for [(η⁶-biphenyl)Ru^{II}(NH₃)₂Cl](PF₆) (**2b**) and 2.4146(4) Å for [(η⁶-cymene)Ru^{II}(NH₃)₂Cl](PF₆) (**2a**)]^[23g] which is in accordance with observations for the mono-ammine complexes [(η⁶-arene)Ru^{II}(NH₃)Cl₂] (**5a,b**) (2.421(2), 2.427(2) and 2.4246(9), 2.4284(8) for cymene/biphenyl respectively).^[17] In contrast, the Ru–Cl bond in the ethylenediamine complexes [(η⁶-arene)Ru^{II}(en)Cl]PF₆ (**7a,b**) is remarkably longer in the cymene complex [2.4418(8) Å (**7a**) vs. 2.4080(15) Å (**7b**)].^[19] The Ru–N bond lengths in **2b**, **3a**, **4b**, and **6a** are in the range 2.120–2.152 Å, and N–Ru–N angles vary between 79 and 88°. These values are similar to those reported previously for related Ru^{II}(arene) complexes.^[19,23g] The Ru–Ph_{centroid} distance in **2b** (1.662 Å) is slightly longer than that of its cymene analogue **2a** (1.659 Å), which is again in accordance with mono-ammine complexes, although less pronounced (1.670 Å for **5b** vs. 1.657 Å for **5a**).^[17] Furthermore, the slightly longer bond lengths for Ru–biphenyl correlate with the higher π acidity compared to *p*-cymene, which leads to a partial filling of the antibonding orbitals of the Ru–arene bonds. All structures feature longer Ru–C_{substituted} than Ru–CH bonds. In the X-ray structure of **2b**, but not of **4b**, intermolecular π stacking was observed in a parallel offset fashion (Figure 1) with a shortest interatomic distance of 3.347 Å and a Ph_{centroid}⋯Ph_{centroid} distance of 3.823 Å. In contrast to structurally related ruthenium(II) half-sandwich complexes bearing biphenyl moieties, in which one phenyl ring is twisted out of the plane by around 23.3(9)° (**7b**)^[19] or 39.5(5)° (**5b**),^[17] the biphenyl ligand in **2b** is surprisingly almost planar (0.3(3)°). In **4b**, the phenyl rings of the biphenyl ligand are tilted from coplanarity by 28.6(3)°.

Hydrolysis and stability studies: Hydrolysis and stability tests were carried out for the complexes prior to investigation of their reactivity toward biomolecules. The stability of the complexes was investigated in water and in 0.1 M (simulating blood plasma conditions) and 1 M aqueous NaCl solutions by means of ¹H NMR spectroscopy. It is known that **2a,b**,^[23g] **5a,b**^[19] and **7a,b**^[17] form mono- and diaqua complexes in water through substitution of chlorido ligands with water molecules. While aquation of the ammine complexes **2a,b**, **5a,b** and **6a** was not suppressed even in 1 M NaCl solution, the ethylenediamine species **7a,b** remained intact for 24 h in 0.1 M NaCl. The complexes without labile chlorido ligands (i.e., **1a,b**, **3a,b** and **4b**) are inert toward hydrolysis in aqueous solution. In long-term stability studies (up to 90 d), a second set of peaks was observed in the NMR spectra after about 10 d (shifted upfield by ca. 0.3 ppm and at 6% relative intensity, see Figure S1 in the Supporting Information). The intensity of this set of peaks remained constant

over the following 80 d, which is indicative of the establishment of an equilibrium. Off-line electrospray ionization mass spectrometry (ESI-MS) measurements of the NMR samples containing **1b** and **3b** showed identical species as observed after 24 h (see below). However, additional hydroxido- and methoxido-bridged dimers were detected in the mass spectrum of **1b**. This suggests that the above-mentioned hydrolysis products may be formed after ammine ligand cleavage.

Furthermore, the stability of the biphenyl compounds in aqueous solution was assayed by ESI-MS, which largely confirmed the observations made by NMR spectroscopy. However, labile monodentate ligands, such as ammine or chlorido, attached to a ruthenium center may be cleaved to a considerable extent even during the soft electrospray process. Such cleavage is observed at a dry gas temperature as low as 80 °C and leads to the formation of dinuclear hydrolysis products with bridging solvent molecules, which are usually regarded as an inactive form of Ru^{II} arene anticancer agents.^[25] Accordingly, the most abundant signal in the mass spectrum of **2b** was assigned to a dinuclear hydrolysis product after cleavage of the monodentate ligands, namely, [(bip)₂Ru₂(μ-OCH₃)₃]⁺ (*m/z* 604.87 ± 0.1, *m_{ex}* = 605.02; bip = η⁶-biphenyl), observed throughout the entire incubation period. Similar dinuclear methoxido-containing hydrolysis products were also observed in the mass spectra of **5b**. The methoxide ligands probably stem from the dilution process with water:methanol (1:1) prior to ESI-MS measurements. In case of **1b**, the most abundant signal was found at *m/z* 288.92 ± 0.01, corresponding to a [(bip)Ru(NH₃)(NH₂)]⁺ fragment (*m_{ex}* = 289.03). The isotope pattern suggests an Ru^I/Ru^{II} redox couple in form of [(bip)Ru(NH₃)₂]⁺ and [(bip)Ru(NH₃)–H]⁺ and a ratio of 1:0.75, while dimeric hydrolysis products were not observed. Due to the lability of the investigated monodentate ligands under the conditions applied in the MS experiments, unequivocal conclusions could not be drawn on the stability of the complexes in aqueous solution. In contrast, complexes containing chelating di- or triamines (e.g., **3b**, **4b**, and **7b**) exhibited higher stability during the spraying process. Their mass spectra remained constant over the entire incubation period, and therefore these compounds are believed to be stable for at least 48 h in aqueous solution. The most abundant signals in the mass spectra of **7b** were assigned to [(bip)Ru(en)Cl]⁺ (*m/z* 350.91 ± 0.01, *m_{ex}* = 351.02) and [(bip)Ru(en)–H]⁺ (*m/z* 314.93 ± 0.01, *m_{ex}* = 315.04); the latter was also observed in the spectra of **4b**. This provides further proof of the lability of monodentate ammine ligands during the electrospray process, since no further assignable signals were detected for **4b**. The mass spectrum recorded for dicationic **3b** showed solely the doubly charged [M]²⁺ ion (*m/z* 179.44 ± 0.01, *m_{ex}* = 179.55).

Reactivity toward proteins: Understanding the interaction of novel metallodrugs with proteins is of particular interest, since anticancer drugs are mostly administered intravenously into the blood stream, where they are exposed to plasma

proteins. Electrospray ionization mass spectrometry (ESI-MS) has proven to be a very suitable tool for the investigation and monitoring of such interactions. In this study, incubations were carried out at 2:1 compound-to-protein molar ratio in aqueous solution. The reactivity of **2b**, **3b**, and **7b** was investigated toward ubiquitin (ub), cytochrome c (cyt), and a mixture containing equimolar amounts of ub and cyt. The MS studies were carried out in high-resolution time-of-flight (ToF) mode. Mass spectra of the incubation mixtures were recorded under denaturing conditions by adding 50% methanol and 0.2% formic acid prior to injection to ensure proper unfolding and protonation of the protein. Because of the absence of labile ligands, **3b** was used as a negative control, and accordingly no protein adducts were observed when it was incubated with ub, cyt, or the ub–cyt mixture for 48 h.

Compound **2b** reacted readily with ub, and after 48 h extensive depletion of free ub (3%) in favor of mono- (45%) and bis-adducts (52%) was observed (Figure 3). The detected masses correspond to a mono-adduct of the type

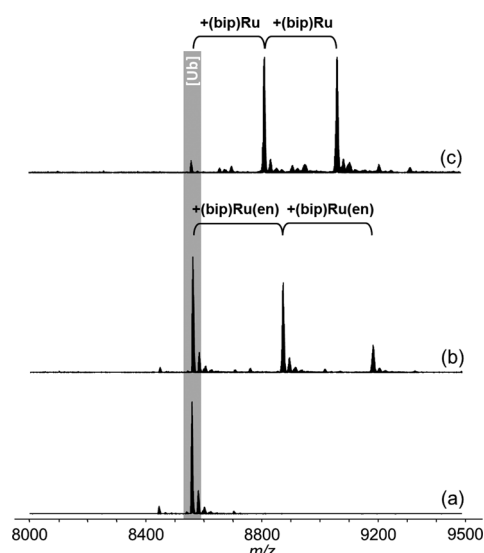


Figure 3. Deconvoluted mass spectra recorded for the incubation mixtures containing ub and **3b** (a), **7b** (b), or **2b** (c) after 48 h. The reaction mixtures were incubated at a compound-to-protein ratio of 2:1 at 37°C in the dark.

$[\text{ub} + (\text{bip})\text{Ru}]^+$ (8818.6031 Da, $m_{\text{ex}} = 8818.6051$ Da, 0.2 ppm), while free ub was found at 8564.6299 Da ($m_{\text{ex}} = 8564.6304$ Da, 0.1 ppm) in the deconvoluted mass spectrum (Figure S2 of the Supporting Information), and a bis-adduct with two (bip)Ru moieties was detected at 9071.5659 Da ($m_{\text{ex}} = 9071.5800$ Da, 1.6 ppm). In case of **2b** the interaction with pro-

teins is accompanied by cleavage of the ammine ligands, as observed previously with pyridonato complexes,^[18d] although in-source ligand cleavage cannot be completely excluded (see above). The interaction between **2b** and cyt resulted in extensive metallation of the protein including higher order adducts at low abundance relative to cyt (12358.4023 Da, $m_{\text{ex}} = 12358.3405$ Da, 5 ppm). In particular, adducts corresponding to $[\text{cyt} + \text{Ru}(\text{HCOO})]^+$ (12504.3070 Da, $m_{\text{ex}} = 12504.2310$ Da, 6 ppm, 15%), $[\text{cyt} + (\text{bip})\text{Ru}]^+$ (12613.3526 Da, $m_{\text{ex}} = 12613.3244$ Da, 2 ppm, 26%), and $[\text{cyt} + (\text{bip})\text{Ru} + \text{Ru}(\text{HCOO})]^+$ (12757.2472 Da, $m_{\text{ex}} = 12757.1985$ Da, 4 ppm, 18%) were detected after 48 h. Similar to the stability studies, no adducts bearing monodentate ammine ligands were observed. Of interest is the observation of the signal at 12504.33 Da. A previous study attributed this signal to $[\text{cyt} + \text{PF}_6^-]$ (12505 Da).^[23f] However, in the present case, the high-resolution mass spectrometric data and isotopic distribution suggest that it rather corresponds to a $[\text{cyt} + \text{Ru}(\text{HCOO})]^+$ adduct (12504.23 Da), in which all of the ligands including the arene were cleaved (see Figure S2 in the Supporting Information). This may be related to oxidation of ruthenium to an Ru^{III} species. This difference in adduct formation between the two data sets may be attributed to differences in experimental conditions. Low metal (and therefore PF_6^-) concentrations and small metal-to-protein molar ratios thereby seem to favor formation of the $[\text{cyt} + \text{Ru}(\text{HCOO})]^+$ adduct. Additionally, no comparable adduct was observed in the reaction with ub. The reaction of **2b** with a 1:1 ub:cyt mixture yielded similar results to the single-protein incubations. Complex **2b** seems to bind preferentially to ub forming mainly $[\text{ub} + (\text{bip})\text{Ru}]^+$ mono-adducts, whereas mono-adduct formation with cyt was only observed at low relative abundance (Table 1).

Compound **7b** formed monofunctional adducts with ub of the type $[\text{ub} + (\text{bip})\text{Ru}(\text{en})]^+$ (8878.6821 Da, $m_{\text{ex}} = 8878.6676$ Da, 2 ppm, 42%), as reported for the undecapeptide substance P.^[26] Retention of the ethylenediamine ligand is related to the stability of the coordinative bond between the *N,N*-bidentate ligand and the Ru center. In addition, the bis-adduct $[\text{ub} + 2(\text{bip})\text{Ru}(\text{en})]^+$ (9191.7175 Da, $m_{\text{ex}} = 9191.7038$ Da, 2 ppm, 15%) was detected after 48 h. Incubation of **7b** with cyt yielded several metal–protein adducts within 48 h, and both mono- and bis-adducts were observed in considerable quantities. Similar to ub, these adducts corresponded to the $[(\text{bip})\text{Ru}(\text{en})]^+$ moiety attached to the pro-

Table 1. List of the detected metallodrug–protein adducts and their associated relative intensities during 2:1 incubation of **2b**, **3b**, or **7b** with ubiquitin (ub), cytochrome c (cyt), or an ub–cyt mixture after 48 h.

Compound	ub		cyt		ub–cyt mixture	
	adduct type	<i>I</i> [%]	adduct type	<i>I</i> [%]	adduct type	<i>I</i> [%]
2b	+(bip)Ru	45	+(bip)Ru	26	ub+(bip)Ru	84
	+2(bip)Ru	52	+Ru(HCOO)	15	ub+2(bip)Ru	5
			+(bip)Ru+Ru(HCOO)	18	cyt+(bip)Ru	9
3b	–	–	–	–	–	–
7b	+(bip)Ru(en)	42	+(bip)Ru(en)	30	ub+(bip)Ru(en)	22
	+2(bip)Ru(en)	15	+2(bip)Ru(en)	6	cyt+(bip)Ru(en)	13
			+Ru(HCOO)	8		

tein, that is, [cyt+(bip)Ru(en)]⁺ (12672.4068 Da, $m_{\text{ex}} = 12672.3790$ Da, 2 ppm, 30%) and [cyt+2(bip)Ru(en)]⁺ (12986.4451 Da, $m_{\text{ex}} = 12986.4169$ Da, 2 ppm, 8%). Like for **2b**, the [cyt+Ru(HCOO)]⁺ adduct was observed, albeit at low abundance (Table 1). When **7b** was incubated with the ub–cyt mixture, it reacted primarily with ub to form [ub+(bip)Ru(en)]⁺, similarly to **2b**, whereas the analogous cyt adducts are much less pronounced.

In analogy to the proposed inverse correlation between extent of protein binding of a metallodrug and cytotoxic activity,^[18g] **2b** is expected to be only active to a limited extent in in vitro assays due to pronounced binding to proteins and ligand cleavage. In contrast, **7b** displays a reduced rate of binding to proteins and also retains the ligand, which is anticipated to result in elevated anticancer activity. Compound **3b** does not react at all with proteins and would in principle be expected to show increased cytotoxicity. However, the absence of a leaving group does not allow conclusions on antitumor properties to be made in this case.

Interaction with 9-ethylguanine as a model for DNA binding: DNA binding is responsible for the antitumor activity of platinum anticancer agents.^[14b] To evaluate the binding capability of representative complexes to DNA, **2b**, **5b**, and **7b** were treated with the DNA model 9-ethylguanine (EtG) and the reaction mixtures were analyzed by ESI-MS. In contrast to **5b** and **2b**, for which no interaction with EtG was observable, **7b** interacts specifically with the model purine. Mono-adducts are believed to form through hydrolysis of the chlorido leaving group and subsequent coordination of EtG to the Ru^{II} center. ESI-IT mass spectra featured peaks assignable to [(bip)Ru(en)(EtG)PF₆]⁺ (m/z 639.93 ± 0.01, $m_{\text{ex}} = 640.10$), [(bip)Ru(en)(EtG)]⁺ (m/z 493.97 ± 0.01, $m_{\text{ex}} = 494.12$), and [(bip)Ru(en)(EtG)]²⁺ (m/z 247.45 ± 0.01, $m_{\text{ex}} = 247.57$), as well as free EtG (m/z 180.01 ± 0.01). CID tandem mass spectrometric experiments on the parent signal at m/z 494 gave peaks at m/z 180.01 and 314.93 for EtG and [(bip)Ru(en)]⁺, respectively, confirming adduct formation of **7b** with EtG. The total percentage of signals attributable to **7b**–EtG adducts increased from 12% after 3 h to 78% after 48 h compared to all signals assigned to free **7b** (Table S4 in the Supporting Information). The stability of the **7b**–DNA adducts may be related to additional C6=O...HN hydrogen-bond formation between guanine and the ethylenediamine ligand.^[27]

Inhibition of cancer cell growth: The in vitro anticancer activity of the Ru complexes was determined in ovarian (CH1), colon (SW480), and non-small cell lung carcinoma (A549) cells by means of the colorimetric MTT assay with an exposure time of 96 h (see Table 2 for IC₅₀ values; concentration–effect curves are shown in Figure S3 in the Supporting Information). CH1 cells are significantly more chemosensitive to the complexes under investigation than SW480 and A549 cells. In general, the biphenyl complexes are more cytotoxic than their *p*-cymene counterparts,^[16b] and only in case of **7a** and **7b** were both compounds approxi-

Table 2. Cytotoxicity of ruthenium complexes **1–7** and cisplatin given as 50% inhibitory concentrations (IC₅₀) in CH1 (ovarian carcinoma), A549 (non-small cell lung cancer), and SW480 (colon carcinoma) cells, determined by means of the MTT assay. Values are means plus/minus standard deviations obtained from at least three independent experiments with exposure times of 96 h.

Compound	IC ₅₀ [μM]		
	CH1	SW480	A549
1a	404 ± 29	474 ± 9	550 ± 16
1b	91 ± 17	272 ± 20	494 ± 54
2a	400 ± 20	586 ± 15	> 640
2b	3.3 ± 0.3	16 ± 2	68 ± 11
3a	> 640	> 640	> 640
3b	54 ± 5	204 ± 16	376 ± 20
4b	30 ± 3	78 ± 8	258 ± 12
5a	258 ± 21	360 ± 26	> 640
5b	85 ± 13	298 ± 21	566 ± 8
6a	343 ± 50	454 ± 19	580 ± 8
7a	7.3 ± 0.1	5.9 ± 0.7	8.8 ± 0.4
7b	6.2 ± 0.5	12 ± 2	9.2 ± 1.9
cisplatin ^[28]	0.14 ± 0.03	3.3 ± 0.4	1.3 ± 0.4

mately equally potent in all cell lines, with IC₅₀ values mostly lower than 10 μM. This might be related to improved accumulation of more lipophilic complexes in cells, facilitated by diffusion of such compounds across membrane barriers. Furthermore, the arene ligand influences the reaction with biological targets. Biphenyl complexes may undergo π–π stacking interactions with nucleobases, leading to intercalation into DNA. However, it seems that the cytotoxicity of the compounds is strongly related to their ability to form covalent bonds, and indeed complexes with labile chlorido ligands were found to undergo quick aquation and yield the lowest IC₅₀ values in the in vitro assays (**2b**, **7a**, **7b**), whereas **1a**, **1b**, **3a**, **3b**, and **4b** with three monodentate ammine or a tridentate amine ligand are virtually noncytotoxic, which may be attributed to the absence of a leaving group. Interestingly, **4b** shows medium in vitro activity, but seems drastically more active in CH1 and SW480 cell lines than **1a,b** and **3a,b**. This may be due to the monodentate ammine ligand, which under cellular conditions may nonetheless be cleaved. The resulting complex is then identical to hydrolyzed **7b**. However, the doubly charged complexes are expected to show less efficient cellular uptake compared to **2b** and **7a,b** and therefore reduced cytotoxicity. These results also confirmed the predictions from protein binding assays. On the contrary, the low activity of **2a**, **5a**, **5b**, and **6a** may be attributed to their instability in organic and especially in aqueous media, in which hydrolysis is not suppressible even by addition of 1 M NaCl, and side reactions may occur already in the cell culture medium prior to contact with the cells. This may also explain why the presence of two labile chlorido ligands (**5a**, **5b**, and **6a**) does not seem to be more advantageous than the presence of only one (**2a**, **2b**) despite the charge of the latter complexes, although the presence of two labile ligands is one of the prerequisites for the strong cytotoxicity of cisplatin (Table 2). Remarkably, neutral ruthenium complexes **5a** and **6a**, which contain noncova-

lently bound base–HPF₆ ion pairs, show a difference in cytotoxicity, which may depend on the base strength, whereby the former is slightly more active.

Conclusion

Ruthenium arene complexes of the bidentate ligand ethylenediamine are potent anticancer agents and have the potential to overcome resistance of tumors to cisplatin. In a systematic study by varying the am(m)ine and arene ligands of Ru half-sandwich compounds, several important parameters for structure–activity relationships could be derived when evaluating the in vitro anticancer activity of the compounds in human tumor cell lines (CH1, A549, and SW480). The cytotoxicity of the complexes strongly depends on the denticity of the ligand, and IC₅₀ values varying by several orders of magnitude were observed. The activity of the complexes appears to be related to their aqueous stability. It is known that classic metal-based drugs serve as prodrugs and are activated by aquation to undergo interactions with biomolecules and exert antiproliferative activity. Inside the cell, activation can be achieved by slow hydrolysis of anionic ligands such as chloride in environments of low chloride concentration, while outside the cell the higher chloride ion concentration shifts the equilibrium to the chlorido complex, preventing formation of the active species. Compounds which are quickly hydrolyzed in aqueous (NaCl-containing) solution were found to be inactive in the anticancer assays, as were compounds which are too reactive towards proteins. These properties are of relevance to incubation with tumor cells in cell culture medium. These observations are in line with previous reports on organoruthenium complexes with three monodentate ligands such as acetonitrile or isonicotinamide,^[19] and also with some more weakly bonding bidentate ligands.^[18a,c,g] Furthermore, compounds lacking leaving groups were less active due to their too high stability. Overall, these facts indicate the necessity of covalent bond formation of the anticancer agent with the intracellular target for exerting anticancer activity.

Acknowledgements

This work was supported by the Platform Austria for Chemical Biology of the Genome Research Program Austria (GEN-AU, BMWF-70.081/0018-II/1a/2008), COST D39, and CM0902. We gratefully acknowledge Prof. Vladimir Arion for the refinement of X-ray diffraction data and Prof. Markus Galanski for recording the 2D NMR spectra.

- [1] B. Rosenberg, L. VanCamp, J. E. Trosko, V. H. Mansour, *Nature* **1969**, *222*, 385–386.
 [2] a) P. Koepf-Maier, *Eur. J. Clin. Pharmacol.* **1994**, *47*, 1–16; b) F. Caruso, M. Rossi, *Met. Ions Biol. Syst.* **2004**, *42*, 353–384.
 [3] a) M. J. Clarke, *Coord. Chem. Rev.* **2003**, *236*, 209–233; b) Y. K. Yan, M. Melchart, A. Habtemariam, P. J. Sadler, *Chem. Commun.* **2005**, 4764–4776; c) I. Kostova, *Recent Pat. Anti-Cancer Drug Discovery* **2006**, *1*, 1–22; d) I. Bratsos, A. Bergamo, G. Sava, T. Gianfer-

- rara, E. Zangrando, E. Alessio, *J. Inorg. Biochem.* **2008**, *102*, 606–617.
 [4] a) J. M. Rademaker-Lakhai, D. Van Den Bongard, D. Pluim, J. H. Beijnen, J. H. M. Schellens, *Clin. Cancer Res.* **2004**, *10*, 3717–3727; b) C. G. Hartinger, M. A. Jakupec, S. Zorbas-Seifried, M. Groessl, A. Egger, W. Berger, H. Zorbas, P. J. Dyson, B. K. Keppler, *Chem. Biodiversity* **2008**, *5*, 2140–2155; c) D. Thompson, G. J. Weiss, S. F. Jones, H. A. Burris, K. Ramanathan, J. R. Infante, J. C. Bendell, A. Ogden, D. D. von Hoff, at *ASCO Annual Meeting* **2012**, Abstract 3033.
 [5] a) M. J. Clarke, S. Bitler, D. Rennert, M. Buchbinder, A. D. Kelman, *J. Inorg. Biochem.* **1980**, *12*, 79–87; b) P. Schluga, C. G. Hartinger, A. Egger, E. Reisner, M. Galanski, M. A. Jakupec, B. K. Keppler, *Dalton Trans.* **2006**, 1796–1802.
 [6] M. A. A. F. d. C. T. Carrondo, W. P. Griffith, J. P. Hall, A. C. Skapski, *Biochim. Biophys. Acta Gen. Subj.* **1980**, *627*, 332–334.
 [7] a) W. L. Ying, J. Emerson, M. J. Clarke, D. R. Sanadi, *Biochemistry* **1991**, *30*, 4949–4952; b) C. Zazueta, G. Zafra, G. Vera, C. Sanchez, E. Chavez, *J. Bioenerg. Biomembr.* **1998**, *30*, 489–498; c) C. Zazueta, M. E. Sosa-Torres, F. Correa, A. Garza-Ortiz, *J. Bioenerg. Biomembr.* **1999**, *31*, 551–557.
 [8] C. M. Bastos, K. A. Gordon, T. D. Ocain, *Bioorg. Med. Chem. Lett.* **1998**, *8*, 147–150.
 [9] D. Frasca, J. Ciampa, J. Emerson, R. S. Umans, M. J. Clarke, *Met.-Based Drugs* **1996**, *3*, 197–209.
 [10] F. Bottomley, *Can. J. Chem.* **1977**, *55*, 2788–2791.
 [11] a) K. A. Marx, R. Kruger, M. J. Clarke, *Mol. Cell. Biochem.* **1989**, *86*, 155–162; b) K. A. Marx, C. Seery, P. Malloy, *Mol. Cell. Biochem.* **1989**, *90*, 37–45.
 [12] a) M. J. Clarke, *ACS Symp. Ser.* **1980**, *140*, 157–180; b) M. J. Clarke, F. Zhu, D. R. Frasca, *Chem. Rev.* **1999**, *99*, 2511–2533.
 [13] a) J. E. Earley, P. M. Smith, T. Fealey, J. V. Silverton, *Inorg. Chem.* **1971**, *10*, 1943–1947; b) P. Nagababu, J. N. L. Latha, S. Satyanarayana, *Chem. Biodiversity* **2006**, *3*, 1219–1229; c) S. P. Mulcahy, K. Gruendler, C. Frias, L. Wagner, A. Prokop, E. Meggers, *Dalton Trans.* **2010**, *39*, 8177–8182; d) M. Shilpa, P. Nagababu, Y. P. Kumar, J. N. L. Latha, M. R. Reddy, K. S. Karthikeyan, N. Gabra, S. Satyanarayana, *J. Fluoresc.* **2011**, *21*, 1155–1164.
 [14] a) S. van Zutphen, J. Reedijk, *Coord. Chem. Rev.* **2005**, *249*, 2845–2853; b) Y. Jung, S. J. Lippard, *Chem. Rev.* **2007**, *107*, 1387–1407.
 [15] a) I. Bratsos, S. Jedner, T. Gianferrara, E. Alessio, *Chimia* **2007**, *61*, 692–697; b) C. G. Hartinger, P. J. Dyson, *Chem. Soc. Rev.* **2009**, *38*, 391–401; c) G. Sava, A. Bergamo, P. J. Dyson, *Dalton Trans.* **2011**, *40*, 9069–9075.
 [16] a) R. E. Morris, P. J. Sadler, H. Chen, D. Jodrell, Half-sandwich ruthenium(II) compounds comprising nitrogen containing ligands for treatment of cancer, **2001**, WO2001030790 A1; b) A. Habtemariam, M. Melchart, R. Fernandez, S. Parsons, I. D. H. Oswald, A. Parkin, F. P. A. Fabbiani, J. E. Davidson, A. Dawson, R. E. Aird, D. I. Jodrell, P. J. Sadler, *J. Med. Chem.* **2006**, *49*, 6858–6868.
 [17] S. Betanzos-Lara, A. Habtemariam, G. J. Clarkson, P. J. Sadler, *Eur. J. Inorg. Chem.* **2011**, 3257–3264.
 [18] a) W. Kandioller, C. G. Hartinger, A. A. Nazarov, C. Bartel, M. Skocic, M. A. Jakupec, V. B. Arion, B. K. Keppler, *Chem. Eur. J.* **2009**, *15*, 12283–12291; b) W. Kandioller, C. G. Hartinger, A. A. Nazarov, J. Kasser, R. John, M. A. Jakupec, V. B. Arion, P. J. Dyson, B. K. Keppler, *J. Organomet. Chem.* **2009**, *694*, 922–929; c) W. Kandioller, C. G. Hartinger, A. A. Nazarov, M. L. Kuznetsov, R. O. John, C. Bartel, M. A. Jakupec, V. B. Arion, B. K. Keppler, *Organometallics* **2009**, *28*, 4249–4251; d) M. Hanif, H. Henke, S. M. Meier, S. Martic, M. Labib, W. Kandioller, M. A. Jakupec, V. B. Arion, H. B. Kraatz, B. K. Keppler, C. G. Hartinger, *Inorg. Chem.* **2010**, *49*, 7953–7963; e) M. Hanif, P. Schaaf, W. Kandioller, M. Hejl, M. A. Jakupec, A. Roller, B. K. Keppler, C. G. Hartinger, *Aust. J. Chem.* **2010**, *63*, 1521–1528; f) W. Kandioller, A. Kurzwernhart, M. Hanif, S. M. Meier, H. Henke, B. K. Keppler, C. G. Hartinger, *J. Organomet. Chem.* **2011**, *696*, 999–1010; g) S. M. Meier, M. Hanif, W. Kandioller, B. K. Keppler, C. G. Hartinger, *J. Inorg. Biochem.* **2012**, *108*, 91–95.

- [19] R. E. Morris, R. E. Aird, S. Murdoch Pdel, H. Chen, J. Cummings, N. D. Hughes, S. Parsons, A. Parkin, G. Boyd, D. I. Jodrell, P. J. Sadler, *J. Med. Chem.* **2001**, *44*, 3616–3621.
- [20] M. A. Bennett, A. K. Smith, *J. Chem. Soc. Dalton Trans.* **1974**, 233–241.
- [21] M. R. Pressprich, J. Chambers, *SAINT+Integration Engine, Program for Crystal Structure Integration*, Bruker Analytical X-ray systems, Madison, **2004**.
- [22] G. M. Sheldrick, *Acta Crystallogr. Sect. A* **2008**, *64*, 112–122.
- [23] a) D. R. Robertson, T. A. Stephenson, T. Arthur, *J. Organomet. Chem.* **1978**, *162*, 121–136; b) R. O. Gould, C. L. Jones, D. R. Robertson, T. A. Stephenson, *Cryst. Struct. Commun.* **1978**, *7*, 27–32; c) Y. Hung, W.-J. Kung, H. Taube, *Inorg. Chem.* **1981**, *20*, 457–463; d) W. Weber, P. C. Ford, *Inorg. Chem.* **1986**, *25*, 1088–1092; e) E. A. Ganja, T. B. Rauchfuss, C. L. Stern, *Organometallics* **1991**, *10*, 270–275; f) F. Wang, J. Bella, J. A. Parkinson, P. J. Sadler, *J. Biol. Inorg. Chem.* **2005**, *10*, 147–155; g) S. Grguric-Sipka, I. N. Stepanenko, J. M. Lazic, C. Bartel, M. A. Jakupec, V. B. Arion, B. K. Keppler, *Dalton Trans.* **2009**, 3334–3339.
- [24] M. N. Bell, A. J. Blake, M. Schroeder, T. A. Stephenson, *J. Chem. Soc. Chem. Commun.* **1986**, 471–472.
- [25] A. F. A. Peacock, M. Melchart, R. J. Deeth, A. Habtemariam, S. Parsons, P. J. Sadler, *Chem. Eur. J.* **2007**, *13*, 2601–2613.
- [26] J. P. Williams, J. M. Brown, I. Campuzano, P. J. Sadler, *Chem. Commun.* **2010**, *46*, 5458–5460.
- [27] H. Chen, J. A. Parkinson, S. Parsons, R. A. Coxall, R. O. Gould, P. J. Sadler, *J. Am. Chem. Soc.* **2002**, *124*, 3064–3082.
- [28] Y. Y. Scaffidi-Domianello, A. A. Legin, M. A. Jakupec, V. B. Arion, V. Y. Kukushkin, M. Galanski, B. K. Keppler, *Inorg. Chem.* **2011**, *50*, 10673–10681.

Received: July 26, 2012

Revised: December 12, 2012

Published online: January 22, 2013

CHEMISTRY

A EUROPEAN JOURNAL

Supporting Information

© Copyright Wiley-VCH Verlag GmbH & Co. KGaA, 69451 Weinheim, 2013

Am(m)ines Make the Difference: Organoruthenium Am(m)ine Complexes and Their Chemistry in Anticancer Drug Development

**Maria V. Babak,^[a] Samuel M. Meier,^[a, b] Anton A. Legin,^[a] Mahsa S. Adib Razavi,^[a]
Alexander Roller,^[a] Michael A. Jakupec,^[a, b] Bernhard K. Keppler,^[a, b] and
Christian G. Hartinger ^{*[a, b, c]}**

chem_201202657_sm_miscellaneous_information.pdf

Am(m)ines make the Difference: Organometallic Ruthenium Am(m)ine Complexes and Their Chemistry in Anticancer Drug Development

Maria V. Babak^a, Samuel M. Meier^{a,b}, Anton A. Legin^a, Mahsa S. Adib Razavi^a, Alexander Roller^a, Michael A. Jakupec^{a,b}, Bernhard K. Keppler^{a,b}, Christian G. Hartinger^{a-c,*}

^a *Institute of Inorganic Chemistry, University of Vienna, Waehringer Str. 42, A-1090 Vienna, Austria.*

^b *Research Platform “Translational Cancer Therapy Research”, University of Vienna, Waehringer Str. 42, A-1090 Vienna, Austria.*

^c *School of Chemical Sciences, The University of Auckland, Private Bag 92019, New Zealand*

Table S1. Crystal data and details of data collection for **2b**, **3a**, **4b** and **6a**.

Table S2. Key bond lengths and angles observed in the molecular structures of **2b**, **3a**, **4b**, and **6a** as compared to **2a**, **5a**, **5b**, **7a** and **7b**.

Table S3. ¹H NMR (500 MHz) data for diethylenetriamine, the ruthenium precursors **A** and **B** and for **3a** and **3b**.

Table S4. Relative time-dependent intensity changes (%) of the signals assigned to **7b** and its EtG adduct.

Figure S1. ¹H NMR study on the stability of **1b** in D₂O for 10 days.

Figure S2. The figure shows part of the deconvoluted spectrum of the incubation between **2b** and cytochrome-c after 48 h. The mixture was incubated at a molar ratio of 2 : 1 at 37 °C in the dark. The signal at 12504.3320 Da indicates formation of a [Cyt + Ru(HCOO)]⁺ mono-adduct, with Ru in oxidation state 3+. The upper spectrum corresponds to the recorded spectrum, whereas the lower refers to the simulated spectrum.

Figure S3. Concentration–effect curves of the biphenyl complexes **1b**, **2b**, **3b**, **4b** and **7b** in the human ovarian cancer cell line CH1. Values were obtained by the MTT assay and are means ± standard deviations from at least three independent experiments using exposure times of 96 h

Table S1. Crystal data and details of data collection for **2b**, **3a**, **4b** and **6a**.

Complex	2b	3a	4b	6a
CCDC no.	885890	885889	885888	885891
Empirical formula	C ₁₂ H ₁₆ ClF ₆ N ₂ PRu	C ₁₄ H ₂₇ ClF ₆ N ₃ PRu	C ₁₄ H ₂₁ F ₁₂ N ₃ P ₂ Ru	C ₁₆ H ₃₃ Cl ₂ F ₆ N ₂ PRu
Fw	469.76	518.88	622.35	570.38
Crystal system	monoclinic	monoclinic	monoclinic	monoclinic
Space group	<i>P</i> 2 ₁ / <i>c</i>	<i>P</i> 2 ₁ / <i>n</i>	<i>P</i> 2 ₁ / <i>n</i>	<i>P</i> 2 ₁ / <i>m</i>
<i>a</i> , Å	9.0395(3)	12.8138(5)	12.0792(11)	10.7107(3)
<i>b</i> , Å	16.8786(6)	12.6133(6)	12.1344(9)	9.2077(3)
<i>c</i> , Å	10.4512(4)	13.2356(6)	14.2723(12)	11.9450(3)
α , deg	90	90	90	90
β , deg	96.517(2)	112.266(2)	95.277(4)	99.347(10)
γ , deg	90	90	90	90
<i>V</i> , Å ³	1584.28(10)	1979.68(15)	2083.1(3)	1162.39(6)
<i>Z</i>	4	4	4	2
λ , Å	0.71073	0.71073	0.71073	0.71073
ρ_{calcd} , g cm ⁻³	1.969	1.741	1.984	1.630
Crystal size, mm ³	0.20 × 0.10 × 0.10	0.20 × 0.10 × 0.03	0.25 × 0.25 × 0.03	0.25 × 0.22 × 0.10
<i>T</i> , K	100(2)	296(2)	150(2)	100(2)
μ , cm ⁻¹	1.319	1.066	1.020	1.025
Reflns collected/unique	36393 / 3820	77548 / 3867	135141 / 6095	13305 / 2429
[<i>R</i> _{int}]	0.0501	0.0424	0.0462	0.0379
<i>R</i> 1 ^a	0.0209	0.0471	0.0257	0.0292
<i>wR</i> 2 ^b	0.0513	0.1238	0.0668	0.0725
GOF ^c	1.053	1.037	1.085	1.067

^a $R_1 = \sum ||F_o| - F_c| / \sum |F_o|$, ^b $wR_2 = \{\sum w(F_o^2 - F_c^2)^2 / \sum w(F_o^2)^2\}^{1/2}$. ^c $GOF = \{\sum [w(F_o^2 - F_c^2)^2] / (n - p)\}^{1/2}$, where *n* is the number of reflections and *p* is the total number of parameters refined.

Table S2. Key bond lengths and angles observed in the molecular structures of **2b**, **3a**, **4b**, and **6a** as compared to **2a**, **5a**, **5b**, **7a** and **7b**.

Bond lengths (Å) and angles (°)	Compound			
	2a ^a	2b	3a	4b
Ru–arene _{centroid} / Å	1.659	1.662	1.676	1.675
Ru–arene _{average} / Å	2.1829(84)	2.1826(35)	2.190(1)	2.1937(52)
Ru–C _{substituted} / Å	2.1995(17)	2.1964(17)	2.216(6)	2.2194(18)
	2.2043(18)		2.199(6)	
Ru–C _{unsubstituted} / Å	2.1631(17)	2.1829(18)	2.183(6)	2.1936(18)
	2.1660(18)	2.1712(19)	2.162(6)	2.1764(19)
	2.1889(17)	2.1738(18)	2.200(6)	2.1853(18)
	2.1760(17)	2.1953(19)	2.177(6)	2.1969(19)
		2.1761(18)		2.1908(18)
Ru–Cl1 / Å	2.4146(4)	2.4125(4)		
Ru–N1 / Å	2.1504(15)	2.1417(14)	2.130(5)	2.1388(17)
Ru–N2 / Å	2.1425(15)	2.1324(14)	2.127(5)	2.1324(17)
Ru–N3 / Å			2.120(5)	2.1515(17)
N1–Ru–Cl1 / °	84.60(4)	83.53(4)		
N2–Ru–Cl2 / °	84.68(4)	83.36(4)		
N1–Ru–N2 / °	82.70(6)	82.88(6)	79.4(2) (NH)	84.79(7) (NH ₃)
N2–Ru–N3 / °			77.61(19) (NH)	88.35(7) (NH ₃)
N1–Ru–N3 / °			88.39(19) (2NH ₂)	79.39(7) (2NH ₂)
π-π stacking	No	Yes	No	No
Ph _{centroid} –Ph _{centroid} / Å		3.823		
Shortest contact / Å		3.347		

^a taken from Cambridge Structural Database, CCDC no. 707426

Table S2. Continued.

Bond lengths (Å) and angles (°)	Compound				
	5a ^b	5b ^c	6a	7a ^d	7b ^e
Ru–arene _{centroid} / Å	1.657	1.670	1.645	1.669	1.662
Ru–arene _{average} / Å	2.182(4)	2.190(3)	2.170(8)	2.187(6)	2.178(7)
Ru–C _{substituted} / Å	2.214(1)	2.233(3)	2.198(4)	2.202(3)	2.244(6)
Ru–C _{unsubstituted} / Å	2.212(9)			2.218(3)	
	2.158(9)	2.202(3)	2.179(3)	2.163(3)	2.190(5)
	2.185(9)	2.201(3)	2.153(2)	2.164(3)	2.138(5)
	2.177(8)	2.175(3)	2.153(2)	2.195(3)	2.185(6)
	2.145(1)	2.164(3)	2.170(2)	2.182(3)	2.160(6)
		2.165(3)	2.170(2)		2.152(5)
Ru–Cl1 / Å	2.421(2)	2.4245(9)	2.4157(6)	2.4418(8)	2.4080(15)
Ru–Cl2 / Å	2.427(2)	2.4284(8)	2.4157(6)		
Ru–N1 / Å	2.124(7)	2.135(3)	2.130(3)	2.136(2)	2.110(5)
Ru–N2 / Å				2.130(3)	2.121(5)
N1–Ru–Cl1 / °	83.80(2)	84.29(8)	83.26(6)	83.46(8)	85.60(12)
N1–Ru–Cl2 / °	84.30(2)	84.73(8)	83.26(6)		
Cl1–Ru–Cl2 / °	85.11(8)	85.26(3)	85.10(3)		
N2–Ru–Cl1 / °				85.29(7)	82.88(11)
N1–Ru–N2 / °				78.98(10)	79.20(18)
π–π stacking	No	Yes	No	No	Yes
Ph _{centroid} –Ph _{centroid} / Å		3.687			3.942
Shortest contact / Å		3.587			3.659

^b taken from Cambridge Structural Database, CCDC no. 809024

^c taken from Cambridge Structural Database, CCDC no. 809025

^d taken from Cambridge Structural Database, CCDC no. 170360

^e taken from Cambridge Structural Database, CCDC no. 170362

Table S3. ^1H NMR (500 MHz) spectroscopy data for diethylenetriamine, the ruthenium precursors **A** and **B** and for **3a** and **3b**.

Compound	solvent	chemical shift, ppm					
		ligand		arene			
		2NH ₂ , NH	2CH ₂ CH ₂	<i>i</i> -Pr	CH ₃	Ring	
				η^6 -coordinated	uncoordinated		
diethylenetriamine (dien)	CDCl ₃	1.06 (s, 5H)	2.51 (m, 4H) 2.64 (m, 4H)				
	DMSO-d ⁶	1.44 (s, br)	2.48 (m, 4H) 2.57 (m, 4H)				
	CD ₃ OD	4.83 (s, 5H)	2.69 (m, 4H) 2.77 (m, 4H)				
	D ₂ O	-	2.59 (m, 4H) 2.67 (m, 4H)				
A	DMSO-d ⁶			1.20 (d, 6H) 2.84 (sept, 1H)	2.10 (s)	5.78 (d, 2H) 5.83 (d, 2H)	
B	DMSO-d ⁶					6.08 (m, 3H) 6.44 (d, 2H)	7.51 (m, 3H) 7.84 (d, 2H)
3a	DMSO-d ⁶	5.14 (m, 2H) 6.48 (m, 2H) 7.92 (m, 1H)	2.48 – 2.55 (m, 4H) 2.61 (m, 2H) 2.76 (m, 2H)	1.21 (d, 6H) 2.96 (sept, 1H)	2.25 (s)	5.61 (d, 2H) 5.73 (d, 2H)	
	D ₂ O	4.14 (m, 2H) 6.07 (m, 2H) 7.39 (m, 1H)	2.58 (m, 2H) 2.66 (m, 2H) 2.73 (m, 2H) 2.93 (m, 2H)	1.22 (d, 6H) 2.78 (sept, 1H)	2.21 (s)	5.57 (d, 2H) 5.72 (d, 2H)	
3b	DMSO-d ⁶	4.31 (m, 2H) 5.92 (m, 2H) 8.32 (m, 1H)	2.41 – 2.60 (m, 6H) 2.72 (m, 2H)			5.92 (t, 2H) 6.04 (t, 1H) 6.30 (d, 2H)	7.55 (m, 3H) 7.80 (d, 2H)
	CD ₃ OD	4.21 (m, 2H) 6.29 (m, 2H) 8.04 (m, 1H)	2.62 (m, 2H) 2.72 (m, 4H) 2.96 (m, 2H)			6.00 (t, 1H) 6.06 (t, 2H) 6.31 (d, 2H)	7.61 (m, 3H) 7.82 (d, 2H)
	D ₂ O	4.21 (m, 2H) 5.97 (m, 2H) 7.83 (m, 1H)	2.53 (m, 2H) 2.61 (m, 2H) 2.66 (m, 2H) 2.89 (m, 2H)			5.88 (t, 1H) 5.97 (t, 2H) 6.21 (d, 2H)	7.57 (m, 3H) 7.73 (d, 2H)

Table S4. Relative time-dependent intensity changes (%) of the signals assigned to **7b** and its EtG adducts.

time / h	EtG-adducts	7b
0	0	100
3	12	88
6	25	75
24	31	69
48	78	22

Figure S1. ^1H NMR study on the stability of **1b** in D_2O for 10 days.

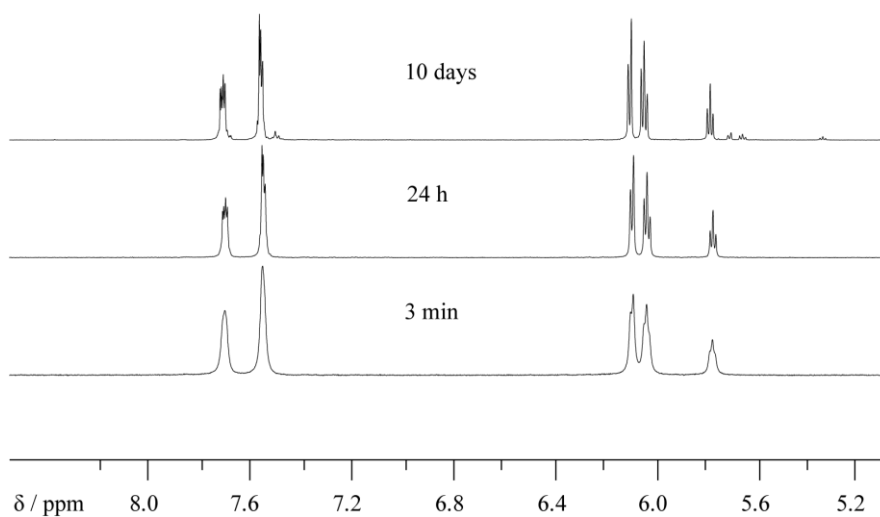


Figure S2. The figure shows part of the deconvoluted spectrum of the incubation between **2b** and cytochrome-c after 48 h. The mixture was incubated at a molar ratio of 2 : 1 at 37 °C in the dark. The signal at 12504.3320 Da indicates formation of a $[\text{Cyt} + \text{Ru}(\text{HCOO})]^+$ mono-adduct, with Ru in oxidation state 3+. The upper spectrum corresponds to the recorded spectrum, whereas the lower refers to the simulated spectrum.

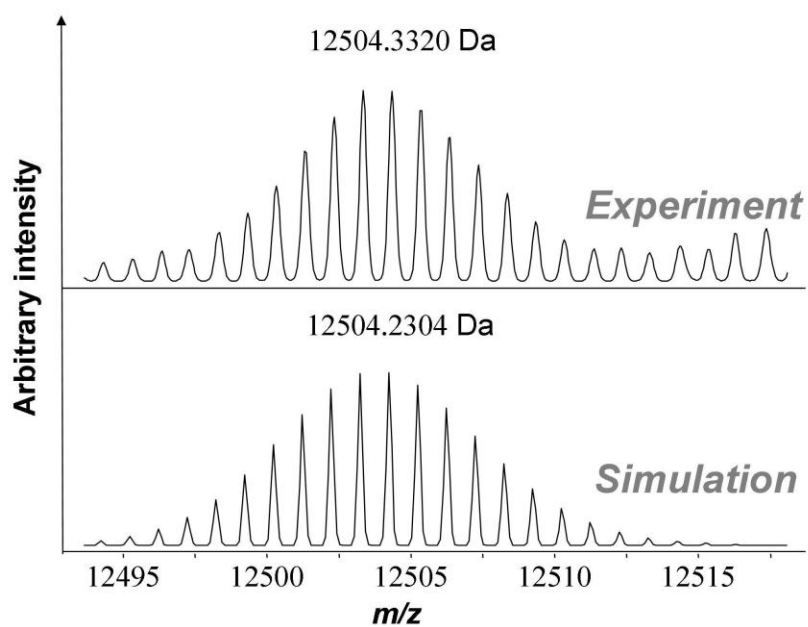
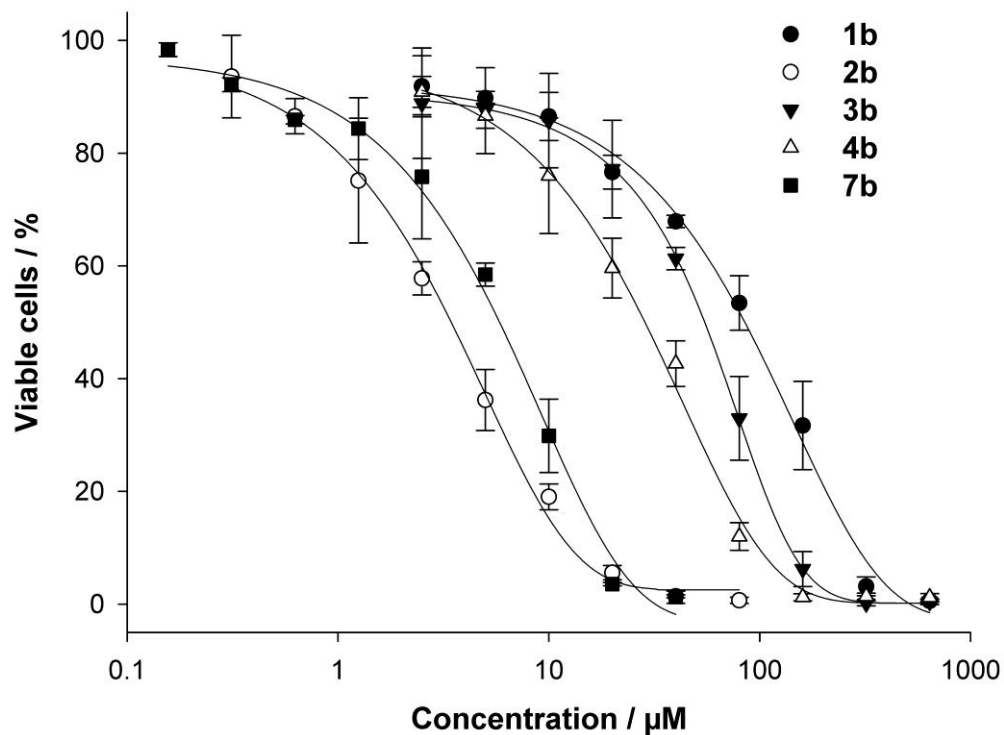


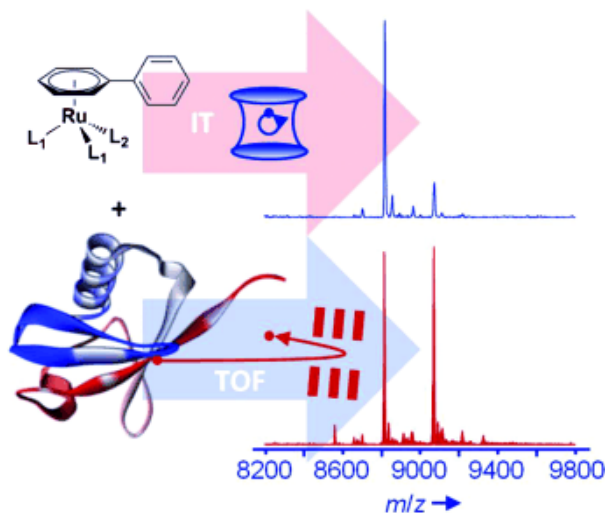
Figure S3. Concentration–effect curves of the biphenyl complexes **1b**, **2b**, **3b**, **4b** and **7b** in the human ovarian cancer cell line CH1. Values were obtained by the MTT assay and are means \pm standard deviations from at least three independent experiments using exposure times of 96 h.



4. Efficiently detecting metallodrug-protein adducts: ion trap versus time-of-flight mass analyzers

Samuel M. Meier, *Maria V. Babak*, Bernhard K. Keppler, Christian G. Hartinger

ChemMedChem, published online, **2014**, DOI: 10.1002/cmdc.201400020



Weighing the alternatives: Mass spectrometry is increasingly employed for metallodrug–protein binding studies. However, a methodical investigation on mass analyzers and especially their influence on the efficiency of adduct detection has not been carried out so far. We show that mass analyzers can exhibit pronounced differences on adduct detection efficiencies, influencing investigations on potential cellular targets and for the screening of metallodrugs.

DOI: 10.1002/cmdc.201400020

Efficiently Detecting Metallodrug–Protein Adducts: Ion Trap versus Time-of-Flight Mass Analyzers

Samuel M. Meier,^[a, b] Maria V. Babak,^[a, b, c] Bernhard K. Keppler,^[a, b] and Christian G. Hartinger^{*[c]}

Modern mass spectrometry techniques have increasingly found use in studies on the binding of anticancer metallodrugs to potential cellular targets. In this context, investigations on the detection efficiency of adduct formation between antiproliferative Ru(arene) complexes and proteins in dependence of the mass analyzer used in the electrospray ionization (ESI) mass spectrometer are presented. The potential in detecting adducts between the metal center and the protein was found to be dependent on the mass analyzer and the denticity of the metal–protein interaction. This might be related to the design of the mass analyzers with different conditions in the ion travelling pathways, which affects adducts when the protein acts as a monodentate ligand more highly than in cases when the protein is a multidentate ligand. This could also impact the biological activity and indicate different pathways of metabolism of biomolecule adducts.

The appreciation that certain organometallic Ru^{II} anticancer agents might exert their biological effect by interacting with targets different from genomic DNA has prompted detailed investigations on the modes of action for this compound class.^[1] Interactions with proteins have proven to be of particular interest due to their signaling, enzymatic, and regulatory functions in cells and their high abundance in blood plasma. Metallodrug–protein interactions have gained additional relevance due to the observation that cisplatin binding to proteins in blood might be associated with unwanted side effects in patients undergoing chemotherapy.^[2] Consequently, several recent reports have been devoted to the analysis of metallodrug–protein interactions on a molecular level, in particular using mass spectrometry to establish the nature of binding,^[3] the location of binding sites,^[4] and to analyze the conformational changes that occur upon metallation.^[4d,e,5]

The preferred binding partners on proteins for metallodrugs are still a matter of debate; however, it is widely accepted that the covalent interaction depends on the nature of the metal center, its oxidation state, and the accessibility to the ligand donor atoms, for which nucleophilic character is known to be essential. Furthermore, it is possible to determine pseudokinetics of metallodrug–protein interactions by monitoring the time-dependent formation of adducts. The combined evaluation of pseudokinetics and the nature of binding allowed the proposition of an inverse relationship between the extent of adduct formation and cytotoxic activity, at least for Ru^{II}(arene) complexes containing (thio)pyr(id)onato ligands, providing a convenient method for a first cost-effective activity screen in the development of such anticancer agents.^[3h]

During the last few years, metallodrug–protein binding was probed using various types of mass spectrometry and efforts were primarily focused on adduct characterization. However, the impact of the instrumental setup was not extensively investigated with respect to the nature of adduct formation or to the efficiency of adduct detection. One of the few reports that looked at different methodical approaches involved the study of different ion sources,^[4b] which underlined the superiority of electrospray ionization (ESI) over matrix-assisted laser desorption/ionization (MALDI) due to decreased in-source fragmentation of the metallodrug–protein adduct. Surprisingly, the influence of the mass analyzer on adduct detection efficiencies is still unexplored. For this purpose, the reactivity of three biphenyl-capped Ru^{II} complexes (1–3; Figure 1) containing am(m)ine ligands was investigated towards ubiquitin (ub) and cytochrome C (cyt) employing ESI-ion trap (IT) and ESI-time-of-flight (ToF) mass spectrometry (Figure 1). Compound 1 contains two amines and one labile chlorido ligand, whereas in compound 2, the amines are linked by an ethylene unit forming a bidentate ligand, which is more inert towards ligand substitution. Compound 3 contains the tridentate bis(ethylene)triamine ligand and represents a probe for electro-

[a] Dr. S. M. Meier, M. V. Babak, Prof. B. K. Keppler
Institute of Inorganic Chemistry, University of Vienna
Waehringer Str. 42, 1090 Vienna (Austria)

[b] Dr. S. M. Meier, M. V. Babak, Prof. B. K. Keppler
Translational Cancer Research Center, University of Vienna
Waehringer Str. 42, 1090 Vienna (Austria)

[c] M. V. Babak, Prof. C. G. Hartinger
School of Chemical Sciences, University of Auckland
Private Bag 92019, Auckland 1142 (New Zealand)
E-mail: c.hartinger@auckland.ac.nz
Homepage: <http://hartinger.wordpress.fos.auckland.ac.nz/>

Supporting information for this article is available on the WWW under <http://dx.doi.org/10.1002/cmdc.201400020>.

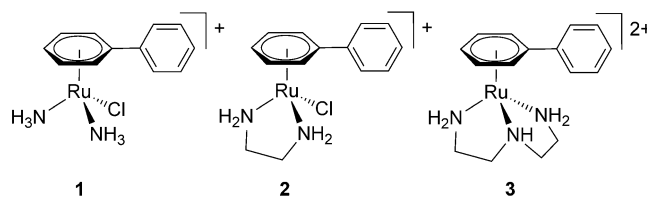


Figure 1. The chemical structures of the investigated organometallic Ru^{II} compounds.

static, and therefore nonspecific (noncovalent), adduct formation.^[6]

Compounds **1–3** were incubated with ub or cyt at molar ratios of both 1:1 and 2:1 and a mixture of ub/cyt at molar ratios of 1:1:1 and 2:1:1 for up to 48 hours. The proteins were chosen due to their frequent use in previous metaldrug binding studies by mass spectrometry, thus enabling comparison.^[7] We used identical Bruker Apollo ion sources and standard ESI sprayers on both instruments. The ESI parameters were set as similar as possible for the ESI-IT and ESI-ToF mass spectrometry measurements, and identical samples and solvent compositions were employed for both instruments. The capillary voltage did not affect the type of the detected metal–protein adducts. Therefore, capillary voltages were set individually on each instrument for optimal signal intensity. The ion life time on the IT and ToF are also comparable. On the ToF instrument, it is mainly determined by the transfer time and the pre-pulse storage time (ca. 130 μ s), while on the IT, the ion life time is mainly determined by the accumulation and the sweep time in the ion trap (ca. 160 μ s). Finally, the ToF instrument features a higher mass accuracy and resolving power than the IT.

Analysis of equimolar incubation mixtures of **1** with ub using ESI-IT and ESI-ToF MS yielded very similar results. The Ru complex forms essentially mono-adducts, which correspond to $[\text{ub} + (\text{bip})\text{Ru} - \text{H}]^+$, where bip represents η^6 -biphenyl (Table 1 and Figure 2A; see also Table S1 in the Supporting Information). The IT and the ToF measurement yielded 77% and 73% relative adduct intensity, respectively, and most of the ub was consumed within 48 hours. Relative intensities refer to percentage of signal area with respect to all assignable mass signals in

Table 1. Experimental (m/z) and theoretical (m_{ex}) deconvoluted masses of the metaldrug–protein adducts measured on ion trap (IT) and time-of-flight (ToF) mass spectrometers.

Adduct	m/z (IT)	m/z (ToF)	m_{ex}
$[\text{ub} + (\text{bip})\text{Ru} - \text{H}]^+$	8818.1	8818.60	8818.61
$[\text{ub} + 2(\text{bip})\text{Ru} - 3\text{H}]^+$	n.d.	9071.58	9071.57
$[\text{ub} + (\text{bip})\text{Ru}(\text{en}) - \text{H}]^+$	8877.5	8878.68	8878.67
$[\text{ub} + 2(\text{bip})\text{Ru}(\text{en}) - 3\text{H}]^+$	n.d.	9191.72	9191.70
$[\text{cyt} + (\text{bip})\text{Ru} - \text{H}]^+$	12612.8	12613.35	12613.32
$[\text{cyt} + (\text{bip})\text{Ru}(\text{en}) - \text{H}]^+$	n.d.	12672.41	12672.38
$[\text{cyt} + 2(\text{bip})\text{Ru}(\text{en}) - 3\text{H}]^+$	n.d.	12986.44	12986.42

Abbreviations: η^6 -biphenyl (bip), cytochrome C (cyt), ethylenediamine (en), not detected (n.d.), ubiquitin (ub).

the deconvoluted spectrum. Ubiquitin contains Met1 and His68 as the two major nucleophilic amino acids suitable for metal binding. A bidentate binding mode of Met1 involving the thioether and the N-terminal amine was suggested to be responsible for forming an exceptionally stable and kinetically favored adduct with respect to His68.^[8] The binding of **1** to Met1 or His68 of ub is accompanied by cleavage of the monodentate ammine ligands, and hence, a bidentate binding mode might occur at both binding sites. In the case of His68, this may be achieved by interaction with a donor atom of a neighboring amino acid. The mass signal of the $[\text{ub} + (\text{bip})\text{Ru} - \text{H}]^+$ adduct is composed of two types of adducts: a major population of the (bip)Ru moiety bound to Met1 and a minor population of the (bip)Ru moiety bound to His68. These mono-adducts are equally well detected on both instru-

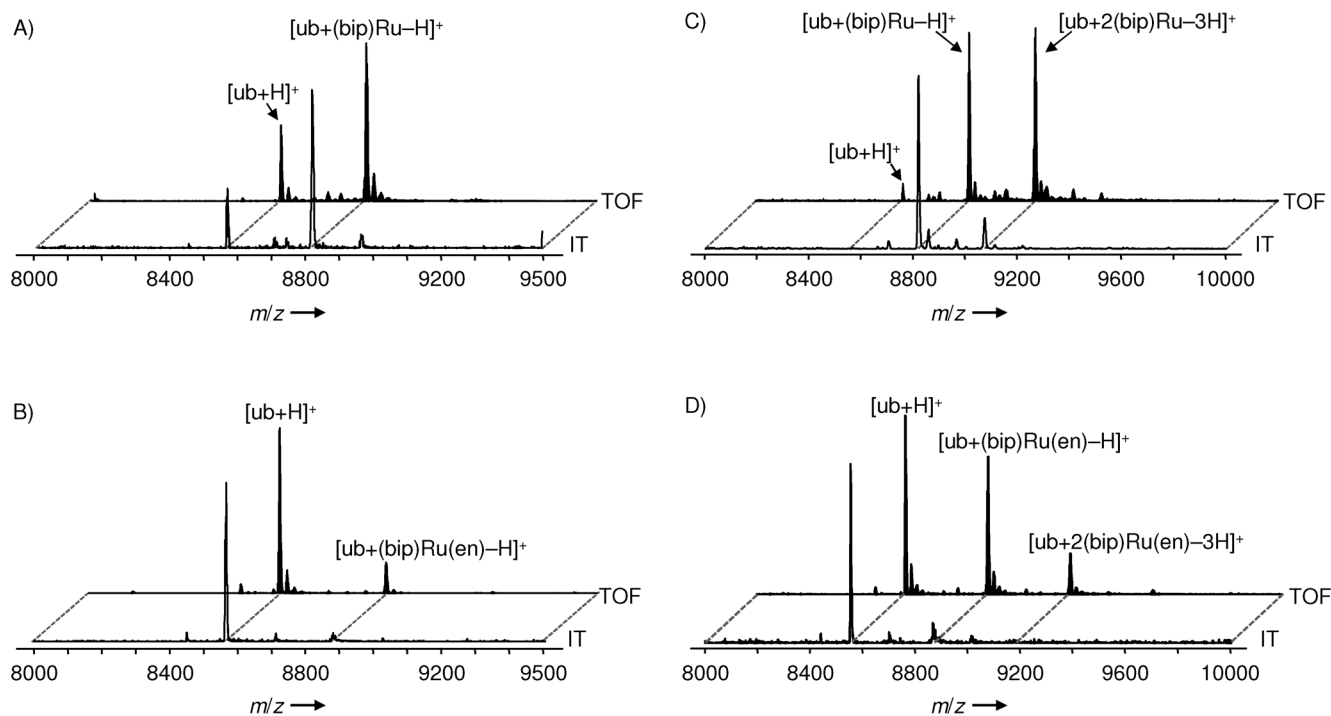


Figure 2. The deconvoluted mass spectra show the efficiency of adduct detection for the reaction of **1** and **2** with ubiquitin (ub) at different molar ratios after 48 h: A) **1** + ub (1:1), B) **2** + ub (1:1), C) **1** + ub (2:1) and D) **2** + ub (2:1). Identical samples were analyzed by ion trap (IT) and time-of-flight (ToF) electrospray (ESI) mass spectrometry.

ments. The interaction product between **2** and ub, that is $[\text{ub} + (\text{bip})\text{Ru}(\text{en}) - \text{H}]^+$, was detected in ESI-ToF mass spectra (18%) and only to a very minor extent by ESI-IT MS (Figure 2B). The bidentate ethylenediamine (en) ligand is retained at the metal center, which leads exclusively to a monofunctional binding mode to the protein. This leads to lower kinetics of adduct formation between **2** and ub, as compared with **1**. Notably, the detection efficiency of this interaction product varies significantly between the mass analyzers and is lower on the IT instrument.

A 2:1 metal-to-protein ratio results in pronounced differences of adduct detection efficiencies on the two mass analyzers. The IT mass spectrum of the reaction between **1** and ub yielded primarily mono-adducts, while the mass signal of unreacted ub vanished completely (Figure 2C). Bis-adducts corresponding to $[\text{ub} + 2(\text{bip})\text{Ru} - 3\text{H}]^+$ (16%) were observed in small amounts. ToF measurements yielded nearly equal amounts of the mono- (45%) and bis- (52%) adducts, and this exemplifies an increased efficiency for detecting the bis-adduct compared with the IT. Again, the primary binding site on ub (Met1) seems to be responsible for forming a stable adduct with **1**, which is detectable to similar degrees on both mass spectrometers probably due to the bidentate nature of the binding site. The efficiency of detecting the adduct with His68, however, seems substantially hampered using IT and the bis-adduct is much less abundant. The analogous reaction between **2** and ub illustrates the differences between the analyzers further. In the recorded IT mass spectrum, the mono-adduct $[\text{ub} + (\text{bip})\text{Ru}(\text{en}) - \text{H}]^+$ is only indicated by a broad signal (22%) in the deconvoluted spectrum (Figure 2D), whereas ToF MS allowed the detection of significant amounts of mono- and even bis-adducts of $[\text{ub} + n(\text{bip})\text{Ru}(\text{en}) - m\text{H}]^+$, where $n=1$ (42%, $m=1$), 2 (15%, $m=3$) (Figure 3).

The equimolar reaction between cyt and **1** yielded only minor amounts of mono-adducts corresponding to $[\text{cyt} + (\text{bip})\text{Ru} - \text{H}]^+$. Cytochrome C adducts from the reaction with **1** were detected with similar efficiency with both mass analyzers, that is, 19% and 11% on the ToF and IT instrument, re-

spectively (Figure S1 in the Supporting Information). Incubations with cyt were in general characterized by a lower rate of adduct formation. In contrast to ub, cyt features three potential monodentate binding partners (His26, His33 and Met65), and it is acetylated at the N terminus. The equimolar reaction of **2** with cyt showed mainly unreacted cyt on both instruments. The deconvoluted mass spectra of the IT and ToF MS display, in both cases, an additional mass signal, which was attributed to an adduct between cyt and $\text{Ru}^{\text{III}}(\text{HCOO}^-)$ and could stem from a redox reaction at the metal center, which induces arene cleavage.^[6] This adduct was also detected in the mass spectra when using slight excess of the metallodrug.

The incubation of **1** with cyt at a molar ratio of 2:1 yielded, with both instrument types, primarily mono-adducts corresponding to $[\text{cyt} + (\text{bip})\text{Ru} - \text{H}]^+$ and $[\text{cyt} + \text{Ru}^{\text{III}}(\text{HCOO}^-) - \text{H}]^+$ with similar abundances. The incubation between **2** and cyt under similar conditions yielded mono- and bis-adducts corresponding to $[\text{cyt} + (\text{bip})\text{Ru}(\text{en}) - \text{H}]^+$ (31%) and $[\text{cyt} + 2(\text{bip})\text{Ru}(\text{en}) - 3\text{H}]^+$ (7%), respectively, as identified with the ToF MS (Figure S2 in the Supporting Information). Strikingly, IT measurements of the same reaction mixture showed only unreacted cyt.

Overall, cyt features monodentate binding partners and adducts are difficult to detect with IT even if the metal offers two coordination sites.

Compounds **1** and **2** were additionally reacted with a mixture of ub and cyt at a 1:1:1 molar ratio (Figure S3 in the Supporting Information). By using an excess of the proteins, this approach should reveal one of the proteins as the preferred binding partner for the Ru complexes. The resulting mass spectra showed that **1** and **2** tend to bind to ub over cyt. This might be due to the formation of a stable and potentially bidentate adduct involving Met1. Comparison of the adduct intensities on both instruments of the reaction between **1** and ub/cyt reveals a higher efficiency of adduct detection with the ToF instrument, in particular for $[\text{ub} + (\text{bip})\text{Ru} - \text{H}]^+$ (85%) but also for $[\text{cyt} + (\text{bip})\text{Ru} - \text{H}]^+$ (16%) compared with 39% of the ub mono-adduct on the IT instrument, where cyt adducts were

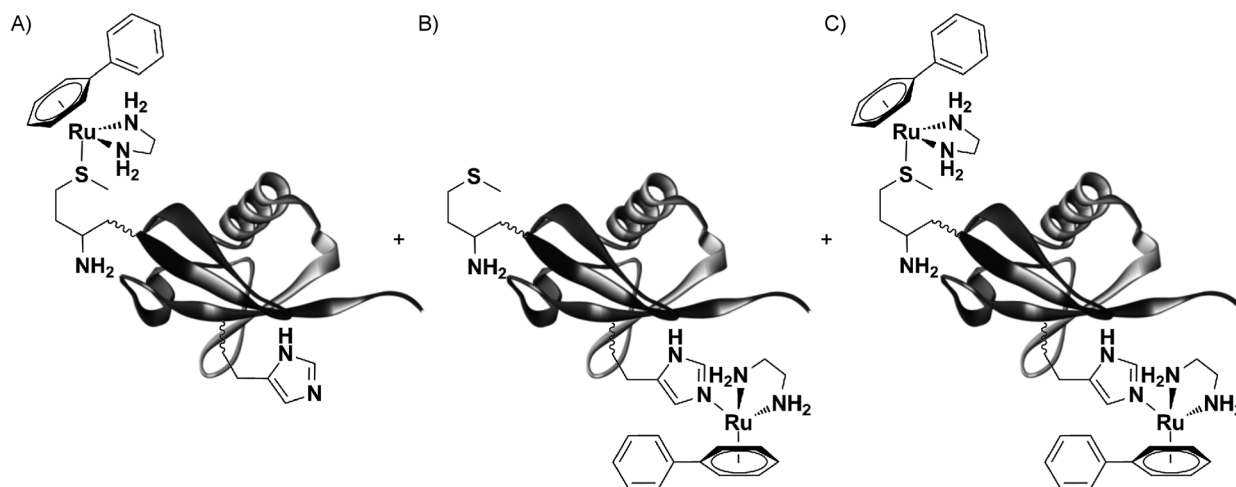


Figure 3. The reaction between **2** and ubiquitin (ub) (PDB: 1UBQ) can yield a mixture of adducts corresponding to two mono-adducts A) $[\text{ub}(\kappa\text{-S-Met1}) + (\text{bip})\text{Ru}(\text{en}) - \text{H}]^+$, B) $[\text{ub}(\kappa\text{-N-His68}) + (\text{bip})\text{Ru}(\text{en}) - \text{H}]^+$ and a bis-adduct C) $[\text{ub} + 2(\text{bip})\text{Ru}(\text{en}) - 3\text{H}]^+$, where bip = η^6 -biphenyl and en = ethylenediamine.

not observed. When using the same protein mixture for **2**, again lower levels of adducts were detected. Mono-adducts corresponding to $[\text{ub} + (\text{bip})\text{Ru}(\text{en})-\text{H}]^+$ (8%) were observed only in low abundance with the ToF analyzer, and the cyt mono-adduct was not detected. In the IT mass spectrum, only free proteins were observed.

The incubation of **1** and **2** with the ub/cyt mixture at a 2:1:1 molar ratio featured again selectivity for ub and only mono-adducts were observed (Figure S4 in the Supporting Information). The mass spectrum of the reaction containing **1** was thereby largely identical on both instruments, which is in accordance with the above findings. The ToF mass spectrum of the protein mixture incubated with **2** also showed a slight preference for $[\text{ub} + (\text{bip})\text{Ru}(\text{en})-\text{H}]^+$ (22%) compared with $[\text{cyt} + (\text{bip})\text{Ru}(\text{en})-\text{H}]$ (13%), while only free ub and cyt were detected in the deconvoluted IT mass spectrum.

The tridentate bis(ethylene)triamine ligand is known to be strongly bound to the Ru center, and a ligand exchange reaction is unfavorable. As expected, incubation of **3** with the protein mixture yielded only mass signals assignable to the unreacted proteins. This supports the conclusion that nonspecific adducts through electrostatic attraction do not form during the spraying process, and the detected adduct signals stem from coordinated metal fragments to the biomolecules.

In conclusion, the investigation and identification of possible cellular targets of anticancer metallodrugs is crucial in drug development and a challenging task.^[7] Mass spectrometry is increasingly being used in this area of research and has already contributed significantly to the understanding of the targets of metallodrugs on the molecular level. However, as the results herein show, the efficiencies of adduct detection seem to be dependent on the mass analyzer and the denticity of the metal–protein interaction, while the types of adducts are not. For this purpose, the performance of an IT and ToF instrument with similar ion focusing and ion guide technologies were compared. The principal difference between the instruments is the mass analyzer and, therefore, the crucial part with regard to adduct detection efficiency. The striking differences in adduct detection efficiencies are believed to be related to the ion cooling processes occurring in the IT during which the stationary helium buffer gas cools the kinetically excited ions and forces them via multiple collisions into the center of the IT. These collisions might just provide enough energy randomization to cleave a fraction of the metal–protein adducts, in particular the monodentate Ru–S/N bonds, while this seems less probable for the S,N-bidentate binding mode.

In comparison, the ions are orthogonally accelerated into the high-vacuum reflectron ToF mass analyzer after being focused by ion cooling. Ion beam trapping is not necessary, hence potential collisions with gas molecules are less energetic and frequent, which results in a better efficiency of adduct detection. This is underlined by the fact that the transfer time in the ToF (cooling) accounts for 100 μs , while ion trapping in the IT did not exceed 10 μs on average.

For the complexes studied herein, it seems that stable adducts form when the metallodrug and the protein engage a bidentate binding mode such as **1** binding to Met 1 of ub. In this

case, ESI-IT and ESI-ToF MS are equally powerful methods for detecting the resulting adducts. If, however, one of the binding partners offers solely monofunctional binding such as **2**, cyt or the second binding site on ub (His68), then the ToF shows a drastically improved efficiency of adduct detection compared to the IT instrument and useful information regarding adduct formation can be obtained. This information also has, however, impact on the biological activity. Mono- and bidentate adducts could be metabolized in a different way, and important biological defense mechanisms might be more effective against monofunctional biomolecule binders than against bifunctional adducts.

Experimental Section

Compounds **1–3** were synthesized according to published procedures.^[6] Stock solutions of **1–3** (400 μM , 1% dimethylsulfoxide) and of ubiquitin (bovine erythrocytes, Sigma) and cytochrome C (horse heart, Sigma) each 200 μM were prepared in ultrapure water (Advantage A10, 18.2 M Ω , ultrapure water system, Millipore, France). The stock solutions were mixed at 1:1 and 2:1 molar ratios and kept stirring in the dark at 37 °C. Mass spectra (MS) of the incubation solutions were recorded after 0, 3, 6, 24 and 48 h. Furthermore, the compounds were incubated under comparable conditions with an ubiquitin–cytochrome C mixture (1:1).

The samples were analyzed using a MaXis ultra-high resolution (UHR) electrospray ionization (ESI) time-of-flight (ToF) mass spectrometer (Bruker Daltonics, Bremen, Germany) employing the following parameters: capillary –4.5 kV, gas flow 8 psi, dry gas 6 L min⁻¹, dry temperature 150 °C, 400 Vpp funnel RF, 4 eV quadrupole ion energy, 50 Vpp ion cooler RF, 90–110 μs transfer time and 10 μs pre-pulse storage. The samples were diluted before injection to 2–5 μM using water/methanol/formic acid (50:50:0.2) and injected by direct infusion into the mass spectrometer at a flow rate of 180 $\mu\text{L min}^{-1}$.

Additionally, samples from the same incubation mixtures were analyzed on an Amazon SL ESI-ion trap (IT) mass spectrometer (Bruker Daltonics, Bremen, Germany). Typical parameters were as follows: capillary –3.5 kV, end plate offset –500 V, capillary exit 140, gas flow 8 psi, dry gas 6 L min⁻¹, dry temperature 150–180 °C, trap drive 78, 10 μs trap accumulation time and 148 μs sweep. Protein samples were diluted to 5 μM using water/methanol/formic acid (50:50:0.2) and quickly introduced by direct infusion into the mass spectrometer at a flow rate of 180–240 $\mu\text{L min}^{-1}$.

All spectra were recorded in positive ion mode over 0.5 min and averaged. The Data Analysis 4.0 software package from Bruker Daltonics (Bremen, Germany) was used for processing. Maximum entropy deconvolution was applied with automatic data point spacing, 0.5 peak width for IT and 30 000 instrument resolving power for ToF. Identical ion sources (Apollo ESI source with standard ESI spray chamber, Bruker Daltonics) and standard ESI sprayers (S/N 602147-00672 for the IT and S/N 602147-00809 for the ToF, Bruker Daltonics) were used on both instruments.

Acknowledgements

S.M.M. would like to thank the Mass Spectrometry Center, University of Vienna (Austria), for providing access to the UHR ESI-ToF mass spectrometer. This work was supported by the Platform

Austria for Chemical Biology (PLACEBO) project of the Austrian Genome Research Programme, Gen-AU (BMWF-70.081/0018-II/1a/2008), the European Cooperation in Science and Technology (COST) action CM1105 "Functional Metal Complexes that Bind to Biomolecules", and the Royal Society of New Zealand.

Keywords: detection efficiency · ion trap · mass spectrometry · metallodrugs · ruthenium · time-of-flight

- [1] a) C. G. Hartinger, M. A. Jakupec, S. Zorbas-Seifried, M. Groessl, A. Egger, W. Berger, H. Zorbas, P. J. Dyson, B. K. Keppler, *Chem. Biodiversity* **2008**, *5*, 2140–2155; b) M. Groessl, Y. O. Tsybin, C. G. Hartinger, B. K. Keppler, P. J. Dyson, *J. Biol. Inorg. Chem.* **2010**, *15*, 677–688; c) P. Nowak-Sliwinska, J. R. van Beijnum, A. Casini, A. A. Nazarov, G. Wagnieres, H. van den Bergh, P. J. Dyson, A. W. Griffioen, *J. Med. Chem.* **2011**, *54*, 3895–3902; d) B. Wu, M. S. Ong, M. Groessl, Z. Adhireksan, C. G. Hartinger, P. J. Dyson, C. A. Davey, *Chem. Eur. J.* **2011**, *17*, 3562–3566.
- [2] J. Lokich, N. Anderson, *Ann. Oncol.* **1998**, *9*, 13–21.
- [3] a) D. Gibson, C. E. Costello, *Eur. Mass Spectrom.* **1999**, *5*, 501–510; b) T. Peleg-Shulman, D. Gibson, *J. Am. Chem. Soc.* **2001**, *123*, 3171–3172; c) F. Y. Wang, J. Bella, J. A. Parkinson, P. J. Sadler, *J. Biol. Inorg. Chem.* **2005**, *10*, 147–155; d) C. G. Hartinger, A. Casini, C. Duhot, Y. O. Tsybin, L. Messori, P. J. Dyson, *J. Inorg. Biochem.* **2008**, *102*, 2136–2141; e) A. Casini, G. Mastrobuoni, M. Terenghi, C. Gabbiani, E. Monzani, G. Moneti, L. Casini, L. Messori, *J. Biol. Inorg. Chem.* **2007**, *12*, 1107–1117; f) A. Casini, G. Mastrobuoni, W. H. Ang, C. Gabbiani, G. Pieraccini, G. Moneti, P. J. Dyson, L. Messori, *ChemMedChem* **2007**, *2*, 631–635; g) A. Casini, C. Gabbiani, E. Michelucci, G. Pieraccini, G. Moneti, P. J. Dyson, L. Messori, *J. Biol. Inorg. Chem.* **2009**, *14*, 761–770; h) S. M. Meier, M. Hanif, W. Kandioller, B. K. Keppler, C. G. Hartinger, *J. Inorg. Biochem.* **2012**, *108*, 91–95.
- [4] a) C. S. Allardyce, P. J. Dyson, J. Coffey, N. Johnson, *Rapid Commun. Mass Spectrom.* **2002**, *16*, 933–935; b) C. G. Hartinger, W. H. Ang, A. Casini, L. Messori, B. K. Keppler, P. J. Dyson, *J. Anal. At. Spectrom.* **2007**, *22*, 960–967; c) H. Li, T. Y. Lin, S. L. Van Orden, Y. Zhao, M. P. Barrow, A. M. Pizarro, Y. Qi, P. J. Sadler, P. B. O'Connor, *Anal. Chem.* **2011**, *83*, 9507–9515; d) S. M. Meier, Y. O. Tsybin, P. J. Dyson, B. K. Keppler, C. G. Hartinger, *Anal. Bioanal. Chem.* **2012**, *402*, 2655–2662; e) N. Zhang, Y. Du, M. Cui, J. Xing, Z. Liu, S. Liu, *Anal. Chem.* **2012**, *84*, 6206–6212.
- [5] J. P. Williams, H. I. Phillips, I. Campuzano, P. J. Sadler, *J. Am. Soc. Mass Spectrom.* **2010**, *21*, 1097–1106.
- [6] M. V. Babak, S. M. Meier, A. A. Legin, M. S. A. Razavi, A. Roller, M. A. Jakupec, B. K. Keppler, C. G. Hartinger, *Chem. Eur. J.* **2013**, *19*, 4308–4318.
- [7] C. G. Hartinger, M. Groessl, S. M. Meier, A. Casini, P. J. Dyson, *Chem. Soc. Rev.* **2013**, *42*, 6186–6199.
- [8] W. Kandioller, E. Balsano, S. M. Meier, U. Jungwirth, S. Goschl, A. Roller, M. A. Jakupec, W. Berger, B. K. Keppler, C. G. Hartinger, *Chem. Commun.* **2013**, *49*, 3348–3350.

Received: January 7, 2014

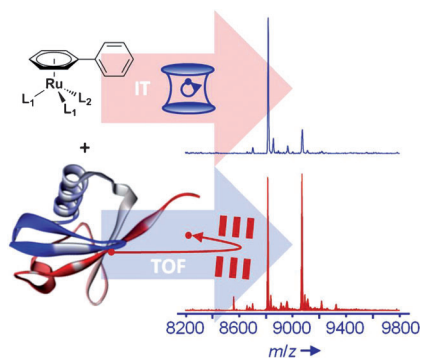
Published online on ■ ■ ■ ■, 0000

COMMUNICATIONS

S. M. Meier, M. V. Babak, B. K. Keppler,
C. G. Hartinger*



Efficiently Detecting Metallodrug– Protein Adducts: Ion Trap versus Time-of-Flight Mass Analyzers



Weighing the alternatives: Mass spectrometry is increasingly employed for metallodrug–protein binding studies. However, a methodical investigation on mass analyzers and especially their influence on the efficiency of adduct detection has not been carried out so far. We show that mass analyzers can exhibit pronounced differences on adduct detection efficiencies, influencing investigations on potential cellular targets and for the screening of metallodrugs.

Supporting Information

© Copyright Wiley-VCH Verlag GmbH & Co. KGaA, 69451 Weinheim, 2014

Efficiently Detecting Metallodrug–Protein Adducts: Ion Trap versus Time-of-Flight Mass Analyzers

Samuel M. Meier,^[a, b] Maria V. Babak,^[a, b, c] Bernhard K. Keppler,^[a, b] and Christian G. Hartinger^{*[c]}

cmdc_201400020_sm_miscellaneous_information.pdf

Content

Table S1. The nature and the intensities of the detected adducts formed between the proteins and the metal complexes. The left block displays the results from ion trap experiments and the right block results from time-of-flight experiments of the same samples. Relative intensities refer to percentages of signal area with respect to all assignable mass signals in the deconvoluted spectra.

Figure S1. ESI-IT and ESI-TOF mass spectra of identical samples of **1** (A) or **2** (B) incubated with cytochrome C at a metal-to-protein ratio of 1:1 for 48 hours.

Figure S2. ESI-IT and ESI-TOF mass spectra of identical samples of **1** (A) or **2** (B) incubated with cytochrome C at a metal-to-protein ratio of 2:1 for 48 hours.

Figure S3. ESI-IT and ESI-TOF mass spectra of identical samples of **1** (A) or **2** (B) incubated with a mixture of ubiquitin and cytochrome C at a metal-to-protein ratio of 1:1:1 for 48 hours.

Figure S4. ESI-IT and ESI-TOF mass spectra of identical samples of **1** (A) or **2** (B) incubated with a mixture of ubiquitin and cytochrome C at a metal-to-protein ratio of 2:1:1 for 48 hours.

Table S1. The nature and the intensities of the detected adducts formed between the proteins and the metal complexes. The left block displays the results from ion trap experiments and the right block results from time-of-flight experiments of the same samples. Relative intensities refer to percentages of signal area with respect to all assignable mass signals in the deconvoluted spectra.

		Ion Trap		Time-of-Flight			
compound	protein	adduct	rel. Int. (%)	adduct	rel. Int. (%)		
equimolar ratio	1	ub	[ub + (bip)Ru ²⁺ – H] ⁺	77	[ub + (bip)Ru ²⁺ – H] ⁺	73	
		cyt	[cyt + (bip)Ru ²⁺ – H] ⁺	11	[cyt + (bip)Ru ²⁺ – H] ⁺	19	
		ub/cyt	[ub + (bip)Ru ²⁺ – H] ⁺	39	[ub + (bip)Ru ²⁺ – H] ⁺	85	
	2	ub	[ub + (bip)Ru(en) ²⁺ – H] ⁺	8	[ub + (bip)Ru(en) ²⁺ – H] ⁺	18	
		cyt	n.d.	-	n.d.	-	
		ub/cyt	n.d.	-	[ub + (bip)Ru(en) ²⁺ – H] ⁺	8	
	3	ub/cyt	n.d.	-	n.d.	-	
	2 : 1 metal-to-protein ratio	1	ub	[ub + (bip)Ru ²⁺ – H] ⁺	84	[ub + (bip)Ru ²⁺ – H] ⁺	45
				[ub + 2(bip)Ru ²⁺ – 3H] ⁺	16	[ub + 2(bip)Ru ²⁺ – 3H] ⁺	52
cyt			[cyt + (bip)Ru ²⁺ – H] ⁺	18	[cyt + (bip)Ru ²⁺ – H] ⁺	26	
			[cyt + (bip)Ru(HCOO) ⁻] ²⁺ – H] ⁺	16	[cyt + (bip)Ru(HCOO) ⁻] ²⁺ – H] ⁺	18	
			ub/cyt	[ub + (bip)Ru ²⁺ – H] ⁺	85	[ub + (bip)Ru ²⁺ – H] ⁺	84
2		ub	[ub + (bip)Ru(en) ²⁺ – H] ⁺	22	[ub + (bip)Ru(en) ²⁺ – H] ⁺	42	
			[ub + 2(bip)Ru(en) ²⁺ – 3H] ⁺	-	[ub + 2(bip)Ru(en) ²⁺ – 3H] ⁺	15	
		cyt	n.d.	-	[cyt + (bip)Ru ²⁺ – H] ⁺	31	
			n.d.	-	[cyt + 2(bip)Ru ²⁺ – 3H] ⁺	7	
			ub/cyt	n.d.	-	[ub + (bip)Ru(en) ²⁺ – H] ⁺	22
3		ub/cyt	n.d.	-	[cyt + (bip)Ru ²⁺ – H] ⁺	13	
					n.d.	-	

n.d. not detected

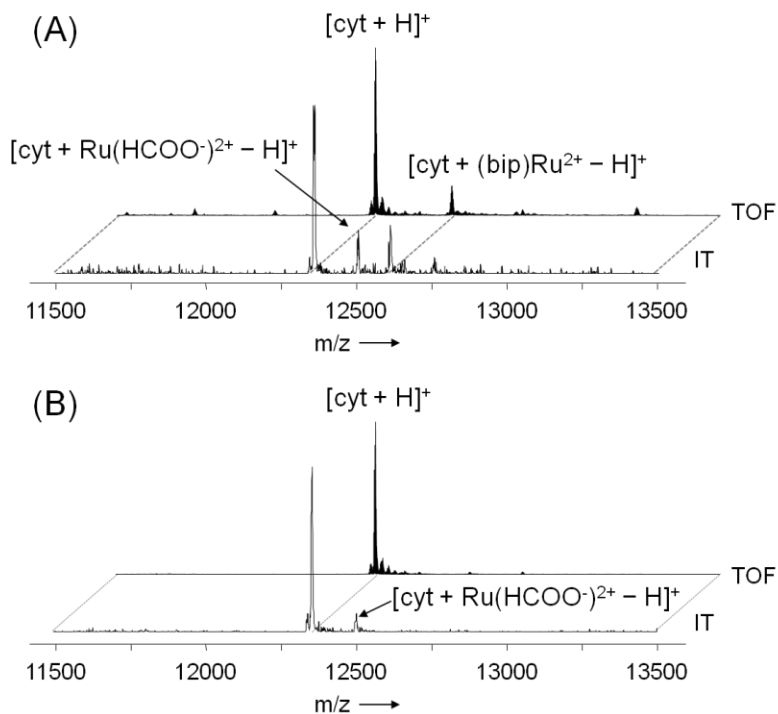


Figure S1. ESI-IT and ESI-TOF mass spectra of identical samples of **1** (A) or **2** (B) incubated with cytochrome C at a metal-to-protein ratio of 1:1 for 48 hours.

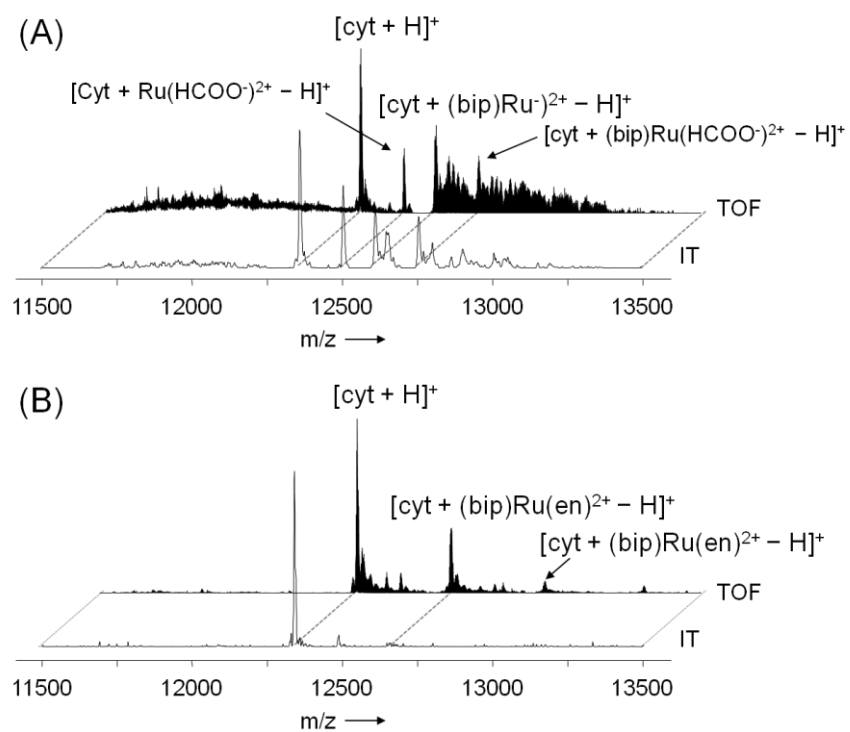


Figure S2. ESI-IT and ESI-TOF mass spectra of identical samples of **1** (A) or **2** (B) incubated with cytochrome C at a metal-to-protein ratio of 2:1 for 48 hours.

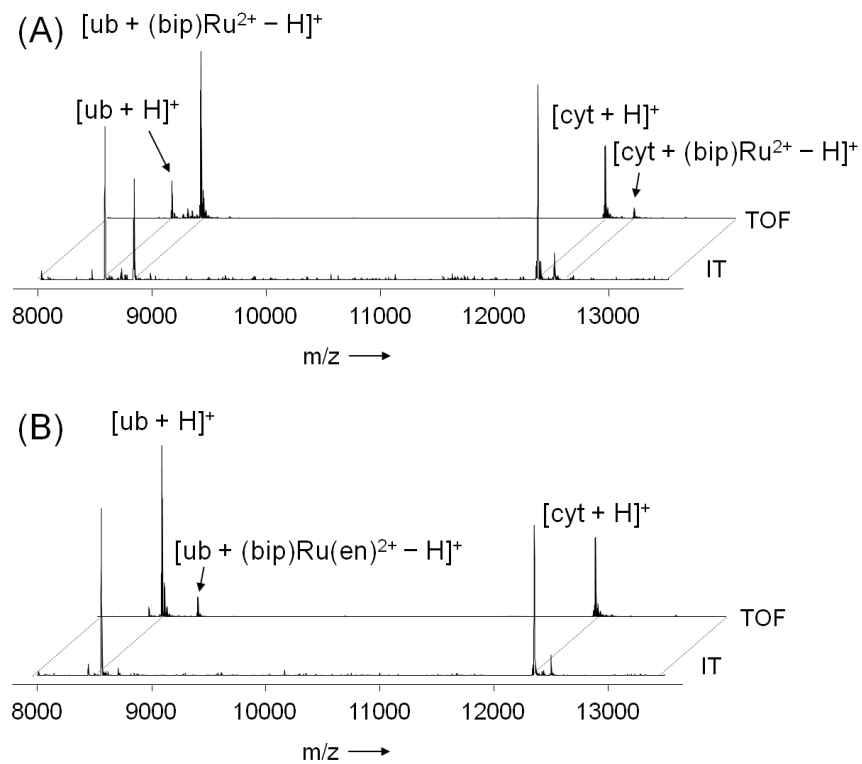


Figure S3. ESI-IT and ESI-TOF mass spectra of identical samples of **1** (A) or **2** (B) incubated with a mixture of ubiquitin and cytochrome C at a metal-to-protein ratio of 1:1:1 for 48 hours.

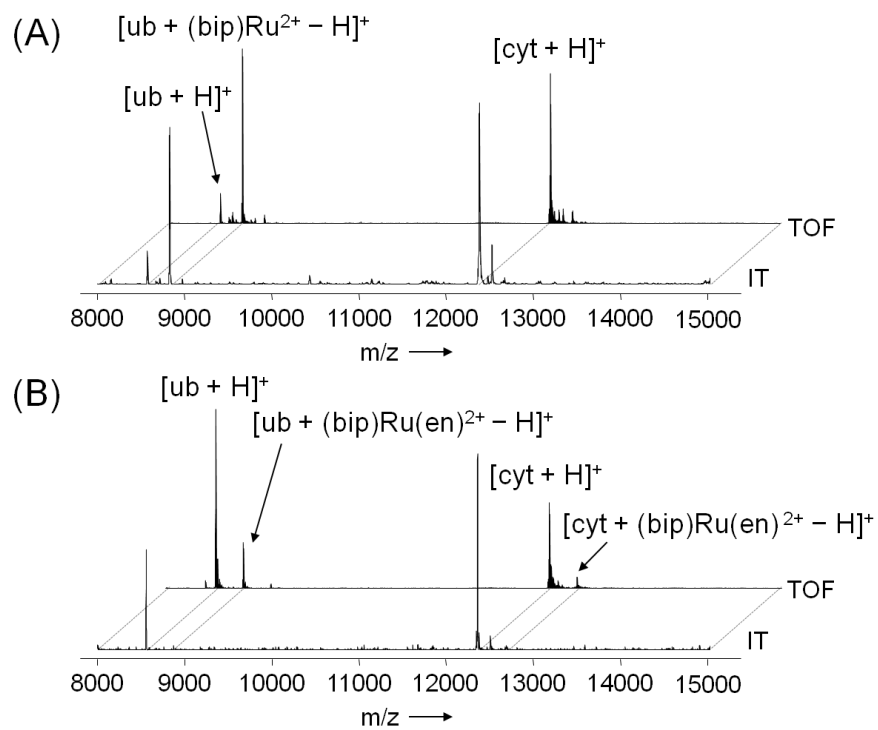


Figure S4. ESI-IT and ESI-TOF mass spectra of identical samples of **1** (A) or **2** (B) incubated with a mixture of ubiquitin and cytochrome C at a metal-to-protein ratio of 2:1:1 for 48 hours.

III. Conclusions and prospects

One of the major flaws of conventional cancer therapeutics is low selectivity towards cancer cells over normal cells, which results in severe toxicity. The successful design of personalized medicines is markedly dependent on the identification of molecular targets of drugs. Paradoxically, the targets of commonly used drugs as well as promising metal-based compounds in clinical trials still remain unknown. There are analytical tools, e.g., mass spectrometry, capillary electrophoresis, NMR spectroscopy and X-ray diffraction, which allow for identification and analysis of adducts between metal-based drugs and biomolecules. However, the routine screening of such interactions is time-consuming and does not provide information about the whole target profile of the drugs. The choice of biomolecules to be tested is usually based on several well-known hypotheses. Thus, in the field of metal-based anticancer drugs there are several biomolecules of interest, which are commonly investigated, such as transferrin, albumin, cytochrome C, ubiquitin, glutathione. Taking into account thousands of estimated druggable targets, common methods for the identification of targets of metal-based drugs provide only a small bit of information. Hitting uncommon targets can even enable a drug to be applied in several unrelated diseases. Traditional chemical proteomic methods are known for decades. However, they do not allow for the determination of the “natural” target profile of the drug (natural binding partners, expression levels, competitive cellular environment). Within the frame of this PhD thesis a novel metal-based drug pull-down method was developed based on a combination of drug affinity purification with subsequent high-end mass spectrometry and bioinformatics. This method opens the door to previously uncharacterized biomolecular targets of metal-based drugs. The method was tested on RAPTA complexes and more than 300 proteins were identified. A more complete picture of the interactions of RAPTA compounds helped to improve understanding of their mode of action.

In addition, a series of RAPTA complexes with appended biotin ligands was reported and their potential as guided molecular missiles was investigated. The hypothesis for development of such complexes was based on the high requirements of cancer cells for vitamins. It is known that the main biotin uptake system in humans is the sodium-dependent multivitamin transporter (hSMVT) system. Therefore, the ability of novel RAPTA complexes to inhibit cancer cell growth was tested in cancer cells with different levels of SMVT expression. It was shown that complexation of non-toxic biotin ligands to

the organometallic Ru^{II} scaffold resulted in the formation of highly antiproliferative anticancer agents. The activity of the complexes was markedly higher in cell lines with a high level of SMVT transporter. As a result, novel complexes may act as highly efficacious biological vectors to cancer cells. In order to estimate the likelihood of binding of ruthenium complexes to the SMVT transporter, docking studies with avidin and streptavidin were conducted. The results of the docking studies were in agreement with *in vitro* anticancer activity data.

Further research effort was directed into the establishment of structure-activity relationships for non-specifically targeting ruthenium compounds, namely Ru^{II}(arene) complexes with am(m)ine ligands. In a systematic study by varying the am(m)ine and arene ligands of Ru half-sandwich compounds, several important parameters for structure-activity relationships were derived. The cytotoxicity of the complexes was strongly dependent on the denticity of the ligand, and IC₅₀ values varying by several orders of magnitude were observed. The activity of the complexes appeared to be related to their aqueous stability and protein binding. Compounds which were more reactive towards model proteins were less active in cancer cell lines. This is in agreement with the previously proposed inverse correlation between extent of protein binding of a metallodrug and its cytotoxic activity.

In the course of investigations of interactions of Ru^{II}(am(m)ine) complexes with proteins by means of mass spectrometry, we discovered that the efficiency of detecting adducts was dependent on the mass analyzer of the mass spectrometer and the denticity of the metal-protein interaction. To the best of our knowledge, the impact of the mass analyzer on the adduct formation of metallodrugs towards proteins had not been explored. An ESI-MS-ToF instrument was profoundly more efficient in adduct detection than the IT instrument when one of the binding partners offered a solely monofunctional binding. However, when the metallodrug and protein engaged in a bidentate binding mode, both instruments were equally powerful.

In future, further research efforts will be concentrated on the extension of the drug pull-down method to other metal-based drugs, such as NAMI-A, KP1019 or more specifically targeting compounds. The comparison of the obtained data sets will provide additional information about the mechanism of action of these drugs and/or common targets between them. We believe that our novel method can be used not only for RAPTA complexes, but a large number of different metal-based anticancer agents.

IV. Curriculum Vitae

University of Vienna
Institute of Inorganic Chemistry
Währingerstrasse 42
1090 Vienna, Austria
+43 (680) 2321430
maria.babak@univie.ac.at



Personal information:

- Nationality: Russian
- Age: 25
- Date of birth: 23.09.1988
- Place of birth: Taganrog, Russia

Language skills:

Russian (native), English (fluent), German (fluent), French (intermediate), Hungarian (beginner)

Educational background:

- **University of Vienna**, Vienna, Austria
Institute of Inorganic Chemistry
Ph.D in Bioinorganic Chemistry
Dissertation Advisors: O. Univ. Prof. Dr. Dr. Bernhard K. Keppler
A/Prof. Dr. Christian G. Hartinger
Dissertation Title: *Functionalization of metal-based anticancer drugs in the quest for new chemotherapeutics and studies on their mode of action*
- **The Higher Chemical College of Russian Academy of Sciences (HCC RAS)**
Moscow, Russian Federation
Master of Science, Chemistry
Diploma with Honors, June 2010
Diploma Work advisor: Dr. Dmitry S. Perekalin
Diploma Work Title: *Photochemically Controlled Crown-ethers: Transition Metal Pi-complexes of Dibenzo-18-crown-6*
Average grade: **5,0** (max – 5, min – 1)
- **School of Arts with the Profound Knowledge of English Language**
Taganrog, Russian Federation
Diploma with Honors, June 2005
Average grade: **5,0** (max – 5, min – 1)

Research Experience:

- **University of Vienna**, Vienna, Austria **2010-present**
Institute of Inorganic Chemistry, Supervisor: Dr. Bernhard K. Keppler
Synthesis and analysis of organometallic and coordination ruthenium complexes with potential anticancer activity.
- **The University of Auckland**, Auckland, New Zealand **2013**
Institute of Inorganic Chemistry, Supervisor: Dr. Christian G. Hartinger
Synthesis and analysis of ruthenium and platinum complexes with potential anticancer activity.
- **University of Science and Technology of Lille** **2007-2009**
Lille, France
Laboratory of Organic Chemistry and Macromolecules, Supervisor: Dr. Christian Rolando
Synthesis of ruthenium complexes with the special properties for in gel protein staining.
- **A.N. Nesmeyanov Institute of Organoelement Compounds of Russian Academy of Sciences (INEOS RAS)** **2005-2010**
Moscow, Russian Federation
Laboratory of Transition Metal Pi-Complexes, Supervisor: Dr. Dmitry S. Perekalin
Investigation of new arene-exchange reactions in organometallic ruthenium and iron complexes, synthesis and analysis of various new metal-based complexes.

Scientific Interests:

- Medicinal chemistry
- Bioinorganic and bioorganometallic chemistry
- Drug development
- Metal-based anticancer drugs: development, mode of action studies
- Transition metals complexes

Teaching Experience:

- **University of Vienna**, Vienna, Austria **2011-present**
 - **The University of Auckland**, Auckland, New Zealand **2013**
- Teaching first-year graduate students in inorganic chemistry laboratory course, conduction of discussion and examination sessions, grading exams. Supervision of graduate students in research projects.

Additional Teaching Activities:

- *Member of "Kind Lessons" program* **2009-2010**
Tutoring of chemistry students with disabilities.
- *Private Tutor* **2003-present**
Teaching organic, inorganic and biochemistry in university-level and college chemistry, college-level English, English for 6-8 year old children.

Fellowships and Awards:

- First prize of Falling Walls Lab 2012 in Vienna **2012**
Presentation Title: *Breaking the walls of classical anticancer therapy*
- First prize of Young Scientists Work Competition of **2008**
A.N. Nesmeyanov Institute of Organoelement Compounds RAS
- Second prize of D. I. Mendeleev's Competition of Research **2008**
Projects for Undergraduate Students
- Russian Academy of Sciences fellowship **2009**
Faculty honors, The Higher Chemical College of Russian Academy of **2008**
Sciences (awarded to one student each semester) **2007**

Additional Honors:

- Participant of the summer school "Metals in Biological Systems" in Louvaine-la-Neuve, Belgium
- Participant of 59th Nobel Laureates Meeting in Lindau, Germany
Siemens Fellow

Hobbies:

- Playing piano
- Singing
- Travelling
- Learning new languages
- Dancing zouk

Publications:

1. *Maria V. Babak*, Samuel M. Meier, Kilian Huber, Jóhannes Reynisson, Anton A. Legin, Michael A. Jakupec, Alexander Roller, Alexey Stukalov, Manuela Gridling, Keiryn L. Bennett, Jacques Colinge, Walter Berger, Paul J. Dyson, Giulio Superti-Furga, Bernhard K. Keppler, Christian G. Hartinger. Target Profiling of RAPTA-drugs by Chemical Proteomics, *Journal of American Chemical Society*, submitted, **2014**
2. Samuel M. Meier, *Maria V. Babak*, Bernhard K. Keppler, Christian G. Hartinger. Efficiently Detecting Metallodrug-Protein Adducts: Ion Trap versus Time-of-Flight Mass Analyzers. *ChemMedChem*, published online, **2014**
3. *Maria V. Babak*, Damian Plazuk, Samuel M. Meier, John Arabshahi, Jóhannes Reynisson, Błażej Rychlik, Andrzej Błaż, Muhammad Hanif, Sebastian Ströbl, Bernhard K. Keppler, Christian G. Hartinger. Half-sandwich Ruthenium(II) Biotin-Conjugates as Biological Vectors to Cancer Cells, *Chemistry – A European Journal*, to be submitted, **2014**.
4. Muhammad Hanif, *Maria V. Babak*, Christian G. Hartinger. Development of Anticancer Agents: Wizardry with Osmium. *Drug Discovery Today*, submitted, **2014**
5. *Maria V. Babak*, Samuel M. Meier, Alexander Roller, Anton A. Legin, Michael A. Jakupec, Bernhard K. Keppler, Christian G. Hartinger. Am(m)ines Make the Difference: Organometallic Ru(ammine) Complexes and Their Chemistry in Anticancer Drug Development. *Chemistry – A European Journal*, 19(13), 4308-18, **2012**
6. Dmitry S. Perekalin, *Maria V. Babak*, Eduard E. Karslyan, Yulia V. Nelyubina and Alexander R. Kudinov. Synthesis and Reactivity of Iron and Ruthenium complexes $[(\eta^5\text{-Indenyl})M(\eta^6\text{-Indene})]^+$ (M = Fe, Ru). *Inorganica Chimica Acta*, 392, 73-76, **2012**
7. Dmitry S. Perekalin, *Maria V. Babak*, Valentin V. Novikov, Pavel V. Petrovskii, Konstantin A. Lyssenko and Alexander R. Kudinov. (Mesitylene)ruthenium π -complexes with benzo-15-crown-5 and dibenzo-18-crown-6, *Journal of Organometallic Chemistry*, 695(8), 1200-1204, **2010**
8. Dmitry S. Perekalin, *Maria V. Babak*, Valentin V. Novikov, Pavel V. Petrovskii, Konstantin A. Lyssenko, Maddalena Corsini, Pierro Zanello and Alexander R. Kudinov. A new approach to the photochemically controlled crown ethers: (tetramethylcyclobutadiene)cobalt complexes with benzo-15-crown-5 and dibenzo-18-crown-6, *Organometallics*, 27, 15, 3654-3658, **2007**

Selected Abstracts (National and International Meetings)

Oral Presentations:

1. *Maria V. Babak*, Samuel M. Meier, Kilian Huber, Giulio Superti-Furga, Paul J. Dyson, Bernhard K. Keppler, Christian G. Hartinger. How to Find the Needle in a Haystack: Target Profiling of RAPTA Drugs by Chemical Proteomics. Second Whole Action Meeting of the COST Action CM1105, Barcelona, Spain, **2013**.
2. *Maria V. Babak*, Samuel M. Meier, Michael A. Jacupec, Giulio Superti-Furga, Paul J. Dyson, Bernhard K. Keppler, Christian G. Hartinger. Target Profiling of RAPTA Drugs by Chemical Proteomics. Modern Trends in Organometallic Chemistry and Catalysis, Moscow, Russian Federation, **2013**, O16
3. *Maria V. Babak*, Samuel M. Meier, Bernhard K. Keppler, Christian G. Hartinger. Organometallic Ru(amine) Complexes and Their Chemistry in Anticancer Drug Development. 7. Workshop Anorganische Chemie in Österreich, Innsbruck, Austria, **2012**, O18

Poster Presentations:

1. *Maria V. Babak*, Samuel M. Meier, Bernhard K. Keppler, Christian G. Hartinger. Am(m)ines Make the Difference: Organometallic Ruthenium Am(m)ine Complexes and Their Chemistry in Anticancer Drug Development. XXV International Conference on Organometallic Chemistry, Lisbon, Portugal, **2012**, PA.203
2. *Maria V. Babak*, Samuel M. Meier, Bernhard K. Keppler, Christian G. Hartinger. Inhibition of Cancer Cell Growth by Ruthenium(II)-Arene Complexes with Various Am(m)ine Ligands. 5th EuCheMS Nitrogen ligands conference, Granada, Spain, **2011**, P 159
3. *Maria V. Babak*, Samuel M. Meier, Bernhard K. Keppler, Christian G. Hartinger. Synthesis and investigation of substituted RAPTA-compounds – new potential anticancer drugs. 13th JCF-Frühjahrssymposium, Erlangen, Germany, **2011**, P28
4. *Maria V. Babak*, Christian Rolando. Novel high-sensitive organometallic dyes for in gel protein staining. 11th JCF-Frühjahrssymposium, Essen, Germany, **2009**, O5. Young Chem 2008, International Congress of Young Scientists, Krakow, Poland, **2008**, T07, P02
5. *Maria V. Babak*, Christian Rolando. Novel fluorescent organometallic dyes for protein detection. XVIII Mendeleev conference of young scientists, Belgorod, Russian Federation, **2008**, 58
6. *Maria V. Babak*, Dmitry S. Perekalin, Alexander R. Kudinov. Pi-complexes of ruthenium and cobalt with crown-ethers. XVII Mendeleev conference of young scientists, Samara, Russian Federation, **2007**, 34

FALLING WALLS LAB 2012 VIENNA

MARIA BABAK

has been awarded

1st PLACE

for BREAKING THE WALL OF

CLASSICAL ANTICANCER THERAPY

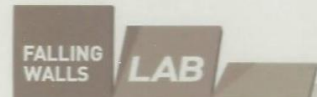
*at the Falling Walls Lab Vienna, organised by the Falling Walls Foundation
and A. T. Kearney on June 15, 2012.*

Ernst Rietschel

Prof. Dr. Drs. h. c. mult. Ernst Th. Rietschel
Chairman of the Board of Trustees
Falling Walls Foundation

Martin Sonnenschein

Dr. Martin Sonnenschein
Managing Director Central Europe
A. T. Kearney



In cooperation with **ATKearney**

I tried to contact all the people who hold the intellectual rights to the figures, in order to get their consent for the usage of the figures in this dissertation. Should there be any claims of copyright infringement, do not hesitate to get in contact with me.

Maria Babak

April, 2014